Demonstration and Theoretical Basis of Energy-Efficient High Recovery, Small-Scale Brackish Reverse Osmosis System

by

Bryan D. Schuetze, Jr., M.S., P.E.

A Dissertation

In

Civil Engineering

Submitted to the Graduate Faculty
of Texas Tech University in
Partial Fulfillment of
the Requirements for
the Degree of

DOCTOR OF PHILOSOPHY

Approved

Lianfa Song, Ph.D.
Chair of Committee

Kenneth Rainwater, Ph.D.

Annette Uddameri, Ph.D.

Dominick Casadonte
Interim Dean of the Graduate School

December 2013

ACKNOWLEDGMENTS

I would like to thank the members of my committee, Dr. Lianfa Song, Dr. Kenneth Rainwater, and Dr. Annette Uddameri, for their invaluable support and technical and editorial assistance. I would also like to thank the Texas Water Development Board and the Lubbock Chapter of Achievement Rewards for College Scientists (ARCS) for their generous financial support in the completion of this research, and Mr. Brad Thornhill of the Department of Civil and Environmental Engineering at Texas Tech University for assisting in the maintenance and operation of the experimental apparatus. Finally, I would like to express my gratitude to the staff of the U.S. Bureau of Reclamation Brackish Groundwater National Desalination Research Facility in Alamogordo, New Mexico, for the use of their facility and for their generous assistance in the completion of this research, and to Ms. Malynda Cappelle of the University of Texas at El Paso for her technical expertise in the use of antiscalants.

.

TABLE OF CONTENTS

ACKNOWLEDGMENTS ii

TABLE OF CONTENTS iii

SUMMARY ABSTRACT vi

LIST OF TABLES vii

LIST OF FIGURES ix

LIST OF ABBREVIATIONS AND SYMBOLS xv

I. INTRODUCTION 1

Control of Test Conditions and Repeatability of Results 5

II. LABORATORY DETERMINATION OF ENERGY CONSUMPTION FOR SMALL-SCALE REVERSE OSMOSIS SYSTEM 7

Abstract 7

Introduction 7

Materials and Methods 11

RO System Design 11

Chemicals 16

Experimental Method 16

Results and Discussion 18

Assessment of Basic System Performance: Driving Pressure versus Recovery 21

Impact of Feed Salinity and Recovery on Feed Pump Energy Consumption 25

Effect of Feed Salinity and Recovery on Circulation Pump Specific Energy 29

Effect of Permeate Flux on Feed Pump Energy Consumption and Specific Energy 31

Effect of Permeate Flux on Circulation Pump Specific Energy 33

Effect of Circulation Flowrate on Feed Pump Energy Consumption 34

Effect of Circulation Flowrate on Circulation Pump Specific Energy 38

Assessment of VCCC 41

Impact of Circulation Flowrate on Permeate Quality 46

Conclusions 49

III. IMPACT OF CROSSFLOW VELOCITY ON TIMING AND SEVERITY OF ADVERSE EFFECTS ON RO SYSTEM PERFORMANCE FROM COLLOIDAL FOULANTS 52

Abstract 52

Introduction 53

Materials and Methods 58

RO System Design 58
Chemicals 61
Experimental Method 61

Results and Discussion 65

Feed Pump Pressure Increase vs. Operating Time at Constant Permeate Flux 66
General Trends 74
Impact of Crossflow Velocity on Severity and Timing of Adverse Effects from Colloidal Foulant 75
Impact of Foulant Concentration on Severity and Timing of Colloidal Foulant Effects 77
Feed Pump Pressure Increase vs. Recovery at Constant Permeate Flux 77
Impact of Foulant Concentration and Crossflow Velocity on Permeate Quality 87
Assessment of Closed Concentrate Circulation for Fouling Reduction in SSBRO 92

Conclusions 92

IV. FIELD DETERMINATION OF ENERGY CONSUMPTION AND OVERALL PERFORMANCE FOR SMALL-SCALE BRACKISH REVERSE OSMOSIS SYSTEM 94

Abstract 94

Introduction 95

Materials and Methods 101

RO System Design 101
Chemicals 104
Experimental Method 104

Results and Discussion 107

Contributions to Total Specific Energy for Small-Scale RO System 110
Assumption of Reversible Fouling and Baseline Membrane Performance 112
Effect of Antiscalant Concentration on Feed Pump Specific Energy 112
Effect of Antiscalant Concentration on Circulation Pump Specific Energy 118
Effect of Permeate Flux on Feed Pump Specific Energy 120

Combined Effects of Permeate Flux and Antiscalant Concentration on Feed Pump Specific Energy 126
Effect of Permeate Flux on Circulation Pump Specific Energy 128
Effect of Circulation Flowrate on Feed Pump Specific Energy 131
Desalination of Well 1 Groundwater at an Antiscalant Concentration of 10.0 mg/L 141
Desalination of Well 1 Groundwater at an Antiscalant Concentration of 5.4 mg/L 141
Desalination of Well 2 Groundwater at an Antiscalant Concentration of 30.6 mg/L 142
Desalination of Well 3 Groundwater at an Antiscalant Concentration of 15.3 mg/L 142
Combined Effects of Circulation Flowrate and Antiscalant Concentration on Feed Pump Specific Energy 144
Effect of Circulation Flowrate on Circulation Pump Specific Energy ... 146
Effect of Multiple Operating Cycles on Feed Pump Specific Energy 149
Effect of Feed Chemistry on Feed Pump Specific Energy 152
The van't Hoff Equation and the Effect of Heavy Ions on Osmotic Pressure and Feed Pump Specific Energy 155
Additional Scenarios for Observed Behavior 156
Assessment of Energy Consumption by the Small-Scale RO System 156
Assessment of VCCC 158
Factors Impacting Permeate Quality 160

Conclusions 168

BIBLIOGRAPHY 170

APPENDIX A: TEMPERATURE CORRECTION FACTORS FOR SELECTED TESTS 175

APPENDIX B: RESULTS OF DUPLICATE TESTS 193

SUMMARY ABSTRACT

A small-scale reverse osmosis (RO) system was developed for energy-efficient brackish desalination at high-recovery. The small-scale RO system used such features as closed (pressurized) circulation of concentrate, parallel single membrane configuration and operating pressure based on constant (operator-specified) target permeate flux. Tests were conducted to determine energy consumption for desalination of NaCl solutions at various concentrations. In addition, tests were conducted to determine the impact of crossflow velocity on severity of adverse effects from colloidal foulants on membrane performance. Based on test results, an assessment was made of the effectiveness of variable closed concentrate circulation (VCCC) in the optimization of crossflow velocity to mitigate these adverse effects. In the final phase of this research, the small-scale system was field tested to determine energy consumption for desalination of brackish groundwater from three wells, representing a wide range of chemical compositions, levels of total dissolved solids (TDS) and scaling potentials. Test results indicated that a system with this design could achieve specific energies comparable to those of conventional large-scale brackish RO systems for desalination of NaCl solutions at feed concentrations up to 5,000 milligrams per liter (mg/L), and for desalination of brackish groundwater with moderate to high scaling potential, when operated within the range of permeate flux recommended by the membrane manufacturer. Test results also indicated that VCCC is an effective means to optimize crossflow velocity for the reduction of negative impacts on membrane performance due to colloidal foulants for timeframes as short as three hours.

LIST OF TABLES

Table 2.1 Manufacturer and model information for system measuring devices. 15

Table 2.2 Experimental operating conditions. 20

Table 2.3 Pressure drop between feed pump and circulation pump at various circulation flowrates for 5,000 mg/L NaCl. 25

Table 2. 4 Feed pump specific energy values for tests referenced in Figures 2.7 and 2.8. 37

Table 2. 5 Reported specific energy values for conventional large-scale RO facilities. 41

Table 2.6. Feed Pump and Total Specific Energies at Maximum (First Cycle) Recoveries under Various Operating Conditions 43

Table 3.1 Fouling test operating conditions at a feed NaCl concentration of 2,500 mg/L. 65

Table 3.2 Approximate times required for divergence in rates of feed pump pressure increase at various feed foulant concentrations. 77

Table 3.3 Recovery at which feed pump operating pressure at 0.1 m/s exceeded feed pump pressure at 0.2 m/s. 86

Table 4.1 Chemistry of groundwater supplied by wells at BGNDRF. 104

Table 4.2 Antiscalant concentrations added to groundwater from three wells at BGNDRF. 105

Table 4.3 Operating parameters for testing of the small-scale RO system at BGNDRF. 109

Table 4.4 Increase in feed pump specific energy observed for changes in permeate flux at recoveries of 50 percent and 80 percent. 124

Table 4.5 Increase in feed pump specific energy observed for increases in circulation flowrate, at recoveries of 50 percent and 80 percent. 140

Table 4.6 Feed pump and total specific energy values for test conditions referenced in Chapter IV. 157

Table 4.7 Reported specific energy values for large-scale RO facilities. 158

Table 4.8 Permeate conductivities at select recoveries for desalination of Well 1 and Well 2 groundwater..... 166

LIST OF FIGURES

Figure 2.1 Experimental small-scale RO system design. 12

Figure 2.2 Feed pump pressure vs. first cycle operating time for desalination at feed NaCl (water softener salt) concentrations of 1,000, 2,500, and 5,000 mg/L, at a target feed and permeate flowrate of 0.14 m^3/h, permeate flux of 26 Lmh, and circulation flowrate of 0.68 m^3/h. 23

Figure 2.3 Feed pump specific energy vs. recovery for desalination at feed NaCl (water softener salt) concentrations of 1,000, 2,500, and 5,000 mg/L, at a target feed flowrate of 0.14 m^3/h, permeate flux of 26 Lmh, and circulation flowrate of 0.68 m^3/h..... 26

Figure 2.4 Feed pump specific energy vs. recovery for desalination at feed NaCl (reagent) concentrations of 1,000, 2,500 and 5,000 mg/L, at a target feed flowrate of 0.23 m^3/h, permeate flux of 44 Lmh, and circulation flowrate of 1.14 m^3/h. 27

Figure 2.5 Circulation pump specific energy vs. recovery for desalination at NaCl (reagent) concentrations of 1,000, 2,500 and 5,000 mg/L, at a target feed flowrate of 0.23 m^3/h, permeate flux of 44 Lmh, and circulation flowrate of 1.14 m^3/h. 30

Figure 2.6 Feed pump specific energy vs. recovery for desalination at a feed NaCl (water softener salt) concentration of 1,000 mg/L, target feed and permeate flowrates of 0.18 and 0.23 m^3/h, permeate fluxes of 35 and 44 Lmh, and a circulation flowrate of 0.91 m^3/h. 32

Figure 2.7 Feed pump specific energy vs. recovery at feed NaCl (water softener salt) concentrations of 1,000 mg/L and 2,500 mg/L, a target feed flowrate of 0.23 m^3/h, permeate flux of 44 Lmh, and circulation flowrates of 0.91 m^3/h and 1.14 m^3/h. 35

Figure 2.8 Feed pump specific energy vs. recovery at a feed NaCl (water softener salt) concentration of 5,000 mg/L, target feed flowrate of 0.14 m^3/h, permeate flux of 26 Lmh, and circulation flowrates of 0.55 m^3/h and 0.68 m^3/h. 36

Figure 2. 9 Circulation pump specific energy vs. recovery for desalination at a feed NaCl (water softener salt) concentration of 1,000 mg/L, target feed flowrate of 0.23 m^3/h, and permeate flux of 44 Lmh. Circulation flowrates: 0.91 m^3/h and 1.14 m^3/h. 39

Figure 2. 10 Circulation pump specific energy vs. recovery for desalination at a feed NaCl (water softener salt) concentration of 5,000 mg/L, target feed flowrate of 0.14 m^3/h, and permeate flux of 26 Lmh. Circulation flowrates: 0.55 m^3/h and 0.68 m^3/h. 40

Figure 2.11 Increase in permeate conductivity vs. first cycle recovery. Effect of circulation flowrate and crossflow velocity. Permeate flux: 26 Lmh. Circulation flowrates: 0.68 m^3/h and 0.82 m^3/h. NaCl: 5,000 mg/L. Source of salt: reagent NaCl. 47

Figure 2.12 Increase in permeate conductivity vs. first cycle recovery. Effect of circulation flowrate. Permeate flux: 26 Lmh. Circulation flowrates: 0.55 m^3/h and 0.68 m^3/h. NaCl: 5,000 mg/L. Source of salt: water softener salt. 48

Figure 3.1 Experimental small-scale RO system design. 59

Figure 3.2 Increase in feed pump pressure vs. operating time. Tests conducted at crossflow velocities of 0.1 and 0.2 m/s for (a) feed with foulant concentration of 50 mg/L and (b) feed with no added foulant. 67

Figure 3.3 Increase in feed pump pressure vs. operating time. Tests conducted at crossflow velocities of 0.1 and 0.2 m/s for (a) feed with foulant concentration of 100 mg/L and (b) feed with no added foulant. 68

Figure 3.4 Increase in feed pump pressure vs. operating time. Tests conducted at crossflow velocities of 0.1 and 0.2 m/s for (a) feed with foulant concentration of 200 mg/L and (b) feed with no added foulant. 69

Figure 3.5 Increase in feed pump pressure vs. operating time. Tests conducted at crossflow velocities of 0.1 and 0.2 m/s for (a) feed with foulant concentration of 500 mg/L and (b) feed with no added foulant. 70

Figure 3.6 Increase in feed pump pressure vs. operating time. Tests conducted at crossflow velocities of 0.1 and 0.2 m/s for (a) feed with foulant concentration of 500 mg/L and (b) feed with no added foulant. 71

Figure 3.7 Increase in feed pump pressure vs. operating time. Tests conducted at crossflow velocities of 0.1 and 0.2 m/s for (a) feed with foulant concentration of 1,000 mg/L and (b) feed with no added foulant. 72

Figure 3.8 Increase in feed pump pressure vs. operating time. Tests conducted at crossflow velocities of 0.1 and 0.2 m/s for (a) feed with foulant concentration of 1,500 mg/L and (b) feed with no added foulant. 73

Figure 3.9 Increase in feed pump operating pressure vs. first cycle recovery at inlet crossflow velocities of 0.1 and 0.2 m/s, baseline case, no foulant. NaCl concentration: 2,500 mg/L. 79

Figure 3.10 Increase in feed pump operating pressure vs. first cycle recovery at inlet crossflow velocities of 0.1 and 0.2 m/s and a feed colloidal silica (foulant) concentration of 50 mg/L. NaCl concentration 2,500 mg/L. 80

Figure 3.11 Increase in feed pump operating pressure vs. first cycle recovery at inlet crossflow velocities of 0.1 and 0.2 m/s and a feed colloidal silica (foulant) concentration of 100 mg/L. NaCl concentration: 2,500 mg/L. 81

Figure 3.12 Increase in feed pump operating pressure vs. first cycle recovery at inlet crossflow velocities of 0.1 and 0.2 m/s and a feed colloidal silica (foulant) concentration of 200 mg/L. NaCl concentration: 2,500 mg/L. 82

Figure 3.13 Increase in feed pump operating pressure vs. first cycle recovery at inlet crossflow velocities of 0.1 and 0.2 m/s and a feed colloidal silica (foulant) concentration of 500 mg/L. NaCl concentration: 2,500 mg/L. 83

Figure 3.14 Increase in feed pump operating pressure vs. first cycle recovery at inlet crossflow velocities of 0.1 and 0.2 m/s and a feed colloidal silica (foulant) concentration of 1,000 mg/L. NaCl concentration: 2,500 mg/L. 84

Figure 3.15 Increase in feed pump operating pressure vs. first cycle recovery at inlet crossflow velocities of 0.1 and 0.2 m/s and a feed colloidal silica (foulant) concentration of 1,500 mg/L. NaCl: 2,500 mg/L. 85

Figure 3.16 Change in permeate conductivity vs. operating time at crossflow velocities of 0.1 and 0.2 m/s. Target feed flowrate: 0.09 m^3/h. Target flux: 17 Lmh. Feed foulant concentration: 50 mg/L. 88

Figure 3.17 Change in permeate conductivity vs. operating time at crossflow velocities of 0.1 and 0.2 m/s. Target feed flowrate: 0.09 m^3/h. Target flux: 17 Lmh. Feed foulant concentration: 200 mg/L. 89

Figure 3.18 Change in permeate conductivity vs. operating time at crossflow velocities of 0.1 and 0.2 m/s. Target feed flowrate: 0.09 m^3/h. Target flux: 17 Lmh. Feed foulant concentration: 1,000 mg/L. 90

Figure 3.19 Change in permeate conductivity vs. operating time at crossflow velocities of 0.1 and 0.2 m/s. Target feed flowrate: 0.09 m^3/h. Target flux: 17 Lmh. Feed foulant concentration: 1,500 mg/L. 91

Figure 4.1 Experimental small-scale RO system design. 102

Figure 4.2 Feed pump specific energy vs. recovery. Effect of antiscalant concentration. Groundwater source: Well 1. Permeate fluxes: 26 Lmh and 35 Lmh. Ratio of circulation flowrate to feed flowrate: 5 to 1. 113

Figure 4.3 Feed pump specific energy vs. recovery. Effect of antiscalant. Groundwater source: Well 2. Permeate flux: 35 Lmh. Circulation flowrate: 0.91 m^3/h. 114

Figure 4.4 Feed pump specific energy vs. recovery. Effect of antiscalant. Groundwater source: Well 2. Permeate flux: 35 Lmh. Circulation flowrate: 1.09 m^3/h. 115

Figure 4.5 Circulation pump specific energy vs. recovery. Effect of antiscalant. Groundwater source: Well 2. Permeate flux: 35 Lmh. Circulation flowrate: 0.91 m^3/h. 119

Figure 4.6 Feed pump specific energy vs. recovery. Effect of permeate flux. Groundwater source: Well 1. Permeate fluxes: 26 Lmh and 35 Lmh. Antiscalant concentrations: 5.4 mg/L and 10.0 mg/L. Circulation flowrate: 0.91 m^3/h. 121

Figure 4.7 Feed pump specific energy vs. recovery. Effect of permeate flux. Groundwater source: Well 2. Permeate fluxes: 26 Lmh and 35 Lmh. Antiscalant: 30.6 mg/L. Circulation flowrate: 0.91 m^3/h. 122

Figure 4.8 Feed pump specific energy vs. recovery. Effect of permeate flux. Groundwater source: Well 3. Permeate fluxes: 26 Lmh and 35 Lmh. Antiscalant concentration: 15.3 mg/L. Circulation flowrate: 0.91 m^3/h. 123

Figure 4.9 Circulation pump specific energy vs. recovery. Effect of permeate flux. Groundwater source: Well 1. Permeate fluxes: 22, 26, 35, and 44 Lmh. Circulation flowrates: 0.68 m^3/h and 1.09 m^3/h. 129

Figure 4.10 Circulation pump specific energy vs. recovery. Effect of permeate flux. Groundwater source: Well 2. Permeate fluxes: 22, 26, and 35 Lmh. Circulation flowrates: 0.68 m^3/h and 0.91 m^3/h. Antiscalant concentration: 30.6 mg/L. 130

Figure 4.11 Feed pump specific energy vs. recovery. Effect of circulation flowrate. Groundwater source: Well 1. Permeate flux: 35 Lmh. Circulation flowrates: 0.91 and 1.09 m^3/h. Antiscalant: 10.0 mg/L. 132

Figure 4.12 Feed pump specific energy vs. recovery. Effect of circulation flowrate. Groundwater source: Well 1. Permeate flux: 26 Lmh. Circulation flowrates: 0.68 and 0.91 m^3/h. Antiscalant: 10.0 mg/L. 133

Figure 4.13 Feed pump specific energy vs. recovery. Effect of circulation flowrate. Groundwater source: Well 1. Permeate flux: 35 Lmh. Circulation flowrates: 0.91 and 1.09 m^3/h. Antiscalant: 5.4 mg/L. 134

Figure 4.14 Feed pump specific energy vs. recovery. Effect of circulation flowrate. Groundwater source: Well 1. Permeate flux: 26 Lmh. Circulation flowrates: 0.68 and 0.91 m^3/h. Antiscalant: 5.4 mg/L. 135

Figure 4.15 Feed pump specific energy vs. recovery. Effect of circulation flowrate. Groundwater source: Well 2. Permeate flux: 35 Lmh. Circulation flowrates: 0.91 and 1.09 m^3/h. Antiscalant: 30.6 mg/L. 136

Figure 4.16 Feed pump specific energy vs. recovery. Effect of circulation flowrate. Groundwater source: Well 2. Permeate flux: 26 Lmh. Circulation flowrates: 0.68 and 0.91 m^3/h. Antiscalant: 30.6 mg/L. 137

Figure 4.17 Feed pump specific energy vs. recovery. Effect of circulation flowrate. Groundwater source: Well 3. Permeate flux: 35 Lmh. Circulation flowrates: 0.91 and 1.09 m^3/h. Antiscalant: 15.3 mg/L. 138

Figure 4.18 Feed pump specific energy vs. recovery. Effect of circulation flowrate. Groundwater source: Well 3. Permeate flux: 26 Lmh. Circulation flowrates: 0.68 and 0.91 m^3/h. Antiscalant: 15.3 mg/L. 139

Figure 4.19 Circulation pump specific energy vs. recovery. Impact of circulation flowrate. Groundwater source: Well 1. Permeate flux: 22 Lmh. Circulation flowrates: 0.57 and 0.68 m^3/h. Antiscalant: 5.4 mg/L. 147

Figure 4.20 Circulation pump specific energy vs. recovery. Effect of circulation flowrate. Groundwater source: Well 2. Permeate flux: 26 and 22 Lmh. Circulation flowrates: 0.57, 0.68, and 0.91 m^3/h. Antiscalant concentration: 30.6 mg/L. 148

Figure 4.21 Effect on feed pump specific energy of multiple operating cycles. Groundwater source: Well 2. 150

Figure 4.22 Feed pump specific energy vs. recovery. Effect of feed chemistry. Well 1 groundwater and reagent NaCl solutions.. Permeate flux: 26 Lmh. 152

Figure 4.23 Feed pump specific energy vs. recovery. Effect of feed chemistry. Well 2 groundwater and reagent NaCl solutions. Permeate flux: 26 Lmh. 153

Figure 4.24 Feed pump specific energy vs. recovery. Effect of feed chemistry. Well 3 groundwater and reagent NaCl solutions. Permeate flux: 26 Lmh. 154

Figure 4.25 Permeate conductivity vs. recovery. Effect of permeate flux. Circulation flowrates: 0.68 and 0.91 m^3/h. Groundwater source: Well 2. Antiscalant: 30.6 mg/L. 162

Figure 4.26 Permeate conductivity vs. recovery. Impact of circulation flowrate. Permeate fluxes: 35 and 22 Lmh. Groundwater source: Well 2. Antiscalant: 30.6 mg/L. 163

Figure 4.27 Permeate conductivity vs. recovery. Impact of circulation flowrate. Permeate flux: 26 Lmh. Groundwater source: Well 2. Antiscalant: 30.6 mg/L. 164

LIST OF ABBREVIATIONS AND SYMBOLS

ACS	American Chemical Society
BGNDRF	Brackish Groundwater National Desalination Research Facility
CCD	closed-circuit desalination
cm	centimeter(s)
CP	concentration polarization
in	inch(es)
kWh/m^3	kilowatt-hour(s) per cubic meter
L	liter(s)
Lmh	liters per square meter per hour
L/min	liters per minute
m	meter(s)
m^2	square meter(s) area
Mbar	megabars pressure
m^3/d	cubic meters per day
MF	microfiltration
mg/L	milligrams per liter
m^3/h	cubic meters per hour
μS/cm	microSiemens per centimeter conductivity
NDP	net driving pressure
NF	nanofiltration
NIST	National Institute of Standards and Technology
ppm	parts per million
psi	pounds per square inch pressure
$Q_{Circulation}$	circulation flowrate
Q_{Feed}	feed flowrate
RO	reverse osmosis
rpm	revolutions per minute
SSBRO	small-scale brackish reverse osmosis
TDS	total dissolved solids
TWDB	Texas Water Development Board
UF	ultrafiltration
VCCC	variable closed concentrate circulation

Please note that these are abbreviations and symbols used repeatedly within the main text and on figures and tables. Additional abbreviations and/or symbols are used and defined in equations and are not included here.

I. INTRODUCTION

Today, billions of people have inadequate supplies of drinking water. It was estimated in 2006 (Service, 2006, as cited by Greenlee and others, 2009) that 2.3 billion people suffered from water shortages. As Greenlee and others (2009) pointed out, mismanagement of potential fresh water sources has recently rendered them unusable. Society is increasingly relying on desalination as a means of supplying fresh water, especially in areas with abundant supplies of brackish groundwater or seawater. Methods of desalination include thermal distillation, flash distillation, and reverse osmosis (RO). While thermal desalination has been in use for approximately 60 years, membrane-based desalination has been in use for approximately 40 years (Gleick, 2006).

The overwhelming majority of desalination facilities constructed today are RO facilities (Greenlee and others, 2009). Of these facilities, almost 100 percent are large-scale RO plants that produce anywhere from 100 to several hundred thousand cubic meters per day (m^3/d) of desalinated water. Conventional large-scale brackish RO facilities typically use arrays of parallel pressure vessels containing several RO membrane elements connected in series, with the parallel pressure vessels connected in stages. In these staged configurations, the number of parallel pressure vessels is reduced from one stage to the next, resulting in the term "Christmas tree" being applied to these configurations. The reduction in pressure vessels from one stage to the next is in direct proportion to the recovery ratio in the previous stage and is commonly about 50 percent. This type of configuration permits the system to maintain an adequate crossflow velocity as permeate is removed from the flow and also enables these systems to achieve high recoveries.

These large-scale designs present many challenges, however. Recoveries greater than 50 percent within each stage are achieved by connecting up to eight membrane elements in series. This type of configuration creates extreme changes in hydraulic conditions, including crossflow velocity and shear rate, within the membrane channel. A large reduction in shear rate can increase the severity of concentration polarization (CP) and membrane fouling, which will be described in a

later section. In order to provide sufficient pressure for permeate production, system pumps must maintain an adequate net driving pressure (NDP) to overcome the maximum transmembrane osmotic pressure difference within the RO process. This requirement results in a large excess of NDP at the earlier membranes where the transmembrane osmotic pressure difference is relatively small. Intrastage booster pumps are often required to maintain the required operating pressure, due to head losses within the membrane channels, piping, and other components of the RO system.

Many of these large-scale RO systems reduce energy consumption by incorporating energy recovery devices (ERDs) into system design. These devices, which include pressure exchangers and energy recovery turbines, extract energy remaining in the concentrate stream and are especially well adapted to concentrate streams containing high residual energy, as would be found in large seawater desalination plants.

Some populations suffering from inadequate supplies of fresh water cannot be served by large-scale RO facilities. Many of these populations are geographically isolated and would consume a small fraction of the fresh water supplied by even a modest conventional large-scale RO facility, i.e., less than 100 m^3/d. The small flowrates generated by small-scale RO systems would not be adequate for typical multi-staged RO configurations and could not maintain the hydraulic conditions required for efficient operation. In addition, the concentrate streams within small-scale RO plants would not contain sufficient residual energy for effective extraction by currently available ERDs, especially in small-scale brackish water desalination.

Certain operational issues interfere with the performance of an RO facility, regardless of capacity. These issues include CP and membrane fouling. CP creates a much greater concentration of rejected species at the membrane surface than within the bulk solution and an enhanced transmembrane osmotic pressure difference. Membrane fouling is a process that degrades membrane performance by increasing resistance to permeate flux and decreasing salt rejection. Fouling can increase operating costs in several ways: (1) by increasing the required frequency of membrane replacement and system maintenance, (2) by increasing the required

membrane surface area required for a given permeate flowrate, and (3) by increasing system operating pressure and the associated cost of energy required to produce a given volume of permeate. CP can raise energy costs of the RO process by increasing the effective osmotic pressure that must be overcome to create permeate.

In order to address the need for energy-efficient small-scale brackish desalination, an RO system was developed using features that address the limitations of conventional large-scale RO processes. The small-scale RO system used two parallel single membrane elements and circulating (recycled) concentrate. Concentrate circulated under pressure and combined with incoming raw feed in ratios specified by the operator. Because concentrate was recycled, feed flowrate equaled permeate flowrate. The pressure required to produce permeate was created by a high pressure feed pump, while the circulation of concentrate was accomplished by a secondary pump operating at much lower pressure. Feed pump operating pressure was based on a constant, operator-specified feed flowrate and permeate flux. Feed pump pressure rose in response to gradually increasing salinity and osmotic pressure of the combined feed/concentrate stream. This design eliminated the huge excesses of NDP that occur in conventional large-scale RO facilities. Recycling of pressurized concentrate enabled the small-scale system to achieve high recoveries without large numbers of membrane elements. Variable circulation flowrates enabled the crossflow velocity and shear rate within the membrane channel to be increased without increasing the feed flowrate and permeate flux. While increased permeate flux can increase CP and the potential for membrane fouling, increased crossflow velocity and shear have the potential to reduce CP, membrane fouling, and energy consumption.

In the small-scale RO process, concentrate was discharged as waste at ambient pressure once a target recovery was achieved, a feature that conserved energy, in the form of pressurized concentrate, without the use of ERDs. The concentrate streams in small-scale brackish RO (SSBRO) systems do not provide sufficient energy to be economically extracted by most currently available ERDs. Parallel single membranes eliminated the long membrane channels seen in conventional large-scale brackish RO systems and the extreme changes in hydraulic conditions between the membrane

channel inlet and outlet. This property of the small-scale system further reduced the risk of CP and membrane fouling. A parallel membrane configuration also increased system flexibility by allowing increases in capacity without the need for large numbers of serially connected membrane elements and without increasing required system operating pressure.

The RO system presented in the following three chapters was similar to earlier designs developed by Bratt (1989) and Szucz (1991), and more recent systems patented by Efraty (2009, 2010, and 2011). Efraty's basic process has been successfully used in the desalination of brackish water and water from the Mediterranean Sea at permeate production rates in excess of 800 m^3/d. While these applications are truly "large-scale," the research described in the following chapters represented the adaptation of variable closed concentrate circulation (VCCC), also termed "closed-circuit desalination," or CCD, to small-scale desalination at permeate production rates ranging from 0.09 m^3/h to 0.23 m^3/h.

The research described in the following chapters consisted of three phases. In the first phase, energy consumption of the small-scale RO system was measured for desalination of sodium chloride (NaCl) solutions at three concentrations: 1,000 mg/L, 2,500 mg/L and 5,000 mg/L, for recoveries up to 90 percent. Energy consumption was measured as specific energy, defined as the energy required to produce a given volume of permeate.

In the second phase, the impact of crossflow velocity on RO membrane performance was assessed at two crossflow velocities, 0.1 and 0.2 m/s, and several feed concentrations of colloidal silica foulant, ranging from 50 mg/L to 1,500 mg/L. Additional tests were conducted at the two crosssflow velocities without colloidal silica in order to establish a baseline for membrane performance. For all tests, feed contained 2,500 mg/L NaCl. Severity of foulant effects on membrane performance was assessed based upon the rate of feed pump pressure increase over time at constant permeate flux. The rate of feed pump pressure increase for desalination at each foulant concentration and crossflow velocity was compared to the rate of feed pump pressure increase for desalination at each crossflow velocity without colloidal silica.

In contrast to this methodology, other researchers have typically measured the rate of flux decline while maintaining essentially constant values for other operating parameters. Results of phase two testing were then applied to an assessment of VCCC as a means to increase shear rate and reduce the severity of effects on membrane performance due to colloidal foulants.

In the third phase of testing, the small-scale RO system was field tested at the U.S. Bureau of Reclamation's Brackish Groundwater National Desalination Research Facility (BGNDRF) in Alamogordo, New Mexico. Specific energies were determined for desalination of brackish groundwater from three on-site wells at recoveries up to 90 percent. The three wells represented a wide range of chemical compositions, total dissolved solids (TDS) levels, and potentials for inorganic fouling. Results of all three phases of this research were presented by Song and others (2012) in a report published by the Texas Water Development Board (TWDB).

Control of Test Conditions and Repeatability of Results

In order to ensure validity of comparisons between test results, efforts were made to control variables that impact energy consumption of the RO process. One key variable was temperature. Permeate flux is very sensitive to temperature and seemingly small increases or reductions in feed temperature can result in significant variations in flux, if NDP is held constant, or can result in large variations in operating pressure, if the system is operated at constant flux. The temperature correction factor (TCF) predicts the ratio of permeate flux at a given temperature to permeate flux at a reference temperature and is calculated using Equation 1.1:

$$TCF = \frac{J_T}{J_R} = \exp\left[K\left(\frac{1}{T_R} - \frac{1}{T} \right) \right] \tag{1.1}$$

where TCF is the temperature correction factor, J_T is the predicted permeate flux at the temperature of interest, J_R is the flux at the reference temperature, K is a constant for a particular type of membrane, in this case, assumed to be 2,700, T_R is the reference temperature on the Kelvin scale, and T is the temperature of interest on the Kelvin scale. The system pressure and NDP are assumed to be constant.

For all laboratory tests referenced in Chapters II and III, the temperature of purified water used to create solutions of NaCl was allowed to equilibrate with room temperature for a minimum of 18 hours prior to solution makeup and testing. The temperatures of laboratory NaCl solutions were monitored prior to all tests to ensure that sufficient cooling and temperature equilibration had occurred. Brackish groundwater used in tests referenced in Chapter IV possessed a relatively constant temperature that required little time for stabilization. Nevertheless, temperatures of groundwater from all three sources were monitored to ensure a fairly constant temperature prior to each test. In order to assess the success of efforts to control temperature, the TCF is presented as a function of recovery and/or operating time for selected tests in Appendix A. The reference temperature used in calculations of TCF was 25 C (298 K). The temperature of the circulating concentrate stream at the conductivity sensor immediately upstream of the holding tank was used to compute the TCF. This conductivity sensor is labeled "C3" in Figures 2.1, 3.1, and 4.1.

Duplicate tests were performed for selected test conditions referenced in Chapters II and IV. Although statistical analysis was not performed on duplicate test results, these results are presented side by side in Figures B.1 through B.6 in Appendix B. It should be noted that timespans (in days) between duplicate tests are provided in parentheses on figure legends. Also note that all flowrates reported in figures and in tables throughout this document are target flowrates used by the system operator during testing to control system operation. Actual flowrates, measured with a stopwatch and graduated cylinder, and flowrates measured and logged by the system, varied up to 10 percent from target flowrates. Permeate fluxes and crossflow velocities reported in Chapters II through IV and in Appendices A and B are based on target flowrates and product information provided by Dow Chemical Company (Dow, 2011 and 2013). Please note that the terms "flux" and "permeate flux" are interchangeable throughout this document.

II. LABORATORY DETERMINATION OF ENERGY CONSUMPTION FOR SMALL-SCALE REVERSE OSMOSIS SYSTEM

Abstract

There is a need for small scale desalination of brackish water to meet the water needs of scattered small communities and households in the United States and other parts of the world. Reverse osmosis (RO) would be a viable means to meet this need if it could be adapted to small-scale applications in an energy-efficient manner. However, small-scale RO desalination usually operates with low recovery and/or low energy efficiency because the design features typically used in large-scale RO desalination to improve recovery and energy efficiency cannot be adapted to small-scale applications due to the limited number of membrane elements. In this study, the concept of variable closed concentrate circulation (VCCC) was investigated as a means to increase recovery and energy efficiency of small-scale RO systems with a limited number of membrane elements. Experiments were conducted to determine the energy consumption of an experimental small-scale RO system employing VCCC and parallel single membrane elements under various operating conditions, including feed salinity, permeate flux, crossflow velocity, and recovery. Results demonstrated the potential of the small-scale RO system to produce permeate at energy efficiencies comparable to those published for conventional large-scale RO systems at recoveries greater than 75 percent.

Introduction

Reverse osmosis (RO) desalination is becoming a very important source of potable water in many locations suffering from a shortage of surface freshwater and/or groundwater. Almost all of the desalination capacity in the United States comes from large-scale RO systems that employ several hundred to thousands of membranes and produce from 100 to several hundred thousand m^3/d of potable water. RO systems operating on such a large scale are widely accepted as economically viable desalination technology with high recovery, low energy demand, and specific energy

for permeate production below 1 kWh/m^3 permeate (McHarg, 2010, 2011; Vince and others, 2007; Stover, 2009).

However, there is a great need for small-scale desalination to supplement fresh water supplies in isolated communities scattered throughout the arid and semi-arid regions of the United States. RO systems suited to these populations could be limited to capacities far below 100 m^3/d. For these relatively small capacities and flowrates, a small number of membranes is required, and features widely employed in large-scale RO processes cannot be used. Large-scale RO facilities typically employ parallel arrays of long pressure vessels containing several membrane elements connected in series. The arrays of parallel pressure vessels are arranged in multiple stage "Christmas tree structures." Because RO systems must maximize recovery and the recommended recovery for each membrane element is 15 percent or less, the number of membranes within each pressure vessel is commonly six to eight. These configurations are designed to utilize the driving pressures and to maintain an adequate crossflow velocity to reduce concentration polarization (CP) and membrane fouling.

In the past, small-scale RO systems were characterized by low recovery and high energy demand. Large-scale brackish RO plants have been constructed using pressurized concentrate recycle, i.e., closed-circuit desalination (CCD), to reduce energy consumption at high recoveries (Stover, 2011). Although the capacities of these facilities are far above capacities suited to small-scale RO, concentrate recycle can be incorporated into small-scale RO facilities, enabling these systems to increase recovery with fewer membrane elements and shorter membrane channels, and to drastically reduce energy consumption.

Concentrate recycle is not a new concept. Stover and Efraty (2012) pointed out that the process was first tested in the 1960s. Desaulniers patented an RO process using conductivity-controlled concentrate recycle (1997), wherein the proportion of concentrate recycled was controlled by the conductivity of the concentrate stream. Other individuals who have developed and patented variations on the process include Robbins (2001) and Gross (1974). Stover (2013) described one recent large-scale

brackish RO plant using concentrate recycle, i.e., CCD, that has been operating since 2009. The permeate capacity is 835 m^3/d and the plant desalinates brackish water with a conductivity range of 5,600 to 9,000 μS/cm. "Real-world" demonstrations of CCD up to the present time have been large-scale with permeate capacities much greater than 100 m^3/d. While the numbers of membrane elements in these facilities are much smaller than those seen in the largest brackish RO facilities, working examples of CCD are exclusively large-scale.

Large-scale RO desalination systems commonly improve energy efficiency through the use of energy recovery devices (ERDs) in the concentrate stream such as pressure exchangers and energy recovery turbines (ERTs). These ERDs are currently impractical for small-scale brackish RO processes because the amount of energy remaining in the concentrate stream is too small to justify their cost. Stover (2009) estimates that the energy remaining in a brackish RO concentrate stream may be as little as one-fourth the energy remaining in a seawater RO concentrate stream. There are, however, limited devices capable of energy recovery in SSBRO. These include Clark pumps (Ghermandi, 2009; Wood, 2007) and Pearson pumps (Spectrawatermakers, 2009), both of which are positive displacement reciprocating pumps.

This chapter presents results from recent experimental testing of a small-scale RO system designed to overcome the existing limitations of conventional RO systems. A parallel single membrane configuration and variable closed concentrate circulation (VCCC) were used to increase system recovery and to improve energy efficiency. In an RO process using VCCC, concentrate is not continuously discharged as waste, but recycled under pressure and combined with incoming raw feed at flowrates that are selected by the system operator. Concentrate is only discharged as waste at ambient pressure after a target recovery, salinity limit, or pressure limit has been reached. Experiments were conducted to demonstrate recovery and energy efficiency achievable with this design for comparison to those of conventional large-scale RO systems employing large numbers of membrane elements, long membrane channels, and staged parallel arrays of pressure vessels.

The design described in this chapter is similar to earlier processes patented by Bratt (1989) and Szucz (1991), and to later refinements developed and patented by Efraty (2009, 2010, and 2011). "Real-world" applications of these designs are described by Efraty (2012), Efraty and others (2011), Stover and Efraty (2012), and by Stover (2011 and 2013). Efraty developed a CCD process that is flexible and can use one or more parallel membrane modules, each of which can contain from one to several membrane elements, depending upon capacity and recovery requirements. Efraty's RO process was first designed to operate with one "container" and subsequently designed to operate without auxiliary containers. Efraty and others (2011) described the application of CCD to the desalination of Mediterranean Sea water. The process was able to achieve specific energies in the range from 1.85 to 2.25 kWh/m^3 of permeate at fluxes ranging from 6 to 18 liters per square meter per hour (Lmh). Efraty (2012) also described the application of this technology to large-scale brackish desalination of two waters, with conductivities of 4,000 μS/cm and 6,800 μS/cm, achieving recoveries of 88 percent and 80 percent, respectively, and specific energies of 0.80 and 0.82 kWh/m^3, at permeate fluxes of 27 and 19 Lmh. The process used eight-inch membrane elements, with four membrane elements per module. This RO plant operated at a rate of permeate production between 586 and 835 m^3/d. Efraty (2012) described a large-scale variation of the closed-circuit design incorporating plug-flow in order to replace accumulated concentrated brine within the closed-circuit with fresh feed. This process was used to desalinate water with a conductivity of 6,800 μS/cm and achieved overall (operation in closed-circuit and plug-flow modes) specific energy of 0.94 kWh/m^3 at a recovery of approximately 83 percent and a permeate flux of 19 Lmh. Seawater desalination plants using Efraty's design have been online since December 2010, while brackish desalination plants using his process have been online since February 2009 (Stover, 2011). The brackish RO systems referenced by Stover produce from 737 to 835 m^3/d. The capacities of these facilities are far above the threshold capacity assumed for small-scale RO. Bratt's earlier RO design used concentrate recycle but incorporated two alternating holding tanks that could be used to store accumulated brine. When one tank was

connected to the RO system and the concentrate circulation loop, the other tank could be flushed and restored to starting conditions with fresh feed. According to information provided on the patent, Bratt's system could achieve nearly continuous operation but required permeate production to be halted briefly while tanks were alternately placed online and removed from service. Szucz' system (1991) suffered from the same limitations. Stover and Efraty (2012) categorized Bratt's and Szucz' processes as "batch RO" and asserted that truly continuous operation was first achieved by Efraty's patented CCD process. In contrast to these examples, the research described here focused on the application of closed, or pressurized, concentrate recycle and single parallel membrane elements to brackish RO on a very small scale. Because the flowrate of circulating, pressurized concentrate was operator-specified, the small-scale RO system described in this chapter will be viewed as an example of VCCC. For purposes of comparison, when focusing on major features, VCCC and CCD represent very similar processes.

Materials and Methods

RO System Design

The custom-built RO system described in this chapter was similar to Efraty's CCD process using one auxiliary container. The RO system was designed using the features of parallel single membrane element configuration and VCCC. The RO system design is presented in Figure 2.1. Components labeled C1 through C3 were conductivity sensors; components labeled F1 through F4 were flow meters; and components labeled P1 through P4 were pressure sensors. Valves are identified with labels V1 through V6.

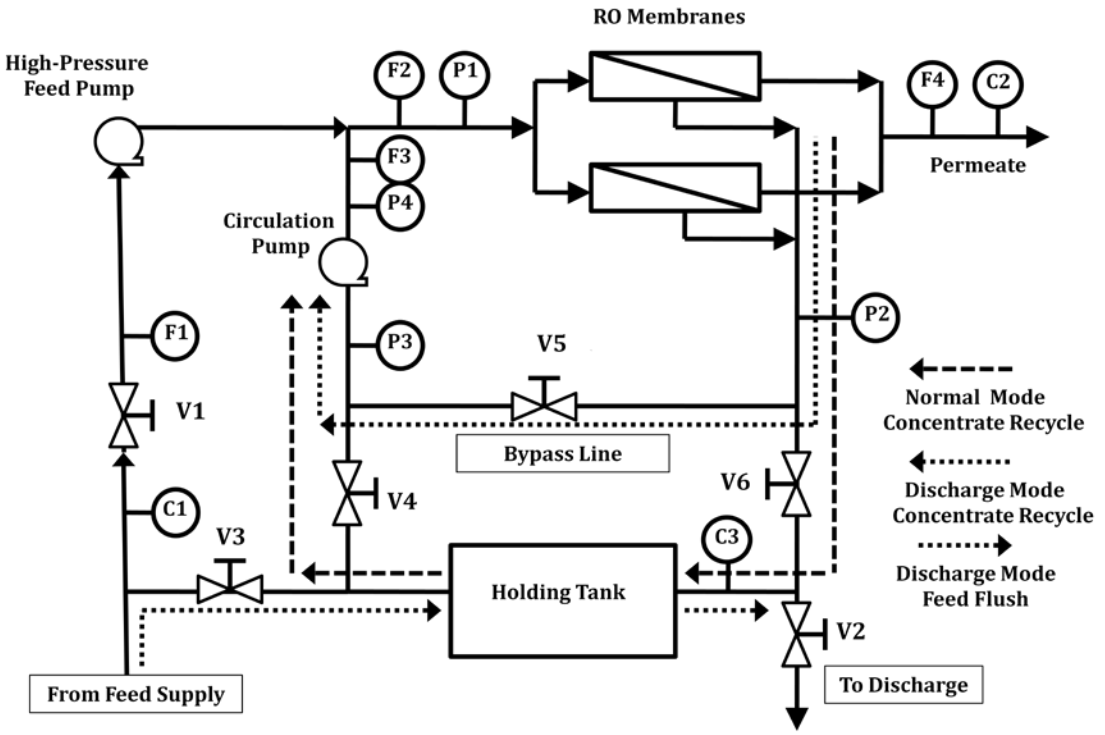

Figure 2.1 Experimental small-scale RO system design.

A key component of the RO system consisted of two parallel Filmtec BW30-2540 2.5-in. (6.2 cm) diameter brackish RO membrane elements (Dow Corporation, Midland, Michigan). The membrane elements were housed within ceramic pressure vessels (Applied Membranes, Vista, California). The number of membrane elements could be reduced to one or increased to a larger number, depending on the capacity requirement. Raw feed was supplied to the RO system by a Hydra-Cell model D-04-S high-pressure diaphragm pump (Wanner Engineering, Inc., Minneapolis, Minnesota), capable of delivering 7.2 L/min at 500 psi (35 bar) pressure and 1750 rpm. A 43.5 L ceramic pressure vessel (Pentair CodeLine, Minneapolis, Minnesota) acted as a holding tank to store concentrated brine during process operation. The concentrate was circulated and mixed with raw feed water, prior to entry into the pressure vessels containing the parallel membrane elements, by a Tonkaflo model AS1608HZ1.5HP centrifugal pump (GE Osmonics, Minnetonka, Minnesota). The Tonkaflo centrifugal pump had a power rating of 1.5 hp, an efficiency rating of 61 percent, and a flow range of 1.14 to 5.22 m^3/h.

The system had two modes of operation: filtration ("normal") mode and discharge mode. The shift between the two modes of operation was accomplished by stainless steel actuated ball valves V2 through V6 (Sharpe Valves, Chicago, Illinois). The flow of feed into the system was controlled by PVC ball valve V1 (Georg Fischer, Tustin, California). During normal mode of operation, circulating concentrate flowed from the membranes through valve V6 and the holding tank and through valve V4 and the circulation pump to combine with the incoming raw feed prior to entry into the RO membrane pressure vessels. The operation of the RO system changed to discharge mode at a pre-determined recovery or feed pump operating pressure.

The recovery of the RO system at any time during one operating cycle was determined using Equation 2.1:

$$R = \frac{\int_0^t Q_f \, dt}{\int_0^t Q_f \, dt + V_H} \tag{2.1}$$

where R is the recovery, Q_f is the feed flowrate, t is the elapsed operating time during one operating cycle from the commencement of normal mode to the completion of the corresponding discharge cycle, and V_H is the volume of the holding tank, or approximately 43.5 L. Calculations of recovery based on Eq. 2.1 assumed that one holding tank volume exited the system during discharge. In order to ensure the discharge of only one tank volume, discharge flowrate was measured with a stopwatch and graduated cylinder a minimum of two times. The required time for discharge of one holding tank volume was determined using the average of the flow measurements. The integration term in Equation 2.1 was the total volume of feed water pumped into the RO system during one operating cycle and was also equal to the volume of permeate produced. The total volume of desalinated feed was approximated by the summation $\Sigma \, Q_f \Delta t$ over short time intervals. For the small-scale RO system, the data logging frequency for all flowrate, pressure, and conductivity measurements was one measurement every 60 seconds. It should be noted that recovery, as defined by

Equation 2.1, was a projected value, based on total volume of desalinated feed and feed used to flush the holding tank at the end of each cycle's discharge operation. During normal mode of operation, prior to initiation of discharge, recovery was essentially 100 percent, with permeate produced equal to feed entering the system.

During discharge, valves V2, V3 and V5 were opened and valves V4 and V6 were closed. Feed flowed into the system not only through valve V1 and the feed pump but also through valve V3 and the holding tank to flush accumulated concentrate from the tank and restore the system to initial conditions. Feed desalination, i.e., permeate production, continued during the discharge process. Circulating concentrate bypassed valves V4 and V6 and the holding tank and flowed through valve V5, the "bypass line", and the circulation pump. Accumulated concentrated brine from the holding tank was discharged as waste through valve V2. The opening and closing of the valves were controlled by a programmable logic controller (PLC) (ABB, Zurich, Switzerland). One operating cycle was defined as the period of time from the start of normal mode to the end of the corresponding discharge operation. Following each discharge process, a new operating cycle commenced and cycle recovery returned to 0 percent. It should be noted that the holding tank also helped to dampen pressure spikes due to sharp increases in concentrate salinity during the discharge process.

Feed flowrates were measured with flow meter F1. Permeate flowrates were measured with flow meter F4. Circulation flowrates were measured with flowmeter F3, while flowrates for the combined feed and circulating concentrate stream were measured with flow meter F2. Flow meters F1 through F3 were "paddlewheel" type flow meters, while flow meter F4 was a magnetic type flow meter. Duplicate measurements of permeate flowrate were made using a stopwatch and graduated cylinder.

Feed pump operating pressures were measured using pressure sensor P1. Fluid pressures of circulating concentrate between the membrane elements and the holding tank were measured using pressure sensor P2. Fluid pressures of circulating concentrate on the upstream side of the circulation pump were measured using pressure sensor P3, while fluid pressures immediately downstream of the circulation

pump were measured using pressure sensor P4. Pressures created by the circulation pump were determined by subtracting the readings obtained from sensor P3 from readings obtained from sensor P4. NIST-certified digital pressure gauges manufactured by Ashcroft (Stratford, Connecticut) were used for duplicate pressure measurements.

Conductivities of raw feed were measured using conductivity sensor C1. Permeate conductivities were measured using conductivity sensor C2, while conductivities of the circulating concentrate stream, prior to entry into the holding tank, were measured using conductivity sensor C3. Conductivity sensor C3 also contained a temperature probe that measured the temperature of the circulating concentrate. Because of the sensitivity of required feed pump pressure and energy consumption to fluid temperature, this temperature was monitored during all testing. Duplicate feed and permeate conductivity measurements were made with an Orion Three-Star conductivity meter (Thermo Fischer Scientific, Waltham, Massachusetts). Manufacturer and model information for each system measuring device are provided in Table 2.1.

Table 2.1 Manufacturer and model information for system measuring devices.

Measuring Device Label	Manufacturer	Model No.
C1	Georg Fischer, Tustin, CA	3-2821
C2	Georg Fischer	3-2821
C3	ABB, Zurich, Switzerland	TB461-0E020002-NV-EN-01-102-J-1-A
F1	Georg Fischer	3-2537-6C-P0
F2	Georg Fischer	P525-1S
F3	Georg Fischer	P525-1S
F4	Georg Fischer	3-2551
P1	Prosense, Oosterhout, Netherlands	PTD25-20-1000H
P2	Prosense	PTD25-20-1000H
P3	Prosense	PTD25-20-1000H
P4	Prosense	PTD25-20-1000H

The RO system used stainless steel pipe, ranging from 0.64 cm to 2.54 cm in

diameter, in all pressurized portions of the RO system, and 1.27 cm diameter Schedule 80 PVC pipe in all non-pressurized portions of the system. Data from various meters and sensors were logged by the system using an AS400 data acquisition system (ABB, Zurich, Switzerland).

Chemicals

Synthetic brackish feed waters of different salinities were used in this study. Sodium chloride (NaCl) from two sources was dissolved in purified water to provide brackish water at three concentrations: 1,000 mg/L, 2,500 mg/L, and 5,000 mg/L. The first set of experiments used Diamond Crystals Solar Salt (Cargill Salt, Minneapolis, Minnesota), which is a coarse crystalline form of sodium chloride with a purity of 99.5 percent claimed by the manufacturer. Because this material is used in water softeners, it will be referred to hereafter as "water softener salt." The second set of experiments used Fisher Scientific ACS-certified NaCl (Thermo Fisher Scientific, Waltham, Massachusetts) . For each laboratory experiment, NaCl was dissolved in purified water supplied by a two-pass, permeate staged RO unit operated by Texas Tech University Physical Plant, capable of producing permeate with an average conductivity of 5 μS/cm and a maximum conductivity below 10 μS/cm.

Experimental Method

Approximately 850 L of purified water were first placed in a plastic tank. Because of the relatively high temperature of the water, it was allowed to cool for at least 18 hours at room temperature prior to test solution makeup in order to maintain a feed water temperature between 23 and 30 C . Because of the sensitivity of required feed pump pressure and energy consumption to feed water temperature, care was exercised to maintain starting and ending test temperatures for circulating concentrate, as measured with conductivity sensor C3 (Figure 2.1), within a 5 C temperature range for all tests. Sufficient salt to create the desired salinity was then added to water with continuous stirring for 20 minutes to achieve complete dissolution and mixing.

During the experiments, raw feed was filtered prior to entry into the RO system. In the first phase of experiments, a 50-μm filter was used. In the second

phase of experiments, water was treated by passage through a 25-μm filter and subsequent passage through a 5-μm filter. In order to "prime" the system prior to all tests, feed was allowed to flow through the system for approximately two minutes. Flow during the first minute consisted of feed flow at the target test feed flowrate, while flow during the second minute consisted of feed flow and circulation flow at the target test feed and circulation flowrates. Flow was then halted and the system (including the holding tank) was flushed for three minutes with the test solution. Flow through the holding tank was approximately 50 L/min during the flush cycle. Tests were commenced following the system flush.

Filtration experiments were conducted at a constant feed and permeate flowrate and permeate flux. The applied pressure from the feed pump was regulated by the PLC, which maintained feed flowrate and permeate flux during the RO process. Likewise, the PLC also controlled circulation pump pressure to maintain target circulation flowrates. It should be noted that the feed flowrate equaled the permeate flowrate for the small-scale RO system. Tests were run in filtration, i.e., normal, mode, followed by discharge, both of which defined one complete operating cycle. The duration of filtration mode satisfied one of the following criteria (first to occur): (a) sufficient time to achieve approximately 90 percent projected recovery following discharge, based on Eq. 2.1; or (b) a feed pump operating pressure of approximately 300 bar. It was necessary to operate tests within this pressure limit due to rapid pressure increases during the discharge process and safe operating pressure limits of the pressure vessels and system piping. Once the target recovery or pressure limit had been reached, operation switched to discharge mode for sufficient time to allow one holding tank volume of raw feed to flow through the holding tank to discharge. Discharge duration was dependent upon the flowrate of the discharge stream. This flowrate varied from approximately 6.8 L/min to 8.7 L/min and was measured at least twice with a stop watch and graduated cylinder. Discharge duration was determined by dividing the holding tank volume by the average of flowrate measurements and entering the time on the appropriate data entry keypad. Once discharge mode had been completed, operation returned to normal mode and cycle recovery returned to 0

percent. At the completion of each test, the RO system was flushed with diluted feed, followed by permeate from the Texas Tech Physical Plant RO system, for several minutes.

Results and Discussion

Desalination experiments were conducted for various combinations of feed flowrate and circulation flowrate at three feed NaCl concentrations: 1,000, 2,500 and 5,000 mg/L, and for recoveries from 0 percent to approximately 90 percent. Operating conditions for each test are presented in Table 2.2 and are reported in units consistent with Dow technical guidance for Filmtec membranes (Dow, 2011). As stated previously, feed flowrate and permeate flowrate were assumed to be equal. It should be noted that all flowrates reported in Table 2.2 were nominal or target flowrates used to control operation of the system. Although total permeate flowrate was measured by the system with flow meter F4, duplicate measurements of permeate flowrate were made volumetrically using a stopwatch and graduated cylinder. Permeate flowrates measured volumetrically differed from target feed and permeate flowrates by as much as 10 percent. The average of feed flowrate measurements from flow meter F1 and permeate flowrate measurements from flow meter F4 most closely matched the timed volumetric measurements of permeate flowrate; therefore, the feed flowrate used in the calculation of recovery was equal to the average of readings from flow meters F1 and F4. It was also assumed that each membrane element contributed 50 percent of total permeate flow. Although the operation of the system was based on target feed flowrates, permeate flux is a much more meaningful parameter for discussions and analyses of test results and has been included in the table as an average value with the corresponding target feed flowrate. Average permeate flux was calculated by dividing 50 percent of the target permeate flowrate by the membrane surface area, or 2.6 m^2 (Dow, 2011). While the feed flowrate used in the calculation of recovery was equal to the average of two simultaneous flow meter readings, the permeate flowrate used to estimate average permeate flux was equal to the target feed flowrate for each test. This assumption was based on the following: (1) the decision to report one approximate value of permeate flux for each experiment, (2) greater perceived

uncertainty in estimating permeate flux within the membrane channel, and (3) the fact that permeate flux was used to analyze and discuss experimental results in a less quantitative and more qualitative manner. Average permeate flux has been reported in Table 2.2 in liters of permeate per hour per square meter of membrane surface area (Lmh). All discussions that follow will be based on permeate flux. Calculations of recovery and estimates of permeate flux in Chapters III and IV also used this methodology.

First cycle recoveries reported in Table 2.2 do not represent maximum recoveries achievable by the process for the conditions specified. These recoveries merely represent the points at which the first cycle normal mode was discontinued, either to meet the initial target of 90 percent recovery, or to avoid system shutdown due to excessive feed pump pressures. Flowrates, conductivities, and system pressures were collected from flow meters F1 through F4, conductivity sensors C1 through C3, and pressure sensors P1 through P4, and recorded by the data acquisition system for all experiments. Flowrate and presssure data were then used to determine the specific energy for permeate production at all recoveries for each experiment.

Table 2.2 Experimental operating conditions.

Feed (NaCl) Salinity (mg/L)	Target Feed/Permeate Flowrate (m^3/h)	Permeate Flux (Lmh)	Target Circulation Flowrate (m^3/h)	First Cycle Recovery Achieved
1,000	0.09	17	0.45	90
1,000	0.14	26	0.68	90
1,000	0.18	35	0.91	91
1,000	0.23	44	0.91	90
1,000	0.23	44	1.14	90
2,500	0.09	17	0.45	90
2,500	0.14	26	0.68	89
2,500	0.18	35	0.82	88
2,500	0.23	44	0.91	80
2,500	0.23	44	1.14	86
5,000	0.09	17	0.45	82
5,000	0.11	22	0.57	81
5,000	0.14	26	0.55	81
5,000	0.14	26	0.68	81
5,000	0.14	26	0.82	80
5,000	0.18	35	0.91	68
5,000	0.23	44	1.14	71

Specific energy was defined as the energy consumed by the RO process per unit volume of permeate produced. The specific energy for the small-scale system consisted of two components: the specific energy requirement for the feed pump and the specific energy requirement for the circulation pump. The specific energy requirement for the feed pump was calculated using Equation 2.2:

$$\hat{E}_f = \frac{\int_0^t Q_f \Delta P_f \, dt}{\int_0^t Q_f \, dt} \tag{2.2}$$

where $\hat{E}_f$ is the specific energy for the feed pump, Q_f is the feed flowrate, dt is the data logging interval, in this case, 60 seconds, and ΔP_f is the operating pressure of the feed pump.

The circulation pump specific energy was determined using Equation 2.3:

$$\hat{E}_c = \frac{\int_0^t Q_c \Delta P_c \, dt}{\int_0^t Q_f \, dt} \tag{2.3}$$

where $\hat{E}_c$ is the specific energy for the circulation pump, Q_c is the circulation flowrate, ΔP_c is the pressure created by the circulation pump, and other variables are defined as in Equation 2.2. For calculations of feed pump and circulation pump specific energy, the integrals in Equations 2.2 and 2.3 were actually approximated by a summation of energy increments (numerator) and flow volume increments (denominator) for each 60 second interval. Total specific energy determined for the small-scale process was simply the sum of the two contributions. Efficiencies of the feed and circulation pumps were not considered in determinations of specific energy.

Assessment of Basic System Performance: Driving Pressure versus Recovery

In a conventional large-scale RO system, the salinity of the fluid in the membrane channel at any given point in the system is fairly constant over time. The osmotic pressure difference between fluid within the channel and permeate at any given point is also reasonably constant. In an RO system using VCCC, the fluid in the membrane channel consists of raw feed and recycled concentrate. The salinity of the recycled concentrate increases with operating time and recovery, causing a corresponding increase in the salinity of the fluid in the membrane channel and an increase in the osmotic pressure difference between the fluid in the channel and the permeate. This assumption is based on a salt rejection not subject to large temporal variation.

Zhu and others (2009) determined the operating pressure profile that produced the lowest theoretical specific energy in scenarios involving fluctuating feed salinity, expressed in terms of feed osmotic pressure. Two operating pressure profiles were investigated for systems with ERDs and for systems without ERDs. One pressure profile assumed a constant operating pressure maintained at twice the calculated average osmotic pressure for a given recovery over the model test duration. The second scenario assumed a variable operating pressure maintained at twice the calculated instantaneous osmotic pressure at each point in time during the model time period. The theoretical specific energy for processes without ERDs was lowest for the variable operating pressure profile, whereas the theoretical specific energy was essentially equal for the two operating pressure profiles for processes with ERDs of 100 percent efficiency.

In the experimental small-scale RO system, the feed pump was designed to maintain a constant feed flow and permeate flux. Operating pressure rose in response to gradual increases in the osmotic pressure difference between fluid in the membrane channel and permeate. To demonstrate this feature, feed pump pressure was plotted as a function of operating time in Figure 2.2 for a target feed flowrate of 0.14 m^3/h, target permeate flux of 26 Lmh, and target circulation flowrate of 0.68 m^3/h. Data is presented for desalination at feed NaCl concentrations of 1,000, 2,500 and 5,000 mg/L for the first operating cycle.

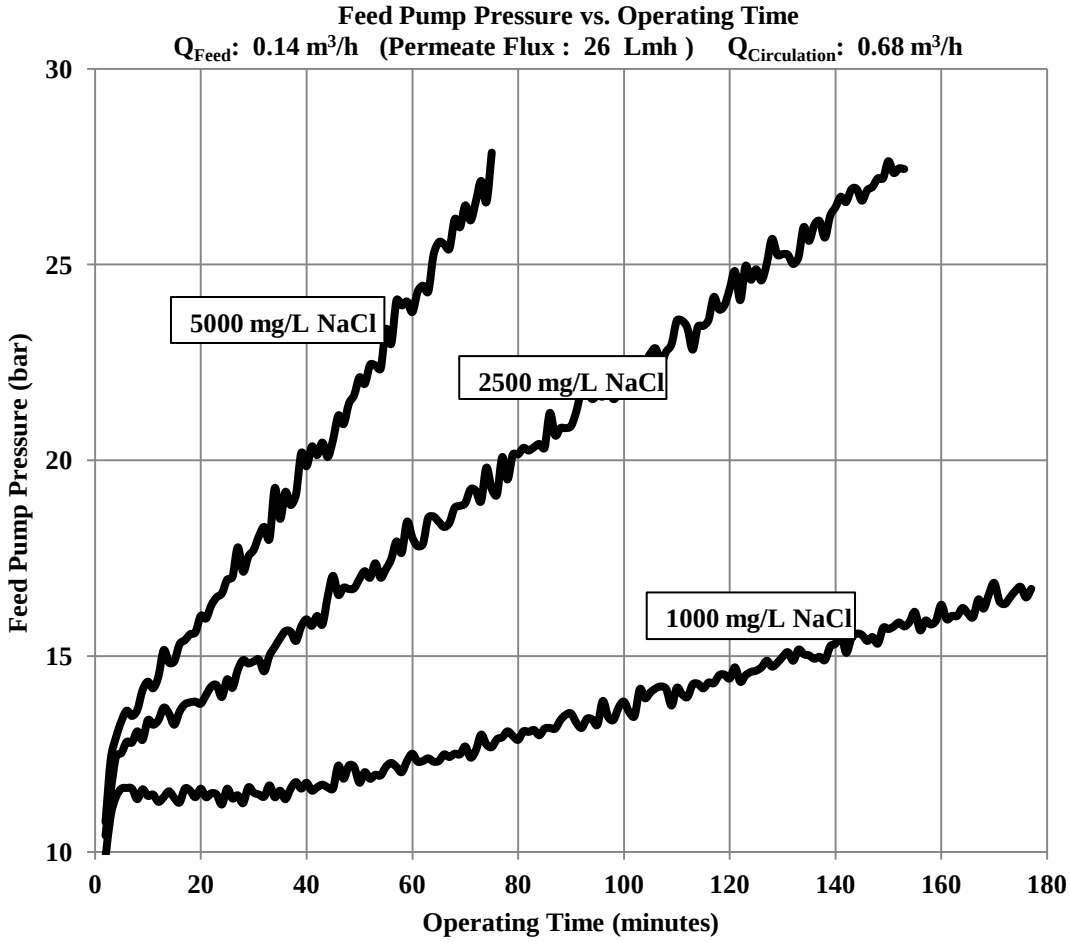

Figure 2.2 Feed pump pressure vs. first cycle operating time for desalination at feed NaCl (water softener salt) concentrations of 1,000, 2,500, and 5,000 mg/L, at a target feed and permeate flowrate of 0.14 m^3/h, permeate flux of 26 Lmh, and circulation flowrate of 0.68 m^3/h.

Results indicated that feed pump pressure rose with operating time in a relatively linear fashion and that this feature of the experimental small-scale RO system functioned as designed.

Although the feed pump pressure rose over time for all test conditions studied, circulation pump operating pressure demonstrated relatively small variations over time for any given feed water salinity. Because the function of the circulation pump was to equalize pressure between circulating concentrate and incoming feed pressurized by the feed pump, circulation pump operating pressure was equal to the pressure drop within the concentrate circulation loop. For the tests referenced in Figure 2.2, the average pressure drop was approximately 2.8 bar for a feed salinity of 1,000 mg/L NaCl, 3.3 bar for a feed salinity of 2,500 mg/L NaCl, and 3.0 bar for a feed salinity of 5,000 mg/L NaCl. Test data indicated that the pressure drop was much more strongly influenced by the circulation flowrate than by feed salinity. Average pressure drops for a range of circulation flowrates for a feed salinity of 5,000 mg/L are provided in Table 2.3.

The manufacturer specified a maximum crossflow pressure drop parallel to a 40 in (1.02 m) membrane element of 15 psi (1.0 bar) (Dow, 2011). Therefore the pressure drop observed for the experimental small-scale RO system was higher than what one would expect based on product information. Additional tests indicated that the relatively large pressure drops between the feed pump and the circulation pump were caused by the flow of concentrate through the pipes, expansions, contractions, valves, and tees within the concentrate circulation pipe. Test results indicated that the pipe configuration within the circulation loop did not significantly affect feed pump specific energy.

Table 2.3 Pressure drop between feed pump and circulation pump at various circulation flowrates for 5,000 mg/L NaCl.

Target Feed Flowrate (m^3/h)	Target Circulation Flowrate (m^3/h)	Average Circulation Pressure Drop (bar)
0.09	0.45	1.7
0.14	0.68	3.0
0.18	0.91	4.3
0.23	1.14	6.5

Impact of Feed Salinity and Recovery on Feed Pump Energy Consumption

In order to determine the impact of raw water salinity and recovery on feed pump energy consumption, feed pump specific energy was determined for the experimental small-scale RO process using raw feed NaCl concentrations of 1,000, 2,500, and 5,000 mg/L at recoveries from 0 percent to approximately 90 percent and at target feed flowrates ranging from 0.09 to 0.23 m^3/h. Feed flowrates corresponded to target permeate fluxes ranging from 17 to 44 Lmh. Ratios of circulation flowrate to feed flowrate ranged from 4:1 to 6:1. Feed pump specific energies determined at target feed flowrates of 0.14 m^3/h and 0.23 m^3/h and permeate fluxes of 26 and 44 Lmh were plotted as a function of recovery at feed salinities of 1,000 mg/L, 2,500 mg/L, and 5,000 mg/L NaCl in Figures 2.3 and 2.4.

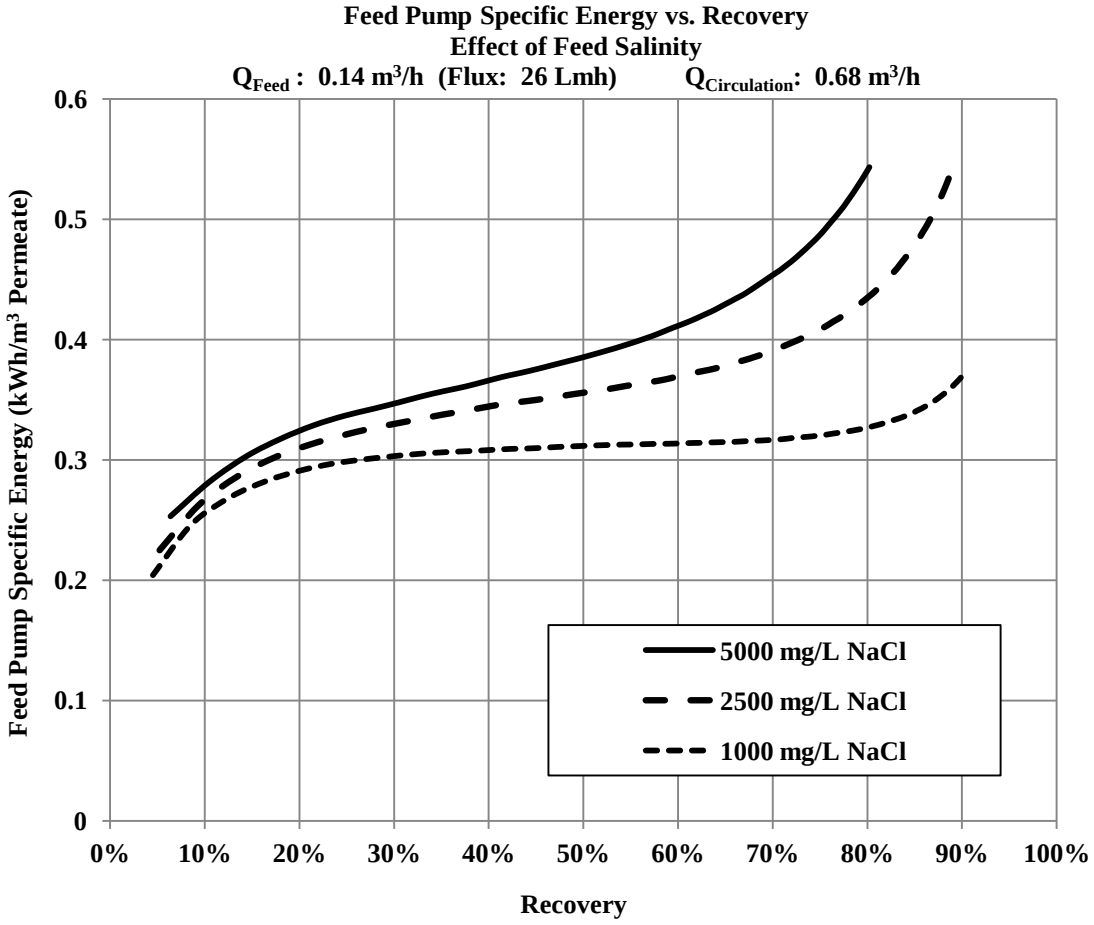

Figure 2.3 Feed pump specific energy vs. recovery for desalination at feed NaCl (water softener salt) concentrations of 1,000, 2,500, and 5,000 mg/L, at a target feed flowrate of 0.14 m^3/h, permeate flux of 26 Lmh, and circulation flowrate of 0.68 m^3/h.

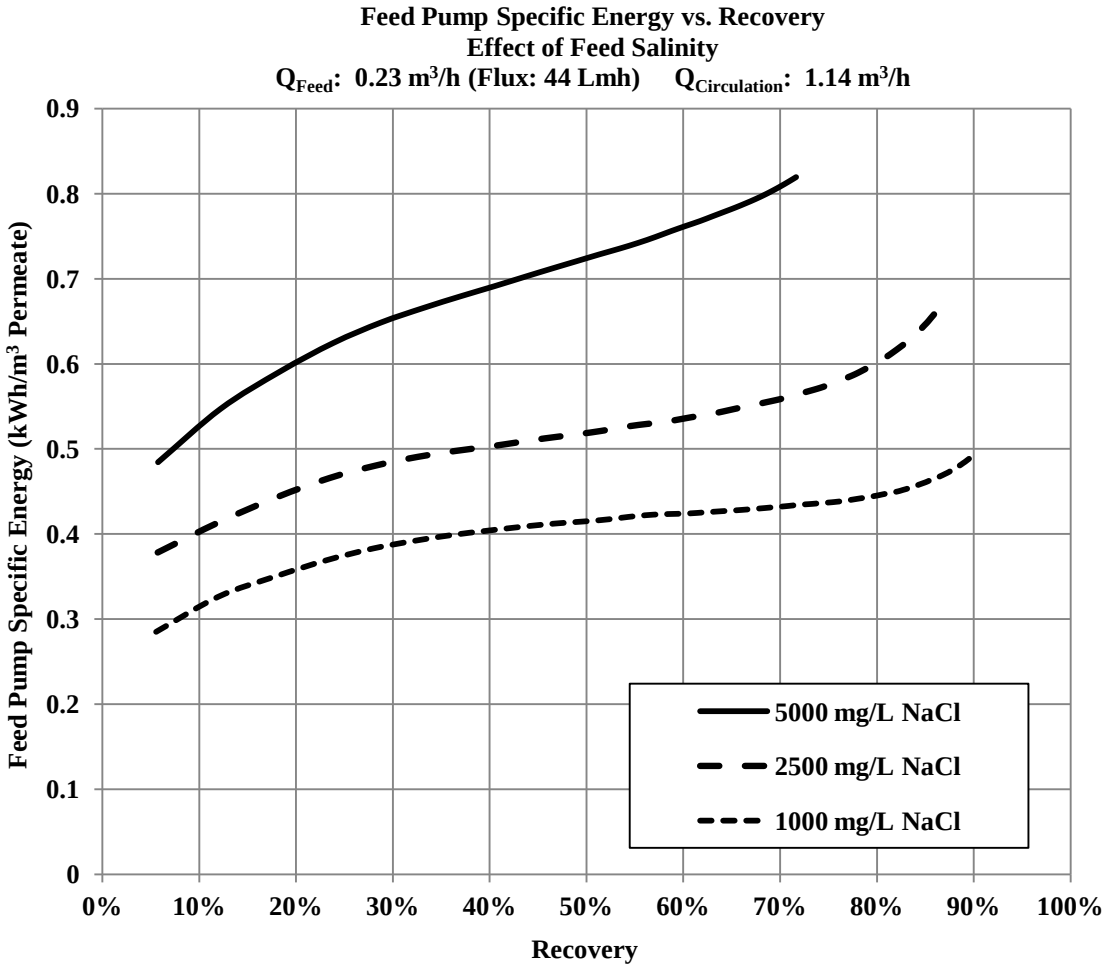

Figure 2.4 Feed pump specific energy vs. recovery for desalination at feed NaCl (reagent) concentrations of 1,000, 2,500 and 5,000 mg/L, at a target feed flowrate of 0.23 m^3/h, permeate flux of 44 Lmh, and circulation flowrate of 1.14 m^3/h.

On inspection of the graphs, very clear relationships and/or trends can be observed. Feed pump specific energy rose with feed salinity and with recovery as a result of increases in salinity of fluid in the membrane channels. Flow within membrane channels consisted of raw feed and circulating concentrate. For the tests referenced in Figures 2.3 and 2.4, the circulation flowrate was approximately five times the feed flowrate.

The RO process must overcome the osmotic pressure difference between the fluid in the membrane channel and the permeate. As the salinity of the feed increases, the salinity of fluid in the membrane channel must also rise proportionately for any

given recovery, resulting in a corresponding increase in the osmotic pressure difference. The osmotic pressure difference between fluid in the channel and permeate rises in spite of the increase in permeate salinity, assuming relatively constant salt rejection, because the salinity of the fluid in the membrane channels rises much more rapidly than permeate salinity. To maintain constant permeate flux, the required NDP must be maintained. System operating pressure must also increase in response to the rise in the osmotic pressure difference, leading to an increase in the energy consumption per unit volume of permeate produced. In simulations performed for an RO plant in Florida, Song and others (2002) demonstrated that the actual relationship between osmotic pressure and salinity, as expressed by the osmotic coefficient, was strongly dependent upon the composition of the feed water and must be determined individually for each feed water under consideration.

The recovery of the process was a function of operating time within an operating cycle. As described previously, an operating cycle was defined as the time between the commencement of normal mode and the end of discharge mode. As operating time and recovery increased, the salinity of the circulating concentrate also increased. Since the ratio of circulating concentrate flow to feed flow entering the membrane channels ranged from approximately 4:1 to 6:1, the osmotic pressure difference between water in the membrane channel and permeate also increased with recovery. This change led to an increase in operating pressure with recovery and a corresponding increase in the energy consumed by the feed pump per unit volume of permeate produced. The impact of recovery on feed pump specific energy was relatively large because the circulating concentrate flowrate was a multiple of the feed flowrate.

For all test conditions, distinct regions were apparent for each curve, following stabilization of flow: (1) a region with a relatively mild slope at intermediate recoveries followed by (2) a relatively steeply-sloped region at high recoveries. The slope of region (1) was smallest for low feed salinities and largest for high feed salinities. In addition, the timing of region (2) was dependent upon the salinity of the feed and upon the feed and circulation flowrates. At any given feed and circulation

flowrate, the onset of region (2) occured at lower recoveries for high salinity feed and at higher recoveries for low salinity feed. If we hold salinity constant and consider only feed and circulation flowrate, the steeply-sloped portion of the curve commenced at lower recoveries for low feed and circulation flowrates and commenced at higher recoveries for high feed and circulation flowrates. This phenomenon was most evident for high feed salinity and less obvious for low feed salinity, and was indicative of potential CP effects.

At a target feed flowrate of 0.23 m^3/h and corresponding permeate flux of 44 Lmh, a target circulation flowrate of 1.14 m^3/h, and a recovery of 70 percent, the ratio of feed pump specific energy for desalination at a feed water salinity of 5,000 mg/L NaCl to feed pump specific energy for desalination at a feed water salinity of 1,000 mg/L was approximately 2:1, much less than the ratio of feed water salinities, i.e., 5:1. This ratio indicated that the influence of hydraulic resistance due to water passage through the membranes was relatively large at the lower salinity when compared to other factors, such as the osmotic pressure difference between the fluid in the membrane channel and the permeate and/or osmotic pressure gradients caused by CP.

It is also worth nothing that desalination of feed containing reagent NaCl resulted in higher feed pump specific energies at any given TDS level and recovery than desalination of feed containing NaCl in the form of water softener salt. This may be due to chemical impurities in the water softener salt that are composed of relatively heavy ions that create less osmotic pressure than pure NaCl for any given TDS level. This effect is discussed further in Chapter IV with respect to the van't Hoff equation. The fact that the supplier of water softener salt claimed 99.5 percent purity does not ensure that 99.5 percent of the water softener salt was NaCl. Depending on process specifics, including location and source of the material, evaporated salt may consist of significant percentages of metal ions other than sodium.

Effect of Feed Salinity and Recovery on Circulation Pump Specific Energy

The impact of feed salinity and recovery on circulation pump specific energy is illustrated in Figure 2.5 for the tests referenced in Figure 2.4.

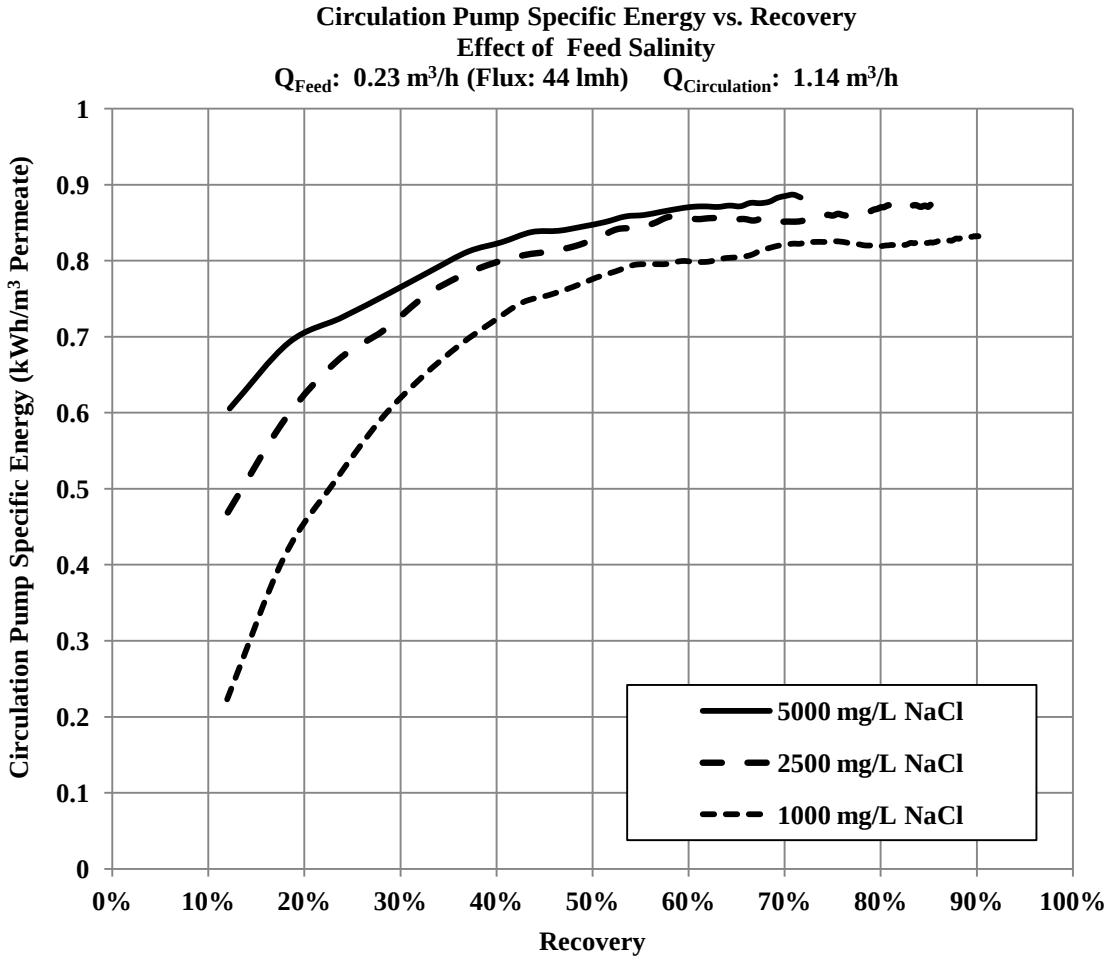

Figure 2.5 Circulation pump specific energy vs. recovery for desalination at NaCl (reagent) concentrations of 1,000, 2,500 and 5,000 mg/L, at a target feed flowrate of 0.23 m^3/h, permeate flux of 44 Lmh, and circulation flowrate of 1.14 m^3/h.

Circulation pump specific energy rose significantly with salinity at lower recoveries. One possible explanation for this behavior is the increase in concentrate viscosity with feed salinity, resulting in greater head losses and energy consumption at higher feed salinity. However, as recovery increased, the relative impact of salinity on specific energy decreased dramatically. This observation can be explained, not in terms of viscosity, but in terms of the fluid temperature in the concentrate circulation loop. As recovery and operating time increased, the temperature of the fluid within the system also increased, reducing the viscosity of the concentrate and the magnitude of associated head losses and energy consumption.

Effect of Permeate Flux on Feed Pump Energy Consumption and Specific Energy

Because feed pump energy consumption is a function of the feed flowrate and the required NDP, permeate flux was expected to have a direct impact on feed pump energy consumption, as predicted by Equation 2.4 that relates NDP to permeate flux and the hydraulic resistance of the membrane:

$$\Delta p - \Delta \pi = J\, R_m \tag{2.4}$$

where Δp is the pressure difference between the membrane channel and the permeate side of the membrane, $\Delta \pi$ is the transmembrane osmotic pressure difference, $\Delta p - \Delta \pi$ is the NDP, J is the permeate flux, and R_m is the hydraulic resistance of the membrane.

In order to demonstrate the effect of permeate flux on feed pump energy consumption, feed pump specific energy was plotted in Figure 2.6 as a function of recovery at target feed flowrates of 0.18 and 0.23 m^3/h, corresponding to permeate fluxes of 35 and 44 Lmh, and a target circulation flowrate of 0.91 m^3/h. The feed NaCl concentration was 1,000 mg/L.

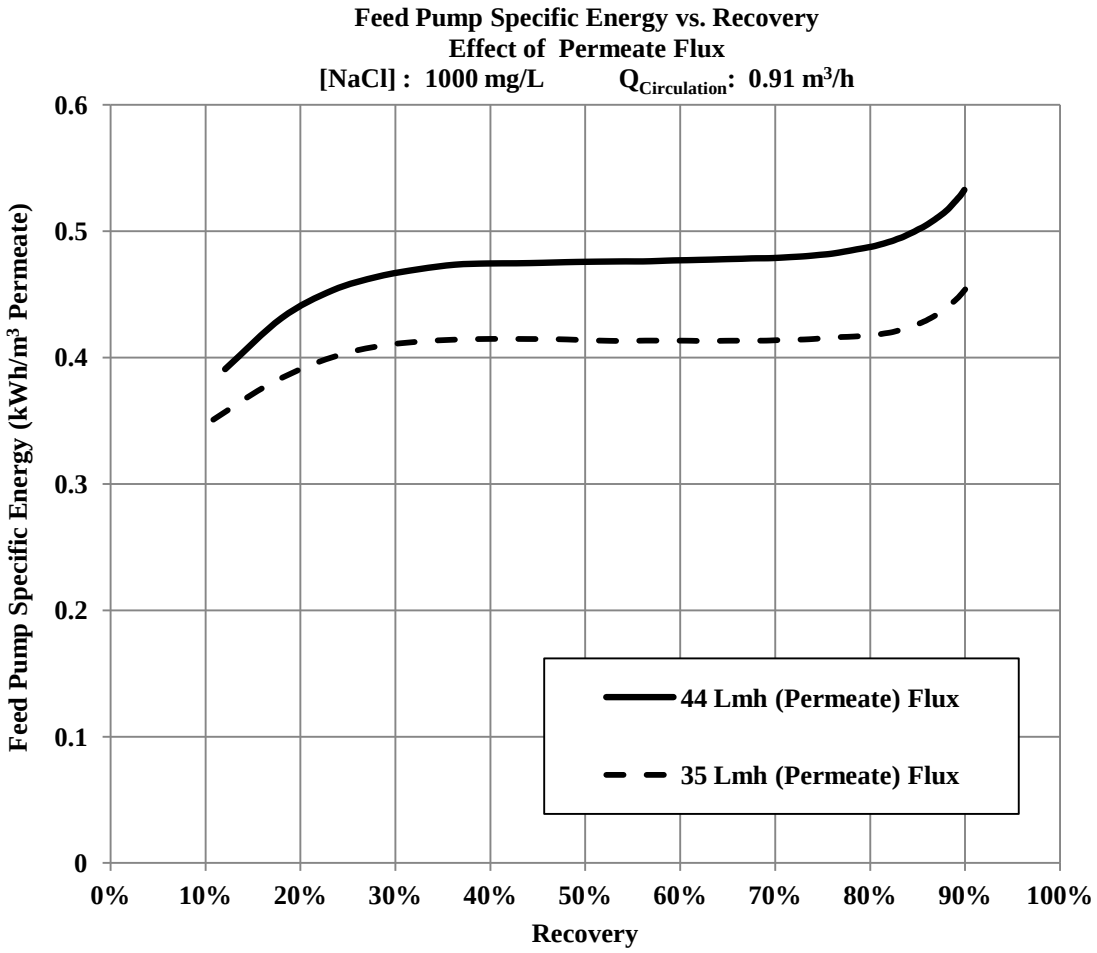

Figure 2.6 Feed pump specific energy vs. recovery for desalination at a feed NaCl (water softener salt) concentration of 1,000 mg/L, target feed and permeate flowrates of 0.18 and 0.23 m^3/h, permeate fluxes of 35 and 44 Lmh, and a circulation flowrate of 0.91 m^3/h.

Certain trends can be observed from Figure 2.6. Increasing permeate flux resulted in an increase in feed pump specific energy for any given recovery. This relationship can be explained by examining the effect of permeate flux on the RO process. The operating pressure required to generate permeate was dependent upon the hydraulic resistance of the membrane, permeate flux, and the osmotic pressure difference between the fluid in the membrane channel and the permeate. Since feed pump energy consumption was directly related to operating pressure, permeate flux had a large impact on energy consumption and it is reasonable that an increase in permeate flux resulted in increased energy consumption per unit volume of permeate.

Increased permeate flux can be associated with increased feed pump specific energy through another mechanism. Because permeate flux was a function of permeate flowrate and permeate flowrate was equal to feed flowrate, increases in permeate flux translated into higher feed flowrates, fluid velocities, and velocity-dependent head losses in the piping between the feed pump and the RO membranes. During testing of the small-scale RO system, these head losses were potentially communicated upstream to the feed pump, which maintained flow by increasing operating pressure. This effect was relatively small when compared to the effect of hydraulic resistance and permeate flux because the piping between the feed pump and the RO membranes was relatively short. It was also expected that the effect of feed flowrate-related head losses on feed pump energy consumption would be relatively small, when compared to the effect of head losses related to the circulation flowrate and occurring within the same portion of the RO system, because the circulation flowrate was much greater than the feed flowrate. This effect will be discussed in the next section.

Effect of Permeate Flux on Circulation Pump Specific Energy

Because feed flowrate and permeate flowrate were equal in the small-scale RO system, feed flowrate had no effect on circulation flowrate and the velocity of circulating concentrate; therefore, the impact of feed flowrate and permeate flux on circulation pump energy consumption was expected to be negligible. However, specific energy is not equal to energy consumption, but rather energy consumption per unit volume permeate. While an increase in permeate flux was not expected to increase the total energy consumed by the circulation pump at a given circulation flowrate, it corresponded to an increase in permeate flowrate and total permeate produced, for the same circulation pump energy consumption. Increased permeate flux at constant circulation flowrate was therefore expected to reduce the contribution to specific energy consumption by the circulation pump.

Effect of Circulation Flowrate on Feed Pump Energy Consumption

The effects of circulation flowrate on feed pump specific energy were examined for desalination at various feed flowrates and circulation flowrates for feed salinities of 1,000, 2,500, and 5,000 mg/L NaCl. Results are presented in Figure 2.7 for NaCl concentrations of 1,000 and 2,500 mg/L and a target feed flowrate of 0.23 m^3/h, corresponding to a permeate flux of 44 Lmh. Circulation flowrates were 0.91 m^3/h and 1.14 m^3/h, corresponding to ratios of circulation flowrate to feed flowrate of 4:1 and 5:1. Results are presented in Figure 2.8 for a feed NaCl concentration of 5,000 mg/L and target feed flowrate of 0.14 m^3/h, corresponding to permeate flux of 26 Lmh. Circulation flowrates were 0.55 m^3/h and 0.68 m^3/h, corresponding to ratios of circulation flowrate to feed flowrate of 4:1 and 5:1. Please note that all discussions based on circulation flowrate reference total circulation flow to both membranes. Circulation flow to each membrane was assumed to be 50 percent of total circulation flow. The exact proportion of total flow to each membrane was not measured during tests referenced in this chapter and in subsequent chapters.

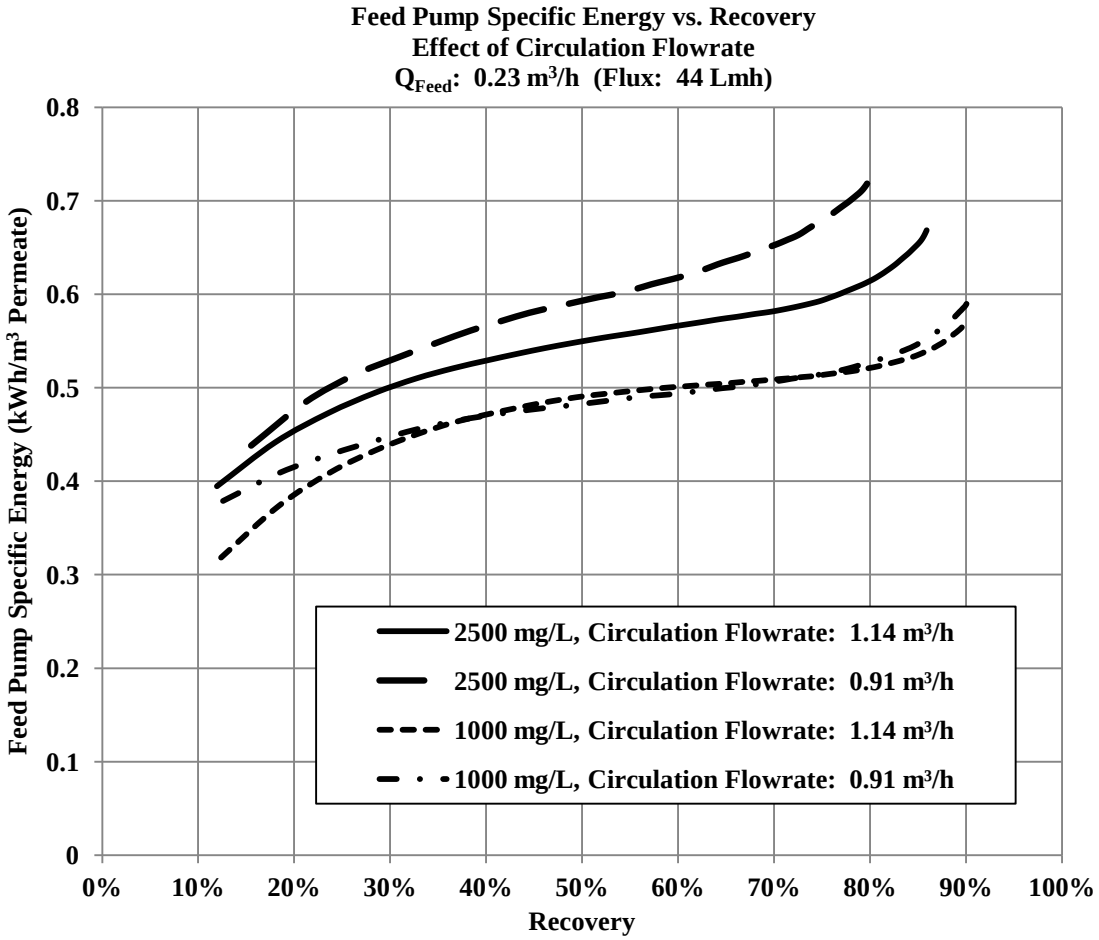

Figure 2.7 Feed pump specific energy vs. recovery at feed NaCl (water softener salt) concentrations of 1,000 mg/L and 2,500 mg/L, a target feed flowrate of 0.23 m^3/h, permeate flux of 44 Lmh, and circulation flowrates of 0.91 m^3/h and 1.14 m^3/h.

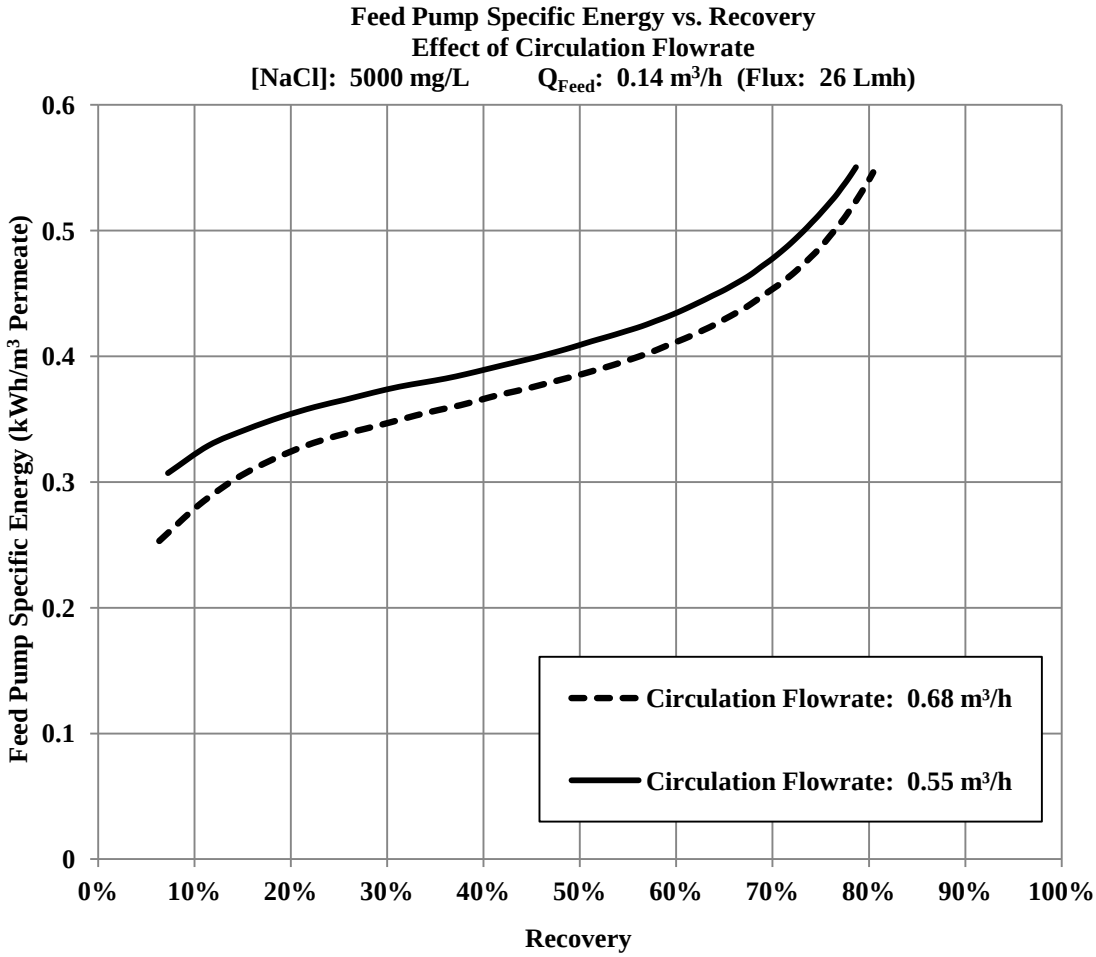

Figure 2.8 Feed pump specific energy vs. recovery at a feed NaCl (water softener salt) concentration of 5,000 mg/L, target feed flowrate of 0.14 m^3/h, permeate flux of 26 Lmh, and circulation flowrates of 0.55 m^3/h and 0.68 m^3/h.

In tests using a raw water salinity of 1,000 mg/L NaCl, feed pump specific energy was slightly higher at the higher circulation flowrate for recoveries from 40 percent to 70 percent, but was slightly lower at the higher circulation flowrate for recoveries below 35 percent and above 75 percent. In tests using feed water with salinities of 2,500 and 5,000 mg/L NaCl, feed pump specific energy was highest at the lower circulation flowrate for all recoveries. In addition, the difference in feed pump specific energy for the two circulation flowrates actually increased with recovery for a feed water salinity of 2,500 mg/L. Feed pump specific energy values for tests referenced in Figures 2.7 and 2.8 are presented for selected recoveries in Table 2.4.

The symbol $\hat{E}$ represents specific energy. In Table 2.4, it denotes feed pump specific energy. The associated subscripts represent the recoveries of interest. This symbol will be used to denote specific energy, in general, throughout this chapter and the following chapters.

Table 2. 4 Feed pump specific energy values for tests referenced in Figures 2.7 and 2.8.

NaCl (mg/L)	Feed Flowrate (m^3/h)	Circulation Flowrate (m^3/h)	$\hat{E}_{30\%}$ (kWh/m^3)	$\hat{E}_{50\%}$ (kWh/m^3)	$\hat{E}_{70\%}$ (kWh/m^3)
1,000	0.23	0.91	0.45	0.48	0.51
1,000	0.23	1.14	0.44	0.49	0.51
2,500	0.23	0.91	0.53	0.59	0.65
2,500	0.23	1.14	0.50	0.55	0.58
5,000	0.14	0.55	0.37	0.41	0.48
5,000	0.14	0.57	0.32	0.37	0.44

These results are reasonable if one considers all of the potential impacts of the circulation flowrate on feed pump specific energy. Changes in the circulation flowrate can affect feed pump energy consumption by altering the crossflow velocity in the membrane channel. An increase in the circulation flowrate increases crossflow velocity and can reduce CP and any enhanced osmotic pressure gradient created by CP, particularly at high salinities. This effect can lead to reduced operating pressure and feed pump energy consumption.

At the same time, increasing circulation flowrate can also increase feed pump operating pressure and feed pump energy consumption. During these experiments, the combined stream containing raw feed and circulating concentrate passed through a tee and split between two narrow pipes prior to entry into the parallel membrane channels. The ratio of pipe diameter upstream of the tee to pipe diameter downstream of the flow split was approximately 4:1. Head losses associated with this drastic change in pipe diameter were a function of flow velocity. Increasing the circulation flowrate potentially caused significant increases in head loss upstream of the RO membranes. These increased head losses were potentially communicated in an upstream direction to the feed pump which would have increased operating pressure to maintain a constant feed flowrate and permeate flux. This would have resulted in increased energy consumption at the higher circulation flowrate.

The relationships between circulation flowrate and feed pump specific energy illustrated in Figures 2.7 and 2.8 were the result of a balance between these competing effects. For feed salinities of 2,500 mg/L and 5,000 mg/L NaCl, the effect of crossflow velocity on CP dominated any effects due to head losses, while at a feed salinity of 1,000 mg/L NaCl, the impact of head losses eliminated any energy savings due to increased crossflow velocity and reduced CP.

Effect of Circulation Flowrate on Circulation Pump Specific Energy

The large impact of circulation flowrate on the circulation pump contribution to specific energy is clearly illustrated by Figures 2.9 and 2.10. In Figure 2.9, circulation pump specific energy was plotted as a function of recovery at two circulation flowrates for a raw feed salinity of 1,000 mg/L NaCl, target feed flowrate

of 0.23 m^3/h, and target permeate flux of 44 Lmh. Circulation flowrates were 0.91 m^3/h and 1.14 m^3/h, corresponding to circulation flowrate to feed flowrate ratios of 4:1 and 5:1. In Figure 2.10, the circulation pump contribution to specific energy was plotted as a function of recovery for the same ratios of circulation flowrate to feed flowrate. For tests referenced in Figure 2.10, the NaCl concentration of the raw feed was 5,000 mg/L. The target feed flowrate was 0.14 m^3/h, corresponding target permeate flux was 26 Lmh, and circulation flowrates were 0.55 m^3/h and 0.68 m^3/h.

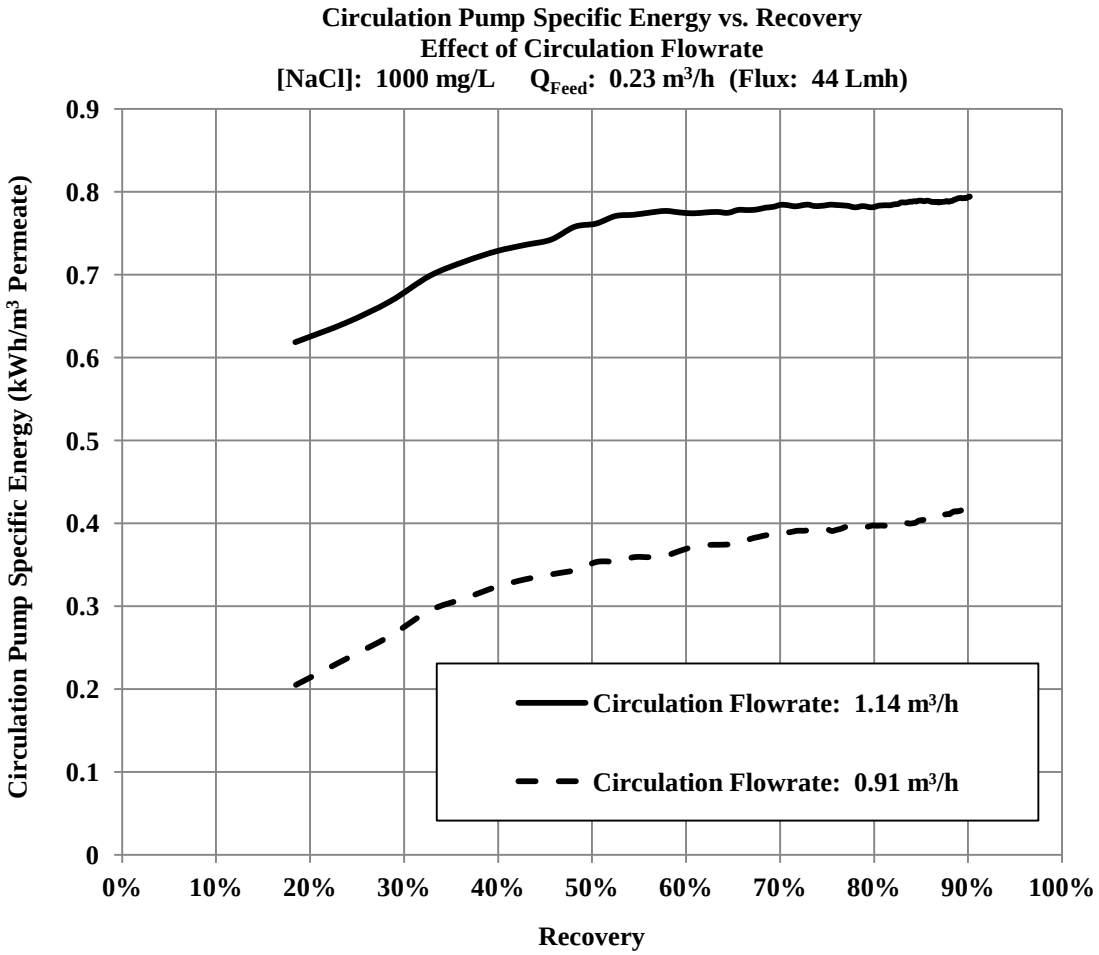

Figure 2. 9 Circulation pump specific energy vs. recovery for desalination at a feed NaCl (water softener salt) concentration of 1,000 mg/L, target feed flowrate of 0.23 m^3/h, and permeate flux of 44 Lmh. Circulation flowrates: 0.91 m^3/h and 1.14 m^3/h.

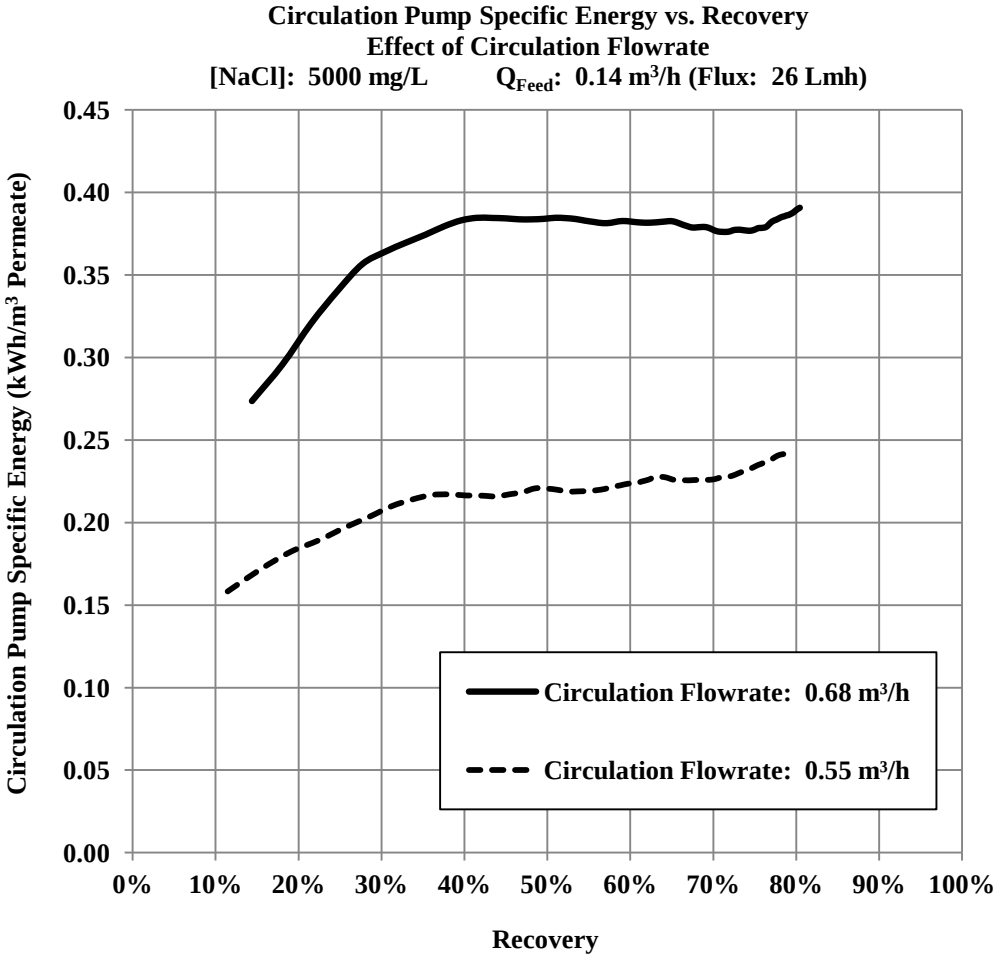

Figure 2. 10 Circulation pump specific energy vs. recovery for desalination at a feed NaCl (water softener salt) concentration of 5,000 mg/L, target feed flowrate of 0.14 m^3/h, and permeate flux of 26 Lmh. Circulation flowrates: 0.55 m^3/h and 0.68 m^3/h.

For both feed salinities, increasing the target circulation flowrate 25 percent roughly doubled the circulation pump specific energy. This is not surprising in light of the circulation pump's function in the small-scale RO system. The circulation pump replaces the head lost by the circulating concentrate. Head losses are a function of fluid velocity squared, and a consequence of viscous flow. One might expect, however, that the concentrate produced from the raw feed with the higher salinity would suffer significantly greater head losses due to its greater viscosity. This is not the case. Results presented in Figure 2.10 demonstrate that any effects due to increased fluid viscosity were dominated by effects due to increased velocity.

Assessment of VCCC

One major focus of this study was the assessment of VCCC as a means to increase recovery and reduce energy consumption for the SSBRO process. As part of that assessment, specific energy values determined for the small-scale RO were compared to values published for conventional large-scale RO systems. Published specific energy values for large-scale RO systems generally ranged from 0.4 to 1.0 kWh/m^3 of permeate. Representative values are provided in Table 2.5.

Table 2. 5 Reported specific energy values for conventional large-scale RO facilities.

Specific Energy (kWh/m^3)	Description	Recovery (%)	Source and Year
1.5	Product information from Lenntech website	65-80	Lenntech, 2011
1.02	Reim 2 brackish RO facility[1]	88	Stover, 2011
0.80	Reim 1 brackish RO facility[2]	88	Stover, 2011
0.61	Kay Bailey Hutchison RO Facility, El Paso, TX	81	McHarg, 2010
0.45	Kay Bailey Hutchison RO Facility, with isobaric ERDs	81	McHarg, 2011
0.8	Representative value for brackish water RO	60	Stover, 2009
0.6 to 0.9	Representative value for brackish water RO	Not Available	Vince and others, 2007

[1]Process uses CCD, coupled with plug-flow desalination.
[2]Process uses CCD only.

For desalination of water with a TDS level of 4,000 ppm at a recovery of 80 percent, Qiu and Davies (2012) provided a theoretical energy requirement for conventional single stage brackish RO of 0.54 kWh/m^3 without ERDs and a corresponding theoretical energy requirement of 0.26 kWh/m^3 for CCD. Based on values provided by several recent sources, and omitting product information provided by manufacturers, an upper limit of 1.0 kWh/m^3 has been used when performing the comparison between the small-scale RO system and conventional large-scale RO systems. Feed pump and total specific energies for the small-scale RO system are provided in Table 2.6 for various circulation flowrates, permeate fluxes, and salinities.

As stated previously, feed pump and circulation pump efficiencies have not been used in calculations of specific energy. Permeate fluxes provided in Table 2.6 are based on target permeate flowrates, assumed to be equal to target feed flowrates, and a membrane surface area of 2.6 m^2 specified by the membrane manufacturer (Dow, 2011). Approximate crossflow velocities based on target feed and circulation flowrates have also been reported in Table 2.6. These crossflow velocities were calculated as averages of estimated inlet and outlet crossflow velocities. Inlet crossflow velocities were estimated using Equation 2.5, based on a membrane feed channel width of 0.93 m (36.56 in) (Dow, 2013), a feed channel spacer height of 7.11 $\times 10^{-4}$ m (28 mil or 0.028 in), and an assumption of 50 percent of feed and circulating concentrate flow entering each membrane channel:

$$u_i = \frac{Q_f + Q_c}{2 \times W \times \delta} \tag{2.5}$$

where u_i is the inlet crossflow velocity in m/s, Q_f and Q_c are the feed and circulation flowrates in m/s, W is the width of the membrane feed channel in m, and δ is the feed channel spacer height in m. The outlet crossflow velocity is estimated using Equation 2.6:

$$u_o = \frac{Q_c}{2 \times W \times \delta} \tag{2.6}$$

where u_o is the outlet crossflow velocity and other variables are as defined in Equation 2.6. Mean crossflow velocities were calculated by averaging inlet and outlet crossflow velocities.

Table 2.6. Feed Pump and Total Specific Energies at Maximum (First Cycle) Recoveries under Various Operating Conditions

Feed (NaCl) Salinity (mg/L)	Permeate Flux (Lmh)	Circulation Flowrate (m^3/h)	Mean Crossflow Velocity (m/s)	Recovery (%)	Feed Pump Specific Energy (kWh/m^3)	Total Specific Energy (kWh/m^3)
1,000[2]	17	0.45	0.11	90	0.26	0.42
1,000[2]	26	0.68	0.16	90	0.32	0.67
1,000[1]	35	0.91	0.21	91	0.46	0.99
1,000[1]	44	0.91	0.21	91	0.54	1.00
1,000[2]	44	1.14	0.26	91	0.50	1.32
2,500[2]	17	0.45	0.11	90	0.43	0.60
2,500[2]	26	0.68	0.16	91	0.50	0.88
2,500[1]	35	0.91	0.21	88	0.59	1.14
2,500[1]	44	0.91	0.21	80	0.73	1.22
2,500[2]	44	1.14	0.26	87	0.68	1.55
5,000[2]	17	0.45	0.11	82	0.54	0.71
5,000[1]	22	0.57	0.13	80	0.58	0.89
5,000[1]	26	0.55	0.13	81	0.59	0.83
5,000[2]	26	0.68	0.16	72	0.63	1.06
5,000[2]	26	0.82	0.19	80	0.73	1.22
5,000[2]	33	0.68	0.16	82	0.69	0.98
5,000[1]	35	0.91	0.21	68	0.69	1.26
5,000[2]	44	1.14	0.26	72	0.82	1.68

[1]Water softener salt
[2]Reagent NaCl

The feed pump contribution to total specific energy for the small-scale RO system was below 1.0 kWh/m^3 for target permeate fluxes ranging from 17 to 44 Lmh for all feed salinities, circulation flowrates, and first cycle recoveries. At a feed salinity of 1,000 mg/L, total specific energy for the small-scale RO system did not exceed 1.0 kWh/m^3 for target permeate flux ranging from 17 to 44 Lmh at circulation flowrates up to 0.91 m^3/h. At a salinity of 2,500 mg/L, total specific energy did not exceed 1.0 kWh/m^3 for target permeate flux of 17 and 26 Lmh at circulation flowrates of 0.45 and 0.68 m^3/h. At a feed salinity of 5,000 mg/L, total specific energy did not exceed 1.0 kWh/m^3 for target permeate flux of 17 and 22 Lmh, at circulation flowrates of 0.45 and 0.57 m^3/h and for target permeate flux of 26 Lmh at a circulation flowrate of 0.55 m^3/h. Manufacturer data for Dow Filmtec brackish RO membranes provided a

"typical" permeate flux of 24 Lmh for surface water treatment and 31 Lmh for well water treatment for "light industrial" applications (Dow, 2011).

The energy demand by the circulation pump is a function of the circulation flowrate and a function of head losses that must be overcome by the circulation pump. Head losses include frictional losses within pipes, losses due to pipe components such as bends, tees, expansions, and contractions, crossflow head losses within the membrane channel, and head losses due to flow entering and exiting the holding tank. Pressure measurements from Sensors P2 and P3 indicated that head losses due to flow through the holding tank were negligible. Measurements of pressure upstream of membrane channel inlets and downstream of channel outlets also indicated that pressure losses from flow through membrane channels were only on the order of 0.14 to 0.35 bar, while frictional head losses and losses due to pipe components ranged from approximately 1.4 bar at the lowest circulation flowrates to approximately 6.2 bar at the highest circulation flowrates used in this study. These velocity-related head losses can be reduced through changes in pipe configuration. Because the circulation pump contribution to total specific energy ranged from approximately 30 percent to 60 percent, eliminating these head losses can potentially lead to large reductions in specific energy. These savings could be achieved through design changes as simple as eliminating small pipe diameters and reducing flow velocity and/or eliminating abrupt changes in pipe diameter or flow direction. An analysis of potential energy savings from reductions in circulation pump operating pressure indicated that maintaining total circulation pressure loss at or below 1.4 bar (20 psi) could potentially lead to total specific energy values for the experimental RO system that are comparable to published values for large-scale RO systems under a much broader range of operating conditions.

The relationship between the circulation pump contribution to total specific energy, circulation flowrate, and circulation pump operating pressure is analogous to the relationship between feed pump specific energy, feed flowrate, and feed pump operating pressure as represented in Equations 2.2 and 2.3. Based upon these relationships and assuming constant circulation flowrate, feed flowrate and circulation

pump operating pressure, the circulation pump specific energy may be estimated from Equation 2.7:

$$\hat{E}_c = (0.028)\left(\frac{Q_c \Delta P_c}{Q_f}\right) \tag{2.7}$$

where Q_c/Q_f is the ratio of circulation flowrate to feed flowrate, ΔP_c is the circulation pump pressure, expressed in bar and $\hat{E}_c$ is the circulation pump specific energy, expressed in kWh/m^3 permeate.

Based on Equation 2.7, a circulation pump pressure of 1.0 bar (15 psi) and a circulation flow to feed flow ratio of 5:1 would result in a circulation pump specific energy of approximately 0.14 kWh/m^3, while a circulation pump pressure of 1.4 bar (20 psi), using the same flow ratio, would result in a circulation pump specific energy of 0.19 kWh/m^3. If these values were added to the feed pump specific energies provided in Table 2.6, all total specific energy values obtained by adding the two specific energy contributions would be below the 1.0 kWh/m^3 upper limit assumed for large-scale RO facilities, with the exception of values reported for a raw feed salinity of 5,000 mg/L, a feed flowrate of 0.23 m^3/h, and permeate flux of 44 Lmh. When considered in light of the low recovery and energy efficiency that have characterized SSBRO up to the present time, these findings indicate that VCCC is a promising technology in the development of energy-efficient small-scale brackish RO.

The primary advantage(s) offered by this technology stem from the fact that conventional large-scale RO configurations without concentrate recycle are impractical for small-scale RO. This technology offers small-scale RO applications the ability to achieve specific energies comparable to conventional large-scale RO facilities at high recovery if permeate flux does not exceed limits appropriate for the type of water being treated.

Impact of Circulation Flowrate on Permeate Quality

The process of CP adversely impacts permeate quality by concentrating ions at the membrane surface relative to the bulk solution and increasing their passage through the membrane. While the severity of CP is believed to increase with permeate flux, increasing crossflow velocity is believed to lessen the severity of CP by increasing shear and back diffusion of ions from the membrane surface to the bulk solution. In the small-scale RO system, crossflow velocity was increased by raising both the feed flowrate and the circulation flowrate. Increasing the circulation flowrate, however, had a much larger relative impact on crossflow velocity because the small-scale system was designed to operate at circulation flowrates that are multiples of the feed flowrate. In order to demonstrate the effect of circulation flowrate and crossflow velocity on permeate quality, permeate conductivity increase is plotted as a function of first cycle recovery in Figure 2.11 for desalination of feed containing 5,000 mg/L reagent NaCl at a target permeate flux of 26 Lmh for circulation flowrates of 0.68 and 0.82 m^3/h. Permeate conductivity data for desalination at circulation flowrates of 0.55 and 0.68 m^3/h at the same feed salt concentration and permeate flux are presented in Figure 2.12. The source of salt for tests referenced in Figure 2.12 was water softener salt.

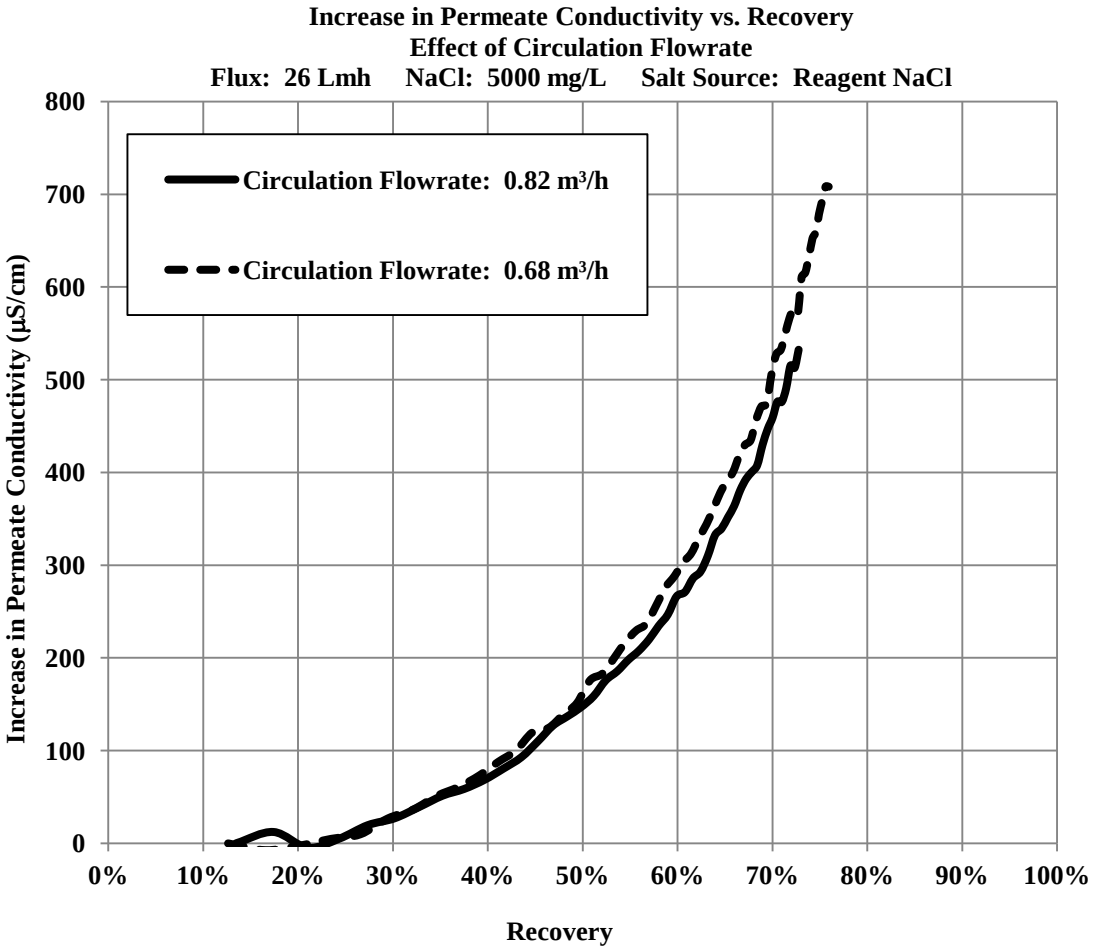

Figure 2.11 Increase in permeate conductivity vs. first cycle recovery. Effect of circulation flowrate and crossflow velocity. Permeate flux: 26 Lmh. Circulation flowrates: 0.68 m^3/h and 0.82 m^3/h. NaCl: 5,000 mg/L. Source of salt: reagent NaCl.

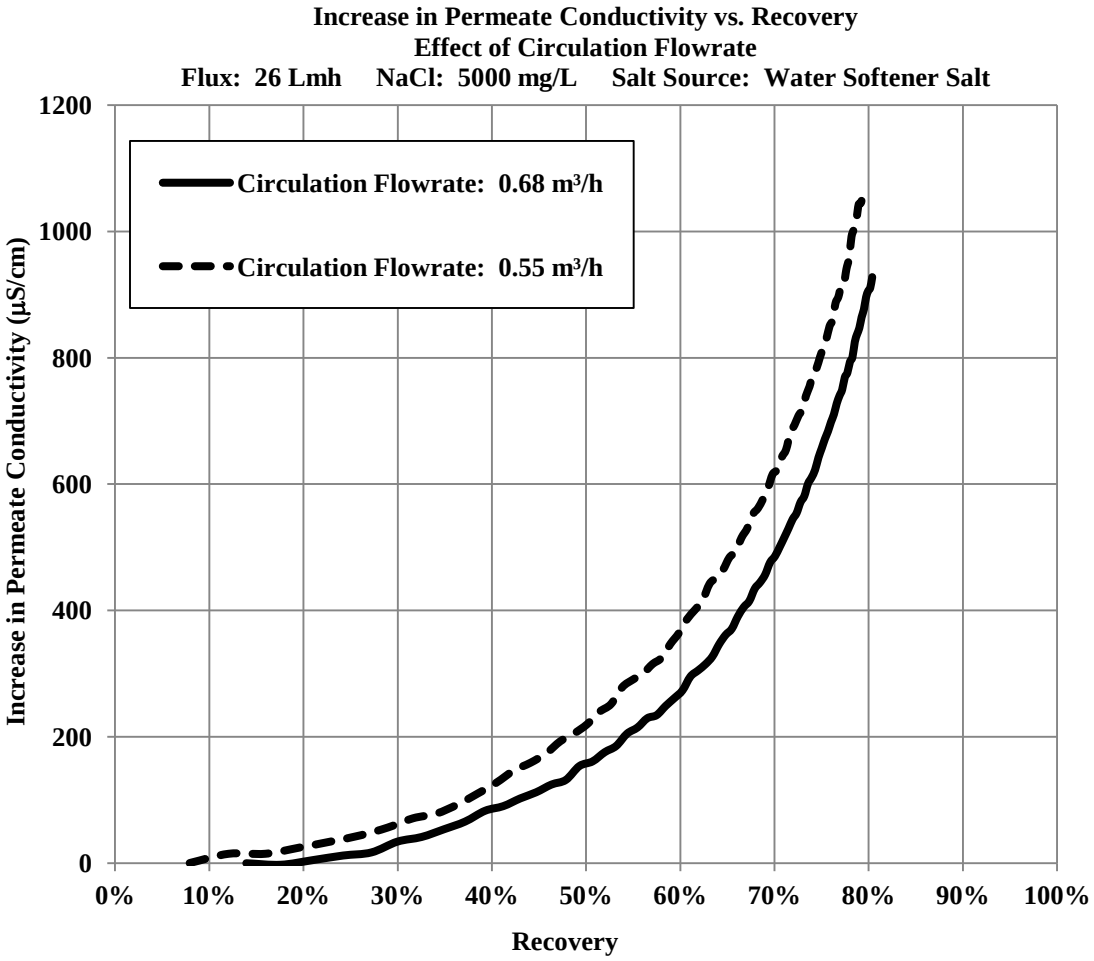

Figure 2.12 Increase in permeate conductivity vs. first cycle recovery. Effect of circulation flowrate. Permeate flux: 26 Lmh. Circulation flowrates: 0.55 m^3/h and 0.68 m^3/h. NaCl: 5,000 mg/L. Source of salt: water softener salt.

As demonstrated by data presented in Figure 2.11, raising the circulation flowrate 20 percent from 0.68 m^3/h to 0.82 m^3/h resulted in a slight improvement in permeate quality, as reflected in conductivity readings, at recoveries above 50 percent. As stated in previous sections, the term "circulation flowrate" refers to total circulation flow to both membranes. Each membrane channel is assumed to receive 50 percent of total circulation flow. At a permeate flux of 26 Lmh, increasing the circulation flowrate from 0.68 m^3/h to 0.82 m^3/h represented an increase in inlet crossflow velocity from 0.17 to 0.20 m/s, an increase in outlet crossflow velocity from 0.14 to 0.17 m/s, and an increase in mean crossflow velocity from 0.16 to 0.19 m/s. This

increase represented an 18 percent change in mean crossflow velocity. The improvement in permeate quality demonstrated by results presented in Figure 2.12 for an increase in circulation from 0.55 m^3/h to 0.68 m^3/h was slightly larger. At a permeate flux of 26 Lmh, increasing the circulation flowrate from 0.55 to 0.68 m^3/h raised the inlet crossflow velocity from 0.14 to 0.17 m/s, the outlet crossflow velocity from 0.11 to 0.14 m/s, and the mean crossflow velocity from 0.13 to 0.16 m/s. This increase represented a 22 percent change in crossflow velocity, which could potentially explain the slightly larger improvement in permeate quality at these conditions.

Conclusions

Test results indicated that incorporation of VCCC into the RO process is a viable means to increase recovery and maximize energy efficiency for SSBRO. This assessment was based on (1) the observation that system pressure rose in response to increasing recovery and osmotic pressure and (2) comparisons between specific energy values determined for the experimental small-scale RO system and values published for conventional large-scale RO systems. Based upon a survey of recent sources, an upper limit of 1.0 kWh/m^3 for specific energy of conventional large-scale brackish RO systems was assumed for the comparison.

Specific energy was determined for permeate production at target feed and permeate flowrates from 0.09 to 0.23 m^3/h, NaCl concentrations of 1,000 mg/L, 2,500 mg/L, and 5,000 mg/L, and for ratios of circulation flowrate to feed flowrate of 4:1, 5:1, and 6:1. Corresponding target permeate fluxes ranged from 17 to 44 Lmh. Actual permeate flux exceeded target flux by as much as 10 percent. It should also be noted that comparisons of specific energy were based on the calculated specific energy for the small-scale RO process at the end of the first operating cycle, which was defined as the time between initial process startup and the end of the first discharge process.

The feed pump specific energy component for the small-scale RO system did not exceed the assumed 1.0 kWh/m^3 upper limit of reported specific energy values for conventional large-scale RO facilities for all salt concentrations, permeate fluxes,

circulation flowrates, and recoveries specified in Table 2.2. Total specific energy for desalination of feed containing 1,000 mg/L NaCl did not exceed 1.0 kWh/m^3 for first cycle recovery to 90 percent at target permeate fluxes ranging from 17 to 35 Lmh and a 5:1 ratio of circulation flowrate to feed flowrate. The ratio of circulation flowrate to feed flowrate will be assigned the term "flow ratio" for the remainder of this section. At a permeate flux of 44 Lmh, total specific energy did not exceed 1.0 kWh/m^3 at 90 percent recovery for a 4:1 flow ratio, i.e., a circulation flowrate of 0.91 m^3/h. At a flow ratio of 5:1, total specific energy for desalination of feed containing 1,000 mg/L NaCl exceeded the 1.0 kWh/m^3 upper limit at a target permeate flux of 44 Lmh by over 30 percent at 90 percent recovery.

Total specific energy for desalination of feed containing 2,500 mg/L NaCl did not exceed 1.0 kWh/m^3 for target permeate fluxes of 17 and 26 Lmh, at a 5:1 flow ratio and first cycle recovery of approximately 90 percent. Total specific energy exceeded 1.0 kWh/m^3 at a target permeate flux of 35 Lmh, 88 percent recovery, and flow ratio of 5:1. Total specific energy also exceeded 1.0 kWh/m^3 for a target permeate flux of 44 Lmh, at flow ratios of 4:1 and 5:1, and recoveries of 80 percent and 87 percent, respectively.

For desalination of feed containing 5,000 mg/L NaCl, total specific energy of the small-scale RO process did not exceed 1.0 kWh/m^3 at fluxes of 17 and 22 Lmh, a flow ratio of 5:1, and first cycle recoveries of 82 and 80 percent, respectively. In addition, total specific energy did not exceed 1.0 kWh/m^3 for permeate flux of 26 Lmh, first cycle recovery of 81 percent, and a flow ratio of 4:1. Total specific energy exceeded 1.0 kWh/m^3 at target permeate flux of 26 Lmh for flow ratios of 5:1 and 6:1, and first cycle recoveries of 72 percent and 80 percent, respectively. Total specific energy also exceeded 1.0 kWh/m^3 at target fluxes of 35 Lmh and 44 Lmh for flow ratios of 5:1 and first cycle recoveries of 68 and 72 percent, respectively. Product technical guidance provided on the Dow Filmtec website for "light industrial applications" provided a typical permeate flux of 24 Lmh for surface water treatment and 31 Lmh for well water treatment (Dow, 2011), suggesting that total specific energy for the small-scale RO system is comparable to published values for large-

scale RO for brackish well or surface water desalination if the system is operated at a "typical" permeate flux.

Tests indicated that a major portion of the total specific energy was due to head loss within the concentrate circulation piping where flow encounters tees, valves, bends, contractions and expansions. These head losses were velocity-dependent and could potentially be reduced by design changes in the piping configuration. Although component head losses are termed "minor losses," their combined effects were significant, as determined by this study. Modifications in system design therefore have the potential to significantly reduce total specific energy of the system. Based on test results from this research, maintaining pressure drops between the feed pump and circulation pump below 1.4 bar (20 psi) could potentially enable the experimental small-scale RO system to achieve specific energies comparable to or superior to those of existing conventional large-scale RO systems at recoveries greater than 75 percent for an even broader range of permeate flux. In addition to its application to energy-efficient small-scale brackish RO, VCCC has potential as a means to improve permeate quality by enabling the operator to uncouple crossflow velocity from feed flowrate and permeate flux, as demonstrated by experimental data.

III. IMPACT OF CROSSFLOW VELOCITY ON TIMING AND SEVERITY OF ADVERSE EFFECTS ON RO SYSTEM PERFORMANCE FROM COLLOIDAL FOULANTS

Abstract

Although significant advances have been made in the development of membranes for reverse osmosis (RO) desalination, membrane fouling continues to be a serious issue affecting the performance of RO processes in many applications. Membrane fouling can drive operating costs upward by increasing energy costs, maintenance and repair costs, shortening useful life of RO membranes, and increasing the required membrane surface area for a given permeate production rate. Research has shown that the severity of membrane fouling can be reduced by increasing crossflow velocity and shear rate. In conventional RO processes, crossflow velocity and shear are increased by increasing the feed flowrate or by reducing the number of membrane elements, i.e., reducing recovery. This paper presents the demonstration of a small-scale RO system using variable closed (pressurized) concentrate circulation (VCCC) for the mitigation of adverse effects caused by colloidal foulants in small-scale brackish reverse osmosis (SSBRO). VCCC permits increases in crossflow velocity without requiring increases in feed flowrate and permeate flux. In addition to VCCC, the system described in this chapter employed a parallel single membrane configuration that reduced membrane channel length to a small fraction of the channel length encountered in conventional large-scale RO systems, resulting in a more uniform crossflow velocity within the membrane channel. Test results indicated that increasing the inlet crossflow velocity from 0.1 m/s to 0.2 m/s significantly reduced adverse effects on RO membrane performance from colloidal silica foulant in desalination of brackish water containing foulant at concentrations of 1,000 and 1,500 mg/L. At these feed foulant concentrations, positive effects of increased crossflow velocity were observed in timeframes as short as three hours. Observed benefits included reduced operating pressure and energy consumption.

Introduction

Reverse osmosis (RO) technology is a viable method for large-scale desalination in many areas of the world suffering from a shortage of fresh water. However, several issues still plague RO processes. One of these issues is membrane fouling. Shirazi and others (2010) pointed out that fouling raises the cost of RO desalination by increasing the membrane surface area required to produce a given permeate flowrate, process downtime, system repair and maintenance costs, and the cost of energy required to produce a given volume of permeate. Membrane fouling is any process that degrades membrane performance and shortens useful life and is caused by several broad classes of substances encountered in the RO process, including sparingly soluble inorganic salts, colloids of inorganic and organic origin, and films caused by biological growth (Amiri and Samiei, 2007; Greenlee and others, 2009). Greenlee and others (2009) pointed out that the type of contaminant responsible for membrane fouling in brackish RO can vary from one location to another. Tran and others (2007) performed an "autopsy" on a membrane in use at a brackish desalination facility after about one year of service to characterize the types of foulants present. They found that different fouling layers formed over time, representing various stages of the fouling process. These layers included amorphous aluminum-phosphorus complexes, polysaccharides, and aluminum silicates, in the order of formation. Vrouwenvelder and others (2000) found that certain classes of antiscalants, intended to prevent inorganic fouling (scaling), could contribute to biofouling. Yiantsios and others (2005) pointed out that other methods used to reduce inorganic scaling, for example, feed acidification, may actually enhance colloidal fouling. Regardless of the type of foulant or the cause of the fouling, the process of membrane fouling degrades membrane performance by reducing water flux and by decreasing salt rejection. Membrane fouling creates serious limitations on the application of RO desalination in many locations and environments (Maeleb and Ayoub, 2011), and for many years has been a major focus of efforts to improve the RO process.

In efforts to optimize RO membrane performance and minimize membrane degradation from colloidal fouling, many researchers have attempted to determine the

factors that either inhibit or enhance the fouling process. These factors include operating parameters and physical and chemical properties of the membranes themselves. Membrane properties, including channel height, surface morphology, surface functional group structure, zeta potential, and contact angle, have been investigated, as well as operating parameters, such as feed salt concentration, crossflow velocity, and rate of shear (Zhu and Elimelech, 1997; Elimilech and others, 1997; Vrijenhoek and others, 2001).

Because RO membranes are classified as non-porous, the mechanism for RO membrane fouling is believed to be very different from the fouling mechanisms that occur in other types of membranes, including those used in microfiltration (MF) and ultrafiltration (UF). Zhu and Elimelech (1995) pointed out that the total resistance to water flux is the sum of the resistance to water flux of the unfouled membrane and the resistance to flux contributed by the fouling layer. They also maintained that the mechanism for colloidal fouling of RO membranes is very different from the mechanisms for membrane fouling by precipitates and materials of biological origin. Greenlee and others (2009) described two types of membrane fouling: "surface fouling" and the fouling that affects pores of membranes used in such processes as MF and UF. Shirazi and others (2010) also distinguish two types of nanofiltration (NF), "loose-end" and "tight-end" NF. Loose-end NF membranes are categorized as porous, while tight-end NF membranes are classified as non-porous. Greenlee and others (2009) pointed out that fouling of non-porous RO membranes is due to surface fouling. In studies conducted on thin-film composite polyamide and cellulose acetate membranes using colloidal silica as a foulant, Zhu and Elimelech (1997) found that surface morphology, feed salt concentration, colloid concentration, and permeate flux were important factors in determining the severity of declines in permeate flux caused by colloidal silica. They found that the effects of colloidal foulants on RO membrane performance were reversible for the operating conditions and type of foulant used in their experiments. They also found that the severity of these effects increased with ionic strength and with the feed concentration of the colloidal particles themselves. It is worth noting that rinsing of membranes exposed to colloidal silica with deionized

water was sufficient to achieve a high degree of membrane restoration in their experiments. Their results indicated that polyamide thin-film composite membranes experienced more severe effects than the smoother cellulose acetate membranes and that increases in permeate flux, feed colloid concentration and feed ionic strength increased the rate and/or severity of effects from colloidal foulant. They attributed higher colloidal fouling at increased flux to "permeation drag." Permeation drag is the force exerted on a particle by the flow of permeate through the membrane (Ramon and Hoek, 2012). This phenomenon is believed to increase as the particle approaches the membrane surface (Kim and Hoek, 2007). The impact of surface roughness and the greater fouling potential of thin-film composite membranes was in agreement with the results of studies described by Elimelech and others (1997).

Vrijenhoek and others (2001) investigated several membrane properties, including chemical structure, contact angle, zeta potential, physical structure of the membrane surface and roughness of the membrane surface, for their effect(s) on colloidal fouling. In aqueous media containing colloidal particles, zeta potential is the potential difference, positive or negative, between the stationary layer of water surrounding the colloidal particle and the aqueous medium in which the particle is dispersed. Zeta potential can be used as an index of the repulsion that exists between neighboring particles. In general, high zeta potentials favor dispersion, while low zeta potentials favor aggregation or flocculation. Of the properties studied, only the physical structure and roughness of the membrane surface demonstrated a conclusive relationship to colloidal fouling potential. In addition, these investigators found that this strong relationship existed even when operating parameters, such as feed composition, permeate flux, and crossflow velocity, were varied. They offered an explanation for this behavior in terms of the relative depths of "valleys" on the membrane surface. These researchers believed that greater depths of these valleys and greater membrane surface roughness resulted in shorter paths for permeate flow and colloidal particle transport. These surface features were thought to contain irregular spaces that could become constricted, but not completely blocked, by the essentially spherical particles.

Lee and others (2011) found that zeta potential at the membrane surface alone was not a predictor of fouling potential in cases where the charge distribution on the membrane surface was relatively uniform. Their research indicated that a heterogeneous charge distribution led to increased fouling potential.

Yu and others (2010) studied the effects of feed water chemistry on organic fouling of polyamide thin-film membranes for desalination at feed ionic strengths of 10 mM and 600 mM, representing typical surface water and seawater TDS levels. These researchers studied the effects of pH and calcium ion concentration on fouling by humic acid and found that permeate flux decline for feed at 10 mM ionic strength was strongly influenced by pH and calcium ion concentration, with more rapid permeate flux decline observed at decreasing pH and increasing calcium ion concentration. Flux decline for desalination of feed at 600 mM, however, was much more insensitive to pH and calcium ion concentration.

In an effort to improve membrane performance at an RO plant in Iran, Amiri and Samiei (2007) studied the effects of switching from lime pretreatment to caustic pretreatment on permeate flux and salt rejection, two operating parameters adversely affected by fouling. They discovered that caustic pretreatment resulted in much more stable permeate flux and greater salt rejection over time. These results led them to conclude that membrane fouling was strongly related to CP. Their results were in agreement with previous findings that calcium ion enhances fouling, possibly due to increased attraction between divalent calcium ions on the membrane surface and negatively charged colloid particles.

Zhu and Elimelech (1995) also studied various factors affecting fouling of cellulose acetate and thin film composite RO membranes by aluminum oxide colloids. Based on results of their studies, they concluded that this type of fouling was influenced by the pH and salinity of the feed, factors which also influenced colloid stability, colloid and membrane surface charge, and permeation drag.

Yantsios and others (2005) found an essentially linear relationship between feed foulant concentration and flux decline for membranes fouled by colloidal iron oxide. As the concentration of iron increased, the rate of flux decline also increased,

in a linear fashion. These researchers believed that resistance to flux had two components: resistance due to "setting" of the membrane and resistance due to deposition of the fouling species. They attributed the relationship between flux decline and foulant concentration to a linear relationship between foulant concentration and the resistance due to foulant deposition.

Hoek and others (2002) studied the effects of shear rate and membrane channel height on fouling by colloidal silica and decline in permeate flux. They found that increasing the shear rate, achieved by decreasing membrane channel height or by increasing crossflow velocity, reduced the formation of a colloid layer or cake on the membrane surface and the rate of flux decline and increased salt rejection. Decreasing channel height, independent of its effect on shear rate, reduced the thickness of the colloidal cake layer, increased its porosity, and reduced what the authors termed "cake-enhanced osmotic pressure." However, they also observed that the beneficial effect(s) of increased crossflow velocity and shear rate did not become evident immediately but required up to ten hours to appear.

Results of numerous studies have indicated that increasing the shear rate within the membrane channel can reduce the severity of colloidal fouling. Shirazi and others (2010) pointed out that CP enhances certain types of membrane fouling. This relationship would explain, in part, the inverse relationship between fouling severity and shear rate, which is a function of crossflow velocity. In conventional RO systems, crossflow velocity is controlled by adjusting the feed flowrate and the recovery.

This chapter describes the testing of an RO system designed for small-scale brackish desalination and using variable closed concentrate circulation (VCCC). This feature permits adjustment of crossflow velocity and shear rate by varying the flowrate of circulating, i.e., recycled, pressurized concentrate. Yiantsios and others (2005) believed that an increase in permeate flux would eliminate any potential benefits of increased shear rate of similar magnitude, because of the much stronger dependence of fouling severity on permeate flux. This effect can lead to potential benefits from any RO system design that uncouples crossflow velocity from other parameters, including feed flowrate and permeate flux. The experimental RO system described in this

chapter also used a parallel configuration of single membrane elements. This feature eliminated the long membrane channels and extreme changes in crossflow velocity between the membrane channel inlet and outlet that result from the multiple connected membranes used in conventional large-scale RO. The objective of this study was the assessment of VCCC as a means to optimize crossflow velocity and minimize or delay adverse effects on membrane performance due to colloidal foulant. These adverse effects include decreased salt rejection and permeate quality and increases in operating pressure required to maintain a target permeate flux. Experiments were not designed to simulate true membrane fouling, which is typically an irreversible process occurring over much longer periods of time, but rather to create negative, relatively short-term, foulant effects on membrane performance. Assessments of VCCC effectiveness were based on observations of the impact of circulation flowrate and crossflow velocity on the timing and severity of increases in feed pump operating pressure at constant permeate flux. Tests were conducted at two inlet crossflow velocities, i.e., 0.1 and 0.2 m/s, and several colloidal silica foulant concentrations, ranging from 50 mg/L to 1,500 mg/L. The rise in feed pump operating pressure with time and with recovery ratio at each feed foulant concentration was compared to the rise in feed pump operating pressure for desalination under baseline conditions in which no foulant was added to the feed.

Materials and Methods

RO System Design

The small-scale RO system employed parallel single membrane elements and VCCC. The design of the RO system is presented in Figure 3.1. The system was similar in design to RO processes developed and patented by Efraty (2009, 2010, 2011), Szucz (1991), and Bratt (1989). "Real-world" large-scale applications of the basic design, also referred to as "closed-circuit desalination" (CCD), are described by Efraty (2012), Efraty and others (2011), Stover and Efraty (2012), and by Stover (2011 and 2013). A key component of the RO system consisted of two parallel Filmtec BW30-2540 2.5 in × 40 in (6.2 cm diameter ×1.02 m length) brackish RO membrane elements (Dow Corporation, Midland, Michigan). The membrane elements

were housed within ceramic pressure vessels (Applied Membranes, Vista, California). In the small-scale RO system, the number of membrane elements could be reduced to one or increased to a larger number depending upon required output. Raw feed water was supplied to the RO system by a Hydra-Cell model D-04-S high-pressure diaphragm pump (Wanner Engineering, Inc., Minneapolis, Minnesota), capable of delivering 7.2 L/min at 35 bar pressure and 1750 rpm. A 43.5 L ceramic pressure vessel (Pentair CodeLine, Minneapolis, Minnesota) acted as a holding tank to store circulating concentrate during process operation and helped to dampen the effects of rising osmotic pressure and prevent pressure spikes. The concentrate was circulated to the feed end of the membrane elements, where it mixed with raw feed prior to reentry into the membrane channels, by a Tonkaflo model AS1608HZ1.5HP centrifugal pump (GE Osmonics, Minnetonka, Minnesota). The Tonkaflo centrifugal pump had a power rating of 1.5 hp, an efficiency rating of 61 percent, and a flow range of 1.14 to 5.22 m^3/h.

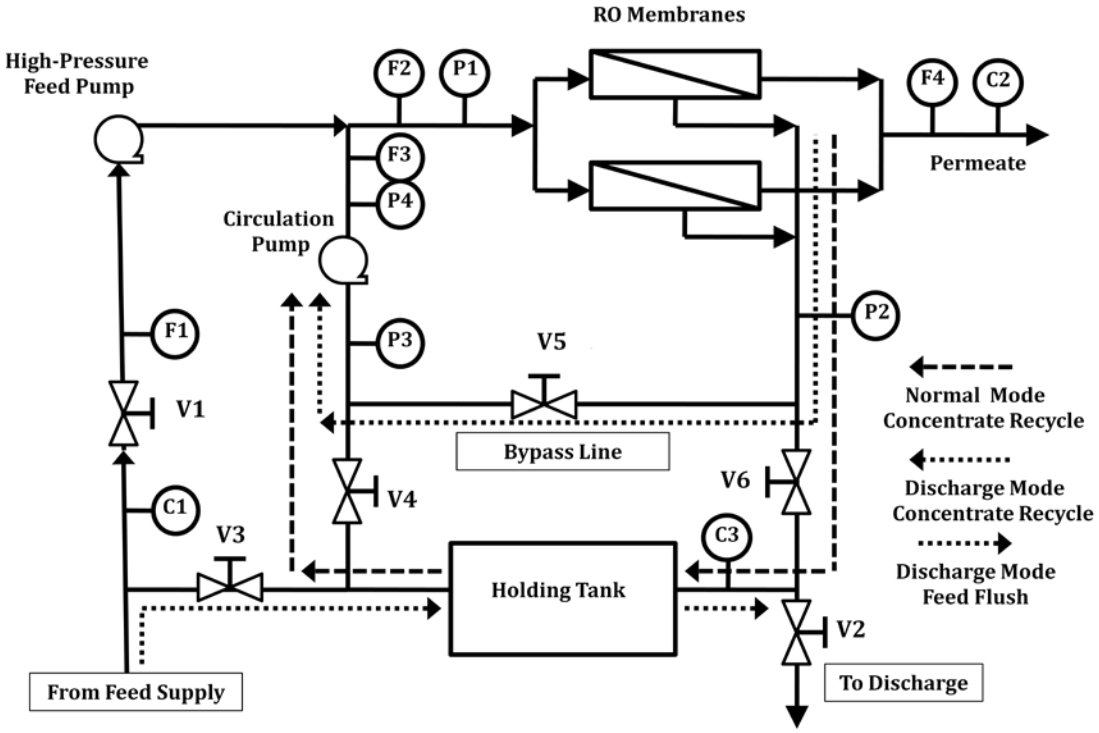

Figure 3.1 Experimental small-scale RO system design.

In Figure 3.1, conductivity sensors are identified with labels C1 through C3, while flow meters are identified with labels F1 through F4, and pressure sensors are identified with labels P1 through P4. Valves are identified with labels V1 through V6. The system had two modes of operation: filtration ("normal") mode and discharge mode. Although the function of discharge mode was to flush the system of concentrated brine and restore the system to initial conditions, permeate production occurred during both modes of operation. The shift between normal mode and discharge mode was accomplished by stainless steel actuated ball valves V2 through V6 (Sharpe Valves, Chicago, Illinois), while PVC ball valve V1 (Georg Fischer, Tustin, California) controlled the flow of raw feed into the RO system. During normal mode of operation, circulating (recycled) concentrate flowed from the membranes through valve V6 and the holding tank and through valve V4 and the circulation pump, prior to mixing with the incoming feed and entering the RO membrane elements.

The operation of the RO system was switched to discharge mode at a pre-determined recovery. During this phase of operation, valves V2, V3 and V5 were opened and valves V4 and V6 were closed. Feed flowed into the system not only through valve V1 and the feed pump, but also through valve V3 and the holding tank to flush accumulated concentrate from the tank. Circulating concentrate bypassed valves V4 and V6 and the holding tank and flowed through valve V5, the "bypass line" and the circulation pump. Accumulated salts and concentrate in the holding tank were discharged as waste through valve V2. The opening and closing of the valves were controlled by a programmable logic controller (PLC) (ABB, Zurich, Switzerland).

The system used stainless steel pipe, ranging from 0.64 cm to 2.54 cm in diameter in all pressurized portions of the RO system and used 1.27 cm diameter Schedule 80 PVC pipe in all non-pressurized portions of the system. Flow meters F1 to F4 (Georg Fischer, Tustin, California) were used to measure flowrates of incoming feed, circulating concentrate, and permeate. Pressure sensors P1 to P4 (Prosense, Oosterhout, Netherlands) were used to measure pressures at various locations within

the system required for the determination of energy consumption by the feed pump and circulation pump. Conductivity sensors C1 and C2 (Georg Fischer, Tustin, California) were used to measure conductivity of incoming feed and permeate, while conductivity sensor C3 (ABB, Zurich, Switzerland) was used measure the conductivity and temperature of circulating concentrate. More detailed information on sensing equipment, including model numbers, is provided in Table 2.1. In addition, duplicate conductivity and temperature measurements of feed and permeate were made with an Orion Three Star conductivity meter (Thermo Fisher Scientific, Waltham, Massachusetts). Data from various meters and sensors were logged by the system once every 60 seconds by an AS400 data acquisition system (ABB, Zurich, Switzerland).

Chemicals

Suspensions of Snowtex ST-ZL colloidal silica were supplied by Nissan Chemical of America (Houston, Texas). The colloidal silica suspensions had a particle size range of 70-100 nm and were approximately 40 percent colloidal silica by mass. ACS grade NaCl was supplied by Thermo Fisher Scientific (Waltham, Massachusetts). Purified water used to create test feed solutions was supplied by an RO system operated and maintained by the Texas Tech University Physical Plant.

Experimental Method

Experiments were designed to assess the impact of crossflow velocity on fouling severity and on the time required to observe the effects of membrane fouling, such as an increase in the rate of feed pump pressure rise at constant permeate flux. Tests were conducted using a feed NaCl concentration of 2,500 mg/L and several foulant concentrations, ranging from 50 mg/L to 1,500 mg/L.

Tests were conducted at two inlet crossflow velocities: 0.1 m/s and 0.2 m/s, based upon target feed and circulation flowrates used to control system operation. The inlet was defined as the location at which combined feed and recycled concentrate enter the membrane channel. Flow meter measurements of feed, permeate, and circulation flowrate logged by the system varied up to 10 percent from target flowrates during testing. It should be noted that feed flowrates were assumed to be equal to

permeate flowrates in the small-scale RO system when calculating the recovery ratio. Although flow meter measurements of feed flowrate were not verified by alternate methods, flow meter measurements of permeate flowrate were verified volumetrically using a stop watch and graduated cylinder. Volumetric measurements of permeate flowrate most closely matched the average of flowrate measurements from Flowmeters F1 (feed) and F4 (permeate). It should also be noted that mean crossflow velocities within the membrane channel were significantly less than inlet crossflow velocities due to the removal of permeate along the membrane channel.

In order to eliminate permeate flux as an additional variable, the same target feed flowrate of 0.09 m^3/h was used at both inlet crossflow velocities. The crossflow velocity was varied by changing the circulation flowrate. Since permeate flowrate equaled feed flowrate in the small-scale RO system, a feed flowrate of 0.09 m^3/h corresponded to an approximate permeate flux of 17 Lmh. To achieve an inlet crossflow velocity of 0.1 m/s, the circulation flowrate was maintained at 0.43 m^3/h. An inlet crossflow velocity of 0.2 m/s was achieved by maintaining the circulation flowrate at 0.95 m^3/h. Inlet crossflow velocities were estimated using Equation 3.1, based on a membrane feed channel width of 0.93 m (36.56 in) (Dow, 2013), a feed channel spacer height of 7.11×10^{-4} m (28 mil or 0.028 in), and an assumption of 50 percent of combined feed and circulating concentrate flow entering each membrane channel:

$$u_i = \frac{Q_f + Q_c}{2 \times W \times \delta} \tag{3.1}$$

where u_i *i*s the inlet crossflow velocity in m/s, Q_f is the feed flowrate in m^3/s, Q_c is the circulation flowrate in m^3/s, W is the width of the membrane feed channel in m, and δ is the feed channel spacer height in m.

In order to determine mean crossflow velocities for analysis of test results, outlet crossflow velocities were estimated using Equation 3.2:

$$u_o = \frac{Q_c}{2 \times W \times \delta} \tag{3.2}$$

where u_o is the outlet crossflow velocity. Other variables are as defined in Equation 3.1. Mean crossflow velocities within membrane channels were calculated by averaging inlet and outlet crossflow velocities.

Prior to each test, approximately 850 L of purified water were placed in a tank and allowed to cool overnight in order to achieve a feed temperature of between 25 and 30 degrees Celcius. After cooling, sufficient reagent-grade sodium chloride (NaCl) was added to create a TDS concentration of 2,500 mg/L. Solutions were mixed by circulating flow through the tank with a pump for approximately 20 minutes. After mixing of the salt solutions, suffcient quantities of Snowtex ST-ZL colloidal silica suspension were added to the sodium solution to create colloidal silica concentrations ranging from 50 mg/L to 1,500 mg/L, based upon the actual mass of colloidal silica per unit volume of solution. Mixing of colloidal silica into the NaCl solutions was achieved by circulating flow through the tank with a pump for an additional 20 min.

Following mixing of NaCl and colloidal silica solutions, the feed solution was processed through the RO system at the target feed flowrate (0.09 m^3/h) for approximately two minutes, in order to prime the system, with the addition of circulation flow during the second minute, at a rate equal to the target circulation flowrate for the test being conducted, either 0.43 m^3/h or 0.95 m^3/h. This process was followed by flushing of the system with the feed solution containing both NaCl and colloidal silica at a flowrate of approximately 49 L/min for at least two minutes. Tests were commenced following the system flush.

Tests were conducted at a constant target feed flowrate of 0.09 m^3/h, corresponding to a permeate flux of approximately 17 Lmh. Feed pump pressure was logged at 60-sec. intervals. The goal of each test was to determine the effect of crossflow velocity on the severity and timing of impacts on membrane performance at

each foulant concentration. Assessment of the severity of foulant impact on membrane performance was based on the rate at which the feed pump pressure increased over time, with steeper rates of feed pump pressure increase assumed to be indicative of more severe impact by colloidal foulant. In designing each test, it was assumed that fouling occurs in stages, with an initial stage in which membrane performance is not significantly affected and feed pump pressure rises linearly and relatively slowly, followed by a second stage in which fouling begins to affect membrane performance and the feed pump pressure rises sharply. Tests were designed to measure the duration of the first stage for the two crossflow velocities in terms of (a) operating time and (b) recovery at each foulant concentration. If a variation in crossflow velocity resulted in a lengthening of stage one and a delay in the appearance of stage two, for example, it was assumed that the change in crossflow velocity had reduced the severity of membrane fouling.

In order to ensure sufficient time to determine the impact of crossflow velocity, the rate of feed pump pressure rise was continuously monitored. Tests were continued until (a) the rate of increase in feed pump pressure had risen sharply from its initial rate and (b) this trend had been maintained for sufficient time to establish a pattern of more rapid feed pump pressure increases. Typically, this time ranged from approximately 30 min. to one hour.

During the experiments, the feed water was filtered before entering the RO system. Feed first passed through a 25 μm pre-filter, followed by a 5 μm filter. Following each test, membranes were washed with RO water supplied by Texas Tech Physical Plant for several hours to remove colloidal silica deposits from the membrane surface. The washing process consisted of processing the purified water through the system at a feed flowrate of 0.23 m^3/h and a circulation flowrate of 0.91 m^3/h, in order to provide sufficient shear for membrane cleaning. The washing continued until (a) a pressure baseline at a given temperature had been reached and (b) flushing of the system in discharge mode produced a visually clear effluent for two consecutive flushes.

Results and Discussion

Tests focused on assessment of the effect(s) of mean crossflow velocity on the timing and severity of adverse effects on membrane performance by colloidal silica. This assessment was based on the assumption that the onset of foulant effects is signaled by an increase in the rate at which the feed pump pressure rises at constant permeate flux, relative to the baseline case in which no foulant has been added to the feed. These results were then used as the basis for an analysis of the effectiveness of VCCC as a means to control crossflow velocity for reduction of foulant effects. For each test, feed pump pressure increase was measured as a function of operating time and as a function of recovery. Operating conditions for each test are presented in Table 3.1.

Table 3.1 Fouling test operating conditions at a feed NaCl concentration of 2,500 mg/L.

Feed Flowrate (m^3/h)	Permeate Flux Lmh	Circulation Flowrate (m^3/h)	Inlet Crossflow Velocity (m/s)	Mean Crossflow Velocity (m/s)	Colloidal Silica Concentration (mg/L)
0.09	17	0.43	0.11	0.10	50
0.09	17	0.43	0.11	0.10	100
0.09	17	0.43	0.11	0.10	200
0.09	17	0.43	0.11	0.10	500
0.09	17	0.43	0.11	0.10	1,000
0.09	17	0.43	0.11	0.10	1,500
0.09	17	0.95	0.22	0.21	50
0.09	17	0.95	0.22	0.21	100
0.09	17	0.95	0.22	0.21	200
0.09	17	0.95	0.22	0.21	500
0.09	17	0.95	0.22	0.21	1,000
0.09	17	0.95	0.22	0.21	1,500

Feed Pump Pressure Increase vs. Operating Time at Constant Permeate Flux

The increase in feed pump operating pressure at constant permeate flux has been plotted as a function of operating time for crossflow velocities of 0.1 and 0.2 m/s at several feed foulant concentrations in Figures 3.2 through 3.8. The increase in feed pump operating pressure over time for desalination of feed containing no added foulant has also been presented in each of the figures for both crossflow velocities in order to provide a basis for comparison of results obtained for each set of operating conditions.

Tests focused on one operating cycle in order to eliminate variables introduced by the discharge cycle. These variables included holding tank flushing efficiency and potential effects resulting from accumulation of foulant between cycles in other parts of the system, including pipes and membrane channels. Data obtained during the first several minutes of each test were not used in the analysis in order to allow system pressures and flowrates to stabilize. In addition, three-minute data averaging was used to reduce the high levels of "noise" seen in the pressure measurements for the feed pump. Plotting was initially performed without data averaging. However, the variation in 60-second readings obscured general trends. Because data averaging did not significantly alter the overall rates of pressure increase when evaluated over the duration of each test, it was used to present experimental results in Figures 3.2 through 3.8. This method of data analysis was also used when plotting feed pump pressure increase as a function of recovery, the results of which are presented in the next section. Figures 3.5 and 3.6 present data obtained for desalination at a feed foulant concentration of 500 mg/L. Data presented in Figure 3.5 for crossflow velocities of 0.1 m/s and 0.2 m/s and a feed foulant concentration of 500 mg/L do not demonstrate overlay during the initial stages of each test and make comparisons between fouling behavior at the two crossflow velocities difficult. To address this issue, data obtained for a crossflow velocity of 0.2 m/s have been "shifted" seven minutes in Figure 3.6 to improve the initial overlay with data obtained at a crossflow velocity of 0.1 m/s. Both unshifted and shifted data have been presented for reference.

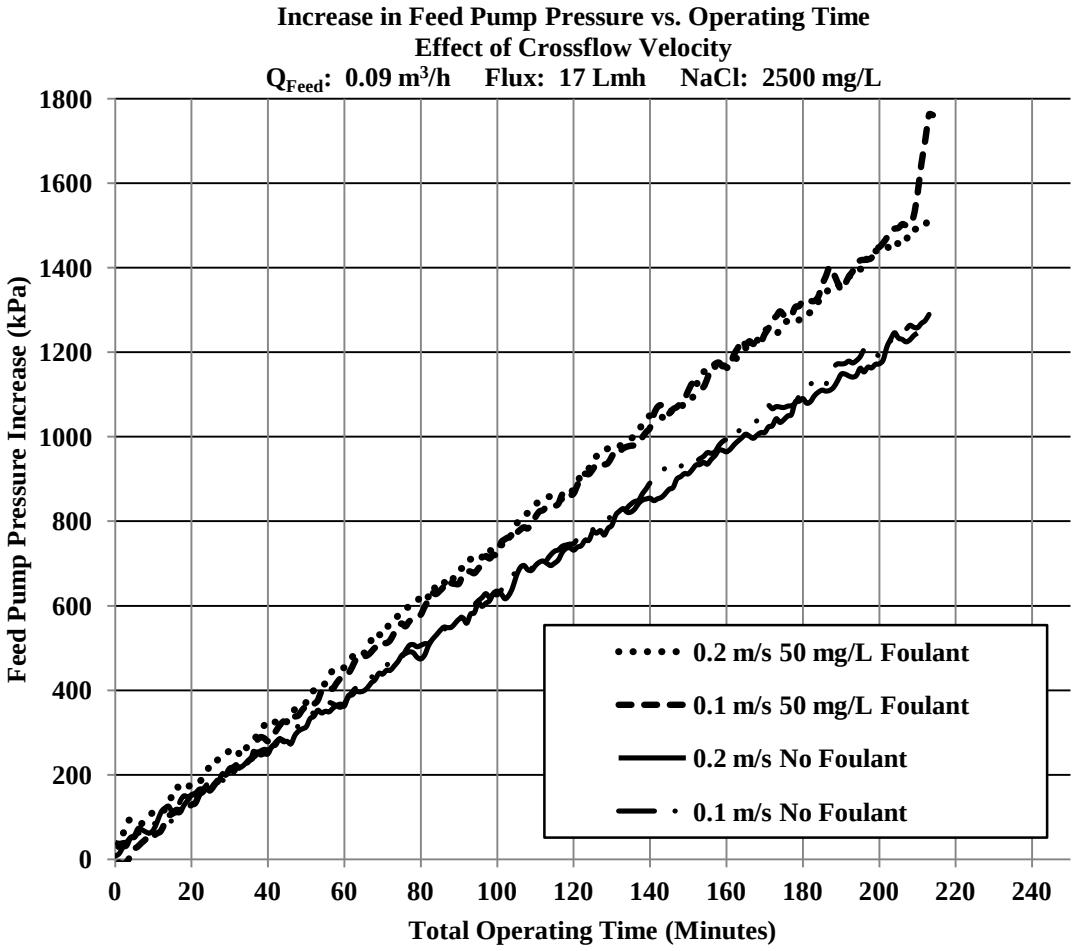

Figure 3.2 Increase in feed pump pressure vs. operating time. Tests conducted at crossflow velocities of 0.1 and 0.2 m/s for (a) feed with foulant concentration of 50 mg/L and (b) feed with no added foulant.

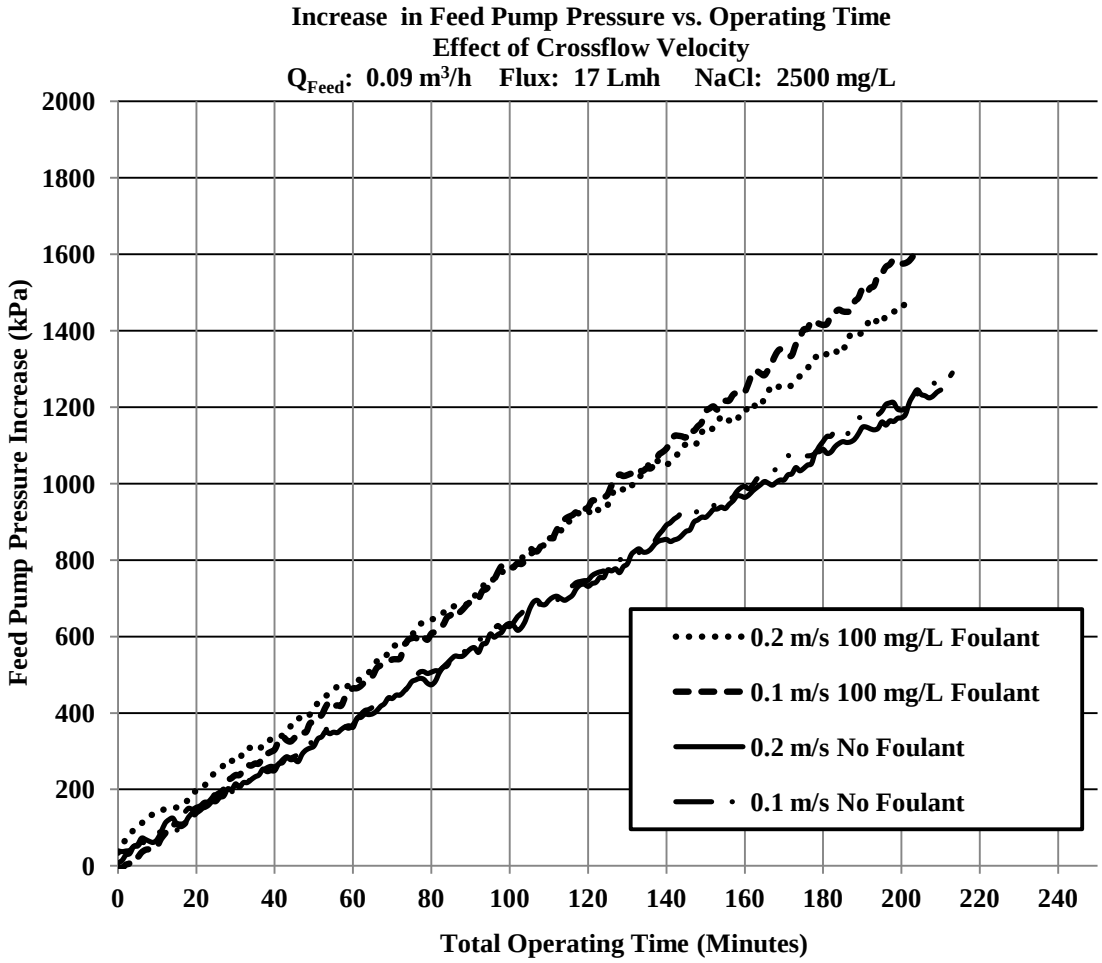

Figure 3.3 Increase in feed pump pressure vs. operating time. Tests conducted at crossflow velocities of 0.1 and 0.2 m/s for (a) feed with foulant concentration of 100 mg/L and (b) feed with no added foulant.

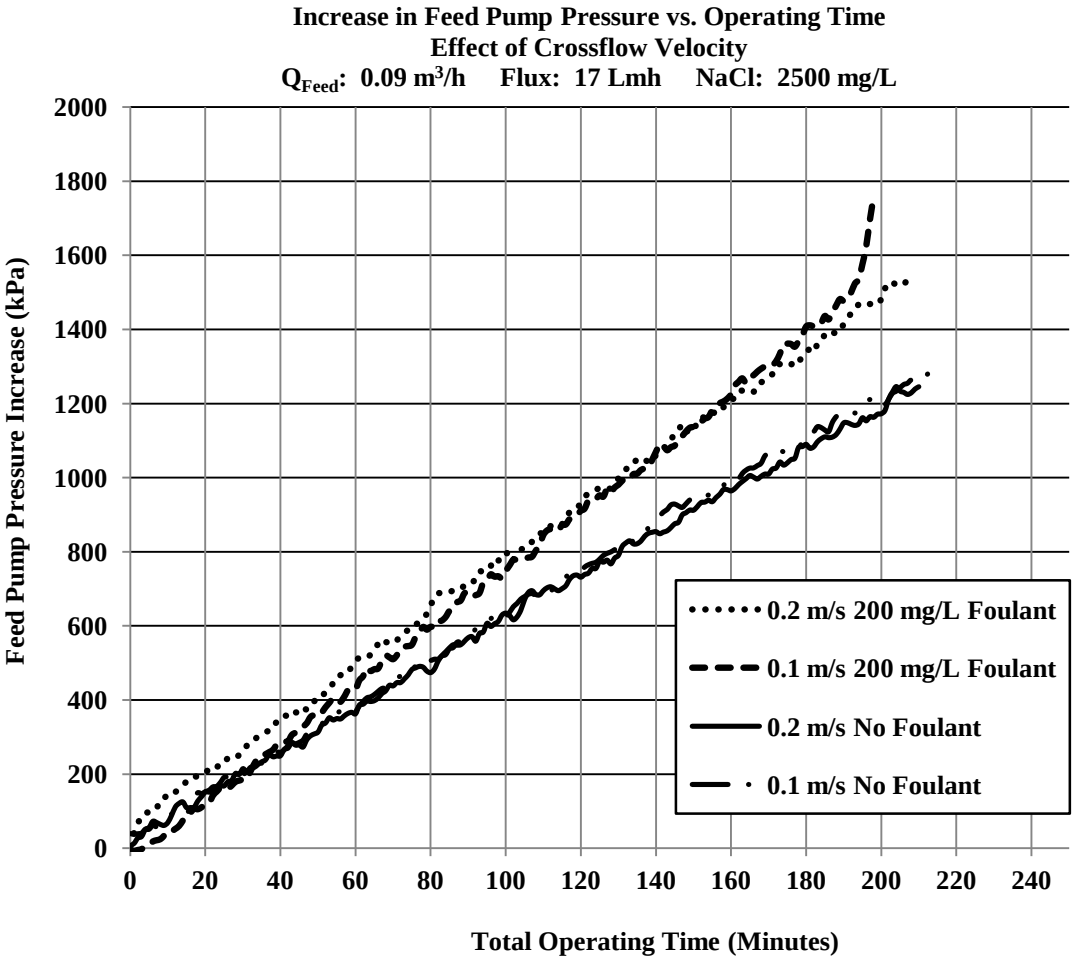

Figure 3.4 Increase in feed pump pressure vs. operating time. Tests conducted at crossflow velocities of 0.1 and 0.2 m/s for (a) feed with foulant concentration of 200 mg/L and (b) feed with no added foulant.

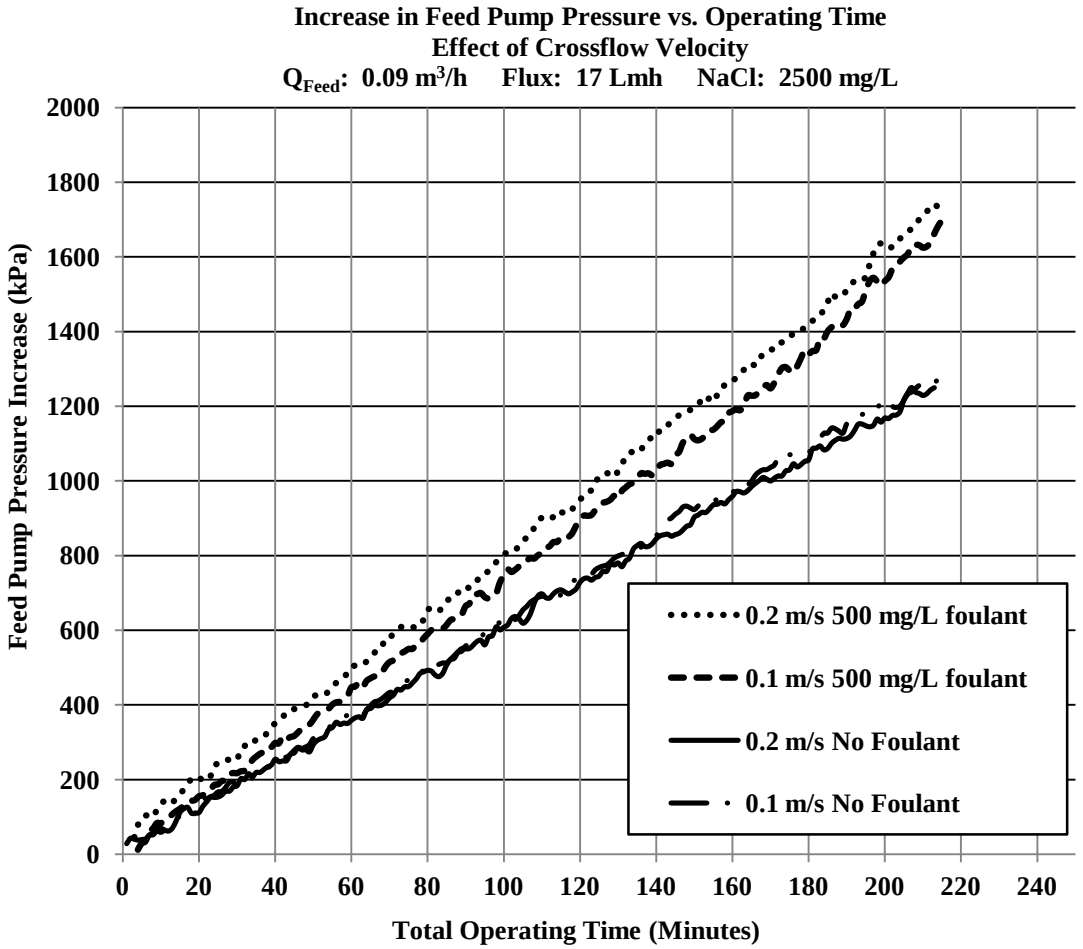

Figure 3.5 Increase in feed pump pressure vs. operating time. Tests conducted at crossflow velocities of 0.1 and 0.2 m/s for (a) feed with foulant concentration of 500 mg/L and (b) feed with no added foulant.

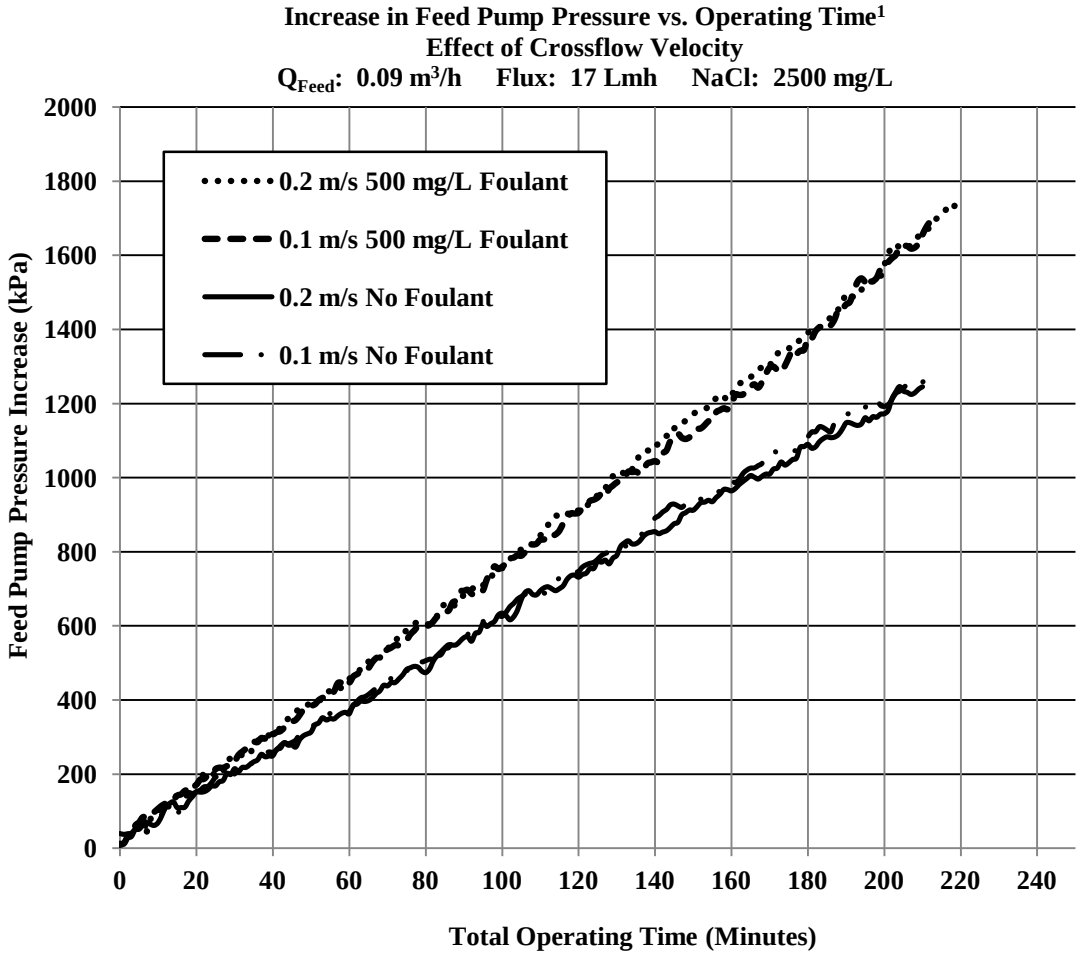

[1]Starting time for 0.2 m/s data shifted 7 minutes relative to 0.1 m/s and baseline data in order to allow 0.2 m/s data to overlay 0.1 m/s data at this foulant concentration.

Figure 3.6 Increase in feed pump pressure vs. operating time. Tests conducted at crossflow velocities of 0.1 and 0.2 m/s for (a) feed with foulant concentration of 500 mg/L and (b) feed with no added foulant.

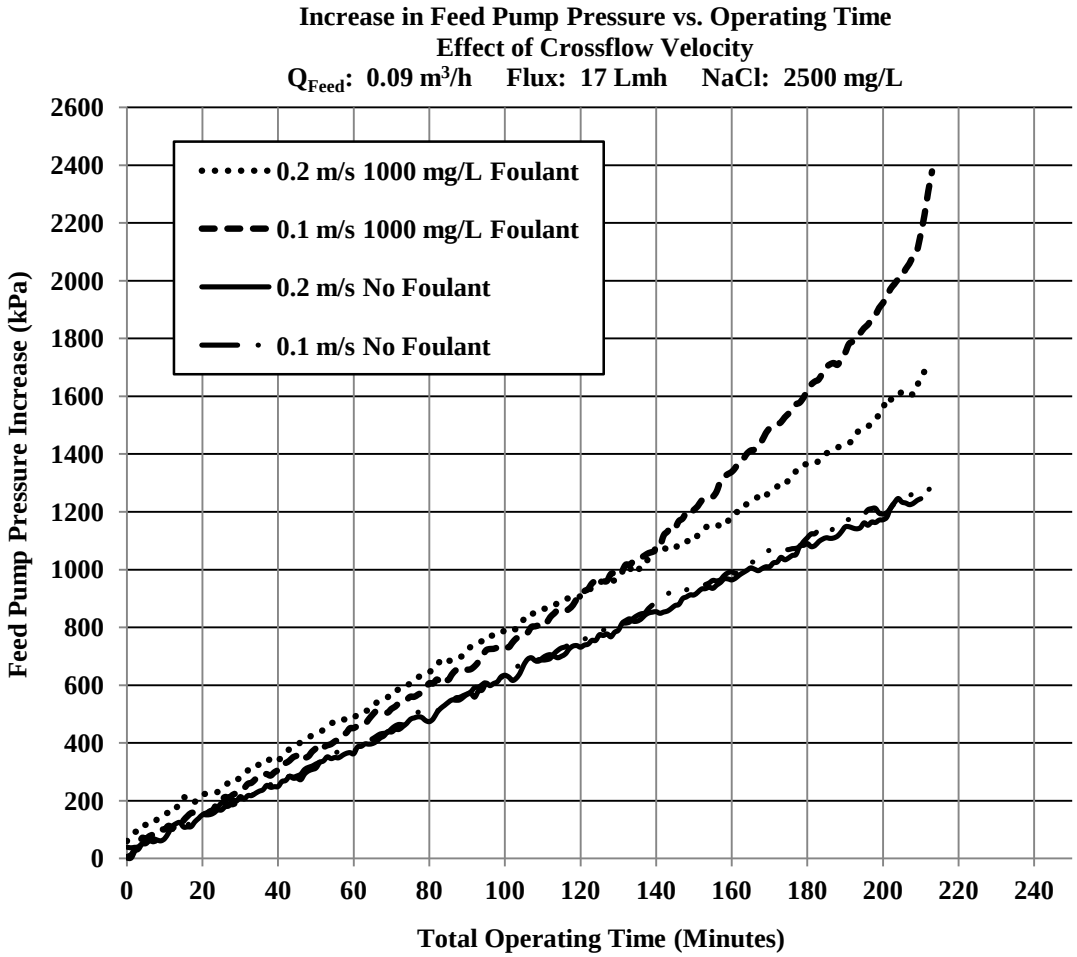

Figure 3.7 Increase in feed pump pressure vs. operating time. Tests conducted at crossflow velocities of 0.1 and 0.2 m/s for (a) feed with foulant concentration of 1,000 mg/L and (b) feed with no added foulant.

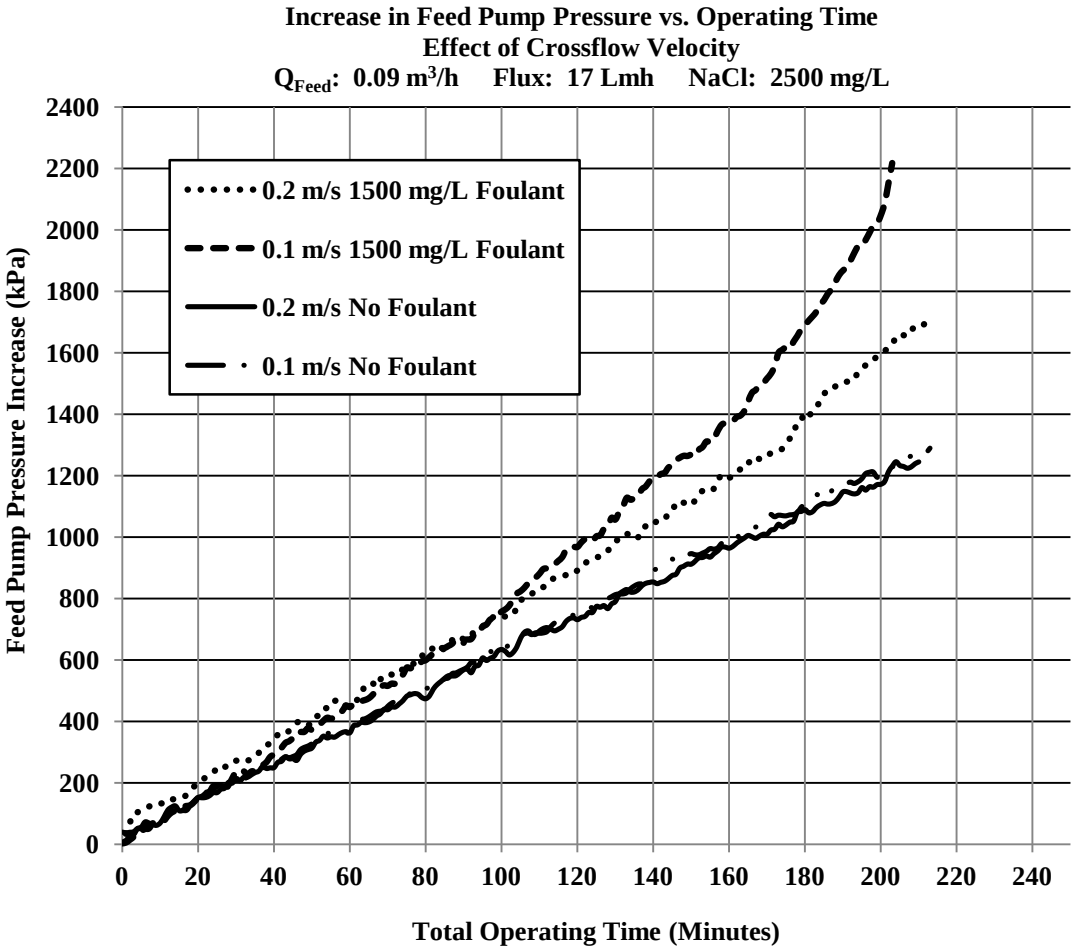

Figure 3.8 Increase in feed pump pressure vs. operating time. Tests conducted at crossflow velocities of 0.1 and 0.2 m/s for (a) feed with foulant concentration of 1,500 mg/L and (b) feed with no added foulant.

General Trends

The addition of foulant to the feed increased the rate of feed pump pressure rise relative to baseline conditions (no foulant added) at inlet crossflow velocities of 0.1 and 0.2 m/s. The steeper rise in feed pump pressure was observed for all foulant concentrations. The rate of pressure increase for desalination with no added foulant was roughly constant at approximately 6 kPa per minute of operation at both crossflow velocities, while the initial rate of pressure increase for desalination with added foulant, regardless of foulant concentration or crossflow velocity, varied between 7 kPa and 8 kPa per minute of operation. For desalination at an inlet crossflow velocity of 0.2 m/s, this initial rate of pressure increase was maintained for the duration of testing for feed foulant concentrations of 50, 100, 200 and 500 mg/L, while the rate of pressure increase rose slightly at approximately three hours elapsed time for the two highest feed foulant concentrations: 1,000 and 1,500 mg/L. For desalination at feed foulant concentrations of 50, 100, 200, 1,000, and 1,500 mg/L and an inlet `crossflow velocity of 0.1 m/s, this initial rate of rise in feed pump operating pressure was not maintained for the duration of testing, but increased significantly at various elapsed operating times that were dependent upon feed foulant concentration. In general, the time required to observe this change was shortest for the higher foulant concentrations (1,000 and 1,500 mg/L) and longest for the lower foulant concentrations (50, 100 and 200 mg/L). No significant change in the rate of feed pump pressure increase was observed at either crossflow velocity for a feed foulant concentration of 500 mg/L.

In addition, feed pump pressure was slightly higher at an inlet crossflow velocity of 0.2 m/s than feed pump pressure at a crossflow velocity of 0.1 m/s for operating times prior to the divergence. This may have been the result of greater head losses at the higher circulation flowrate between the feed pump and the membrane channel. These head losses would require the feed pump to operate at slightly higher pressures to maintain target permeate flux.

The divergence in rates of feed pump pressure increase may be explained in terms of actual foulant concentrations in the combined feed and circulating concentrate stream. As operating time increased, the concentration of foulant in the circulating concentrate stream increased gradually, thereby increasing the concentration in the combined stream. At operating times above 120 minutes, the actual foulant concentration of fluid entering the membrane channels was several times the concentration in the feed. After sufficient operating time, the foulant may have reached a critical concentration at which a crossflow velocity of 0.1 m/s was not sufficient to create the shear required to prevent more rapid or more extensive blockage of surface void spaces, thereby sharply increasing the pressure required to maintain permeate flux. At the highest feed foulant concentrations, fluid in the membrane channels would have reached the critical concentration much earlier.

Impact of Crossflow Velocity on Severity and Timing of Adverse Effects from Colloidal Foulant

For foulant concentrations of 50, 100, 200, 1,000, and 1,500 mg/L, the plots of feed pump pressure increase vs. operating time for crossflow velocities of 0.1 m/s and 0.2 m/s diverged at various operating times. The curves generated at the higher crossflow velocity demonstrated a fairly constant rate of increase for the duration of these tests, while the curves generated at the lower crossflow velocity generally showed a sharp increase in the rate of pressure rise at various elapsed times. If we assume that the steeper slopes observed at the lower crossflow velocity were an indication of more severe effects due to colloidal foulant, these observations were consistent with results of previous studies that indicated that increased crossflow velocity and shear rate reduced the severity of fouling and/or inhibit its development. The conflicting results obtained for a foulant concentration of 500 mg/L might be indicative of competing effects of shear, which would inhibit cake formation and slow the onset of fouling, and increased collisions between particles, resulting in larger particles and more extensive cake development or more effective plugging or blocking of surface void spaces, cancelling out any beneficial effects of increased crossflow velocity and shear rate. A feed foulant concentration 500 mg/L may have represented

an optimal concentration for this behavior to occur, and may explain why it was not observed at concentrations of 1,000 and 1,500 mg/L. At the higher foulant concentrations, greater interparticle repulsions due to surface charges may have prevented the formation of larger particles and greater membrane surface coverage. These interparticle repulsions may have acted to stabilize particle dispersion(s), enabling the beneficial effects of increased shear to once again dominate.

There is an additional factor in this analysis worth considering. As recovery in the small-scale brackish RO process increased, the salinity of the circulating concentrate also increased, leading to increased salinity of fluid within the membrane channels. This is similar to what occurs in conventional RO processes. At a crossflow velocity of 0.1 m/s, circulating concentrate accounted for approximately 83 percent of total flow into the membrane modules, while at a crossflow velocity of 0.2 m/s, circulating concentrate accounted for approximately 91 percent of total flow into the membrane modules. If the salinity of the concentrate increased at the same rate with recovery, regardless of the circulation flowrate, one would expect that the salinity of the combined stream within the membrane channels would be significantly greater at the higher crossflow velocity for any given recovery. Circulating concentrate, however, consisted of dissolved salt and colloidal silica foulant and it would be reasonable to expect that the concentration of colloidal silica in the membrane channels would also be significantly greater at the higher crossflow velocity, assuming 100 percent rejection of the silica by the membranes. Based on these factors, it is possible that the benefits of increased crossflow velocity, achieved through increases in circulation flowrate, may be at least partially offset by the increased concentration of colloidal foulant within the membrane channels. In spite of these potential issues, control of crossflow velocity through the use of VCCC demonstrated significant benefits in terms of the energy efficiency of the small-scale RO system at the highest feed foulant concentrations in this study.

Impact of Foulant Concentration on Severity and Timing of Colloidal Foulant Effects

The time required for divergence of the curves obtained at crossflow velocities of 0.1 and 0.2 m/s was highly dependent on foulant concentration, with the shortest times corresponding to the highest foulant concentrations and the longest times corresponding to the lowest foulant concentrations. These results were consistent with results of research conducted by Zhu and Elimilech (1997) who concluded that increased foulant concentration led to more severe adverse effects on membrane performance. Results are explainable in terms of the increased frequency of collisions between colloidal particles and the membrane surface expected at higher foulant concentrations and greater surface coverage of a foulant cake layer. Approximate times required for divergence in rates of feed pump pressure increase for crossflow velocities of 0.1 and 0.2 m/s are presented below in Table 3.2. The direct relationship between feed foulant concentration and time required for divergence was expected, based on an assumption that the severity of adverse effects from colloidal foulant increases as the feed foulant concentration increases.

Table 3.2 Approximate times required for divergence in rates of feed pump pressure increase at various feed foulant concentrations.

Feed Foulant Concentration (mg/L)	Approximate Time Required for Divergence (min)
50	210
100	160
200	170
500	>210
1,000	140
1,500	110

Feed Pump Pressure Increase vs. Recovery at Constant Permeate Flux

Feed pump pressure increase was plotted as a function of recovery for several feed foulant concentrations in Figures 3.9 through 3.15. Unlike the plots of feed pump pressure increase as a function of operating time, the baseline case (no foulant) was plotted separately, due to the shape of the curves and manner in which the curves

overlay one another, making analysis and comparisons more difficult when baseline curves are displayed on the same plots as results of other tests.

The recovery of the RO system at each point in time within one operating cycle was determined using Equation 3.3:

$$R = \frac{\int_0^t Q_f \, dt}{\int_0^t Q_f \, dt + V_H} \tag{3.3}$$

where R is the recovery, Q_f is the feed flowrate, t is the operating time during one operating cycle, dt is the data logging interval, in this case, 60 seconds, and V_H is the volume of the holding tank, i.e., 43.5 L. The integration term in the equation is the total volume of feed water pumped into the RO system and the total volume of permeate produced during the operating cycle, and was approximated by the summation $\Sigma \; Q_f \; dt$ for the 60 second data recording intervals. Because volumetric measurements of permeate flowrate most closely matched the average of flow meter measurements of feed flowrate and permeate flowrate, and feed flowrate was assumed to be equal to permeate flowrate, Q_f used to calculate recovery was equal to the average of feed and permeate flow meter readings. It should be noted that recovery calculated using Equation 3.3 was a projected recovery for one complete cycle, including discharge, and was based on flushing of the holding tank with one tank volume of feed.

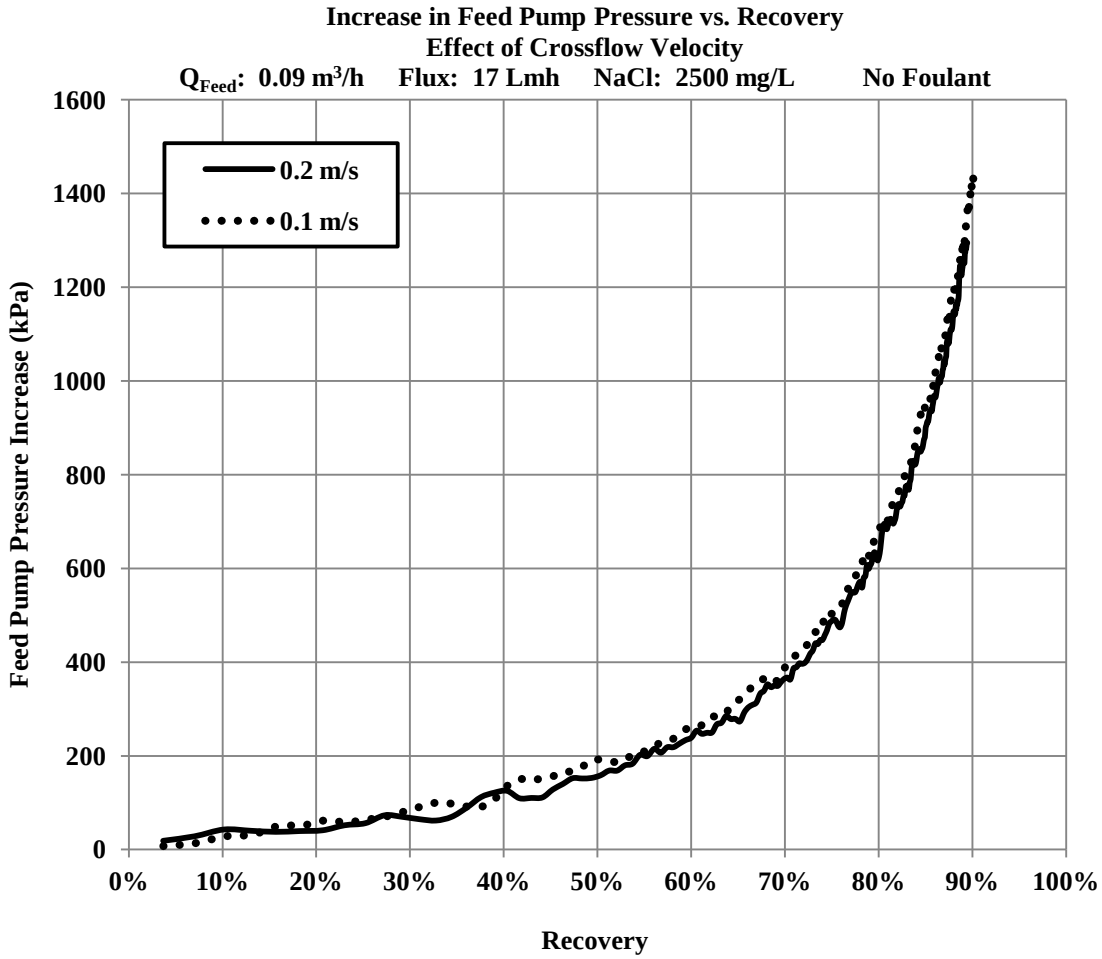

Figure 3.9 Increase in feed pump operating pressure vs. first cycle recovery at inlet crossflow velocities of 0.1 and 0.2 m/s, baseline case, no foulant. NaCl concentration: 2,500 mg/L.

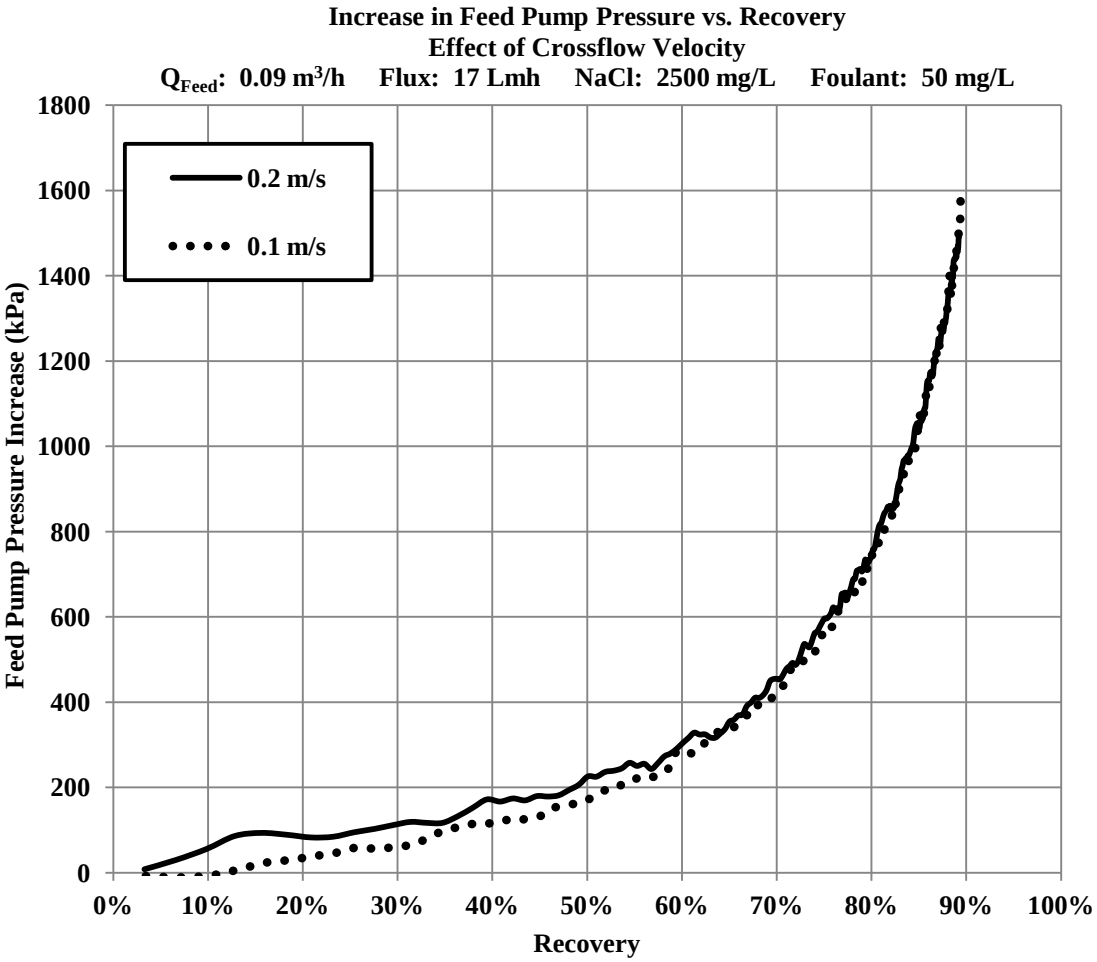

Figure 3.10 Increase in feed pump operating pressure vs. first cycle recovery at inlet crossflow velocities of 0.1 and 0.2 m/s and a feed colloidal silica (foulant) concentration of 50 mg/L. NaCl concentration 2,500 mg/L.

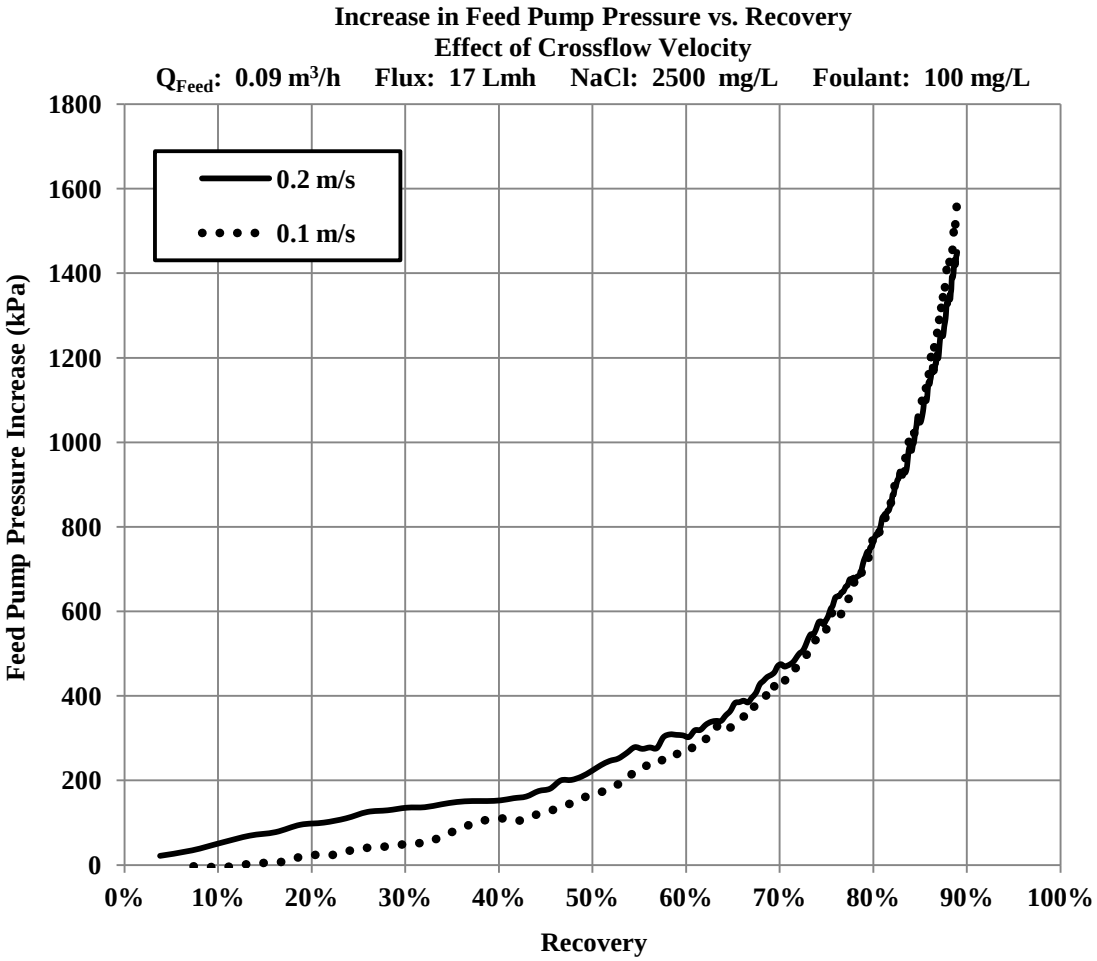

Figure 3.11 Increase in feed pump operating pressure vs. first cycle recovery at inlet crossflow velocities of 0.1 and 0.2 m/s and a feed colloidal silica (foulant) concentration of 100 mg/L. NaCl concentration: 2,500 mg/L.

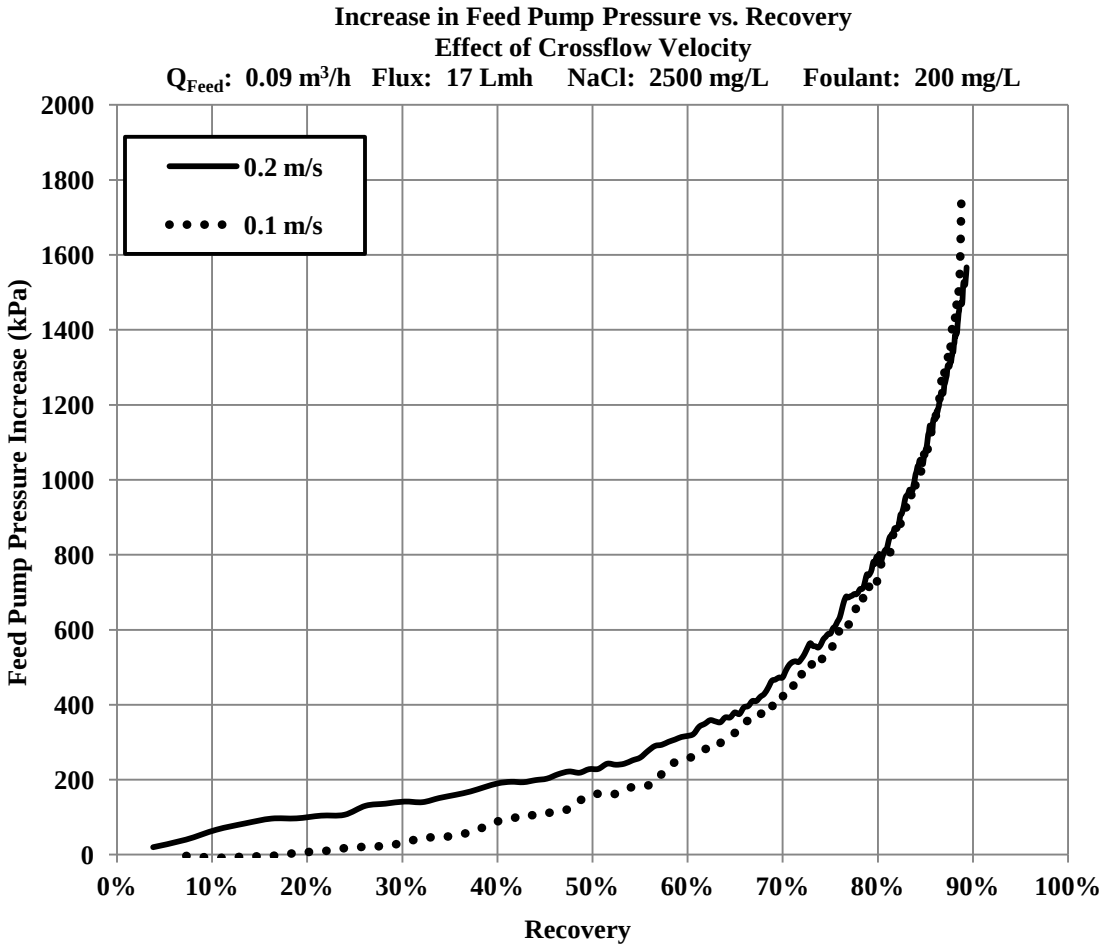

Figure 3.12 Increase in feed pump operating pressure vs. first cycle recovery at inlet crossflow velocities of 0.1 and 0.2 m/s and a feed colloidal silica (foulant) concentration of 200 mg/L. NaCl concentration: 2,500 mg/L.

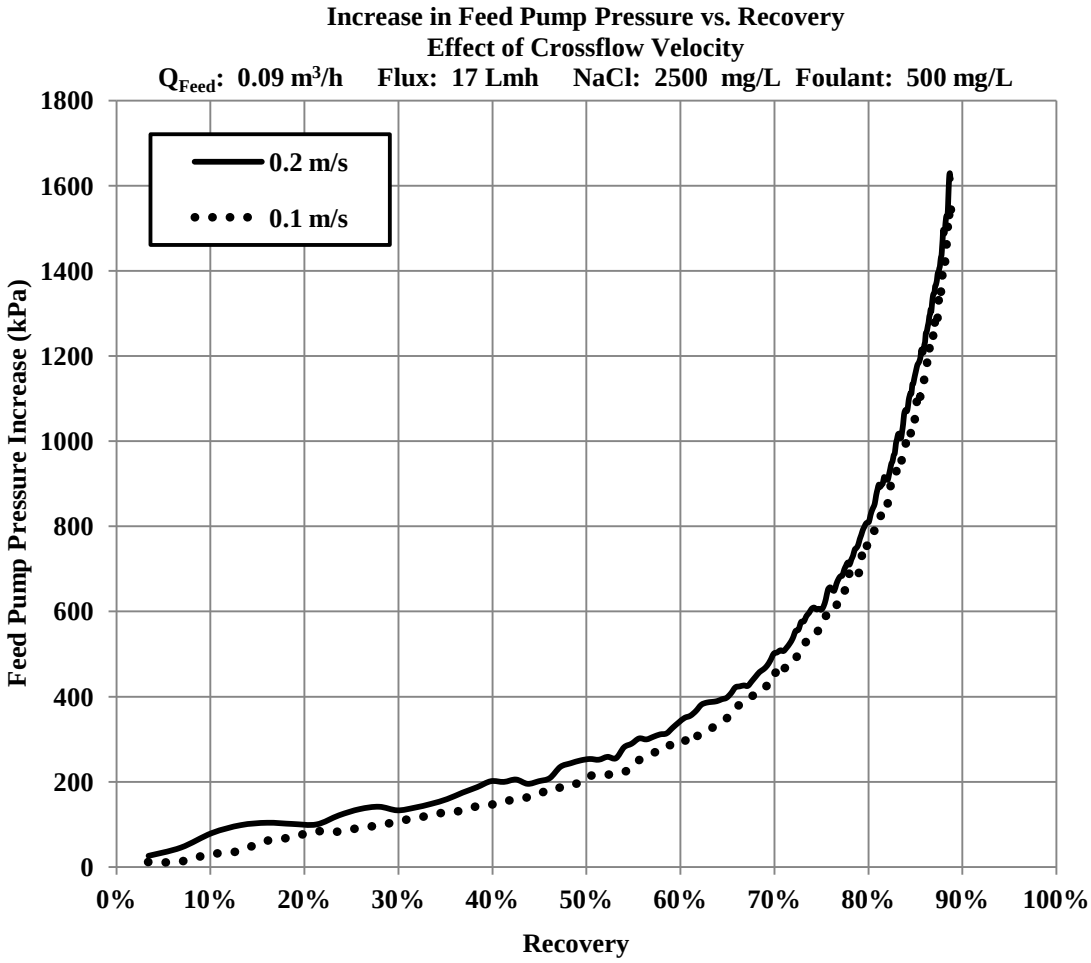

Figure 3.13 Increase in feed pump operating pressure vs. first cycle recovery at inlet crossflow velocities of 0.1 and 0.2 m/s and a feed colloidal silica (foulant) concentration of 500 mg/L. NaCl concentration: 2,500 mg/L.

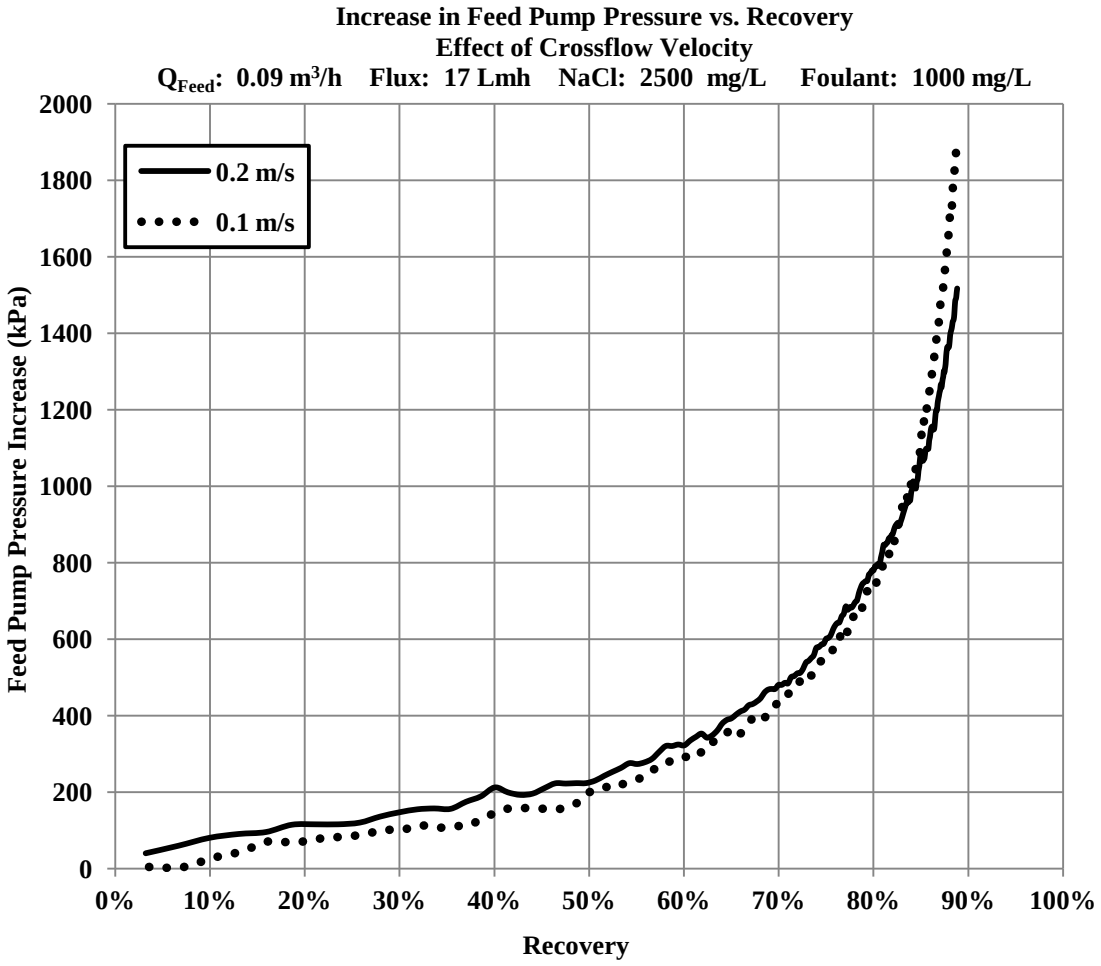

Figure 3.14 Increase in feed pump operating pressure vs. first cycle recovery at inlet crossflow velocities of 0.1 and 0.2 m/s and a feed colloidal silica (foulant) concentration of 1,000 mg/L. NaCl concentration: 2,500 mg/L.

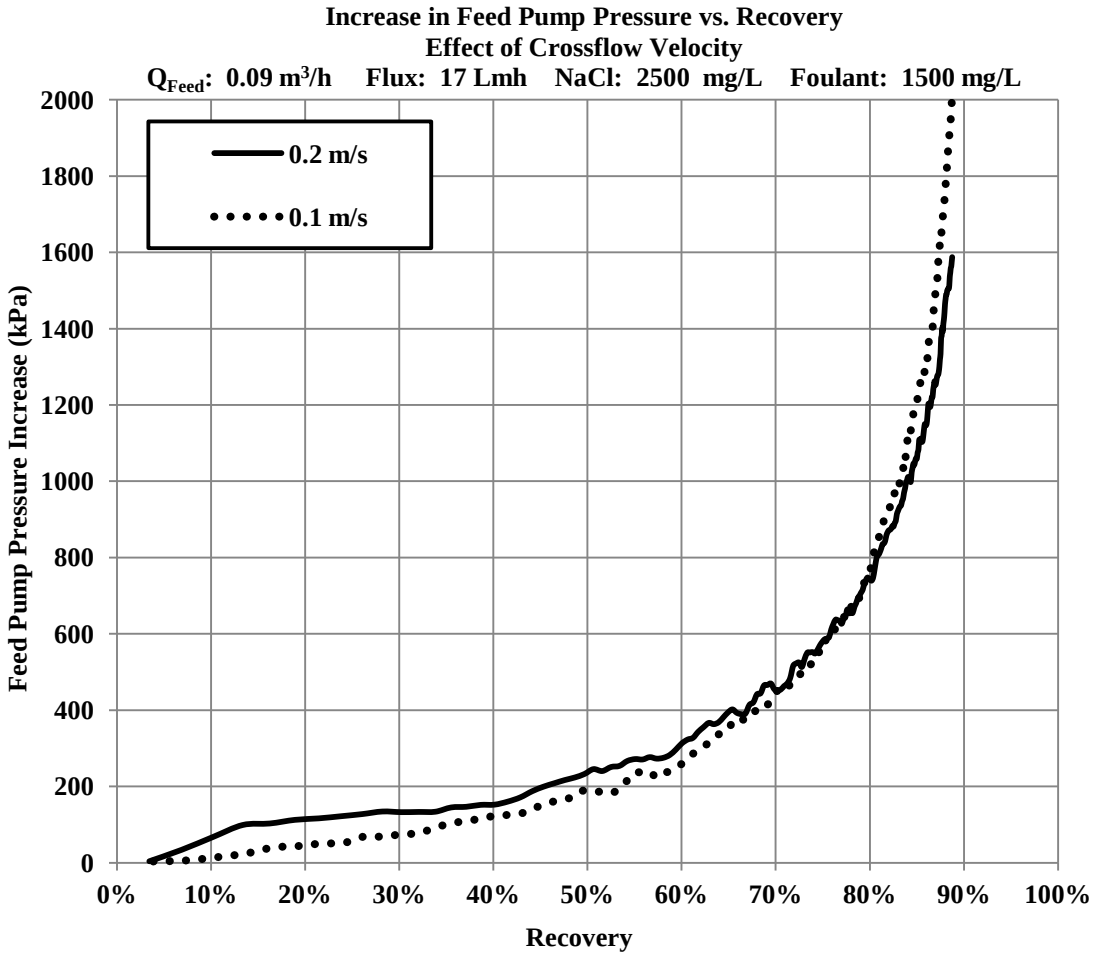

Figure 3.15 Increase in feed pump operating pressure vs. first cycle recovery at inlet crossflow velocities of 0.1 and 0.2 m/s and a feed colloidal silica (foulant) concentration of 1,500 mg/L. NaCl: 2,500 mg/L.

Based on data trends observed in Figures 3.2 through 3.8 for plots of feed pump pressure increase vs. time, we would expect slightly greater feed pump pressures at a crossflow velocity of 0.2 m/s than those observed for a crossflow velocity of 0.1 m/s at lower recoveries. Above a certain threshold recovery dependent upon feed foulant concentration, the 0.1 m/s curve would be expected to diverge in a positive direction from the 0.2 m/s curve. Data presented in Figures 3.9 through 3.15 are consistent with trends observed in Figures 3.2 through 3.8. Initially, at lower recoveries, the feed pump pressure rise was slightly larger at each foulant concentration for the higher crossflow velocity, 0.2 m/s. Consistent with results presented previously in Figures 3.2 through 3.8, the curves in Figures 3.9 through 3.15

eventually crossed and the pressure rise at the lower crossflow velocity, 0.1 m/s, exceeded the pressure rise at the higher crossflow velocity. Recoveries at which the reversals occurred, presented in Table 3.3, generally decreased with feed foulant concentration, although slight anomalies exist for data at intermediate feed foulant concentrations. These anomalies were possibly due to experimental error or to the effects of interparticle interactions, described in the previous section. These results are generally consistent with the assumption that fouling potential and fouling severity increase, at any recovery, with feed foulant concentration and are also consistent with results of previous research that indicated that increases in crossflow velocity and shear rate resulted in reduced fouling severity. It should be noted that data for a feed foulant concentration of 500 mg/L in Figure 3.13 were not shifted in time to enable overlay between the curves for the two crossflow velocities.

Table 3.3 Recovery at which feed pump operating pressure at 0.1 m/s exceeded feed pump pressure at 0.2 m/s.

Feed Foulant Concentration (mg/L)	Threshold Recovery
50	90 percent
100	85 percent
200	86 percent
500	>88 percent
1,000	83 percent
1,500	80 percent

We may also interpret these results as indicators that at lower recoveries where fouling potential was relatively low, it was slightly more energetically expensive to increase the crossflow velocity and shear rate by increasing the circulation flowrate, possibly due to head losses within the piping, connections, valves and tees at the higher velocities. Once the fouling potential had become sufficiently severe at higher recoveries, the energy benefits of increased shear rate predominated, making operation at the higher crossflow velocity more economical from an energy standpoint at high recovery.

Discrepancies between expected behavior and actual results at some intermediate foulant concentrations potentially were due, at least in part, to variations

in feed flowrate , circulation flowrate, and crossflow velocity due to viscosity differences in the feed and concentrate at these foulant concentrations. Viscosity variations may have interfered with the ability of the "paddlewheel" type flowmeters employed by the system to maintain the target feed and circulation flowrates.

Impact of Foulant Concentration and Crossflow Velocity on Permeate Quality

Herzberg and others (2009) reported that biofouling of thin-film composite RO membranes not only reduced permeate flux but also reduced salt rejection. Decrease in salt rejection was believed to be the result of hindered back diffusion of salt by the biofilm layer. Hoek and Elimilech (2003) concluded that colloidal fouling caused declines in flux and salt rejection through creation of an enhanced CP layer. They believed that the enhanced CP layer was the result of poorer back diffusion of ionic species and reduced crossflow velocity and shear within the fouling layer. Based upon these results and the relationship between salt rejection and permeate quality, it is reasonable to expect that any factors that reduce membrane fouling would also increase salt rejection and improve permeate quality. Because of the observed impact of crossflow velocity and foulant concentration on membrane performance, it was predicted that increasing crossflow velocity at high foulant concentrations would result in improved permeate quality. It was also expected that increasing feed foulant concentration would worsen permeate quality. In order to evaluate the impact of crossflow velocity and foulant concentration on permeate quality, the change in permeate conductivity was plotted as a function of operating time at a target feed and permeate flowrate of 0.09 m^3/h and at crossflow velocities of 0.1 m/s and 0.2 m/s in Figures 3.16 through 3.19. A target permeate flowrate of 0.09 m^3/h corresponded to a permeate flux of approximately 17 Lmh. Data are presented for foulant concentrations of 50, 200, 1,000, and 1,500 mg/L. Included in each graph to provide a basis for comparison are data for desalination under baseline conditions, i.e., no foulant added. . As stated previously, the target permeate flowrate varied up to 10 percent from the volumetrically measured flowrate obtained using a stopwatch and graduated cylinder.

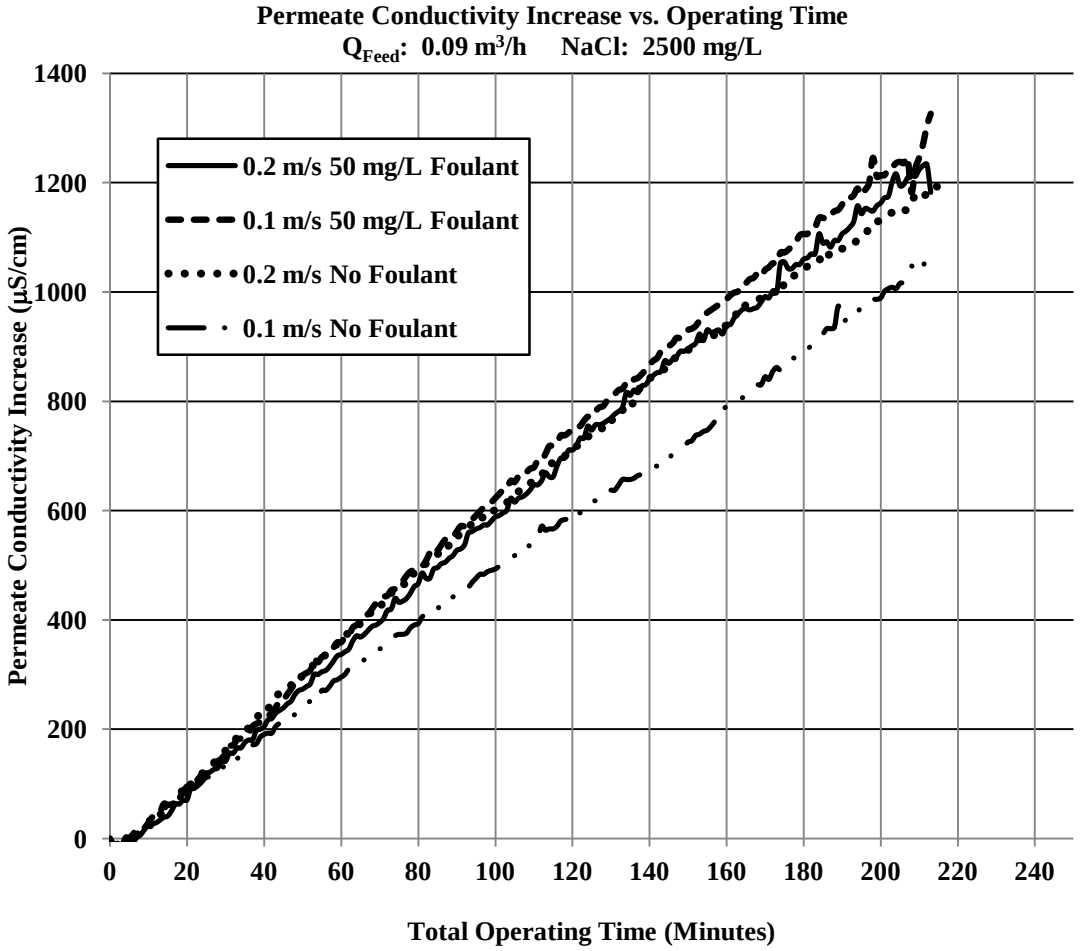

Figure 3.16 Change in permeate conductivity vs. operating time at crossflow velocities of 0.1 and 0.2 m/s. Target feed flowrate: 0.09 m^3/h. Target flux: 17 Lmh. Feed foulant concentration: 50 mg/L.

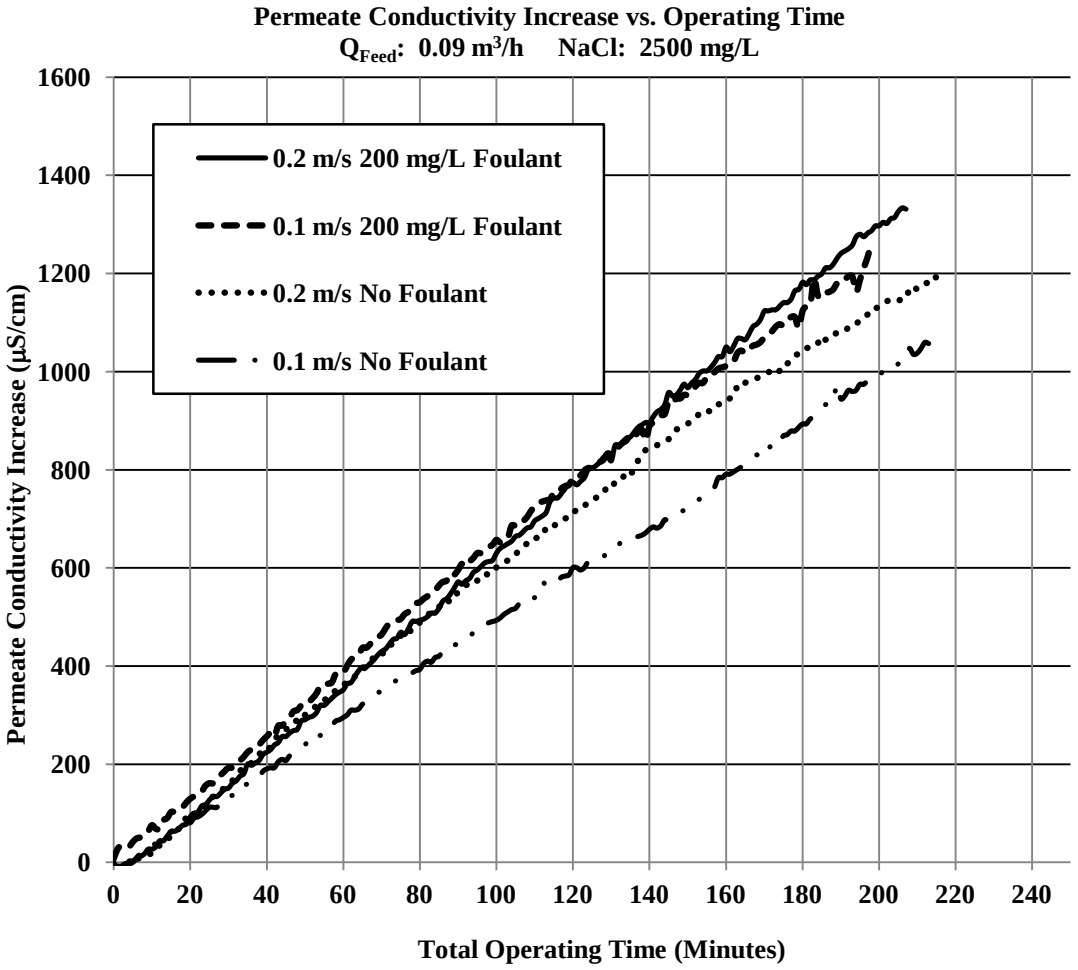

Figure 3.17 Change in permeate conductivity vs. operating time at crossflow velocities of 0.1 and 0.2 m/s. Target feed flowrate: 0.09 m^3/h. Target flux: 17 Lmh. Feed foulant concentration: 200 mg/L.

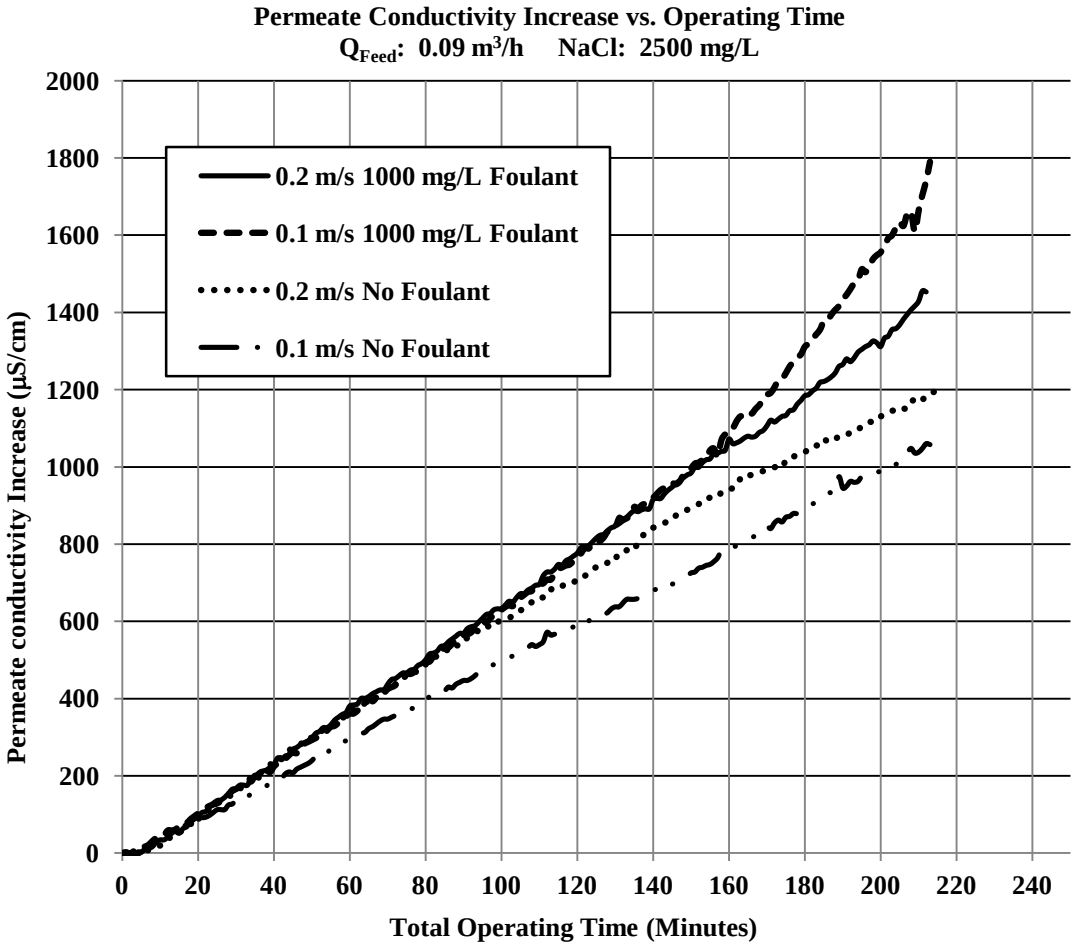

Figure 3.18 Change in permeate conductivity vs. operating time at crossflow velocities of 0.1 and 0.2 m/s. Target feed flowrate: 0.09 m^3/h. Target flux: 17 Lmh. Feed foulant concentration: 1,000 mg/L.

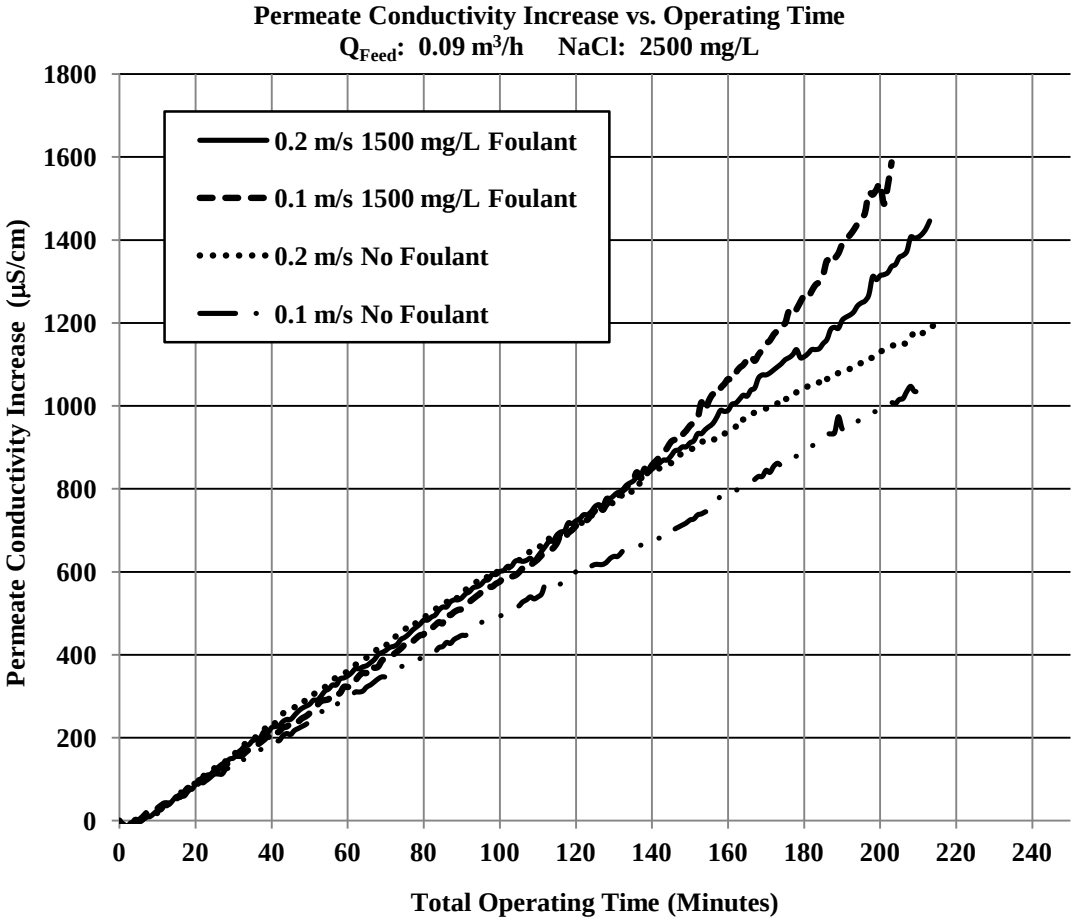

Figure 3.19 Change in permeate conductivity vs. operating time at crossflow velocities of 0.1 and 0.2 m/s. Target feed flowrate: 0.09 m^3/h. Target flux: 17 Lmh. Feed foulant concentration: 1,500 mg/L.

Data presented in Figures 3.16 through 3.19 followed very clear trends. At lower feed foulant concentrations, i.e., 50 and 200 mg/L, there was no significant improvement in permeate quality from increasing crossflow velocity from 0.1 m/s to 0.2 m/s. However, when the feed foulant concentration was raised to 1,000 mg/L, permeate conductivity began to rise much more quickly at the lower crossflow velocity after approximately 160 minutes. At a feed foulant concentration of 1,500 mg/L, the rise in permeate conductivity at the lower crossflow velocity exceeded the rate of rise at the higher crossflow velocity after about 150 minutes. These observations were consistent with the more severe colloidal foulant effects on

membrane performance demonstrated in Figures 3.2 through 3.8 at higher feed foulant concentrations and at a lower crossflow velocity. It was expected, based on data presented in Figures 3.2 through 3.8, that permeate conductivity would rise at similar rates for desalination of feed containing no added foulant at both crossflow velocities. This is what we actually observe in Figure 3.16. Although the curves are shifted relative to one another, the average slopes for the two curves are similar. Because higher crossflow velocity had the potential to reduce CP, a process that can occur in desalination of solutions containing high salt concentrations with no added foulant, it would be reasonable to expect that permeate conductivity would even rise more slowly at the higher crossflow velocity. We do not observe this behavior, indicating that CP is not a significant factor under these conditions. With regard to permeate quality, these results indicated that there is a potential advantage in increasing crossflow velocity, if the foulant concentration is sufficiently high.

Assessment of Closed Concentrate Circulation for Fouling Reduction in SSBRO

Results indicated that VCCC is an effective means to optimize crossflow velocity and shear rate and mitigate negative impacts on RO membrane performance from colloidal foulants in SSBRO. Because these adverse effects lead to increases in the pressure required to maintain permeate flux, VCCC has the potential to reduce the energy consumption of SSBRO desalination of water with high potential for fouling by colloidal silica. The mitigation of colloidal fouling demonstrated at the highest foulant concentrations, however, has implications not only for energy consumption but also for the quality of permeate produced from feed containing high levels of colloidal foulant.

Conclusions

Optimization of crossflow velocity using VCCC was tested as a means to improve RO membrane performance in the presence of colloidal silica foulant. Desalination tests were conducted using feed containing 2,500 mg/L NaCl and colloidal silica at concentrations ranging from 50 mg/L to 1,500 mg/L. Colloid

particle sizes ranged from 70 to 100 nm, based on manufacturer data. Tests were conducted at inlet crossflow velocities of 0.1 m/s and 0.2 m/s.

Tests indicated that control of crossflow velocity and associated shear at the membrane surface through the use of VCCC has the potential to reduce the severity of adverse effects on membrane performance by colloidal foulants and/or delay these effects in SSBRO. Because decreased fouling results in reduced operating pressure at constant permeate flux and reduced operating pressure translates into reduced energy consumption, this feature can lower energy consumption for brackish desalination of waters with high potential for colloidal fouling. Additional benefits demonstrated by the small-scale RO process include improved permeate quality.

The benefits of this technology in the control of membrane fouling can be observed in timeframes as short as three to four hours. Results indicated that the impact of increased crossflow velocity on membrane fouling was most pronounced at high foulant concentrations.

IV. FIELD DETERMINATION OF ENERGY CONSUMPTION AND OVERALL PERFORMANCE FOR SMALL-SCALE BRACKISH REVERSE OSMOSIS SYSTEM

Abstract

A small-scale reverse osmosis (RO) system designed for energy efficient brackish desalination at high recovery was field tested in desalination of brackish groundwater from three sources at the U.S. Bureau of Reclamation's Brackish Groundwater National Desalination Research Facility (BGNDRF) in Alamogordo, New Mexico. The small-scale RO system used variable closed concentrate circulation (VCCC) and two single membranes in a parallel configuration. VCCC minimized energy consumption and allowed crossflow velocity and shear to be varied independently of the feed flowrate and permeate flux. The parallel single membrane configuration prevented extreme changes in crossflow velocity and shear rate between the membrane channel inlet and the channel outlet. The three groundwater sources represented a wide range of total dissolved solids (TDS) levels and potential for inorganic membrane fouling, or scaling. Specific energy of the small-scale RO system, defined as the energy consumption per unit volume of produced permeate, was measured for desalination of groundwater from each well in batch tests using a wide range of feed and circulation flowrates. Tests also focused on the effects of antiscalant concentration on specific energy. Test results indicated that the small-scale RO system can produce permeate from brackish groundwater with variable scaling potential at specific energies comparable to those published for conventional large-scale RO systems at permeate fluxes within the recommended range for desalination of brackish groundwater at recoveries up to 90 percent. Results indicated that the system can achieve these results at antiscalant concentrations in the parts per million (ppm) range. Test results also indicated that increasing antiscalant concentration can reduce energy consumption of the small-scale RO process.

Introduction

Reverse osmosis (RO) desalination has become a very important source of potable water in many locations suffering from a shortage of surface freshwater and/or fresh groundwater. In an attempt to stress the importance of membrane processes to world population, Karagiannis and Soldatos (2008) estimated that 25 percent of the world's population did not have access to water of adequate quality, as of late 2006. Citing predictions by the Worldwatch Institute, they also predicted that almost all of the developed world will suffer from water shortages in the foreseeable future if water consumption is not significantly reduced and/or new sources of fresh water suitable for human consumption are not found. Most of the RO capacity in the United States exists in the form of large-scale systems that employ thousands of membrane elements and can produce up to several hundred thousand m^3/d of potable water.

There are large numbers of isolated populations, scattered throughout the arid and semi-arid regions of the United States, lacking access to adequate supplies of fresh water. RO systems designed for these communities might have capacities that are only a small fraction of large-scale RO system capacities. Small-scale systems serving these populations might generate permeate at rates ranging from several m^3/d to 100 m^3/d and would require a relatively small number of membrane elements that could not support features widely employed in large-scale RO processes. Conventional large-scale RO facilities typically employ parallel arrays of long pressure vessels containing several membrane elements connected in series. The maximum recommended recovery for each membrane element typically does not exceed 15 percent. In order to maximize recovery, the number of membranes within each pressure vessel is commonly six to eight. The arrays of parallel pressure vessels are arranged in multiple stage "Christmas tree" structures. These configurations are designed to utilize the driving pressures and to maintain an adequate crossflow velocity to reduce concentration polarization (CP) and membrane fouling.

In the past, small-scale RO desalination systems were characterized by low recovery and high energy demand. Various features incorporated into large-scale RO facilities to increase energy efficiency include energy recovery devices (ERDs) and closed circuit desalination (CCD), in which concentrate is recycled under pressure and

combined with incoming feed. ERDs employed by conventional large-scale facilities include pressure exchangers and energy recovery turbines (ERTs). Until the present time, these features were not practical for small-scale brackish RO due to the small amount of energy remaining in the concentrate stream. There are, however, limited devices capable of energy recovery in small-scale brackish RO. These include Clark pumps (Ghermandi, 2009; Wood, 2007) and Pearson pumps (Spectrawatermakers, 2009), both of which are positive displacement reciprocating pumps.

The upper limit on energy efficiency by any RO process is imposed by the thermodynamic restriction, an unavoidable requirement that in order to produce permeate the entire length of the membrane channel, the applied pressure on the feed side of the membrane must exceed the osmotic pressure difference between the feed side and the permeate side at the exit of the membrane module, or membrane channel outlet (Gude, 2011; Zhu and others, 2009). When considering the thermodynamic restriction, analyses frequently neglect the hydraulic resistance of the membrane and assume essentially 100 percent salt rejection. Some discussions may also include head losses within the membrane channel. The energy requirement for permeate production can be further increased by the phenomenon known as concentration polarization (CP) and by the formation of a fouling layer on the RO membrane surface, a process which can be enhanced by CP.

In order to increase the energy efficiency of small-scale RO systems, recovery must be increased. Energy consumption, however, is not the only consideration driving efforts to increase recovery. The logistics of concentrated brine disposal, in addition to high disposal costs, make high recovery essential for sustainable inland brackish desalination as asserted by Bartman and others (2011) who have provided an estimate of 85 percent to 95 percent recovery as a desirable target recovery for inland brackish desalination. Although the volume of waste concentrate generated in small-scale RO would only be a small fraction of the volume generated in a typical large scale facility, costs associated with disposal of this waste could potentially represent a large portion of the available budget for a small-scale RO facility. Zhu and others (2009) have pointed out that costs of managing concentrated brine, if high enough, can

significantly impact determinations of target recovery based on the best case scenario for energy costs. Citing the work of Williams and others (2002), Shih and others (2005) provided an estimate, based on economic factors, of 80 percent as a minimum recovery for inland brackish desalination.

High recovery, however, creates additional issues related to membrane fouling, in particular inorganic fouling, or scaling, in cases of feedwaters that contain ions such as sulfate, calcium, barium, or strontium. Greenlee and others (2009) identified membrane scaling as a major limitation to more widespread use of brackish RO. The low flowrates in SSBRO desalination have the potential to further increase the severity of inorganic fouling in these systems. Inorganic fouling can result from high concentrations of ions that can combine to form sparingly soluble salts and the presence of high levels of inorganic colloids, for example, colloidal silica, or colloids containing iron or aluminum. The risk of inorganic fouling is increased by CP which results in extremely high concentrations of fouling species at the membrane surface, leading to large saturation indices for sparingly soluble salts. Amiri and Samiei (2007) distinguished flux decline due to CP from flux decline due to the resistance created by a fouling (scaling) layer, which, they asserted, could be accompanied by increased salt rejection and an improvement in permeate quality. They observed this effect at one RO installation at a petrochemical plant in Iran. The improvement in permeate quality with membrane scaling is the opposite effect to what occurs in cases of colloidal fouling, where salt rejection may actually decrease, leading to worsening permeate quality, as implied by Shirazi and others (2010). They pointed out that CP and the associated risk of fouling rise when permeate flux is increased, but can be reduced by increasing crossflow velocity and shear rate.

Other researchers found additional factors that can enhance inorganic fouling (or scaling). These factors include membrane surface roughness and surface charge, identified by Kang and others (2011) in studies involving membrane fouling by calcium carbonate. They found that the membrane with the lowest degree of surface roughness and the most negative surface charge suffered the least severe inorganic fouling. In tests using four different polyamide composite membranes varying in their

surface roughness, Rahardianto and others (2006) were unable to find a strong association between surface roughness and flux decline. However, they considered the possibility that flux decline is influenced by a more complex interaction between membrane surface chemistry and roughness.

McCool and others (2010) observed large temporal and spatial variations in the quality of San Joaquin Valley, California, agricultural drainage water being treated using plate and frame RO membrane desalination. These variations necessitated the use of widely varying pretreatment methods and target recoveries to prevent scaling or reduce it to a sustainable level. As a result of these observed variations, these researchers recommended the use of real-time, site-specific test methods for the rapid field determination of scaling potential that would enable rapid, real-time modifications to pre-treatment and target recovery.

One promising technology developed to address the balance, or compromise, between energy efficiency, recovery, and membrane fouling is closed-circuit desalination (CCD). CCD is a technology first tested in the 1960s (Stover and Efraty, 2012). In the CCD process, concentrate is recycled, or circulated, under pressure, and combined with incoming raw feed. At a certain point in the process, based upon a target recovery, concentrate salinity, or concentrate conductivity, accumulated concentrate is flushed from the system and discharged as waste and the system restored to initial conditions. Because the concentrate stream remains pressurized, CCD enables RO facilities to maximize energy efficiency with or without ERDs. If desired, ERDs can be integrated into CCD facilities for even greater energy efficiency. In CCD processes, high recovery can be achieved with a small number of membrane elements, eliminating the need for long membrane channels with extreme changes in crossflow velocity and shear rate. This property enables these systems to operate with a reduced risk of fouling and CP. Net driving pressure (NDP) required to generate permeate rises in response to gradually increasing salinity and osmotic pressure of the recycled concentrate, eliminating the large excesses in NDP seen in portions of conventional large-scale RO plants. Because crossflow velocity and shear rate are functions of the flowrate of recycled concentrate, they can be uncoupled from

permeate flux, feed flowrate, and recovery, and increased if required to address issues of CP and fouling.

Since the 1960s, the concept of concentrate recycle in RO desalination has undergone many refinements (Gross, 1974; Bratt, 1989; Szucz, 1991; Desaulniers, 1997; Robbins, 2001; Efraty, 2009, 2010, and 2011). Efraty first designed a CCD RO system using auxiliary containers, but later patented a process that can operate without auxiliary vessels. Recent examples of large-scale brackish RO facilities employing CCD and based on Efraty's concept were provided by Stover (2011). Stover and Efraty (2012) asserted that this process was the first truly continuous application of CCD. It has been applied to the large-scale desalination of brackish water and Mediterranean Sea water at fluxes ranging from 6 to 18 Lmh and permeate capacities ranging from approximately 600 m^3/d to more than 800 m^3/d. Other refinements of Efraty's process have incorporated plug-flow in order to replace accumulated concentrated brine within the closed-circuit with fresh feed. Seawater desalination plants using Efraty's design have been online since December 2010, while brackish desalination plants using his process have been online since February 2009 (Stover, 2011). Earlier applications of concentrate recycle include a process developed by Bratt (1989) that uses concentrate recycle but incorporates two alternating holding tanks that can be used to store accumulated brine. When one tank is connected ("online") to the RO system and the concentrate circulation loop, the other tank can be flushed with fresh feed. Stover and Efraty (2012) classified Bratt's design and a similar design by Szucz (1991) as "batch RO" and asserted that their systems were not totally continuous, requiring brief downtime for system regeneration. Although real-world examples of CCD have essentially been large-scale up to the present time, CCD is a feature that can be adapted to small-scale brackish RO. Recovery is based on operating time rather than the number of membranes, enabling systems employing CCD to achieve high recoveries with a very small number of RO membranes. In addition, operating pressure rises in response to the gradual increase in salinity and osmotic pressure of the circulating concentrate and is governed only by the requirement to maintain a constant permeate flux. This gradual rise in osmotic

pressure eliminates the need for one uniform operating pressure throughout multiple stages of long pressure vessels containing six to eight serially connected membrane elements.

This paper presents results from recent field testing of a small-scale brackish RO system incorporating features of CCD, and designed to overcome the existing limitations of conventional large-scale RO systems, maximize recovery and energy efficiency, and capitalize on the observed benefits of increased shear in the reduction of membrane fouling and CP. The small-scale RO system incorporated a parallel single membrane configuration and operator specified concentrate recycle, or circulation. The small-scale RO system presented in this chapter was similar to Efraty's CCD process using one auxiliary vessel (Efraty, 2009). Because the flowrate of circulating concentrate could be varied by the system operator, this process will be referred to hereafter as variable closed concentrate circulation (VCCC).

The major energy benefits of this design resulted from (1) operating pressures that rose in response to the salinity of the circulating concentrate instead of the uniformly high operating pressures seen in conventional large-scale RO, (2) conservation of energy in the form of pressurized concentrate that was discharged as waste at ambient pressure only after a target recovery or pressure limit had been reached and (3) reductions in membrane fouling, associated pressure increases and energy consumption, due to the ability to increase crossflow velocity and shear, without increasing feed flowrate and permeate flux.

The research described in this chapter specifically focused on determination of the energy consumption and assessment of the overall performance of the small-scale RO process under field conditions that could be considered typical for desalination of brackish water in arid parts of the world. In order to test the small-scale RO process for a range of operating conditions, desalination was performed using three sources of brackish groundwater representing a wide range of TDS levels and potential for inorganic fouling. One groundwater source represented a moderate potential for inorganic fouling, while two additional sources represented more severe potentials for inorganic fouling. Energy consumption was measured as specific energy, defined as

the energy required to produce a given volume of permeate. Values obtained during these tests were then compared to published specific energy values for conventional large-scale RO processes.

Materials and Methods

RO System Design

The small-scale RO system contained features designed to (1) minimize energy consumption and (2) reduce the risk of CP and membrane fouling by enabling increases in crossflow velocity and shear rate, without increasing feed flowrate and permeate flux, and by creating more uniform crossflow velocity and shear rate within the membrane channel. In order to minimize energy consumption, the small-scale system employed VCCC and flux-controlled operating pressure. The incorporation of VCCC into system design served a second major function: to mitigate CP and fouling. In order to eliminate extreme changes in crossflow velocity within the membrane channel, the system used single membrane elements. The parallel arrangement of these elements permitted increases in system capacity without increasing membrane channel length or required system operating pressure. The layout of the RO system is presented in Figure 4.1. The small-scale RO system utilized two Filmtec BW30-2540 2.5 in × 40 in (6.2 cm diameter × 1.02 m length) brackish RO membrane elements (Dow Corporation, Midland, Michigan). The membrane elements were housed within ceramic pressure vessels (Applied Membranes, Vista, California). The capacity of the RO system could be increased, if required, by installing additional parallel membrane elements. Raw feed water was supplied to the RO system by a Hydra-Cell model D-04-S high-pressure diaphragm pump (Wanner Engineering, Inc., Minneapolis, Minnesota), capable of delivering 7.2 L/min at 35 bar pressure and 1750 rpm. A 43.5 L ceramic pressure vessel (Pentair CodeLine, Minneapolis, Minnesota) acted as a holding tank to store concentrated brine during process operation and helped to dampen the effects of rising osmotic pressure and prevent pressure spikes. The concentrate was recycled, i.e., circulated, at operator-specified flowrates, to the feed end of the membrane elements, where it mixed with raw feed prior to entry into the membrane pressure vessels, by a Tonkaflo model AS1608HZ1.5HP centrifugal pump

(GE Osmonics, Minnetonka, Minnesota). The Tonkaflo centrifugal pump had a power rating of 1.5 hp, an efficiency rating of 61 percent, and a flow range of 1.14 to 5.22 m^3/h.

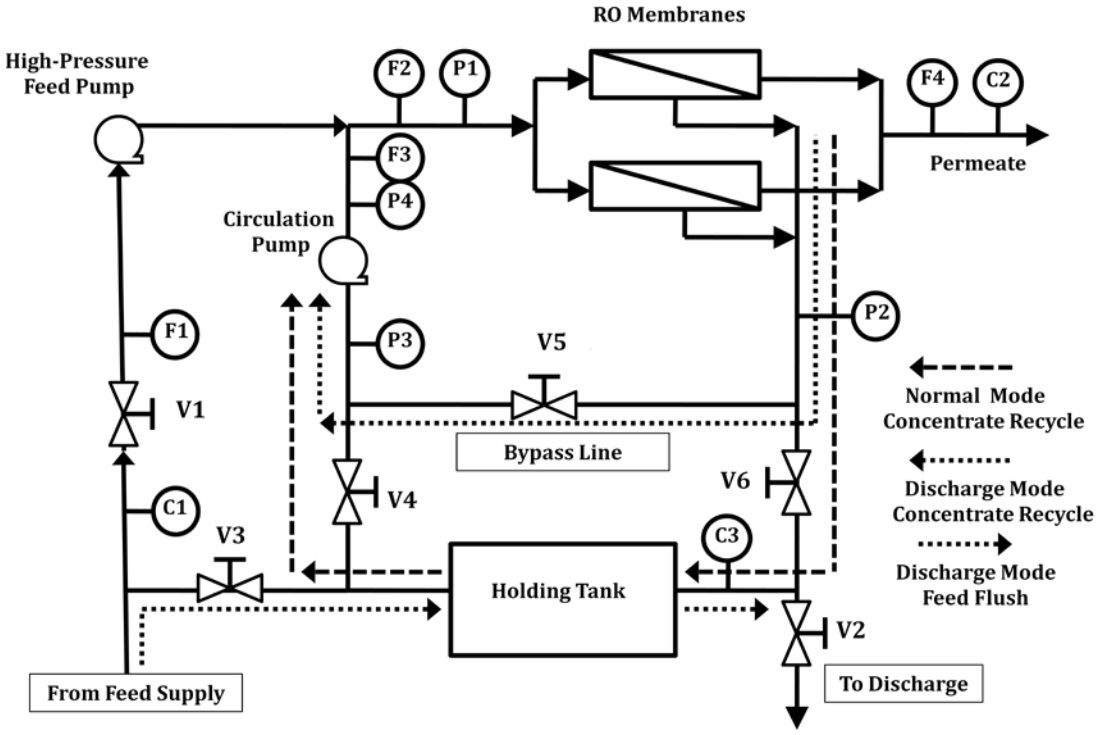

Figure 4.1 Experimental small-scale RO system design.

In Figure 4.1, conductivity sensors are identified by labels C1 through C3, while flow meters are identified by labels F1 through F4, and pressure sensors are identified by labels P1 through P4. Valves are identified by labels V1 through V6.

The system had two modes of operation: filtration ("normal") mode and discharge mode. The shift between the two modes of operation was accomplished by stainless steel actuated ball valves V2 through V6 (Sharpe Valves, Chicago, Illinois), while feed flow into the RO system was controlled by PVC ball valve V1 (Georg Fischer, Tustin, California). During normal mode of operation, circulating recycled concentrate flowed from the membranes through valve V6 and the holding tank and through valve V4 and the circulation pump to combine with pressurized raw feed prior to entry into the RO membrane pressure vessels.

The operation of the RO system was switched to discharge mode at a pre-determined recovery or system pressure in excess of approximately 300 bar. The purpose of the pressure limit was to prevent system shutdown due to pressures in excess of safe operating limits. Once discharge was initiated, valves V2, V3 and V5 were opened and valves V4 and V6 were closed. Feed continued to enter the system through valve V1 and permeate production continued. Feed also flowed through valve V3 and the holding tank to flush concentrated brine and/or accumulated salts from the tank. Circulating concentrate bypassed valves V4 and V6 and the holding tank and flowed through valve V5, the "bypass line" and the circulation pump. The opening and closing of the valves were controlled by a programmable logic controller (PLC) (ABB, Zurich, Switzerland).

Conductivity sensors C1 and C2 (Georg Fischer, Tustin, California) were used to measure conductivity of raw feed and permeate, respectively, while conductivity sensor C3 (ABB, Zurich, Switzerland) was used to measure conductivity and temperature of circulating concentrate immediately upstream of the holding tank. Flow meters F1, F2, F3, and F4 (Georg Fischer, Tustin, California) were used to measure the feed flowrate, flowrate of the combined feed/concentrate stream, the flowrate of circulating concentrate only, and the permeate flowrate, respectively. Pressure sensors P1, P2, P3, and P4 (Prosense, Oosterhout, Netherlands) were used to measure fluid pressure of feed pressurized by the feed pump, fluid pressure of circulating concentrate, prior to entry into the holding tank, fluid pressure of circulating concentrate downstream of the holding tank, and fluid pressure of circulating concentrate after passage through the circulation pump, respectively. Detailed information, including model numbers, is provided in Table 2.1. Duplicate conductivity and temperature measurements of feed and permate were made with an Orion Three-Star conductivity meter (Thermo Fisher Scientific, Waltham, Massachussetts). Duplicate pressure measurements at locations of sensors P1, P3, and P4 were made using NIST-certified digital pressure gauges (Ashcroft, Stratford, Connecticut).

The system used stainless steel pipe, ranging from 0.64 cm to 2.54 cm in diameter, in all pressurized portions of the RO system and 1.27 cm diameter Schedule 80 PVC pipe in all non-pressurized portions of the system. Data from various meters and sensors were logged by the system using an AS400 data acquisition system (ABB, Zurich, Switzerland).

Chemicals

Raw feed consisted of brackish groundwater from three onsite wells (Wells 1, 2, and 3) at BGNDRF, operated by the U.S. Bureau of Reclamation (USBR) in Alamogordo, New Mexico. Groundwater chemistry for each well is provided in Table 4.1. Data are based on results of a sampling event conducted on August 22, 2011 (TetraTech, 2011). Water used to flush the system and remove accumulated scale between tests was provided by USBR from an on-site RO system using four-inch Hydronautics RO brackish water membranes. TriPol 3150 antiscalant, an aqueous solution of polyacrylic acid (<10 percent) and diphosphonic acid (<10 percent), was supplied by TriSep Corporation (Goleta, California).

Table 4.1 Chemistry of groundwater supplied by wells at BGNDRF.

Groundwater source	(TDS) (mg/L)	pH	$CaCO_3$ hardness (mg/L)	Ba^{2+} (mg/L)	Ca^{2+} (mg/L)	SO_4^{2-} (mg/L)	Silica (mg/L)
Well 1	1,240	8.16	230	0.028	63	730	25
Well 2	5,900	7.65	2,600	0.011	550	3,400	23
Well 3	4,290	7.67	2,200	0.011	450	2,200	22

Experimental Method

Experiments were conducted at constant feed flowrate and permeate flux in order to measure specific energy consumption for desalination of brackish groundwater from BGNDRF Wells 1, 2, and 3 for feed flowrates ranging from 0.11 m^3/h to 0.23 m^3/h, corresponding to a range of permeate flux from 22 to 44 Lmh, and ratios of circulation flowrate to feed flowrate ranging from 5:1 to 6.7:1.

In order to prevent fouling of membranes, antiscalant was added to raw groundwater at concentrations based on recommendations provided by the manufacturer of the chemical for assumed recovery ratios ranging from 45 percent to

75 percent with concentrate circulation. The dosages were based on the following parameters for the raw feed water: Langelier Saturation Index, Stiff and Davis Index, calcium carbonate precipitation potential, and the percent saturation for calcium and strontium sulfate. These original recommendations were then scaled upward to provide adequate anti-scaling capacity for levels of TDS and sparingly soluble species in the concentrate, based upon assumed recoveries of 90 percent for desalination of all three groundwater sources. In order to test the effect of antiscalant concentration on specific energy, additional tests were conducted at an elevated antiscalant concentration for desalination of groundwater from Well 1 and without antiscalant for desalination of groundwater from Well 2. Well groundwater fouling indices and antiscalant concentrations are presented in Table 4.2.

Table 4.2 Antiscalant concentrations added to groundwater from three wells at BGNDRF.

Groundwater source	Langelier Saturation Index	Stiff and Davis Index	TriPol 3150 concentration (mg/L)
Well 1 Low Antiscalant	0.59	0.66	5.4
Well 1 High Antiscalant			10.0
Well 2	1.21	0.92	30.6
Well 3	1.07	0.91	15.3

Prior to each test, RO permeate, supplied by USBR from its on-site RO system, flowed through the various components of the small-scale RO system for a minimum of three hours at a combined feed and circulation flowrate of 1.37 m^3/h to flush the system of accumulated scale and salts from previous tests and to reach a pure water baseline feed pump operating pressure for a specific flowrate and temperature. The goal of this process was to standardize and equalize membrane and system conditions for each test and eliminate memory effects from previous tests. The baseline feed pump pressure was established at approximately 1.43 to 1.47 Mbar for a combined feed and circulation flowrate of 1.37 m^3/h, at a temperature of approximately 25^o C, as measured at “C3” (Figure 4.1).

After the pressure baseline was achieved, approximately 850 L of brackish groundwater from one of three wells were placed in a 870 L tank. The temperature of the groundwater was generally between 20 and 25^{o} C. Sufficient antiscalant to create the target concentrations specified above was then added to water with continuous stirring for 20 minutes to achieve complete dissolution and mixing.

During the experiments, the raw feed was filtered before entering the RO system. Brackish groundwater was treated by passage through a 25-μm filter and subsequent passage through a 5-μm filter. In order to "prime" the system prior to all tests, the test solution was allowed to flow through the system at the target test feed flowrate for approximately one minute. Circulation flow was then added at the target test circulation flowrate for an additional minute. Flow was halted and the system (including the holding tank) was flushed for at least two minutes with the test solution. Flow through the holding tank was approximately 50 L/min during the flush cycle, allowing the tank to be flushed with approximately 2.5 volumes of the test solution prior to each test. Tests were commenced following the system flush.

Filtration experiments were conducted at a constant permeate flux. It should be noted that in filtration mode, the feed flowrate into the system equaled the permeate flowrate out of the system because the concentrate flow was completely recycled. The applied pressure from the high pressure feed pump and the circulation pump were regulated by the PLC to maintain constant flowrates and permeate flux during the process.

The recovery of the RO system at any time within one operating cycle was determined from Equation 4.1:

$$R = \frac{\int_0^t Q_f \, dt}{\int_0^t Q_f \, dt + V_H} \tag{4.1}$$

where R is the recovery, Q_f is the feed flowrate, t is the elapsed operating time within one operating cycle, dt is the data recording interval, in this case, 60 seconds, and V_H is the volume of the holding tank, or 43.5 L. The integration term in the equation is

the total volume of feed water pumped into the RO system and the total volume of permeate produced during one operating cycle as of the elapsed time, *t*. The integration term was approximated by the summation $\Sigma\ Q_f\ dt$ for each 60 second data recording interval. It should be noted that recovery calculated using Equation 4.1 was a projected cycle recovery for the entire cycle including discharge. Up to the commencement of discharge mode, recovery was essentially 100 percent, with feed entering the system equal to permeate produced.

Operating conditions and performance data were collected and recorded by the data acquisition system for all experiments. These data were then used to determine the specific energy for permeate production of the RO system for each experiment. The calculation of specific energy will be addressed in a later section. Specific energy was defined as the energy consumed by the RO process divided by the volume of permeate produced.

Tests were run in filtration ("normal") mode to 90 percent projected cycle recovery or approximately 300 bar feed pump pressure, whichever occurred first. Once the target recovery or pressure limit had been reached, operation then changed to "discharge" mode for sufficient time to allow one holding tank volume to flow through the tank to discharge. This time varied depending upon the flowrate of the discharge stream. The flowrate of the discharge stream varied from 6.8 to 8.7 L/min and was measured with a stop watch and graduated cylinder at least twice. Discharge cycle time (for one holding tank volume) was determined by dividing the holding tank volume (43.5 L) by the calculated average discharge flowrate and communicating the time to the system via the appropriate keypad. Once discharge mode was completed, operation returned to filtration mode and cycle recovery returned to 0 percent. At the completion of each test, the RO system was flushed with diluted feed, followed by permeate from the USBR RO system for several minutes.

Results and Discussion

Energy consumption was determined for desalination of groundwater from three wells at the BGNDRF facility operated by the U.S. Bureau of Reclamation in Alamogordo, New Mexico. The three groundwater sources represented a wide range

of variables such as TDS level, potential for membrane fouling, and potential for CP. Other variables studied for their effects on energy consumption included permeate flux, circulation flowrate and antiscalant concentration.

Test conditions, including feed flowrate, circulation flowrate, mean permeate flux, mean crossflow velocity, and antiscalant concentration, are provided in Table 4.3. It should be noted that all flowrates were target flowrates used to control operation of the system. Volumetrically measured flowrates differed from target flowrates by as much as 10 percent. Although the operation of the system was based on target feed flowrates, permeate flux was a much more meaningful parameter for discussions and analyses of test results and has been included in the table with the corresponding feed flowrate. All discussions that follow are based primarily on permeate flux. Inlet crossflow velocities at various feed and circulation flowrates were determined using Equation 4.2, based on a membrane feed channel width of 0.93 m (36.56 in) (Dow, 2013), a feed channel spacer height of 7.11×10^{-4} m (28 mil or 0.028 in), and an assumption of 50 percent of combined feed and circulating concentrate flow entering each membrane channel:

$$u_i = \frac{Q_f + Q_c}{2 \times W \times \delta} \tag{4.2}$$

where u_i is the inlet crossflow velocity in m/s, Q_f is the feed flowrate in m^3/s, Q_c is the circulation flowrate in m^3/s , W is the width of the membrane feed channel in m, and δ is the feed channel spacer height in m. Outlet crossflow velocities for these operating conditions were determined using Equation 4.3:

$$u_o = \frac{Q_c}{2 \times W \times \delta} \tag{4.3}$$

where u_o is the outlet crossflow velocity in m/s and other variables are as defined in Equation 4.2. Mean crossflow velocities were determined by averaging inlet and outlet crossflow velocities.

Table 4.3 Operating parameters for testing of the small-scale RO system at BGNDRF.

Feed Source	Feed/ Permeate Flowrate (m^3/h)	Permeate Flux (Lmh)	Circulation Flowrate (m^3/h)	Mean Crossflow Velocity (m/s)	Antiscalant Concentration (mg/L)
Well 1	0.11	22	0.57	0.13	5.4
Well 1	0.11	22	0.68	0.16	5.4
Well 1	0.14	26	0.68	0.16	5.4
Well 1	0.14	26	0.68	0.16	10.0
Well 1	0.14	26	0.75	0.17	10.0
Well 1	0.14	26	0.82	0.19	5.4
Well 1	0.14	26	0.82	0.19	10.0
Well 1	0.14	26	0.91	0.21	5.4
Well 1	0.18	35	0.91	0.21	5.4
Well 1	0.18	35	0.91	0.21	10.0
Well 1	0.18	35	1.09	0.25	5.4
Well 1	0.18	35	1.09	0.25	10.0
Well 1	0.23	44	1.09	0.25	10.0
Well 2	0.11	22	0.57	0.13	30.6
Well 2	0.11	22	0.68	0.16	30.6
Well 2	0.14	26	0.68	0.16	30.6
Well 2	0.14	26	0.91	0.21	30.6
Well 2	0.18	35	0.91	0.21	30.6
Well 2	0.18	35	0.91	0.21	0.0
Well 2	0.18	35	1.09	0.25	30.6
Well 2	0.18	35	1.09	0.25	0.0
Well 2	0.20	39	1.02	0.24	30.6
Well 3	0.11	22	0.57	0.13	15.3
Well 3	0.11	22	0.68	0.16	15.3
Well 3	0.14	26	0.68	0.16	15.3
Well 3	0.14	26	0.91	0.21	15.3
Well 3	0.18	35	0.91	0.21	15.3
Well 3	0.18	35	1.09	0.25	15.3

Contributions to Total Specific Energy for Small-Scale RO System

Total specific energy for the small-scale RO system had two major components: energy consumption by the feed pump and energy consumption by the circulation pump. The feed pump provided the pressure required to generate permeate, while the circulation pump equalized the pressure between the circulating concentrate stream and incoming feed that had been pressurized by the feed pump. The pressure required of the circulation pump was pressure head lost by the fluid flowing through the system between the membrane channel outlets and the point at which circulating concentrate was combined with incoming pressurized feed. Song and others (2012) described results of previous research on the small-scale RO system that indicated that a large portion of energy consumption by the circulation pump was due to head losses within system piping, valves, tees and other components. Feed pump pressure was most strongly influenced by the salinity of the feed and the target permeate flux. Because it was replacing pressure head lost by the circulating concentrate, circulation pump pressure was most strongly influenced by the velocity of the flowing concentrate.

Specific energy for the feed pump was calculated using Equation 4.4:

$$\hat{E}_f = \frac{\int_0^t Q_f \Delta P_f \, dt}{\int_0^t Q_f \, dt} \tag{4.4}$$

where $\hat{E}_f$ is the specific energy for the feed pump, Q_f is the feed flowrate, t is the total elapsed operating time, dt is the data logging interval, or 60 seconds, and ΔP_f is the pressure created by the feed pump. The circulation pump specific energy was determined using Equation 4.5:

$$\hat{E}_c = \frac{\int_0^t Q_c \Delta P_c \, dt}{\int_0^t Q_f \, dt} \tag{4.5}$$

where $\hat{E}_c$ is the specific energy contribution for the circulation pump, Q_c is the circulation flowrate, ΔP_c is the pressure created by the circulation pump, and other variables are as defined in Equation 4.4. For calculations of feed pump and circulation pump specific energy, the integrals in Equations 4.4 and 4.5 were actually approximated by a summation of energy increments (numerator) and flow volume increments (denominator) for each 60 second interval. Total specific energy determined for the small-scale process was simply the sum of the two contributions. Efficiencies of the feed and circulation pumps were not considered in determinations of specific energy.

In a conventional large-scale RO system, the salinity of the fluid in the membrane channel at any given point in the system and the osmotic pressure difference between that fluid and permeate are fairly constant over time. In an RO system using VCCC, the fluid in the membrane channel consists of raw feed and recycled concentrate. The salinity of the recycled concentrate increases with operating time and recovery, causing a corresponding increase in the salinity of the fluid in the membrane channel and an increase in the osmotic pressure difference between the fluid in the channel and the permeate. In the experimental small-scale RO system, the feed pump was designed to maintain a constant feed flow and permeate flux and increase operating pressure in response to the rise in the osmotic pressure difference. What follows is an analysis of each relevant variable's effect on feed pump specific energy and circulation pump specific energy, followed by comparison of the total specific energy of the small-scale RO system to representative values of specific energy for conventional large-scale RO systems.

Because antiscalant was added to groundwater from each source and had the potential to affect energy consumption through its impact on membrane fouling, antiscalant concentration cannot be isolated from other variables, including feed and circulation flowrate and permeate flux, in the analysis of factors affecting energy consumption. Because of its very important potential effects on energy consumption, antiscalant concentration has been discussed (1) as a separate test variable prior to

analysis of other test variables and (2) in concert with other variables, whenever appropriate.

Assumption of Reversible Fouling and Baseline Membrane Performance

Integral to this study were the following assumptions: (1) the addition of antiscalant to each groundwater ensured that any fouling observed during these tests was reversible; (2) an equivalent baseline membrane state was established for each test with sufficient water washing of the membranes between tests; and (3) the baseline membrane state could be verified through initial pressure and temperature measurements during the first few minutes of each test.

Effect of Antiscalant Concentration on Feed Pump Specific Energy

In order to assess the effect of antiscalant concentration, feed pump specific energy was determined for (1) desalination of groundwater from Well 1 at two antiscalant concentrations, 5.4 and 10.0 mg/L, and for (2) desalination of groundwater from Well 2 at an antiscalant concentration of 30.6 mg/L and without added antiscalant. It should be noted that for desalination of Well 1 groundwater, 5.4 mg/L was the antiscalant concentration based on recommendations from TriSep Corporation and that 10.0 mg/L was the antiscalant concentration used to determine the effect(s) of approximate doubling of the recommended concentration on feed pump specific energy. Feed pump specific energy as a function of first operating cycle recovery for these test conditions is presented in Figures 4.2 through 4.4. Please note that all recoveries referenced in figures are first operating cycle recoveries, unless otherwise specified. Also note that all fluxes and flowrates specified in figures are target values that may be up to 10 percent higher or lower than values obtained through duplicate measurements.

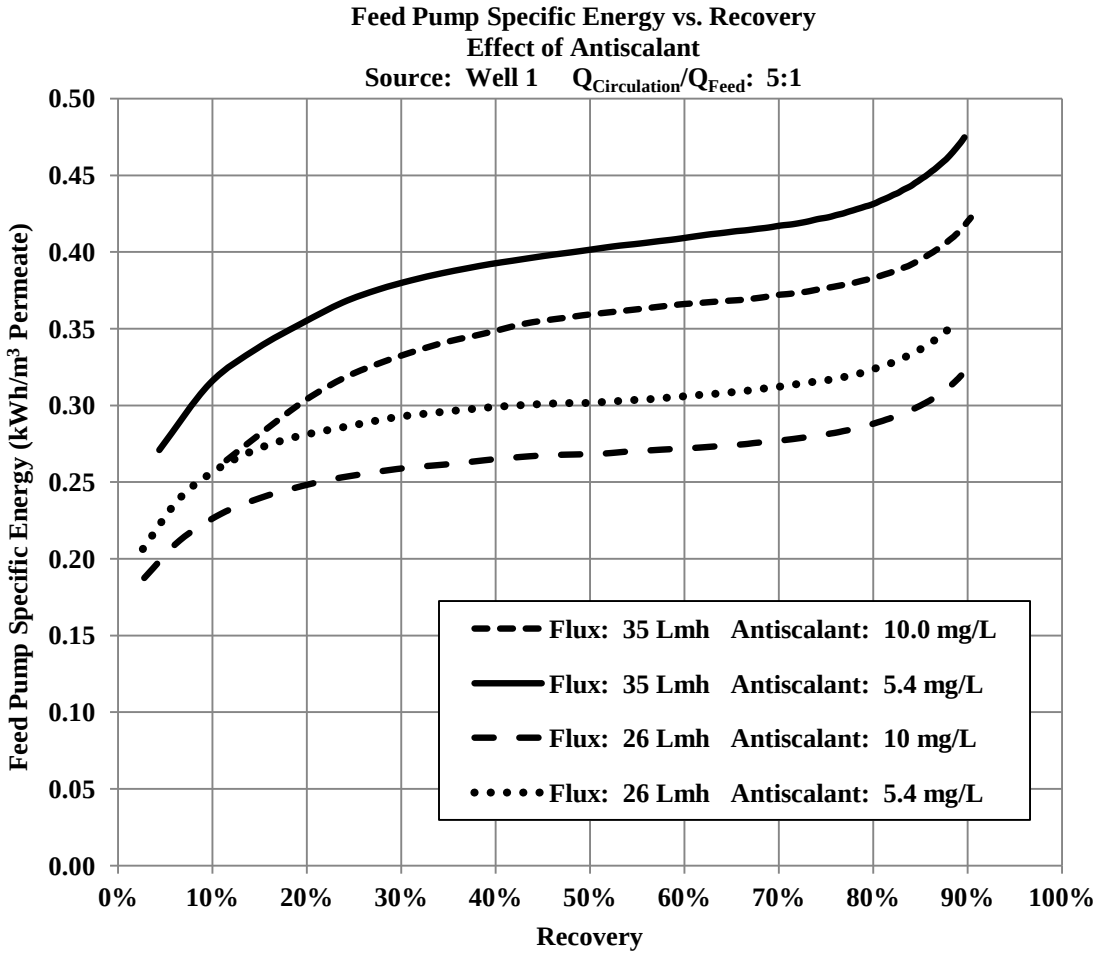

Figure 4.2 Feed pump specific energy vs. recovery. Effect of antiscalant concentration. Groundwater source: Well 1. Permeate fluxes: 26 Lmh and 35 Lmh. Ratio of circulation flowrate to feed flowrate: 5 to 1.

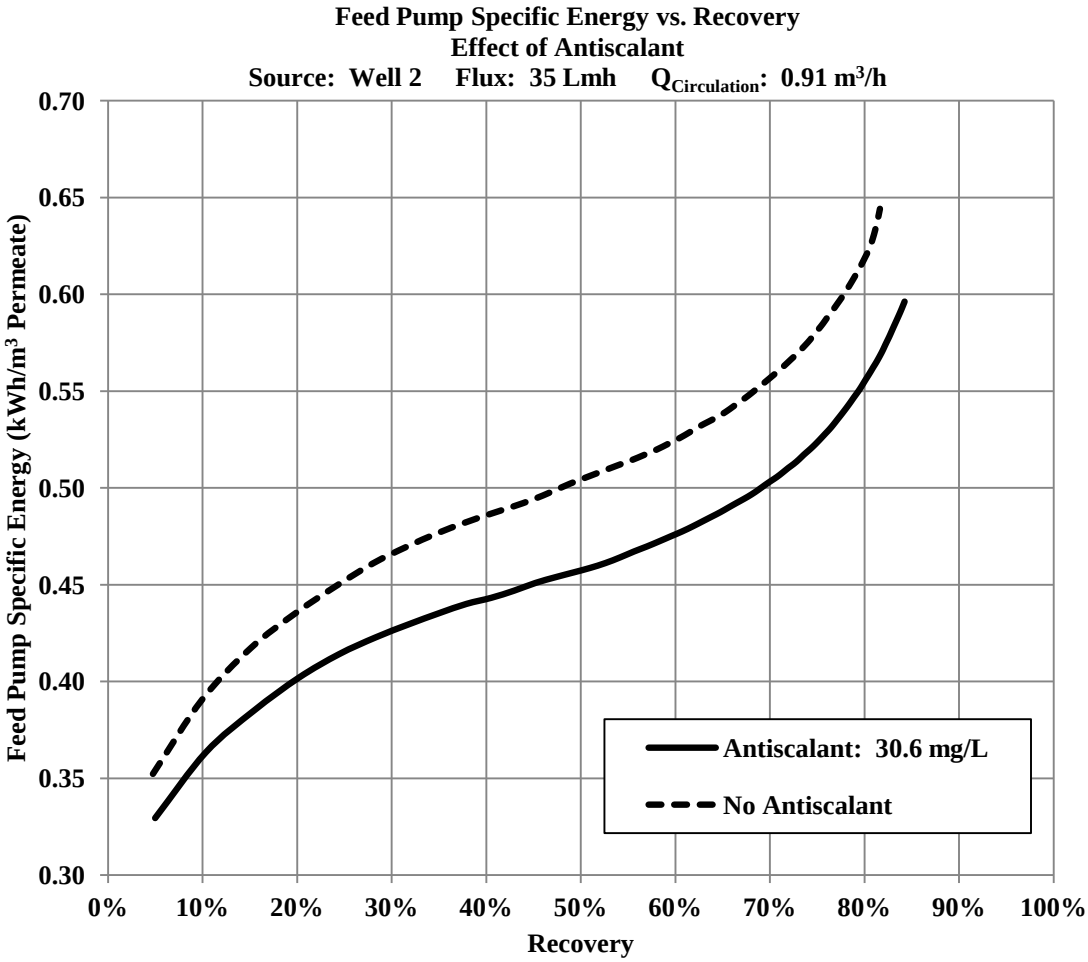

Figure 4.3 Feed pump specific energy vs. recovery. Effect of antiscalant. Groundwater source: Well 2. Permeate flux: 35 Lmh. Circulation flowrate: 0.91 m^3/h.

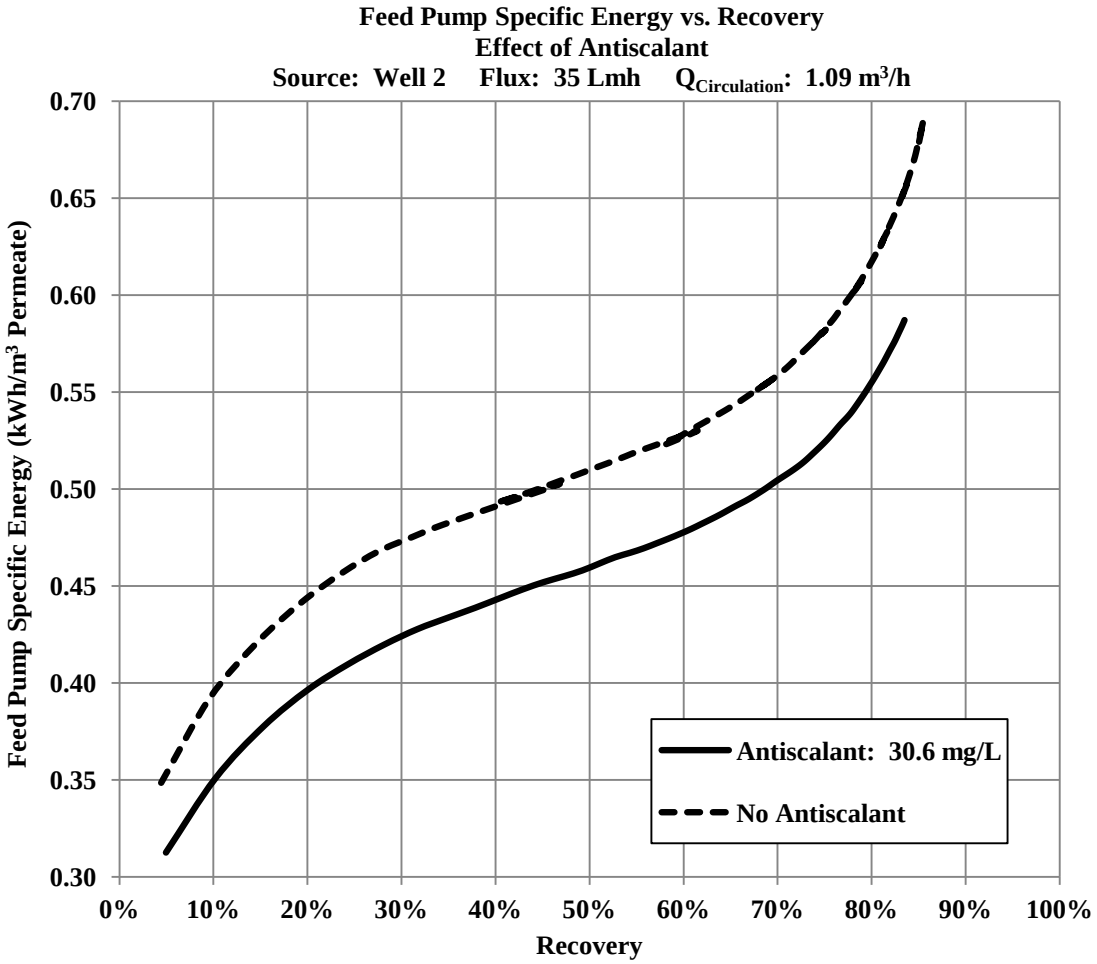

Figure 4.4 Feed pump specific energy vs. recovery. Effect of antiscalant. Groundwater source: Well 2. Permeate flux: 35 Lmh. Circulation flowrate: 1.09 m^3/h.

Several trends can be observed from data presented in Figures 4.2 through 4.4. For desalination of groundwater from Well 1, decreasing the antiscalant concentration from 10.0 mg/L to 5.4 mg/L resulted in an increase in feed pump specific energy of approximately 10 percent at target permeate fluxes of 26 and 35 Lmh for first cycle recoveries up to 90 percent. As noted on Figure 4.2, the ratio of circulation flowrate to feed flowrate was 5:1 for these tests.

Similar changes in feed pump specific energy were observed for desalination of groundwater from Well 2 at a permeate flux of 35 Lmh in tests conducted at an antiscalant concentration of 30.6 mg/L, followed by tests conducted without added antiscalant. At recoveries up to approximately 80 percent and at circulation flowrates

of 0.91 and 1.09 m^3/h, feed pump specific energies were approximately 10 percent greater for desalination without added antiscalant than specific energies for desalination using an antiscalant concentration of 30.6 mg/L. Circulation flowrates of 0.91 and 1.09 m^3/h corresponded to ratios of circulation flowrate to feed flowrate of 5:1 and 6:1, respectively.

If we assume 100 percent rejection of antiscalant and colloidal foulant by the membranes, the concentration of fouling species and the concentration of antiscalant would be expected to increase at roughly the same rate, relative to their original concentrations. Their concentrations would also be expected to increase several fold within the membrane channel at recoveries above 70 percent.

Results observed in Figures 4.2 through 4.4 were in agreement with the intended function of antiscalants and with experimental results from other researchers regarding the impact of antiscalants on the process of inorganic membrane fouling. Antiscalants are designed to inhibit scale formation on membrane surfaces by sparingly soluble salts, for example, calcium sulfate and barium sulfate. A reduction in this type of membrane fouling can reduce resistance to the flux of water across the membrane, lowering required operating pressure and energy consumption. Rahardianto and others (2006) tested antiscalant effectivess in the inhibition of calcium sulfate scale on four polyamide composite membranes and discovered that addition of the antiscalant Vitec 2000, at concentrations as low as 3 ppm, eliminated flux decline due to scale formation. It is worth noting that certain classes of phosphorous- and carboxyl-group-containing antiscalants actually have the potential to contribute to biofouling (Vrouwenvelder and others, 2000), leading to increases in operating pressure and energy consumption.

Greenlee and others (2010) found antiscalant effectiveness to be a function of the structure of the antiscalant molecule and the crystal morphology of the scaling species. They found that spherical crystalline scalants, such as calcium carbonate, were best addressed with antiscalants with a highly branched and relatively compact structure, while needle-like scalants, such as calcium sulfate, were best addressed using antiscalants with a longer, more chain-like structure.

Borden and others (1987) theorized that fouling salts such as calcium sulfate caused flux decline by forming crystals on the membrane surface, causing "surface blockage". The crystals were believed to grow laterally from nuclei distributed on the membrane surface, gradually increasing surface coverage over time. These researchers examined crystal growth patterns and experimental flux decline data in light of the prevailing "cake filtration" model and both laminar and turbulent versions of their surface blockage model. The cake filtration model, as described by these researchers, assumes a porous cake layer that covers the entire membrane surface and gradually increases in thickness. The growing cake layer provides gradually increasing resistance to the passage of water through the membrane. They observed that experimental flux decline data were consistent with predicted behavior based on the surface blockage model. Austin and others (1975) theorized that antiscalants prevented the growth of calcium sulfate crystals by attaching to potential nuclei and displacing the sulfate ions. Their proposed mechanism was based on studies of crystal growth and structure both in the presence and in the absence of antiscalants and on the structures of the antiscalants themselves. They reasoned that the concentrations in the ppm range typically used for these compounds were too small for sequestering or complexing of fouling species. They believed hydroxyl groups to be the active functional groups on antiscalants responsible for their behavior, based on the effectiveness of hydroxyl-containing antiscalants. This class of antiscalants includes phosphonates and compounds containing carboxyl groups.

Shih and others (2005) characterized the development of calcium sulfate dehydrate (gypsum) scale on plate and frame membrane configurations and found differences in crystal morphology and increases in thickness and extent of the scaling layer with respect to the axial direction from the membrane channel entry point to the exit. This trend, they argued, was consistent with CP. They also found that antiscalants inhibited and/or prevented the growth of these crystals at sufficiently high concentrations and reduced associated declines in flux. Rahardianto and others (2006) found that scale development could be completely suppressed or severely inhibited at antiscalant concentrations as low as 3 ppm. They also found that the impact of

antiscalant treatment on scaling was dependent upon location within the membrane channel, due to spatial variations in scale development.

Others pointed out, however, that antiscalants are not a panacea and the ability of antiscalants to inhibit or prevent inorganic fouling is limited. They also pointed out that this type of membrane fouling cannot be avoided if the ions responsible for the fouling become sufficiently high in the RO concentrate (Kang and others, 2011). The observation that feed pump specific energy can be reduced by increasing the antiscalant concentration does not conflict with this assertion, since the optimal antiscalant dosage may actually be much greater than recommended dosages provided by antiscalant manufacturers or predicted by available modeling software. Antiscalant concentrations used in this study were potentially far below optimal levels.

Effect of Antiscalant Concentration on Circulation Pump Specific Energy

In order to assess the effect of antiscalant on circulation pump energy consumption, circulation pump specific energy was plotted as a function of recovery with and without antiscalant for desalination of Well 2 groundwater in Figure 4.5.

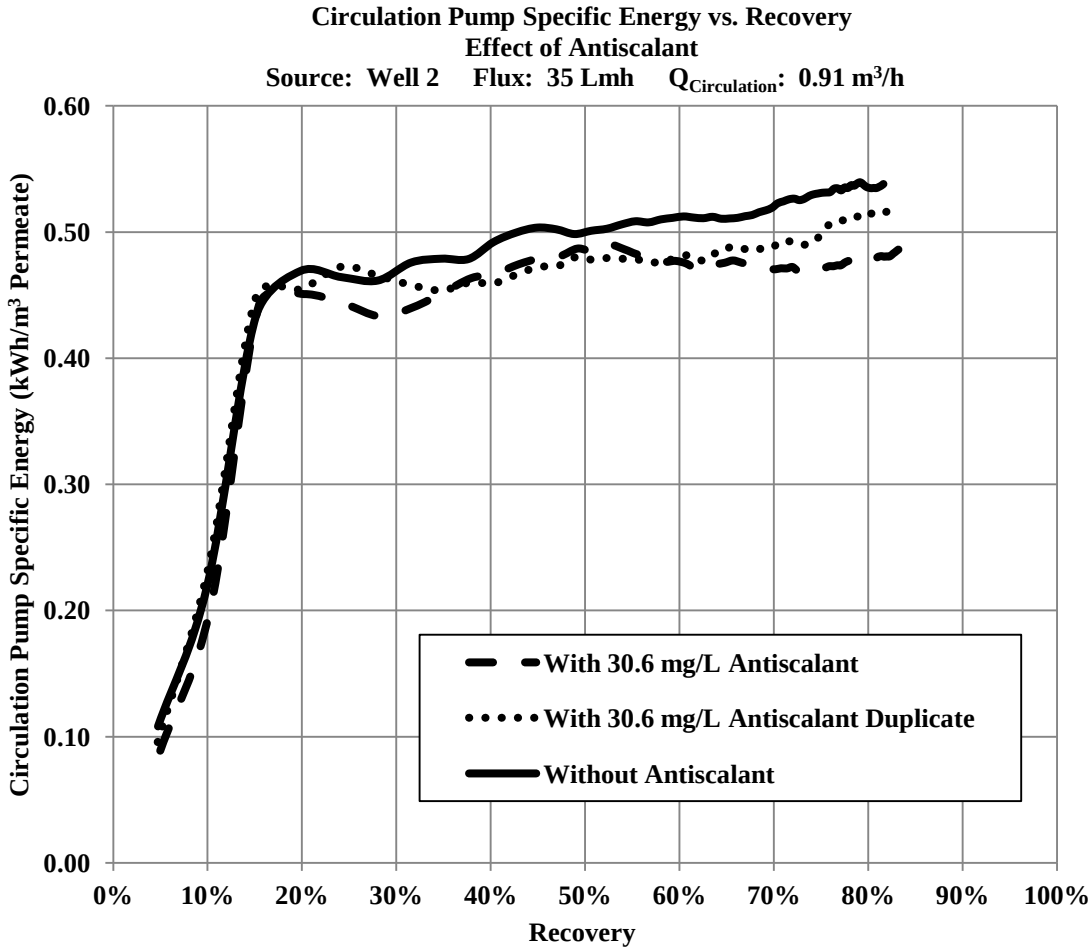

Figure 4.5 Circulation pump specific energy vs. recovery. Effect of antiscalant. Groundwater source: Well 2. Permeate flux: 35 Lmh. Circulation flowrate: 0.91 m^3/h.

The addition of antiscalant appeared to have no significant impact on circulation pump specific energy. This is consistent with the role of antiscalant in the RO process for desalination of brackish groundwater with the potential for inorganic fouling. Antiscalant lessens the potential for inorganic fouling thereby reducing resistance to water flux and energy consumption by the feed pump. Unless the addition of antiscalant either changed the fluid properties of the circulating concentrate, such as viscosity, or altered the deposition rate of scale within the concentrate circulation pipe, we would not expect this strategy to noticeably alter the energy consumption by the circulation pump.

Effect of Permeate Flux on Feed Pump Specific Energy

Feed pump specific energy was determined for desalination of groundwater from Wells 1, 2 and 3 at recoveries from 0 to 90 percent for target permeate fluxes ranging from 22 to 44 Lmh. Ratios of circulation flowrate to feed flowrate ranged from 5:1 to 6.7:1. In order to assess the effect(s) of permeate flux on feed pump energy consumption, feed pump specific energy was plotted as a function of recovery in Figures 4.6 through 4.8 for desalination of groundwater from the three wells at target permeate fluxes of 26 Lmh and 35 Lmh. The circulation flowrate for these tests was 0.91 m^3/h. At a target flux of 26 Lmh, the circulation flowrate was 6.7 times the feed flowrate. For a flux of 35 Lmh, the circulation flowrate was 5 times the feed flowrate. It should be noted that Dow Filmtec technical guidance provided a typical permeate flux for desalination of brackish well water of 18 gfd (31 Lmh), if the silt density index (SDI) of the water was less than 3, and a typical permeate flux for desalination of brackish surface water of 14 gfd (24 Lmh), if the SDI of the water was less than 5 (Dow, 2011). Unfortunately, no SDI data were available for groundwater from Wells 1, 2, and 3 at BGNDRF.

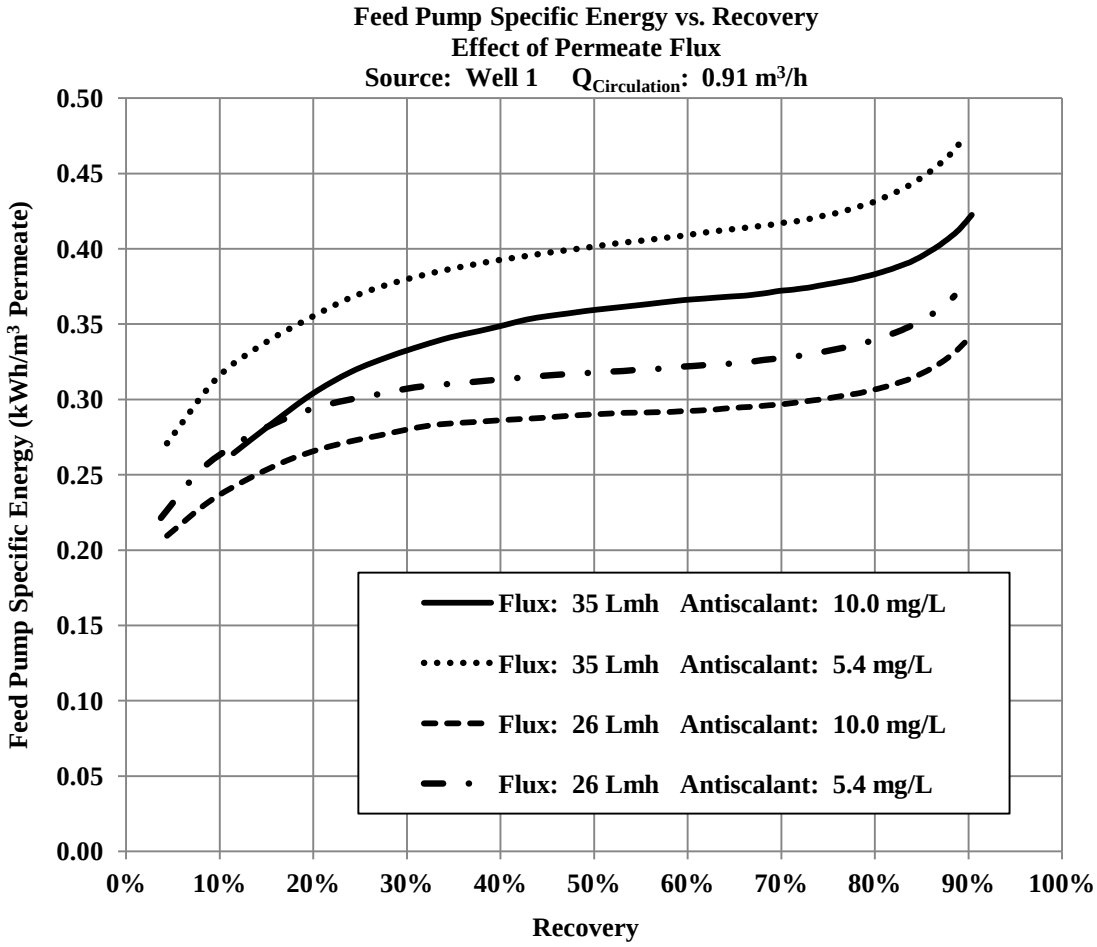

Figure 4.6 Feed pump specific energy vs. recovery. Effect of permeate flux. Groundwater source: Well 1. Permeate fluxes: 26 Lmh and 35 Lmh. Antiscalant concentrations: 5.4 mg/L and 10.0 mg/L. Circulation flowrate: 0.91 m^3/h.

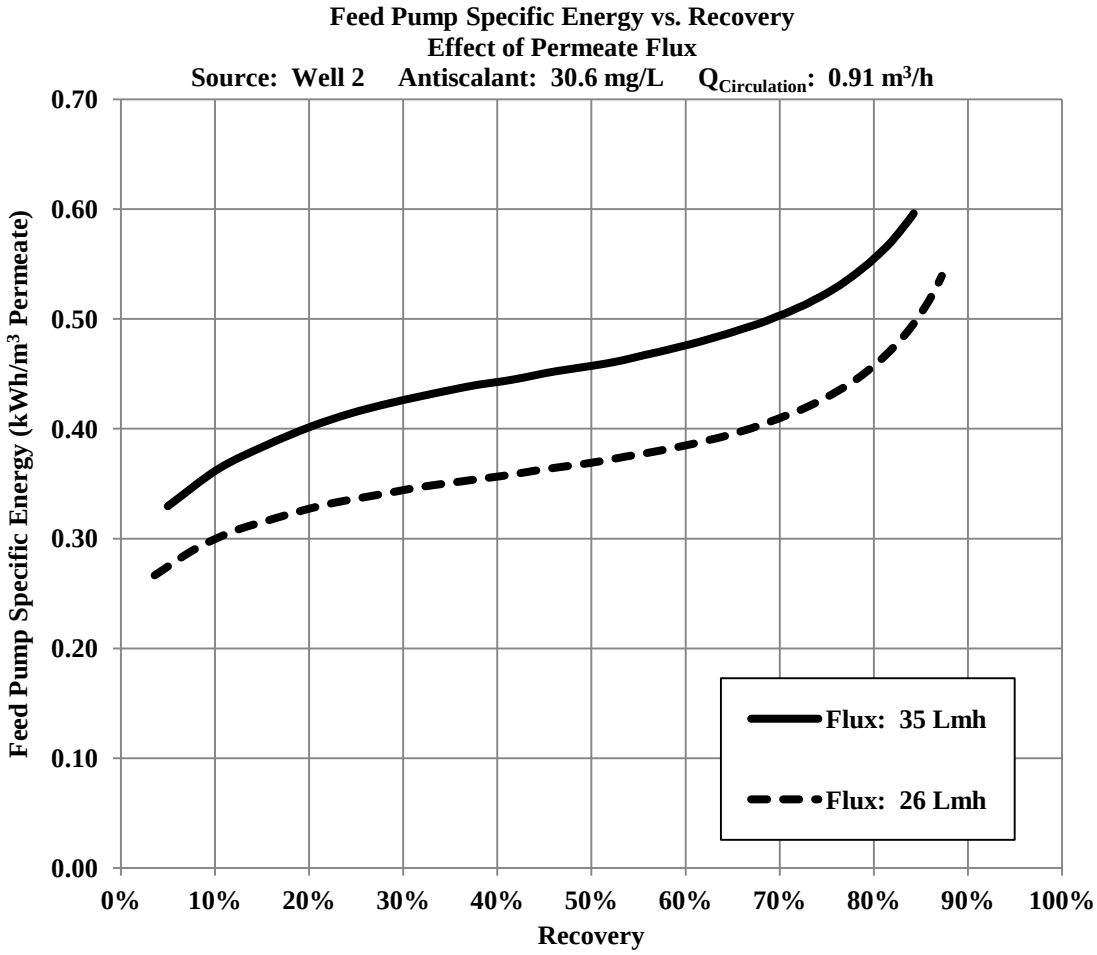

Figure 4.7 Feed pump specific energy vs. recovery. Effect of permeate flux. Groundwater source: Well 2. Permeate fluxes: 26 Lmh and 35 Lmh. Antiscalant: 30.6 mg/L. Circulation flowrate: 0.91 m^3/h.

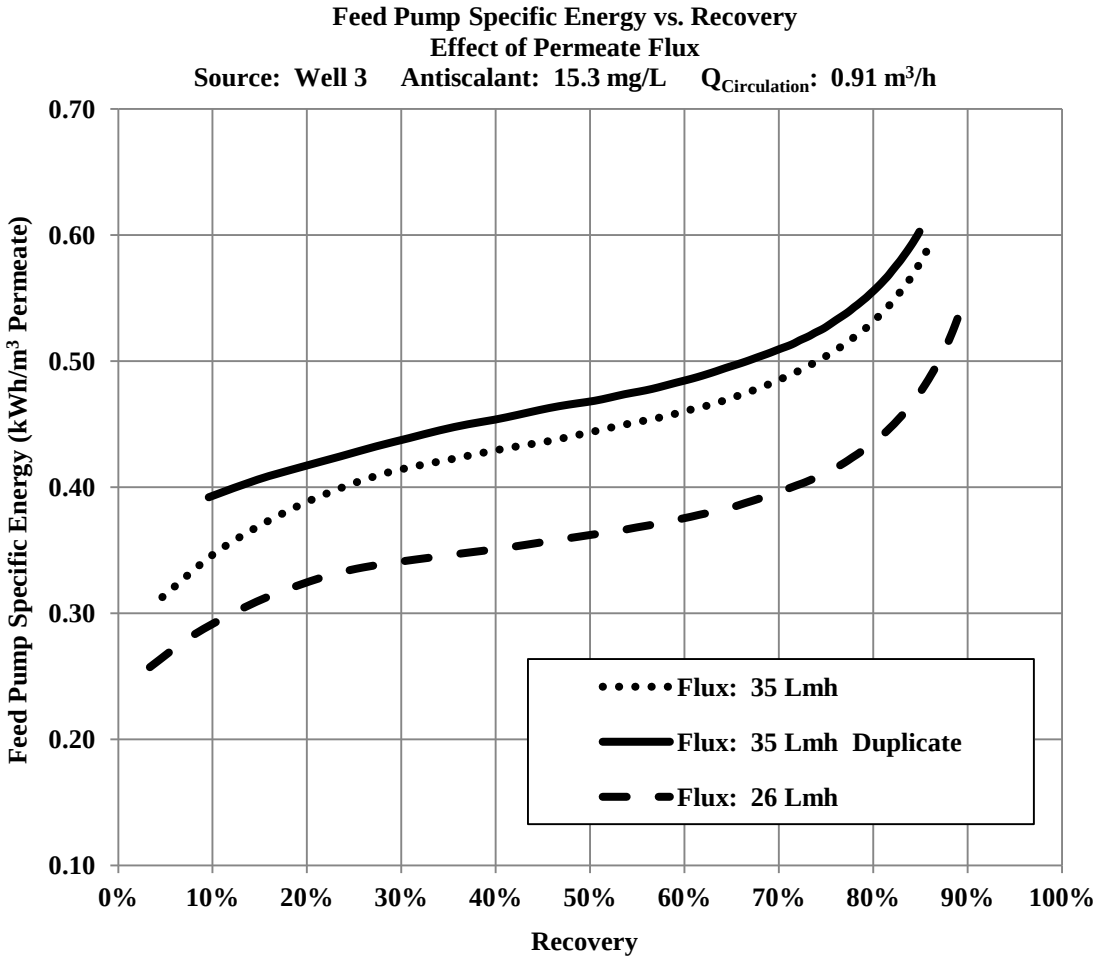

Figure 4.8 Feed pump specific energy vs. recovery. Effect of permeate flux. Groundwater source: Well 3. Permeate fluxes: 26 Lmh and 35 Lmh. Antiscalant concentration: 15.3 mg/L. Circulation flowrate: 0.91 m^3/h.

In order to provide an additional tool for comparison of results for various permeate fluxes, groundwater sources, and antiscalant concentrations, a summary of feed pump specific energies has been presented in Table 4.4 for the test conditions referenced in Figures 4.6 through 4.8 at recoveries of approximately 50 percent and 80 percent. In addition, the percentage change in specific energy due to increasing the permeate flux from 26 to 35 Lmh at each recovery is also presented in Table 4.4 and has been calculated using Equation 4.6:

$$\Delta\hat{E}(\%) = \frac{\hat{E}_{35\ Lmh} - \hat{E}_{26\ Lmh}}{\hat{E}_{26\ Lmh}} \times 100 \tag{4.6}$$

where $\Delta\hat{E}(\%)$ is the percentage change in feed pump specific energy at a given circulation flowrate and recovery for an increase in permeate flux from 26 to 35 Lmh, $\hat{E}_{35\,Lmh}$ is the feed pump specific energy for the same circulation flowrate and recovery at a permeate flux of 35 Lmh and $\hat{E}_{26\,Lmh}$ is the feed pump specific energy for the same circulation flowrate and recovery at a permeate flux of 26 Lmh.

Table 4.4 Increase in feed pump specific energy observed for changes in permeate flux at recoveries of 50 percent and 80 percent.

Source	Antiscalant Concentration (mg/L)	Permeate Flux (Lmh)	$\hat{E}_{50\%}$ (kWh/m^3)	$\Delta\hat{E}_{50\%}$ (%)	$\hat{E}_{80\%}$ (kWh/m^3)	$\Delta\hat{E}_{80\%}$ (%)
Well 1	5.4	26	0.32	26	0.34	27
Well 1	5.4	35	0.40		0.43	
Well 1	10.0	26	0.29	24	0.31	25
Well 1	10.0	35	0.36		0.38	
Well 2	30.6	26	0.37	24	0.46	22
Well 2	30.6	35	0.46		0.56	
Well 3	15.3	26	0.36	23	0.44	22
Well 3	15.3	35	0.44		0.53	

The preceding graphs demonstrate the very clear relationship between permeate flux and feed pump specific energy. Increasing permeate flux from 26 Lmh to 35 Lmh increased the specific energy at 50 percent and 80 percent recovery between 22 percent and 27 percent for all groundwater sources and antiscalant concentrations. These results are in basic agreement with the principles of the RO process. Specific energy is a function of operating pressure which is governed by the NDP required to generate permeate. The required NDP is a function of permeate flux and the hydraulic resistance of the membrane, as predicted by Equation 4.7:

$$\Delta p - \Delta\pi = J\,R_m \tag{4.7}$$

where J is the permeate flux, R_m is the hydraulic resistance of the membrane, Δp is the transmembrane pressure difference or feed pump operating pressure, assuming zero pressure on the permeate side of the membrane, $\Delta\pi$ is the transmembrane osmotic

pressure difference, and $\Delta p - \Delta \pi$ is the NDP. Another source of increased operating pressure and energy consumption is CP, which is increased when the permeate flux is increased (Shirazi and others, 2010). CP not only increases the apparent osmotic pressure gradient at the membrane surface, but also increases the potential for inorganic fouling, if fouling species become concentrated at the membrane surface, relative to their concentrations within the bulk solution.

The experimental small-scale RO process described in this chapter was a crossflow process. In this process, increasing the permeate flux from 26 to 35 Lmh at a circulation flowrate of 0.91 m^3/h was accompanied by an increase in mean crossflow velocity of approximately 2.5 percent, based on Equations 4.2 and 4.3, since permeate flux was dependent upon the feed flowrate. This potentially created two competing processes. Increasing permeate flux can increase the severity of membrane fouling and CP, raising NDP, operating pressure and energy consumption. At the same time, increasing crossflow velocity has the potential to reduce the severity of CP and fouling due to increased shear and back diffusion of sparingly soluble species from the membrane surface into the bulk solution. This can lead to reduced resistance to flux of water across the membrane, operating pressure and energy consumption. The relatively small increase in mean crossflow velocity accompanying the increase in permeate flowrate and permeate flux, however, was not expected to significantly affect CP, fouling, or specific energy.

Although raising the target permeate flux from 26 Lmh to 35 Lmh represented an increase in permeate flux of approximately 33 percent, the corresponding feed pump specific energy increase was expected to be somewhat smaller due to the contribution of the osmotic pressure difference to the required NDP. The observed increase in feed pump specific energy from the increase in permeate flux from 26 Lmh to 35 Lmh was between 20 percent and 30 percent for desalination of groundwater from all three wells for recoveries above 50 percent for the test conditions referenced in Figures 4.6 through 4.8.

Combined Effects of Permeate Flux and Antiscalant Concentration on Feed Pump Specific Energy

Increased permeate flux was also accompanied by a slight increase in crossflow velocity. While increasing permeate flux increases energy consumption of the RO process, increased crossflow velocity has the potential to decrease energy consumption by decreasing CP and fouling caused by CP. Because of the strong direct relationship between flux and energy consumption, and the relatively minor increase in mean crossflow velocity, we would expect the impact of the former to dwarf the impact of the latter factor. The addition of antiscalant can also reduce energy consumption of the RO process by reducing inorganic fouling due to sparingly soluble species. When used at sufficient concentrations, antiscalants can significantly reduce the impact of inorganic fouling on energy consumption in brackish desalination. Increases in crossflow velocity and antiscalant usage can supplement one another with regard to reducing energy consumption. As a result, the relatively minor impact of increasing crossflow velocity on feed pump energy consumption may actually be reduced even further by the addition of antiscalants at sufficient concentrations, due to the reduced importance of membrane fouling as a factor in energy consumption by the feed pump. This is not to say that increasing crossflow velocity will not reduce energy consumption for desalination of feed containing antiscalant. What it does suggest is that the relatively minor (as a percentage) decrease in energy consumption due to increased crossflow velocity and shear could potentially be even less dramatic than it would have been in the absence of antiscalant.

From inspection of data presented in Table 4.4, it was noteworthy that increasing flux from 26 Lmh to 35 Lmh led to the greatest percentage increase in feed pump specific energy for desalination of Well 1 groundwater, groundwater with the lowest potential for inorganic fouling and the lowest TDS level. Based on the impact of flux on the fouling process and the development of CP, this was surprising, in light of the relatively low fouling potential and TDS level of Well 1 groundwater. However, the increase for desalination of Well 1 groundwater was slightly greater for tests conducted at the lower antiscalant concentration: 5.4 mg/L. This was consistent with the greater potential for fouling at the lower antiscalant concentration. The lower

increase in feed pump specific energy observed when permeate flux was raised from 26 Lmh to 35 Lmh for desalination of groundwater from Wells 2 and 3, although unexpected, may be indicative of the greater potential for fouling and/or CP for these two sources and therefore the greatest potential energy savings from even small increases in crossflow velocity.

It was possible that, although antiscalant was added to groundwater from all three sources, there was an optimal amount of antiscalant that would eliminate all potential for fouling and that the actual amount added was far below the optimal concentration in these tests. While antiscalant may have significantly reduced fouling potential, it may not have reduced the potential for CP. Because the potential for CP still existed, increasing the feed flowrate and crossflow velocity had the potential to reduce membrane fouling, resulting in a lower net specific energy increase when the feed flowrate and permeate flux were increased. This potential mechanism does not explain, however, the greater observed energy benefit, i.e., lower specific energy increase, for desalination of Well 1 groundwater at the higher antiscalant concentration, 10.0 mg/L. A much more plausible explanation was the greater reduction in flux-dependent inorganic scaling, and reduced resistance to water flow across the membrane, at the higher antiscalant concentration. Regardless of the impact of fouling potential and the potential for CP, the increase in feed pump specific energy caused by increased permeate flux appeared to be much greater than any energy savings due to increased crossflow velocity, and what was observed from data presented in Figures 4.6 through 4.8 and in Table 4.4 was the dominant effect of higher permeate flux.

Effect of Permeate Flux on Circulation Pump Specific Energy

The role of the feed pump was to supply the necessary NDP to generate the required permeate flux. As predicted by Equation 4.7, permeate flux had a strong direct effect on NDP, which, in turn, had a direct impact on feed pump energy consumption. The role of the circulation pump, however, was to replace the head lost by the circulating concentrate as it traveled from the membrane channel outlet to the point at which it combined with incoming (pressurized) feed. Based on the function of the circulation pump within the small-scale RO system, variations in permeate flux were not expected to significantly influence energy consumption by the circulation pump. In order to test this assumption, circulation pump specific energy has been plotted as a function of recovery for various combinations of permeate flux and circulation flowrate in Figures 4.9 and 4.10.

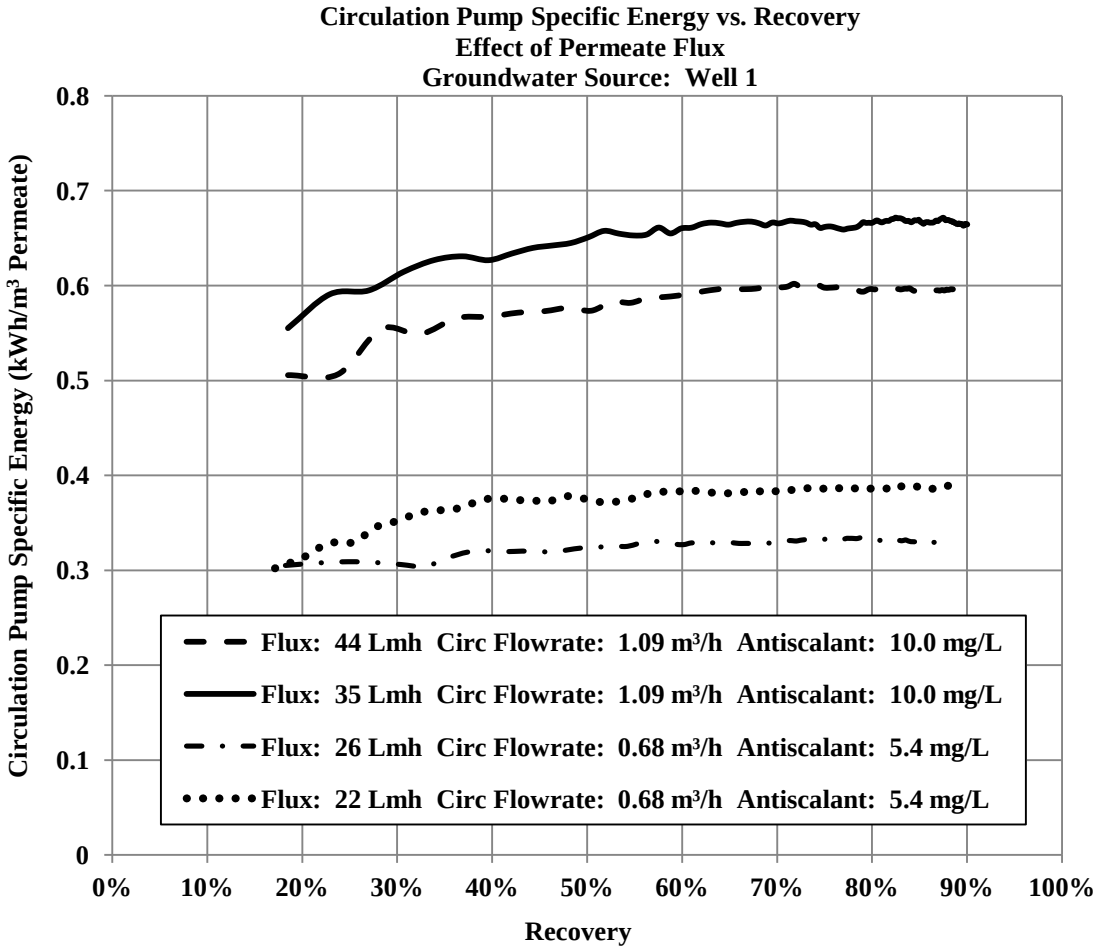

Figure 4.9 Circulation pump specific energy vs. recovery. Effect of permeate flux. Groundwater source: Well 1. Permeate fluxes: 22, 26, 35, and 44 Lmh. Circulation flowrates: 0.68 m^3/h and 1.09 m^3/h.

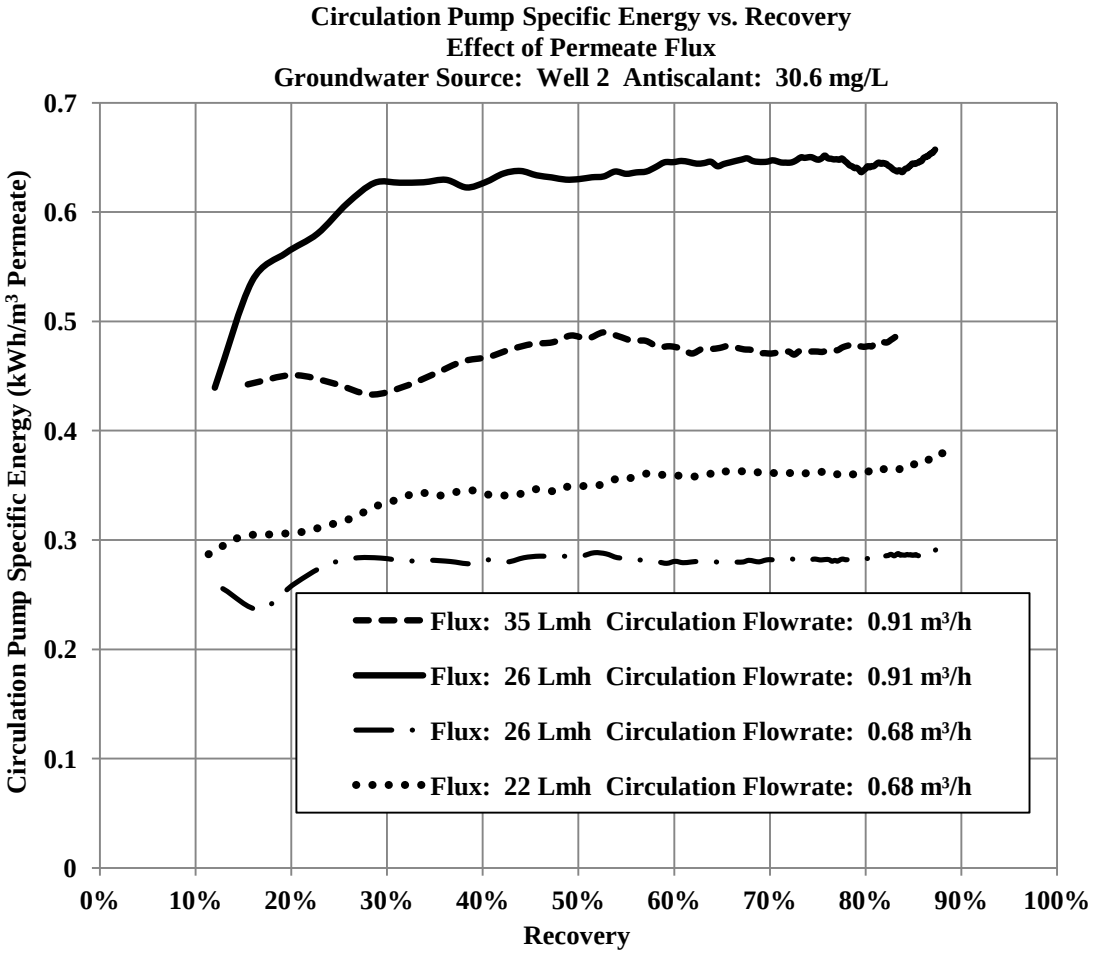

Figure 4.10 Circulation pump specific energy vs. recovery. Effect of permeate flux. Groundwater source: Well 2. Permeate fluxes: 22, 26, and 35 Lmh. Circulation flowrates: 0.68 m^3/h and 0.91 m^3/h. Antiscalant concentration: 30.6 mg/L.

What we observe in Figures 4.9 and 4.10 appears at first glance to contradict our assumptions regarding the relationship between permeate flux and circulation pump energy consumption. For desalination of groundwater from Wells 1 and 2, circulation pump specific energy decreases at a given circulation flowrate and recovery as the flux rises. This relationship is opposite to the relationship between permeate flux and feed pump specific energy. What we must remember is that specific energy is not the actual energy consumed, but the energy consumed per unit volume of permeate produced. Permeate flux is simply the ratio of the permeate flowrate to the permeate producing surface area of the membrane. At a given

circulation flowrate, reducing the permeate flux is equivalent to reducing the permeate flowrate. As the permeate flowrate is reduced, the permeate volume produced per unit time and per unit of energy is also reduced. If we assume that the change in permeate flux does not change the total energy consumed by the circulation pump, based on the role of the circulation pump in the RO system, the ratio of energy consumed to permeate produced, i.e., the circulation pump specific energy, must rise, as the flux is reduced. This is predicted by Equation 4.5.

Effect of Circulation Flowrate on Feed Pump Specific Energy

In order to assess the impact of circulation flowrate on feed pump energy consumption, feed pump specific energies are presented below in Figures 4.11 through 4.18 for desalination of brackish groundwater from Well 1, Well 2, and Well 3 at a target permeate flux of 26 Lmh with target circulation flowrates of 0.68 and 0.91 m^3/h, representing ratios of circulation flow to feed flow of 5:1 and 6.7:1, and at a target permeate flux of 35 Lmh with target circulation flowrates of 0.91 and 1.09 m^3/, representing ratios of circulation flow to feed flow of 5:1 and 6:1. Results for desalination of Well 1 groundwater are presented for both antiscalant concentrations: 5.4 mg/L and 10.0 mg/L. Specific energies were for the first operating cycle only and include the discharge portion of the cycle.

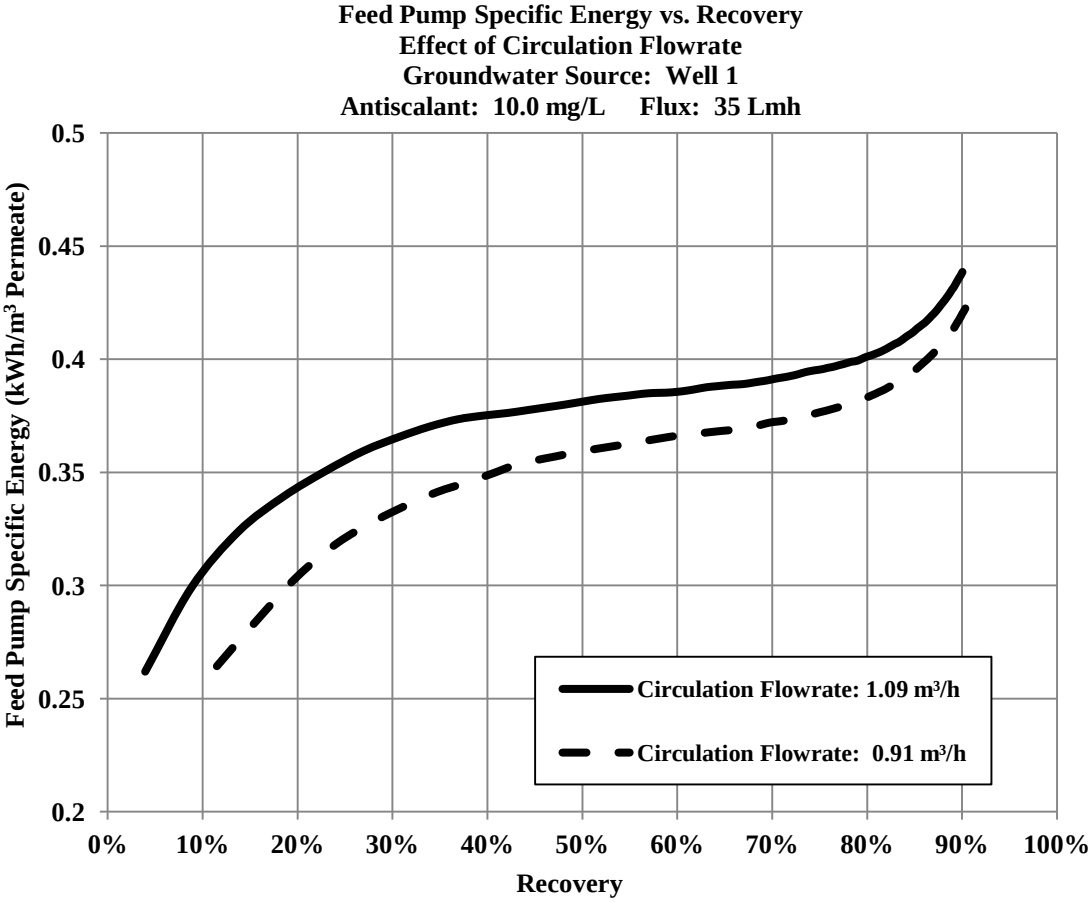

Figure 4.11 Feed pump specific energy vs. recovery. Effect of circulation flowrate. Groundwater source: Well 1. Permeate flux: 35 Lmh. Circulation flowrates: 0.91 and 1.09 m^3/h. Antiscalant: 10.0 mg/L.

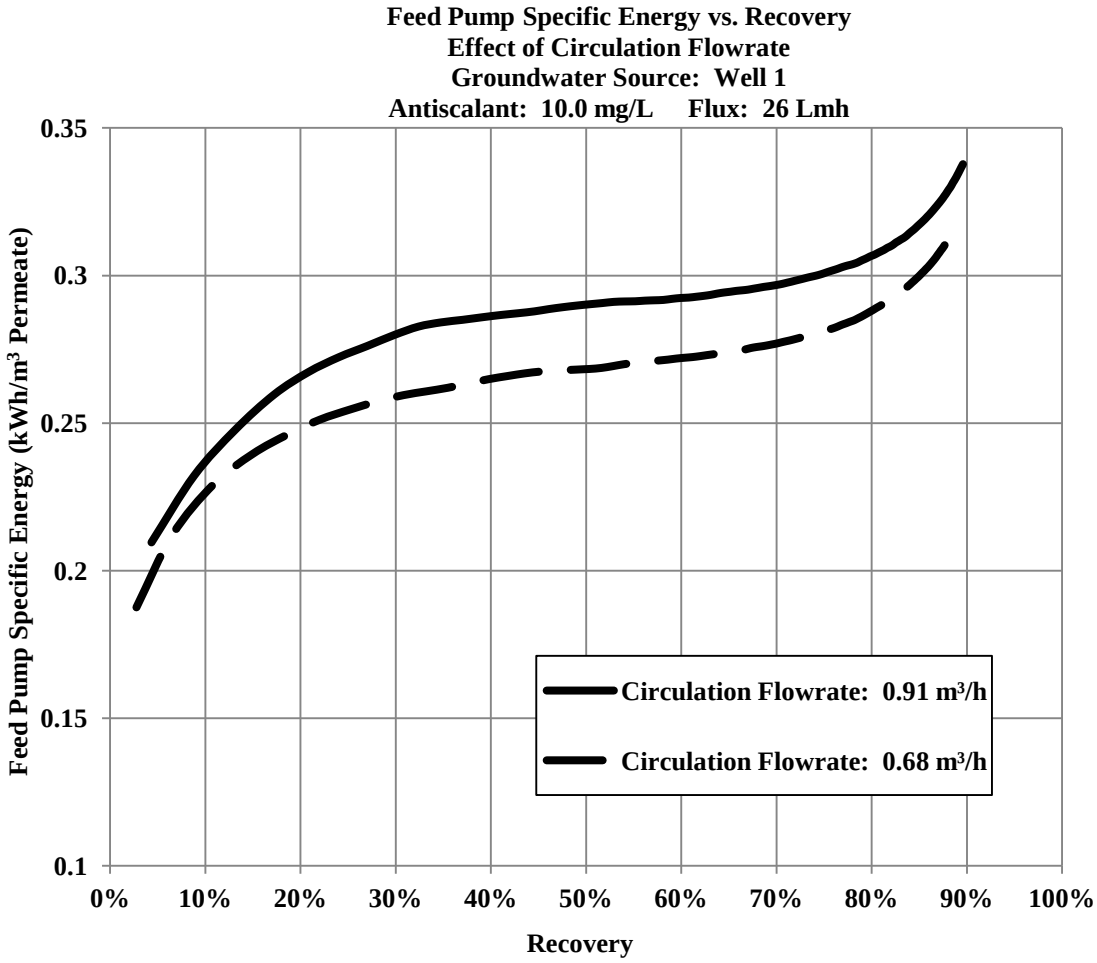

Figure 4.12 Feed pump specific energy vs. recovery. Effect of circulation flowrate. Groundwater source: Well 1. Permeate flux: 26 Lmh. Circulation flowrates: 0.68 and 0.91 m^3/h. Antiscalant: 10.0 mg/L.

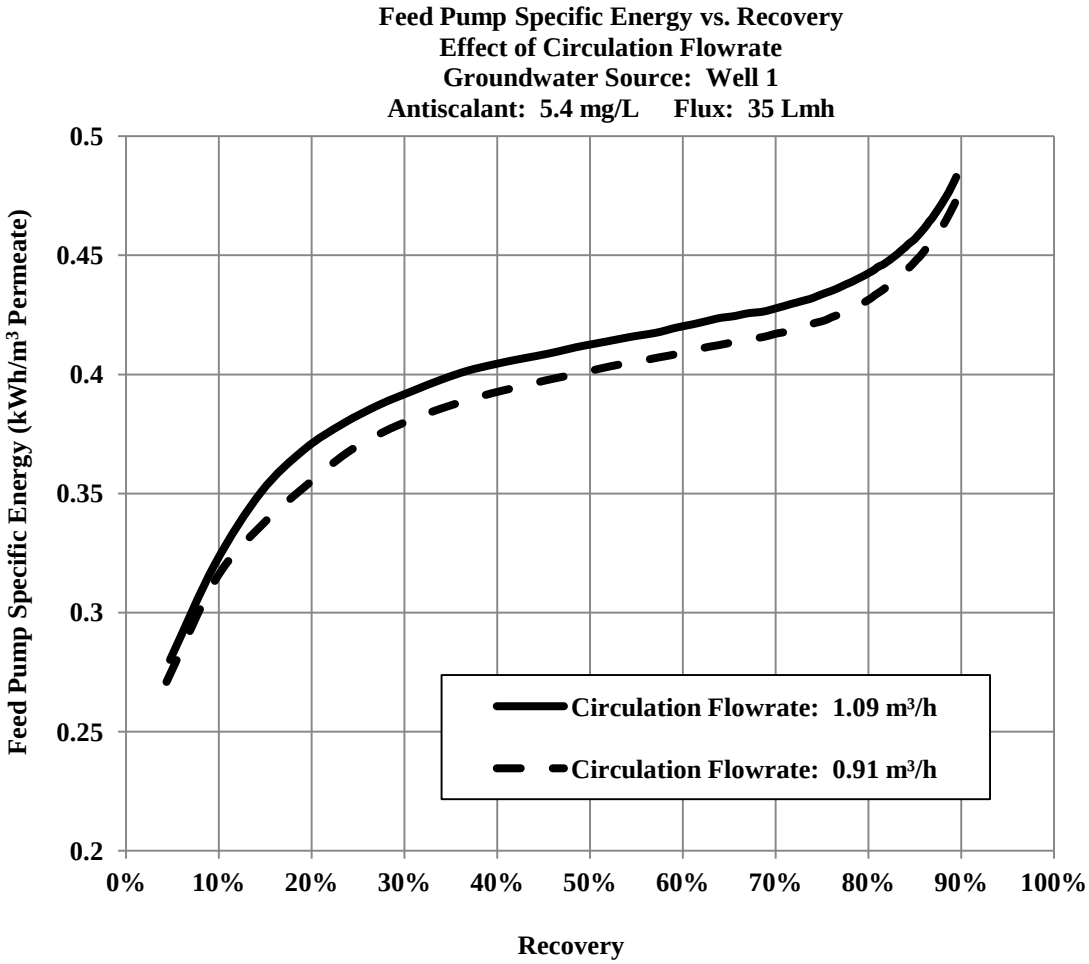

Figure 4.13 Feed pump specific energy vs. recovery. Effect of circulation flowrate. Groundwater source: Well 1. Permeate flux: 35 Lmh. Circulation flowrates: 0.91 and 1.09 m^3/h. Antiscalant: 5.4 mg/L.

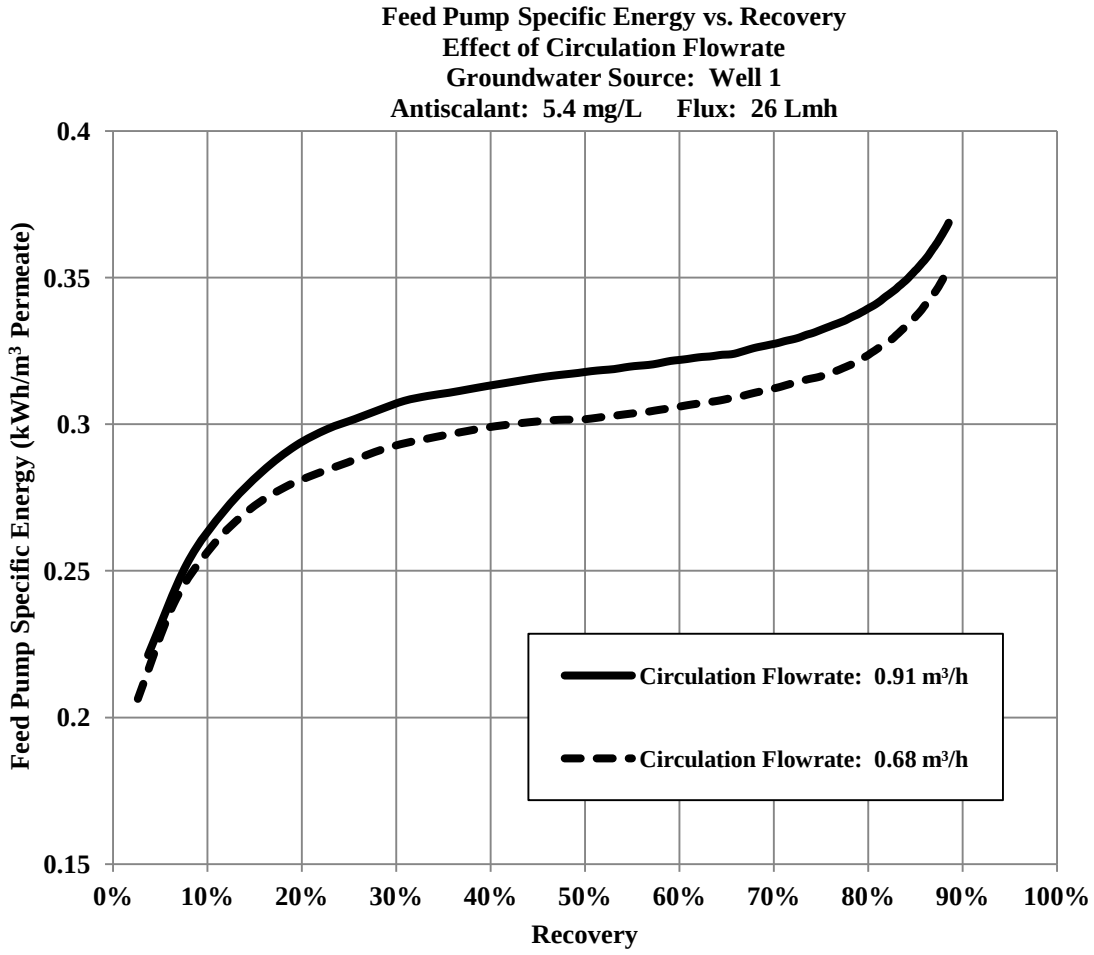

Figure 4.14 Feed pump specific energy vs. recovery. Effect of circulation flowrate. Groundwater source: Well 1. Permeate flux: 26 Lmh. Circulation flowrates: 0.68 and 0.91 m^3/h. Antiscalant: 5.4 mg/L.

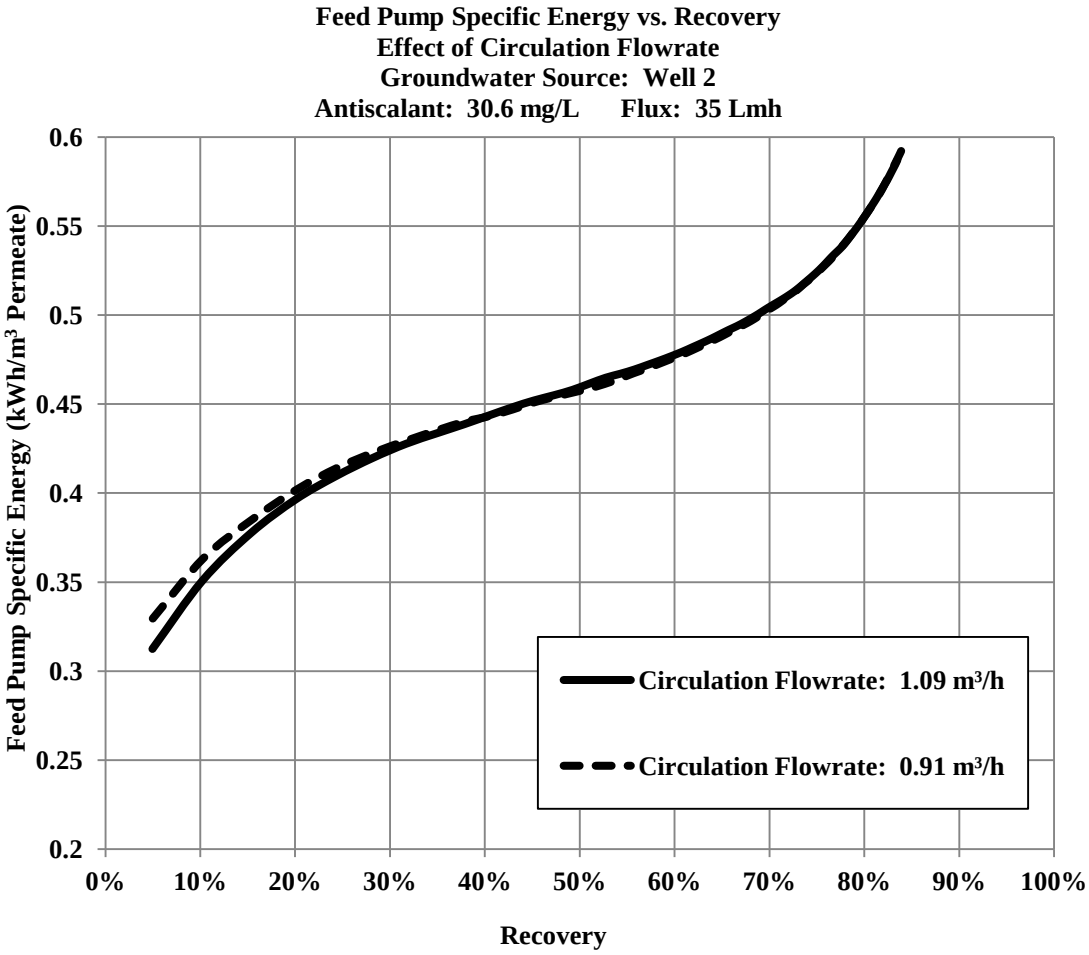

Figure 4.15 Feed pump specific energy vs. recovery. Effect of circulation flowrate. Groundwater source: Well 2. Permeate flux: 35 Lmh. Circulation flowrates: 0.91 and 1.09 m^3/h. Antiscalant: 30.6 mg/L.

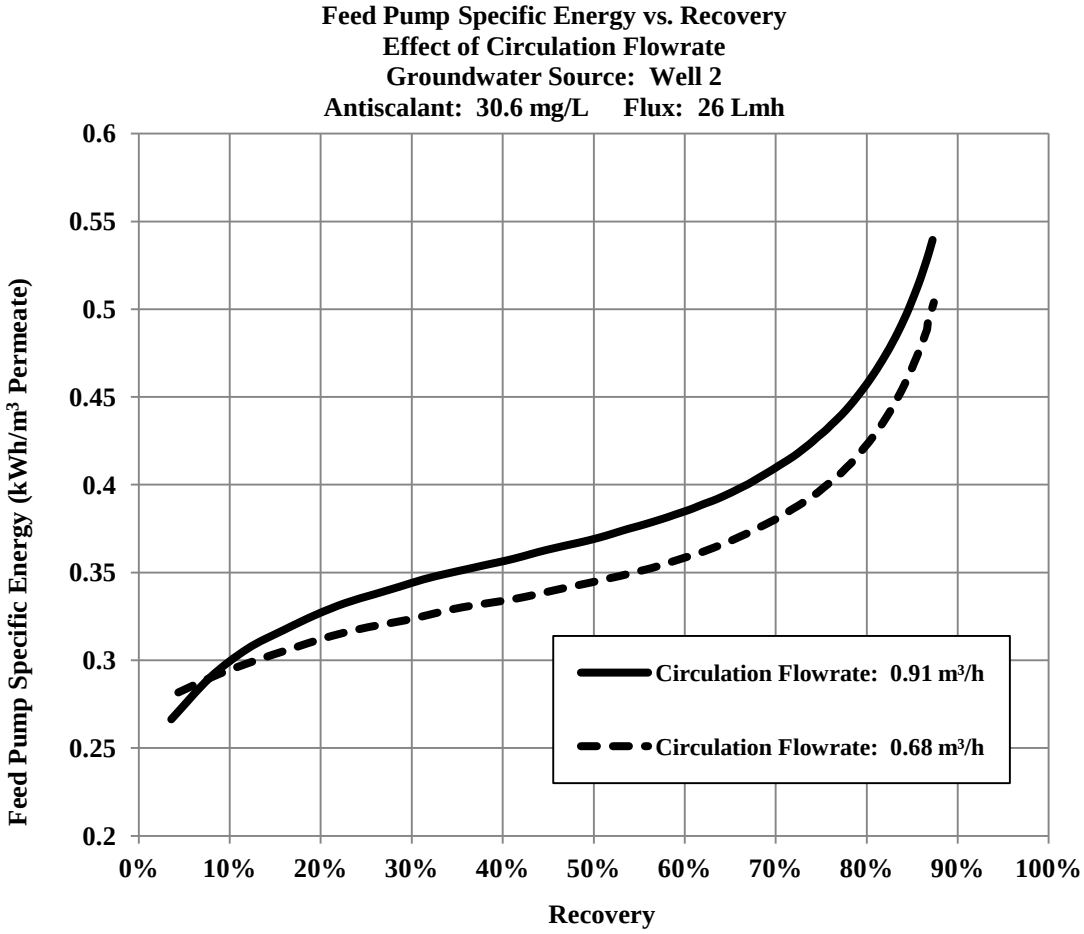

Figure 4.16 Feed pump specific energy vs. recovery. Effect of circulation flowrate. Groundwater source: Well 2. Permeate flux: 26 Lmh. Circulation flowrates: 0.68 and 0.91 m^3/h. Antiscalant: 30.6 mg/L.

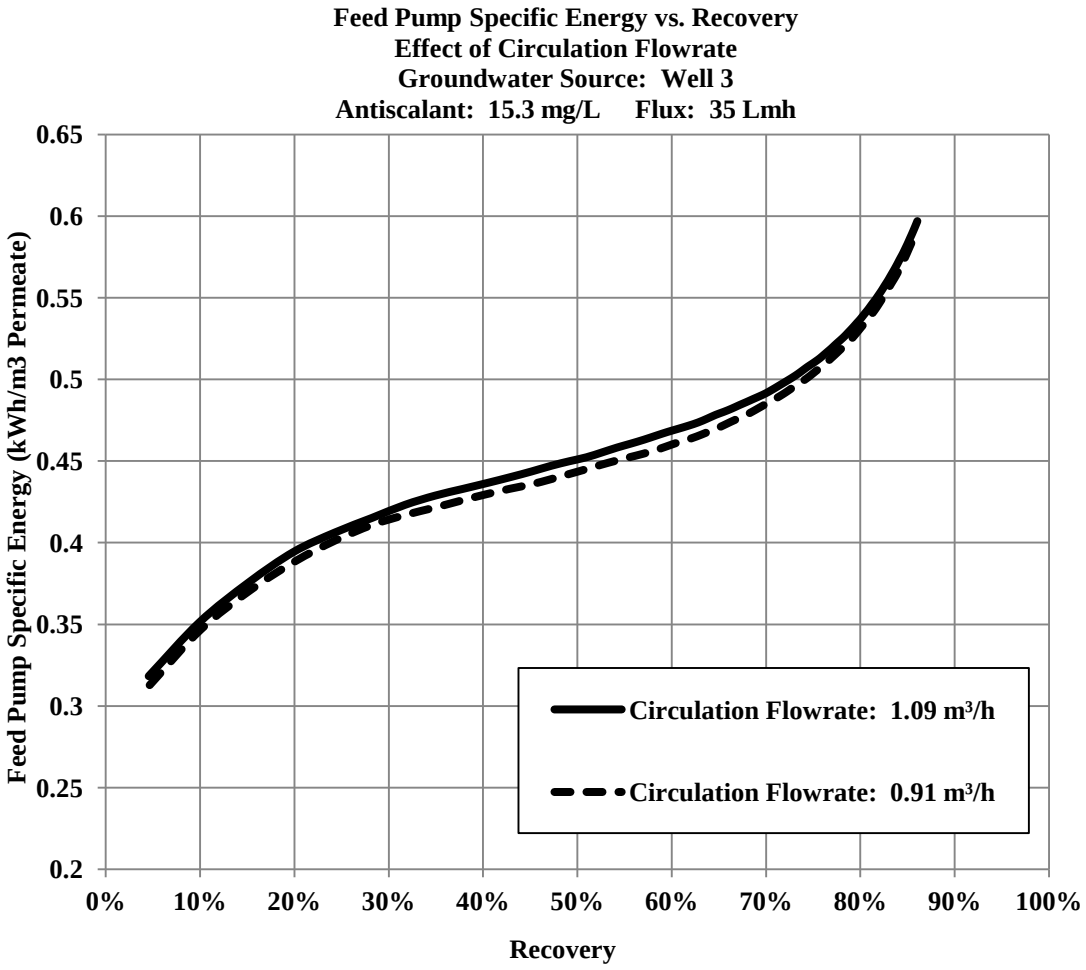

Figure 4.17 Feed pump specific energy vs. recovery. Effect of circulation flowrate. Groundwater source: Well 3. Permeate flux: 35 Lmh. Circulation flowrates: 0.91 and 1.09 m^3/h. Antiscalant: 15.3 mg/L.

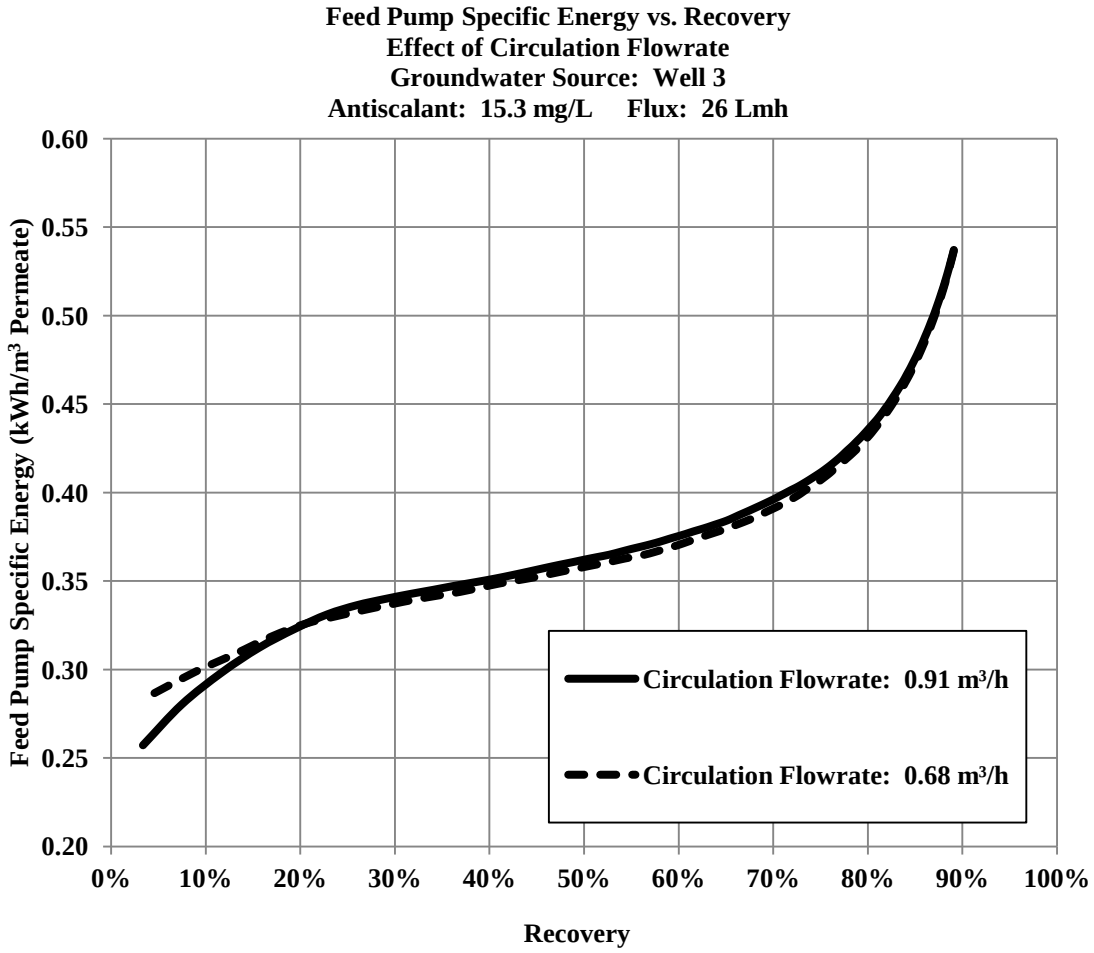

Figure 4.18 Feed pump specific energy vs. recovery. Effect of circulation flowrate. Groundwater source: Well 3. Permeate flux: 26 Lmh. Circulation flowrates: 0.68 and 0.91 m^3/h. Antiscalant: 15.3 mg/L.

To facilitate quantitative comparisons between results from various test conditions, data for recoveries of approximately 50 percent and 80 percent have been summarized in Table 4.5 for the tests referenced in Figures 4.11 through 4.18. In addition, the increases in feed pump specific energy resulting from the increase in circulation flowrate from 0.68 to 0.91 m^3/h at a target permeate flux of 26 Lmh and the increase in the circulation flowrate from 0.91 to 1.09 m^3/h at a target permeate flux of 35 Lmh were calculated using Equations 4.8a and 4.8b.

$$\Delta\hat{E}(\%)_{26\,\mathrm{Lmh}} = \frac{\hat{E}_{0.91} - \hat{E}_{0.68}}{\hat{E}_{0.68}} \times 100 \qquad (4.8a)$$

$$\Delta\hat{E}(\%)_{35\,\mathrm{Lmh}} = \frac{\hat{E}_{1.09} - \hat{E}_{0.91}}{\hat{E}_{0.91}} \times 100 \tag{4.8b}$$

where $\Delta\hat{E}_{26\,\mathrm{Lmh}}$ and $\Delta\hat{E}_{35\,\mathrm{Lmh}}$ are the percentage changes in feed pump specific energy at target permeate fluxes of 26 Lmh and 35 Lmh and recoveries of either 50 percent or 80 percent, resulting from increasing the circulation flowrate from 0.68 m^3/h to 0.91 m^3/h and from 0.91 m^3/h to 1.09 m^3/h. $\hat{E}_{0.91}$ is the feed pump specific energy for the same permeate flux and recovery at a circulation flowrate of 0.91 m^3/h, $\hat{E}_{0.68}$ is the feed pump specific energy for the same permeate flux and recovery at a circulation flowrate of 0.68 m^3/h, and $\hat{E}_{1.09}$ is the feed pump specific energy for the same permeate flux and recovery at a circulation flowrate of 1.09 m^3/h. Results of these calculations are presented in Table 4.5.

Table 4.5 Increase in feed pump specific energy observed for increases in circulation flowrate, at recoveries of 50 percent and 80 percent.

Source	Antisc. Conc.	Perm. Flux	$Q_{Circ.}$	$\hat{E}_{50\%}$	$\Delta\hat{E}_{50\%}$	$\hat{E}_{80\%}$	$\Delta\hat{E}_{80\%}$
	(mg/L)	(Lmh)	(m^3/h)	(kWh/m^3)	(%)	(kWh/m^3)	(%)
Well 1	10.0	26	0.68	0.27	8.20	0.29	6.46
Well 1	10.0	26	0.91	0.29		0.31	
Well 1	10.0	35	0.91	0.36	5.91	0.38	4.75
Well 1	10.0	35	1.09	0.38		0.40	
Well 1	5.4	26	0.68	0.30	5.37	0.32	4.88
Well 1	5.4	26	0.91	0.32		0.34	
Well 1	5.4	35	0.91	0.40	2.87	0.43	2.62
Well 1	5.4	35	1.09	0.41		0.44	
Well 2	30.6	26	0.68	0.34	7.01	0.42	8.01
Well 2	30.6	26	0.91	0.37		0.46	
Well 2	30.6	35	0.91	0.46	0.63	0.56	0.07
Well 2	30.6	35	1.09	0.46		0.56	
Well 3	15.3	26	0.68	0.36	0.97	0.43	0.93
Well 3	15.3	26	0.91	0.36		0.44	
Well 3	15.3	35	0.91	0.47	-3.44	0.53	1.69
Well 3	15.3	35	1.09	0.45		0.54	

Several trends can be observed in Figures 4.11 through 4.18 and in the data summary in Table 4.5. These trends are evaluated in the following sections for each groundwater source.

Desalination of Well 1 Groundwater at an Antiscalant Concentration of 10.0 mg/L

For desalination of Well 1 groundwater at an antiscalant concentration of 10.0 mg/L and a target permeate flux of 35 Lmh, increasing the ratio of circulation flowrate to feed flowrate ("flowrate ratio") from 5:1 to 6:1 increased the feed pump specific energy at all recoveries. An even larger relative increase in feed pump specific energy was observed at a permeate flux of 26 Lmh when the flowrate ratio was raised from 5:1 to 6.7:1. When analyzing the reasons for the larger increase in feed pump specific energy at the lower permeate flux, it should be noted that the relative increase in total flow within the membrane channel was much larger for the increases in the flowrate ratio at the lower permeate flux, 26 Lmh, than it was for the flowrate ratio increase at a target flux of 35 Lmh. When the flowrate ratio was raised from 5:1 to 6.7:1 at a target permeate flux of 26 Lmh, the percentage increase in total flowrate within the membrane channel was approximately 28 percent. When the flowrate ratio was raised from 5:1 to 6:1 at a target permeate flux of 35 Lmh, the percentage increase in total flowrate within the membrane channel was approximately 17 percent.

Desalination of Well 1 Groundwater at an Antiscalant Concentration of 5.4 mg/L

For desalination of groundwater from Well 1 at an antiscalant concentration of 5.4 mg/L and a target permeate flux of 35 Lmh, raising the flowrate ratio from 5:1 to 6:1 increased the feed pump specific energy at all recoveries. Feed pump specific energy was also increased for desalination of the same groundwater and antiscalant concentration at a target permeate flux of 26 Lmh when the flowrate ratio was raised from 5:1 to 6.7:1. Increases in feed pump specific energy were significantly less at an antiscalant concentration of 5.4 mg/L than the increases observed at an antiscalant concentration of 10.0 mg/L for the same permeate fluxes and increases in the flowrate ratio.

Desalination of Well 2 Groundwater at an Antiscalant Concentration of 30.6 mg/L

For desalination of groundwater from Well 2 at an antiscalant concentration of 30.6 mg/L and a target permeate flux of 35 Lmh, raising the flowrate ratio from 5:1 to 6:1 resulted in a much smaller increase in feed pump specific energy than the increase observed for desalination of Well 1 groundwater for the same permeate flux and increase in flowrate ratio at both antiscalant concentrations. At 50 percent and 80 percent recovery, the increase was less than 1 percent. At a target permeate flux of 26 Lmh, raising the flowrate ratio from 5:1 to 6.7:1 resulted in an increase in feed pump specific energy of similar magnitude to that observed in desalination of Well 1 groundwater at an antiscalant concentration of 10.0 mg/L for the same flow conditions. As was mentioned previously, the relative increase in total flowrate and velocity within the membrane channel resulting from increasing the flowrate ratio from 5:1 to 6.7:1 at a target permeate flux of 26 Lmh was nearly double the relative increase in total flowrate and velocity resulting from increasing the flowrate ratio from 5:1 to 6:1 at a target permeate flux of 35 Lmh.

Desalination of Well 3 Groundwater at an Antiscalant Concentration of 15.3 mg/L

For desalination of groundwater from Well 3 at an antiscalant concentration of 15.3 mg/L and a target permeate flux of 35 Lmh, raising the flowrate ratio from 5:1 to 6:1 caused a much smaller increase in feed pump specific energy than that observed for desalination of Well 1 groundwater with the same changes in flow conditions. For a recovery of 50 percent, the calculated feed pump specific energy actually declined, while the feed pump specific energy rose by approximately 1.7 percent at a recovery of 80 percent when the ratio of circulation flowrate to feed flowrate was increased. Increases in feed pump specific energy on the order of 1 percent were observed when the flowrate ratio was increased from 5:1 to 6.7:1 at a target permeate flux of 26 Lmh. As was mentioned previously, the relative increase in total flowrate and velocity within the membrane channel resulting from increasing the flowrate ratio at a target permeate flux of 26 Lmh was nearly double the relative increase in total flowrate and

velocity resulting from increasing the flowrate ratio from 5:1 to 6:1 at a target permeate flux of 35 Lmh.

The observed effects of increases in the ratio of circulation flowrate to feed flowrate on feed pump specific energy can be explained in terms of the various processes occurring in brackish desalination of groundwater with variable potential for membrane fouling. Some processes that affect energy consumption by the feed pump act to increase energy consumption while others act to reduce energy consumption. The net impact of this variable depends upon which process dominates.

During testing, circulation flow was combined with incoming feed upstream of the membrane elements. This combined flow was split via a tee into two approximately equal flowstreams prior to entering the membrane channels. Not only did the combined flow experience frictional head losses but also "minor" or "component" head losses associated with flow through the tee and entry into the ceramic pressure vessels that contained the membranes. These head losses were a function of velocity. Increasing the ratio of circulation flowrate to feed flowrate increased the velocity and associated head losses through this portion of the system. These head losses were observed as reductions in pressure head. At the same time, feed pump operating pressure was determined by target feed flowrate and associated permeate flux. The feed pump was required to maintain a target pressure within the system to maintain target permeate flux. Any losses in pressure head upstream of the membrane elements were communicated to the feed pump which increased pump pressure in targeted feed flowrate and permeate flux, leading to increased energy consumption and specific energy.

Increasing the circulation flowrate can also create the opposite effect by increasing crossflow velocity that can reduce not only the severity of membrane fouling but also CP, causing reductions in operating pressure and energy consumption. Shirazi and others (2010) pointed out that increasing the crossflow velocity also increases the shear rate, which results in increased back diffusion of ions from the membrane surface to the bulk solution, reducing CP and inorganic fouling.

The net impact of these competing processes must be considered in light of the previously mentioned larger relative increase in velocity through the membrane channel for circulation flowrate increases at the lower feed flowrate. In addition, the net effects cannot be discussed separately from the effect of antiscalant concentration. Therefore, analysis of these effects is provided in the next section.

Combined Effects of Circulation Flowrate and Antiscalant Concentration on Feed Pump Specific Energy

The addition of antiscalant to brackish groundwater with potential for membrane fouling can reduce energy consumption by lessening the severity of inorganic fouling and the resulting resistance to transmembrane water flux. Increasing the circulation flowrate can also reduce energy consumption by increasing crossflow velocity within the membrane channel. Increased crossflow velocity and shear rate can reduce energy consumption by reducing inorganic fouling due to CP and the accumulation of fouling species at the membrane surface. However, increases in the circulation flowrate and crossflow velocity can also have the opposite effect on energy consumption by the small-scale RO system described here. Circulating concentrate combines with incoming feed between the feed pump and the pressure vessels containing the membranes. Raising the circulation flowrate also increases velocity within the pipe in this portion of the system. This process then leads to increased head losses that are communicated to the feed pump. In response to these head losses, the feed pump must increase operating pressure and energy consumption to maintain target permeate flux. By lessening the impact of fouling on energy consumption, the addition of antiscalant actually has the potential to reduce the beneficial effects of increased circulation flowrate on energy consumption. Although increasing the circulation flowrate may frequently be a useful strategy to reduce CP and associated fouling through increased shear and back diffusion, it may not be successful in reducing energy consumption, especially in cases of low fouling potential. In these situations, increased head losses may dominate, leading to unanticipated increases in energy consumption.

This effect may explain observed results for desalination of groundwater from Well 1 at the two antiscalant concentrations. At the lower antiscalant concentration, the effect of fouling was greater, increasing the beneficial effects of higher circulation flowrate, crossflow velocity, and shear rate on feed pump specific energy. In other words, greater potential for membrane fouling would translate into a larger reduction in specific energy with increased circulation flowrate, at least partially offsetting any increase in feed pump specific energy due to increased head losses between the feed pump and the membrane channels. It should be noted that while relative increases in feed pump specific energy corresponding to each circulation flowrate increase were much larger for the higher antiscalant concentration at both permeate fluxes, the percentage increase in total flowrate (28 percent at 26 Lmh and 17 percent at 35 Lmh) appeared to determine the relative effect of circulation flowrate on feed pump specific energy, indicating that the effect of flow velocity and associated head losses was still the largest factor in determining the effect of circulation flowrate on feed pump specific energy for desalination of groundwater from Well 1.

When the effects of circulation flowrate increase on feed pump specific energy at a target flux of 35 Lmh were compared to those observed at a target flux of 26 Lmh for desalination of groundwater from Well 2, the results cannot be satisfactorily explained on the basis of the relative increases in total flowrate alone. A lower permeate flux and can translate into reduced CP. Even in the presence of antiscalant, lower permeate flux can potentially result in reduced membrane fouling, if an optimal concentration of antiscalant has not been reached. At the lower permeate flux, the relative magnitude of energy-consuming head losses would be increased when compared to the energy savings resulting from increased crossflow velocity, leading to a larger specific energy increase at the higher circulation flowrate. At the higher target flux (35 Lmh), the impact of fouling and CP could be increased, also increasing the potential benefits of increased crossflow velocity and resulting in a reduced feed pump specific energy increase at a higher circulation flowrate.

For desalination of groundwater from Well 3, the effect of increased circulation flowrate on feed pump specific energy at a target permeate flux of 26 Lmh

was of similar magnitude to the effects observed at the higher target flux, 35 Lmh, in spite of the much larger percentage increase in total flowrate at the lower feed flowrate. This result would seem to indicate that the role of flow velocity and associated head losses was reduced relative to the potential reductions in energy consumption from increased crossflow velocity for Well 3 desalination. Groundwater from Well 3 had a much lower assumed fouling potential than groundwater from Well 2, and the antiscalant concentration was determined based on the lower assumed scaling potential. Potential reasons for the observed effect(s) of circulation flowrate on feed pump specific energy for Well 3 groundwater desalination include the possibility that the fouling potential for Well 3 was more severely underestimated than the fouling potential for groundwater from Well 2 such that the concentration of antiscalant was far below the optimal concentration that would most effectively address issues of fouling for groundwater from Well 3. It is possible that the energy savings from increased crossflow velocity effectively canceled the potential increases in energy consumption from head losses due to higher total velocity.

The net effect observed in Figures 4.11 through 4.18 is the larger effect of flow velocity and associated head losses on feed pump specific energy for operating conditions and feed chemistry that reduce potential for fouling and CP. We observed a much greater beneficial effect of increased crossflow velocity for operating conditions and feed chemistry that favor CP and membrane fouling. For feed chemistry and operating conditions with the highest potential for fouling and CP, the effects of higher flow velocity and associated head losses were essentially neutralized by the energy-saving benefits of increased crossflow velocity.

Effect of Circulation Flowrate on Circulation Pump Specific Energy

The energy consumption of the circulation pump was a function of the circulation flowrate, the required pressure head created by the pump, and the magnitude of head losses within the pipe through which the concentrate traveled. In order to assess the total impact of circulation flowrate on circulation pump specific energy for desalination of brackish groundwater with potential for scaling, specific energy is presented as a function of recovery at various combinations of flux and

circulation flowrate for desalination of groundwater from Wells 1 and 2 in Figures 4.19 and 4.20. These wells have been selected because they represent two sources of moderate to high scaling potential.

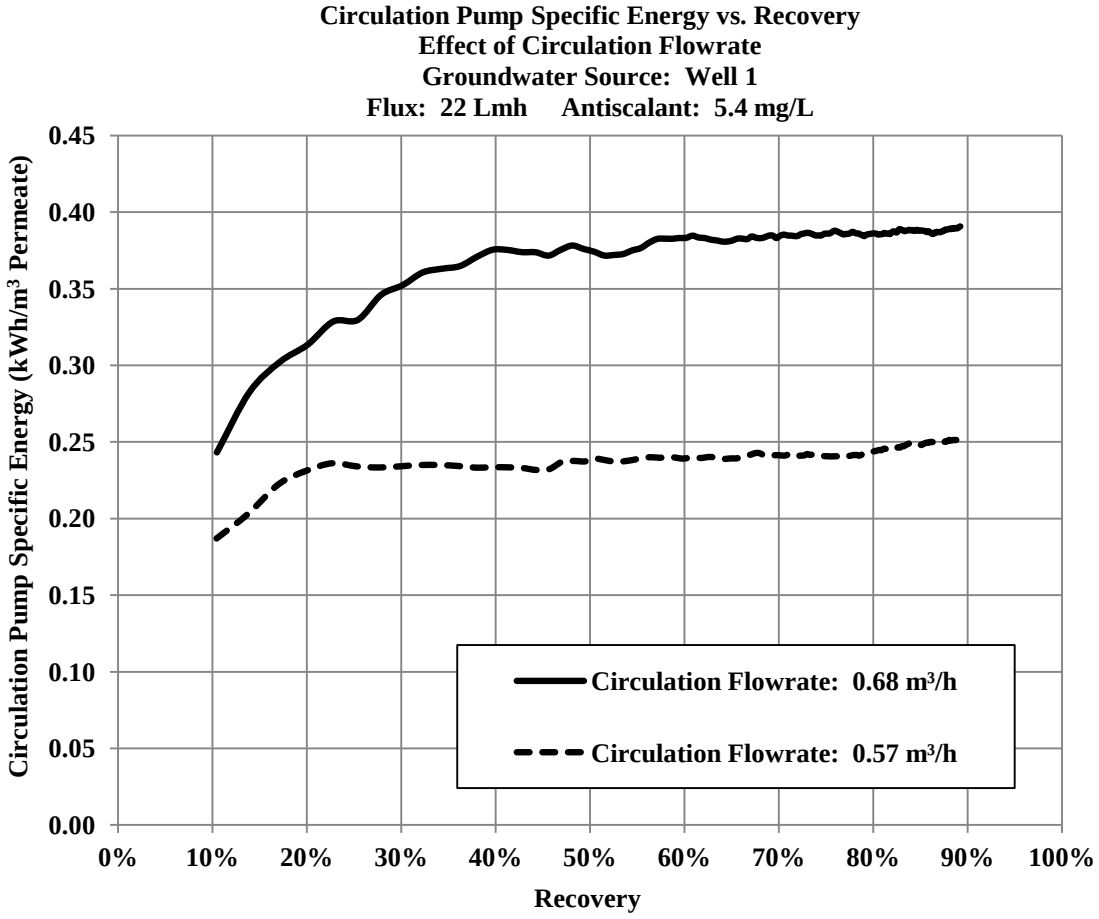

Figure 4.19 Circulation pump specific energy vs. recovery. Impact of circulation flowrate. Groundwater source: Well 1. Permeate flux: 22 Lmh. Circulation flowrates: 0.57 and 0.68 m^3/h. Antiscalant: 5.4 mg/L.

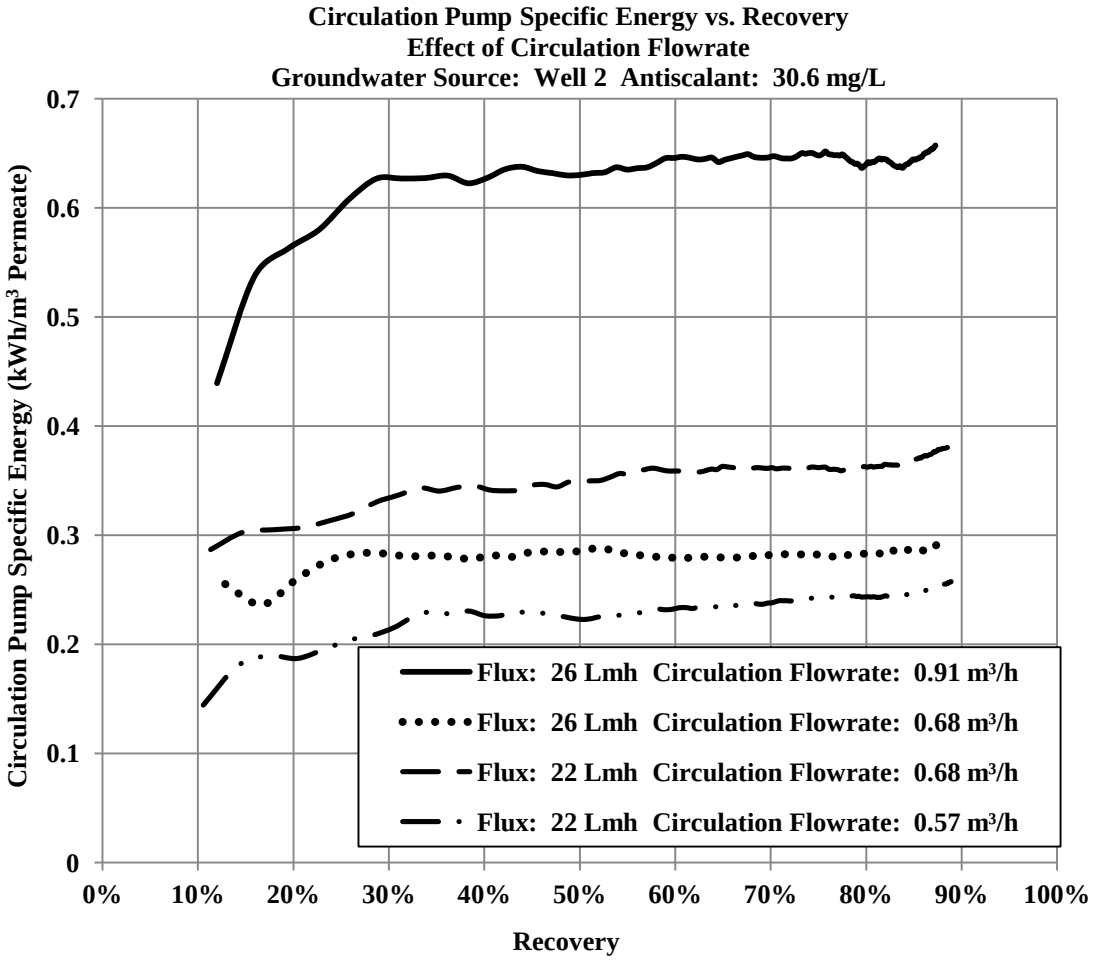

Figure 4.20 Circulation pump specific energy vs. recovery. Effect of circulation flowrate. Groundwater source: Well 2. Permeate flux: 26 and 22 Lmh. Circulation flowrates: 0.57, 0.68, and 0.91 m^3/h. Antiscalant concentration: 30.6 mg/L.

For desalination of groundwater from Well 1, raising the circulation flowrate from 0.57 m^3/h to 0.68 m^3/h at a target permeate flux of 22 Lmh represented an increase of approximately 19 percent. However, the corresponding increase in circulation pump specific energy at recoveries from 40 percent to 90 percent for this change was over 50 percent. For desalination of groundwater from Well 2, raising the circulation flowrate from 0.68 m^3/h to 0.91 m^3/h at a target permeate flux of 26 Lmh represented an increase of nearly 34 percent. The estimated increase in circulation pump specific energy from this change in circulation flowrate was over 100 percent. Clearly, circulation pump specific energy was not a simple linear function of

circulation flowrate alone. The relationship between specific energy and flowrate more closely resembled an exponential relationship that would seem to indicate that head losses, which are a function of flow velocity squared, played a major role, possibly the dominant role, in determining energy consumption by the circulation pump.

Effect of Multiple Operating Cycles on Feed Pump Specific Energy

The previous figures and discussions focused on specific energy as a function of first operating cycle recovery. As defined previously, an operating cycle was the period of time from the commencement of filtration mode to the end of the corresponding discharge operation. During discharge, accumulated concentrate was flushed from the holding tank, which was isolated from the rest of the small-scale RO system. A more representative analysis of the energy consumption of the small-scale RO system would also include multiple operating cycles, since the system would likely be operated for more than one cycle. Figure 4.21 presents specific energy as a function of elapsed operating time for desalination of the groundwater source with the highest scaling potential, Well 2, over more than one operating cycle in order to better estimate the energy consumption during actual use of the system under “real world” conditions. The results are presented for several combinations of feed/permeate flowrate and circulation flowrate.

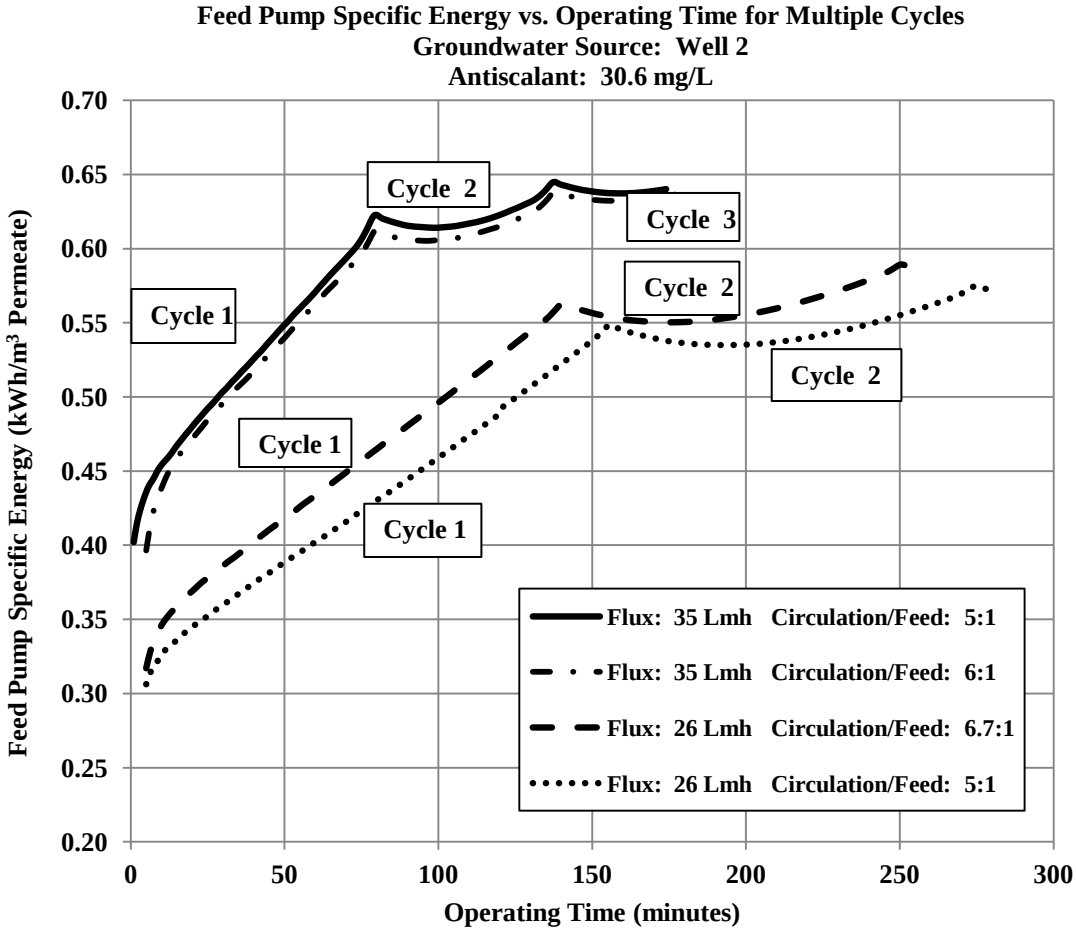

Figure 4.21 Effect on feed pump specific energy of multiple operating cycles. Groundwater source: Well 2.

As shown by these results, the sharpest rise in specific energy with operating time occurred in the first operating cycle. After the first operating cycle, specific energy appeared to level off for all feed and circulation flowrates. In addition to the stabilization of specific energy with operating time after the first operating cycle, the most noticeable features of the graphs include the presence of spikes in specific energy between cycles and the shortening of operating cycles after the first cycle. These spikes corresponded to the discharge processes that typically lasted from six to seven minutes. One explanation for these spikes was the relatively abrupt rise in feed pump pressure that occurred during discharge. These features possibly resulted from the isolation of the system from the holding tank. The holding tank, which must be flushed during discharge, provided a damping effect during filtration mode on the rise

in salinity of the concentrate stream by creating an additional 43.5 L of mixing and dilution volume. Once this tank and its additional volume became unavailable to the process during discharge, the salinity and osmotic pressure of the concentrate stream rose very abruptly, increasing the overall operating pressure and the energy consumption of the process and causing a temporary increase in the slope of the specific energy vs. time curve. One potential means to address this issue would be to supply the system with a backup holding tank that could be connected to the system through automatic valves once discharge had begun. However, care would need to be exercised in the configuration of the valves and the timing of their opening and closing to minimize pressure drops and head losses. The shortening of operating cycles commencing with the second cycle was potentially due to residual salt in the system from previous cycles. The gradual buildup of salts over time enabled the pressure to rise more rapidly over time during "normal" mode of operation. Since the timing of discharge was not only based upon recovery, but was also based upon operating pressure, salt accumulation translated into more rapid pressure rise and shorter cycles. The accumulation of salt was the result of inefficient flushing of the holding tank and other portions of the system during discharge. One potential solution to inefficient flushing of the holding tank would be the installation of baffles to create "plug" flow and reduced mixing within the holding tank.

Equally significant to the assessment of the small-scale system was the evidence provided by these graphs that the specific energy did not rise continuously throughout the process and appeared to approach a limiting value. A permeate flux of 26 Lmh fell within the range recommended by the manufacturer for groundwater or surface water desalination, while a permeate flux of 35 Lmh was above the recommended range. Even at a permeate flux in excess of the manufacturer's recommended range over multiple operating cycles, the feed pump specific energy remained below 1.0 kWh/m^3. These results were obtained for the groundwater source with the highest fouling potential and highest TDS level at an antiscalant concentration of approximately 30 mg/L.

Effect of Feed Chemistry on Feed Pump Specific Energy

Energy consumption for desalination of brackish groundwater is dependent upon fouling potential and the chemistry of feed. To demonstrate the impact of feed chemistry on energy consumption, Figures 4.22 through 4.24 present specific energies for desalination of groundwater from Wells 1, 2 and 3 and for desalination of laboratory reagent solutions of NaCl at concentrations of 1,000, 2,500 and 5,000 mg/L. Results were obtained at a target permeate flux of 26 Lmh and for recoveries up to 90 percent. The target circulation flowrate was 0.68 m^3/h, corresponding to a ratio of circulation flowrate to feed flowrate of 5:1.

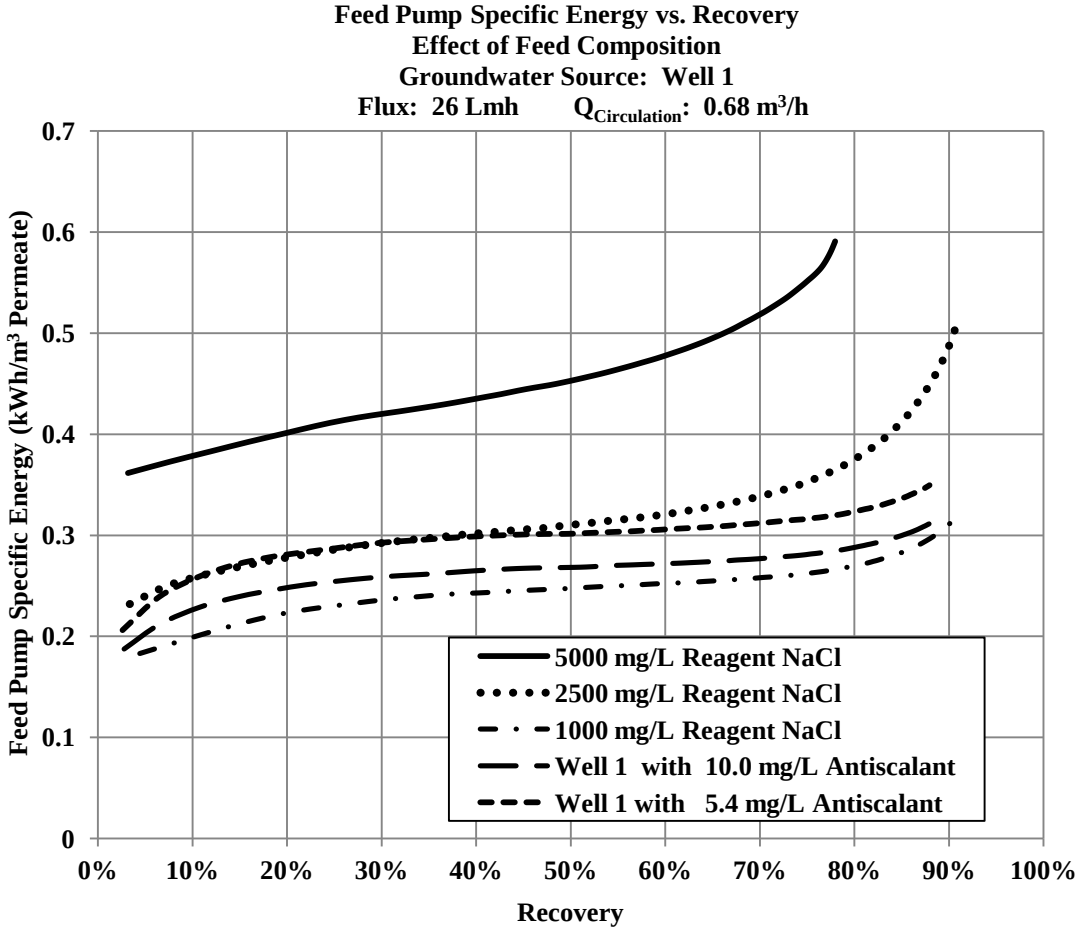

Figure 4.22 Feed pump specific energy vs. recovery. Effect of feed chemistry. Well 1 groundwater and reagent NaCl solutions.. Permeate flux: 26 Lmh.

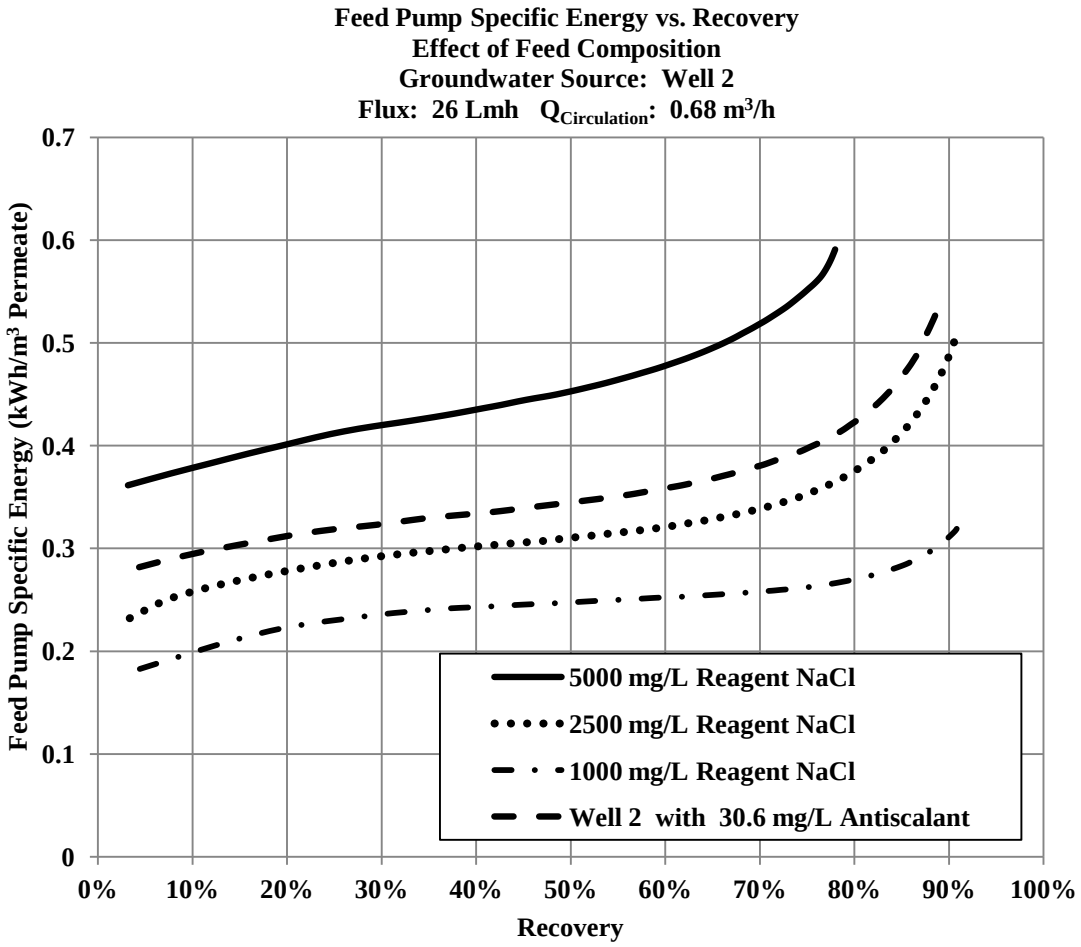

Figure 4.23 Feed pump specific energy vs. recovery. Effect of feed chemistry. Well 2 groundwater and reagent NaCl solutions. Permeate flux: 26 Lmh.

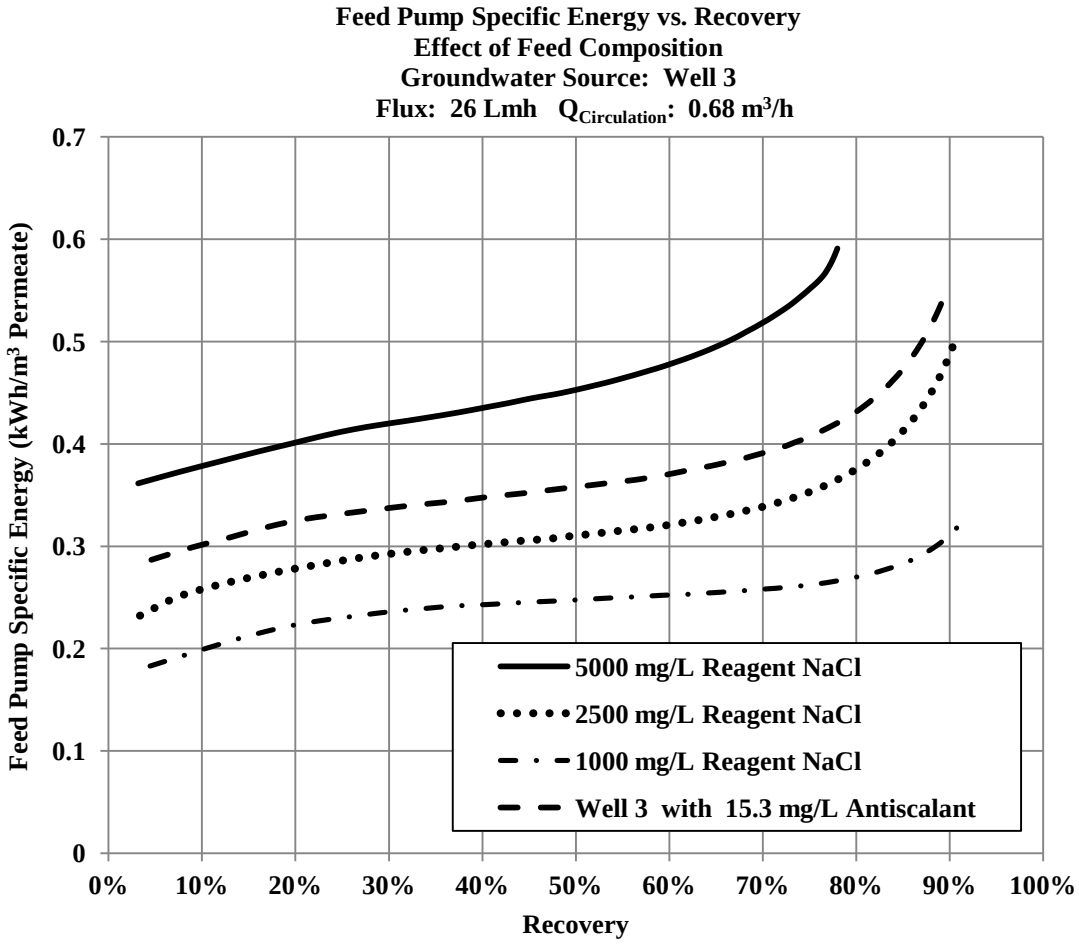

Figure 4.24 Feed pump specific energy vs. recovery. Effect of feed chemistry. Well 3 groundwater and reagent NaCl solutions. Permeate flux: 26 Lmh.

According to the most recent groundwater monitoring data available, from August 2011 (Tetra Tech, 2011), the TDS levels in groundwater from Well 1, 2, and 3 were 1,240 mg/L, 5,900 mg/L, and 4,290 mg/L, respectively. Based on levels of TDS alone and neglecting antiscalant concentration, fouling potential, and potential for CP, we would expect the specific energy curve for Well 1 groundwater desalination to lie between the curve for desalination of 1,000 and 2,500 mg/L NaCl solutions and to more closely coincide with the 1,000 mg/L specific energy curve. We would predict the specific energy curve for desalination of groundwater from Well 3 to lie between the curves for 2,500 mg/L and 5,000 mg/L NaCl, and the specific energy curve for desalination of Well 2 groundwater to lie above the curve for desalination of 5,000

mg/L NaCl. Specific energy vs. recovery curves for desalination of Well 1 groundwater at an antiscalant concentration of 10.0 mg/L and for desalination of Well 3 groundwater at an antiscalant concentration of 15.3 mg/L agreed reasonably well with behavior based on TDS levels alone, while the specific energy curve for desalination of Well 1 groundwater at an antiscalant concentration of 5.4 mg/L more closely coincided with the curve for desalination of 2,500 mg/L NaCl, although the TDS level in the reagent NaCl solution was nearly twice as high as that of Well 1 groundwater. The specific energy curve for desalination of Well 2 groundwater at an antiscalant concentration of 30.6 mg/L was significantly lower than the curve we would predict based on TDS level alone and actually coincided with the specific energy curve for desalination of Well 3 groundwater at an antiscalant concentration of 15.3 mg/L.

The van't Hoff Equation and the Effect of Heavy Ions on Osmotic Pressure and Feed Pump Specific Energy

The impact of brackish groundwater chemical composition and TDS levels on energy consumption by the feed pump may be explained in terms of the van't Hoff equation, provided as Equation 4.9. The van't Hoff equation relates osmotic pressure to total ion molarity:

$$\Delta\pi = RT\sum m_i \tag{4.9}$$

where $\Delta\pi$ is the osmotic pressure, R is the Universal Gas Constant, T is the absolute temperature (K) and m_i is the molar concentration of all ionic species. Because well water from all three wells at BGNDRF had a relatively high concentration of relatively heavy Group IIA ions, i.e., Ba^{2+}, Sr^{2+} and Ca^{2+}, the actual total ionic molarity was much lower for a given TDS level than it would have been for pure NaCl, which consists of relatively light ions. As a result, the ability of well water at BGNDRF to create osmotic pressure was much less for a given TDS level than it would have been for pure NaCl. This lower osmotic pressure would result in lower required system pressure and energy consumption.

Additional Scenarios for Observed Behavior

The following scenarios may offer additional explanations for observed feed pump specific energy curves. At the high antiscalant concentration used for desalination of Well 2 groundwater, membrane fouling was largely eliminated. In addition, CP had potentially increased the osmotic pressure at the membrane surface significantly for solutions at 2,500 and 5,000 mg/L NaCl. Because the molar concentration of ionic species was much less for groundwater from Well 2 than the corresponding concentration in 5,000 mg/L NaCl due to the heavier ions in Well 2 groundwater, this could at least partially explain the position of the Well 2 desalination curve between the specific energy curves for 2,500 mg/L and 5,000 mg/L NaCl.

The concentration of antiscalant used for desalination of Well 3 groundwater was sufficient to eliminate membrane fouling, but had not significantly affected CP. The antiscalant added to Well 3 groundwater created an aqueous environment at the membrane surface that behaved similarly to NaCl at roughly the same concentration, i.e., 4,000 mg/L.

Although an antiscalant concentration of 5.4 mg/L for desalination of groundwater from Well 1 was based on recommendations by the manufacturer, it potentially did not represent an optimal concentration for addressing membrane fouling. Raising the concentration to 10.0 mg/L largely eliminated the potential for membrane fouling, but did not significantly affect CP, creating an environment very similar to aqueous NaCl at a concentration of 1,000 mg/L.

Assessment of Energy Consumption by the Small-Scale RO System

Total specific energies were determined for the small-scale RO system for all test conditions referenced in this chapter by summing the specific energy contribution for the feed pump and the specific energy contribution for the circulation pump. Values for feed pump specific energy and total specific energy at the maximum first cycle recovery are presented in Table 4.6. Maximum recoveries provided were for the first operating cycle and do not represent maximum achievable recoveries, but represent the point in testing during the first operating cycle where operation was

Table 4.6 Feed pump and total specific energy values for test conditions referenced in Chapter IV.

Feed Source	Permeate Flux (Lmh)	Mean Crossflow Velocity (m/s)	Antiscalant Conc. (mg/L)	Recovery (%)	Feed Pump Specific Energy (kWh/m^3)	Total Specific Energy (kWh/m^3)
Well 1	22	0.13	5.4	90	0.31	0.56
Well 1	22	0.16	5.4	90	0.31	0.70
Well 1[1,2]	22	0.16	5.4	82	0.28	0.65
Well 1	26	0.16	5.4	88	0.35	0.68
Well 1	26	0.16	10.0	85	0.32	0.64
Well 1[1]	26	0.16	10.0	90	0.32	0.60
Well 1	26	0.17	10.0	90	0.33	0.66
Well 1	26	0.19	5.4	87	0.32	0.83
Well 1	26	0.19	10.0	88	0.33	0.78
Well 1	26	0.21	5.4	89	0.37	1.02
Well 1	26	0.21	10.0	90	0.34	0.88
Well 1	35	0.21	5.4	90	0.47	0.99
Well 1	35	0.21	10.0	91	0.43	0.83
Well 1	35	0.23	10.0	90	0.43	0.96
Well 1	35	0.25	5.4	90	0.49	1.29
Well 1	35	0.25	10.0	90	0.44	1.10
Well 1	44	0.25	10.0	90	0.53	1.12
Well 2	22	0.13	30.6	90	0.50	0.76
Well 2[1]	22	0.13	30.6	90	0.56	0.85
Well 2	22	0.16	30.6	90	0.51	0.90
Well 2[1]	22	0.16	30.6	90	0.54	0.94
Well 2	26	0.16	30.6	89	0.55	0.85
Well 2	26	0.21	30.6	88	0.56	1.21
Well 2	35	0.21	30.6	85	0.62	1.10
Well 2[1]	35	0.21	30.6	84	0.61	1.12
Well 2[2]	35	0.21	0.0	82	0.64	1.17
Well 2	35	0.25	30.6	85	0.61	1.37
Well 2	35	0.25	0.0	86	0.69	1.55
Well 2	39	0.24	30.6	83	0.64	1.23
Well 3	22	0.13	15.3	90	0.48	0.74
Well 3	22	0.16	15.3	90	0.48	0.88
Well 3[1]	22	0.16	15.3	90	0.49	0.89
Well 3	26	0.16	15.3	90	0.55	0.91
Well 3	26	0.21	15.3	90	0.55	1.22
Well 3	35	0.21	15.3	87	0.61	1.13
Well 3[1]	35	0.21	15.3	86	0.62	1.16
Well 3	35	0.25	15.3	87	0.62	1.42

[1]Duplicate test. [2]Test aborted due to electrical failure during thunderstorm.

switched to discharge mode due to having reached 90 percent recovery or having reached safe operating pressure limits.

Assessment of VCCC

The primary focus of this study was the assessment of VCCC as a means to increase recovery and reduce energy consumption for small-scale brackish desalination under "field" conditions with groundwaters of variable scaling potential. As part of that assessment, comparisons were made between specific energy values determined for the experimental small-scale system and values published for conventional large-scale RO systems. Recent published specific energy values for large-scale systems generally ranged from 0.4 to 1.0 kWh/m^3 of permeate, with some estimates as high as 3.0 kWh/m^3. Exceptionally high values were considered nonrepresentative values for purposes of this analysis. Values considered more representative of specific energies for large-scale brackish RO facilities have been provided in Table 4.7.

Table 4.7 Reported specific energy values for large-scale RO facilities.

Specific Energy (kWh/m^3)	Description	Recovery (%)	Source and Year
1.5	Product information from Lenntech website	65-80 percent	Lenntech, 2011
1.02	Reim 2 brackish RO facility[1]	88	Stover, 2011
0.80	Reim 1 brackish RO facility[2]	88	Stover, 2011
0.61	Kay Bailey Hutchison RO Facility, El Paso, TX	81	McHarg, 2010
0.45	Kay Bailey Hutchison RO Facility, with isobaric ERDs	81	McHarg, 2011
0.8	Representative value for brackish water RO	60	Stover, 2009
0.6 to 0.9	Representative value for brackish water RO	Not Available	Vince and others, 2007

[1]Process uses closed-circuit desalination (concentrate recycle), coupled with plug-flow desalination.
[2]Process uses closed-circuit desalination only.

In addition, one recent source provided a theoretical energy requirement for conventional single stage brackish RO of 0.54 kWh/m^3 without energy recovery devices and a corresponding theoretical energy requirement of 0.26 kWh/m^3 for CCD (Qiu and Davies, 2012). Based on values provided by several recent sources, and omitting product information provided by manufacturers, a range of 0.4 to 1.0 kWh/m^3 for conventional large-scale RO facilities has been used when performing the comparison.

The feed pump contribution to total specific energy for the small-scale RO system was within the assumed specific energy range reported for large-scale RO facilities for target permeate fluxes ranging from 22 Lmh to 44 Lmh for all raw feed salinities, circulation flowrates and recoveries. Manufacturer data provided for Dow Filmtec brackish membranes provides a "typical" target permeate flux of 14 gfd (24 Lmh) for surface water treatment and 18 gfd (31 Lmh) for well water treatment for "light industrial" applications. In addition, total specific energy did not exceed 1..0 kWh/m^3 at permeate fluxes up to 35 Lmh and recoveries up to 90 percent for desalination of Well 1 groundwater at the highest antiscalant dosage and at moderate circulation flowrates. Total specific energy did not exceed 1.0 kWh/m^3 at permeate fluxes up to 26 Lmh and recoveries approaching 90 percent for desalination of Wel1 2 and Well 3 groundwater with antiscalant. A permeate flux of 26 Lmh lies between the Dow Filmtec "typical" values for surface water treatment and groundwater treatment (Dow, 2011).

Test results indicated that VCCC employing pressurized concentrate circulation is a viable technology for maximizing recovery and energy efficiency of small-scale inland brackish RO desalination. Results also indicated that relatively minor design changes have the potential to reduce specific energy of the small-scale RO process further and enable this technology to produce permeate from brackish groundwater with moderate to high inorganic fouling potential at specific energies comparable to or superior to conventional large scale RO systems.

Factors Impacting Permeate Quality

Research has indicated that inorganic fouling can adversely affect salt rejection and permeate quality. Hoek and Elimilech (2003) believed that the fouling layer may trap ionic species at the membrane surface possibly by inhibiting back diffusion. This process can increase the passage of affected ions through the membrane. Foulants of inorganic origin include sparingly soluble salts and inorganic colloids. It is believed that CP can adversely affect permeate quality, also by concentrating ionic species at the membrane surface. It follows that any factor that reduces either inorganic fouling or CP has the potential to improve permeate quality. Increasing permeate flux is believed to enhance CP. If the feed contains fouling species at sufficiently high concentrations, increased flux also translates into higher risk of inorganic fouling. On the other hand, increased crossflow velocity within the membrane channel results in higher shear that not only reduces CP but also reduces the risk of fouling. Although membrane channel crossflow velocity for the small-scale RO system was determined by the feed flowrate and the circulation flowrate, circulation flowrate had a much larger impact on crossflow velocity during testing of the system because the process was designed to operate at circulation flowrates that were multiples of the feed flowrate. Another factor that can reduce the severity of inorganic fouling and potentially improve permeate quality is the use of antiscalants.

In order to demonstrate the impact of permeate flux on permeate quality for groundwater with significant potential for inorganic fouling and for CP, permeate conductivity data are plotted as a function of recovery in Figure 4.25 for desalination of Well 2 groundwater at target circulation flowrates of 0.68 and 0.91 m^3/h. Data are provided for desalination at two permeate fluxes for each circulation flowrate. In order to demonstrate the impact of circulation flowrate and crossflow velocity on permeate quality, permeate conductivity is plotted in Figure 4.26 as a function of recovery for desalination of groundwater from Well 2 at fluxes of 35 Lmh and 22 Lmh. Conductivity data are presented at two circulation flowrates for each flux. Permeate conductivity data are presented in Figure 4.27 for desalination of Well 2 groundwater at a target permeate flux of 26 Lmh for two circulation flowrates.

Flowrates and permeate fluxes were target values used to control the system and varied up to 10 percent during desalination tests.

During testing, permeate conductivity data were subject to significant fluctuations, expecially at low recoveries. These fluctuations obscured trends and made data analysis more difficult. In order to reduce these fluctuations and better represent general trends, permeate conductivity data were reported as three-minute averages. For each recovery, the logged conductivity value at that recovery was averaged with the logged measurement that immediately preceded it and the measurement that immediately followed it. In addition, values that were obvious anomalies, i.e., extremely large or extremely small, when compared to other values within the same three-minute timespan, were not used in the computation. Generally, fluctuations in measured conductivity decreased significantly in magnitude at recoveries above 70 percent. It should also be noted that a calibrated conductivity meter provided duplicate measurements to validate the reliability of reported permeate conductivities.

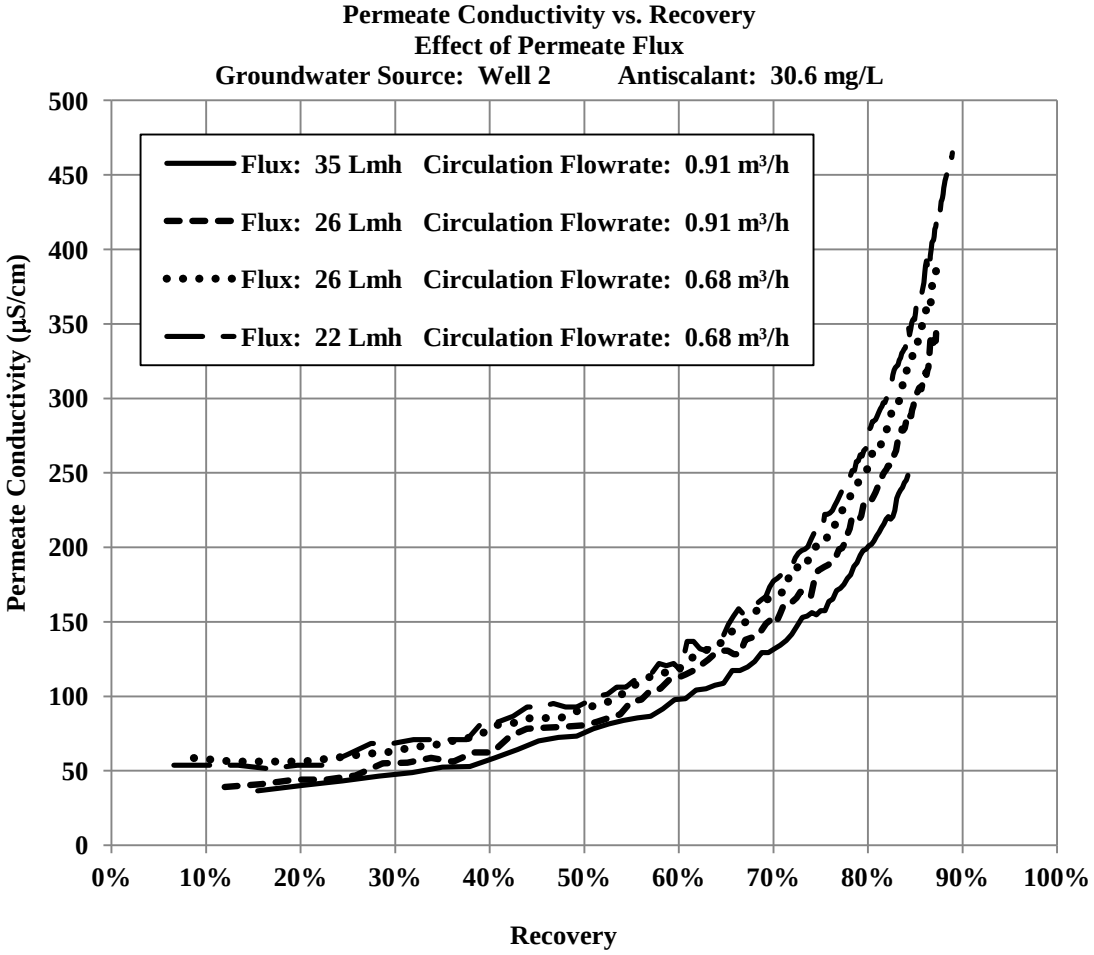

Figure 4.25 Permeate conductivity vs. recovery. Effect of permeate flux. Circulation flowrates: 0.68 and 0.91 m^3/h. Groundwater source: Well 2. Antiscalant: 30.6 mg/L.

Permeate flux can impact salt rejection and permeate quality through two competing processes. While increasing permeate flux can also increase CP, potentially leading to reduced salt rejection and worsening permeate quality, increased flux can also lead to a dilution effect that has the opposite impact on permeate quality. The dilution effect occurs when increases in pressure increase water flux across the membrane but do not increase salt flux, resulting in permeate with a lower TDS concentration. At circulation flowrates of 0.68 and 0.91 m^3/h, increasing permeate flux appeared to reduce permeate conductivity slightly. These results indicated that the dilution effect predominated under these tests conditions

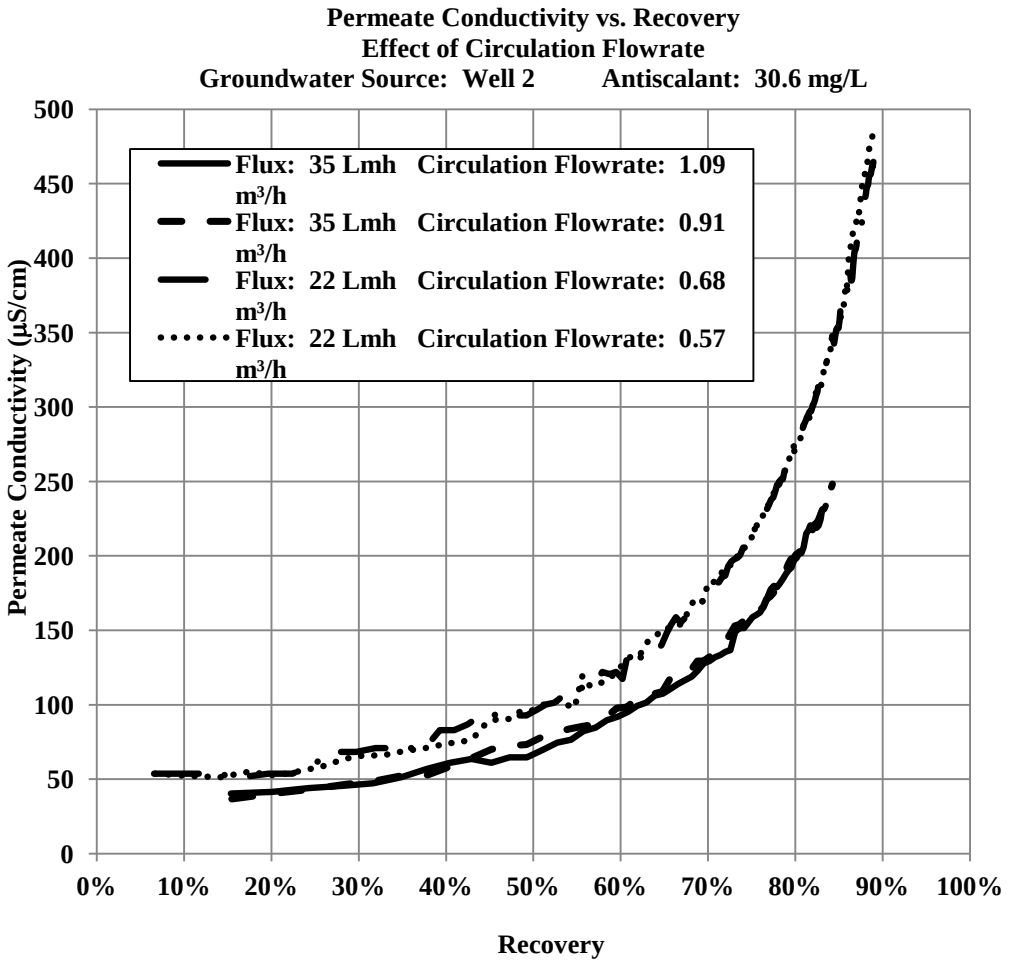

Figure 4.26 Permeate conductivity vs. recovery. Impact of circulation flowrate. Permeate fluxes: 35 and 22 Lmh. Groundwater source: Well 2. Antiscalant: 30.6 mg/L.

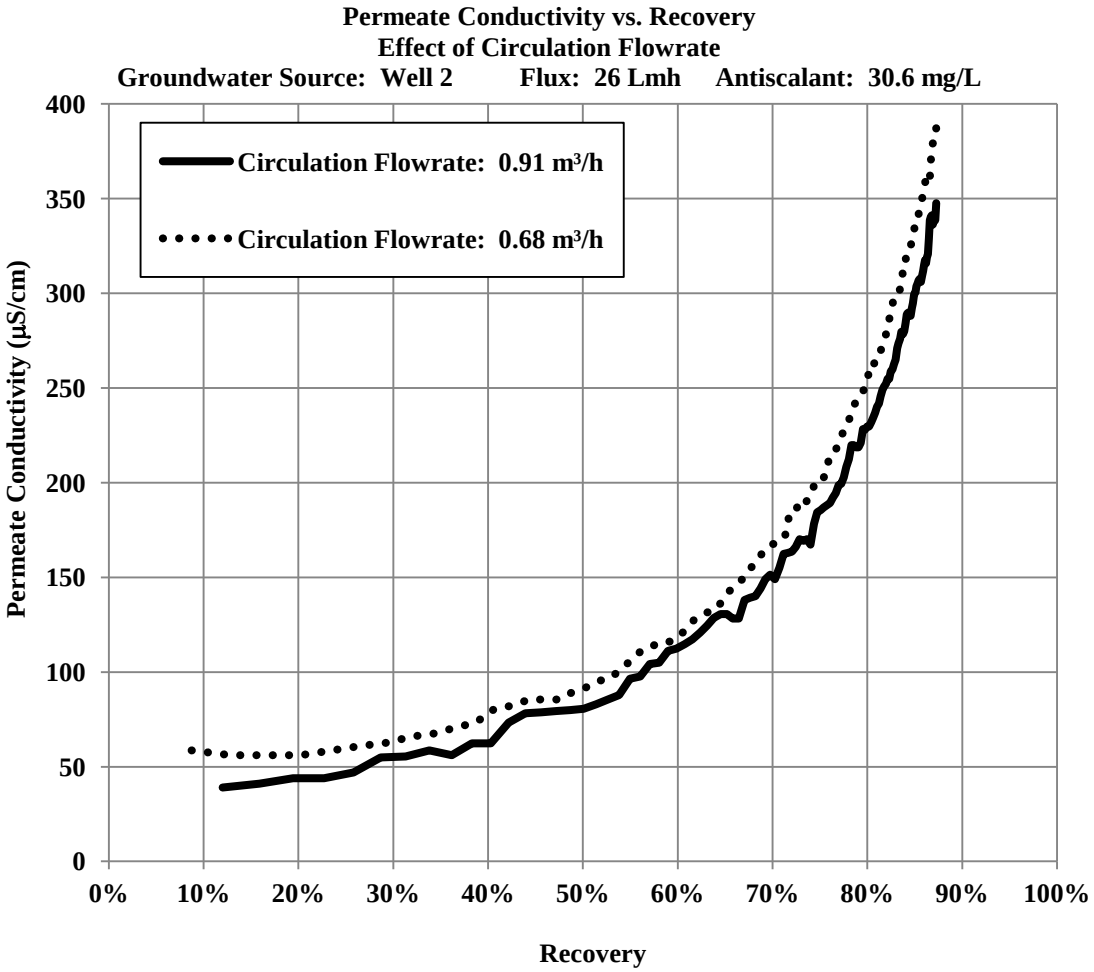

Figure 4.27 Permeate conductivity vs. recovery. Impact of circulation flowrate. Permeate flux: 26 Lmh. Groundwater source: Well 2. Antiscalant: 30.6 mg/L.

Data presented in Figure 4.26 indicated that increasing the circulation flowrate from 0.57 to 0.68 m^3/h at a flux of 22 Lmh had a neglible impact on permeate quality at all first cycle recoveries. In addition, increasing the circulation flowrate from 0.91 m^3/h to 1.09 m^3/h at a flux of 35 Lmh had no significant effect. On the other hand, raising the circulation flowrate from 0.68 m^3/h to 0.91 m^3/h had a small but measurable impact at a flux of 26 Lmh. These results are explainable in terms of the relative increases in crossflow velocity that occurred as the result of these changes in circulation flowrate. Crossflow velocities were estimated using Equations 4.2 and 4.3. Based on a membrane surface area of 2.6 m^2, a permeate flux of 35 Lmh was equivalent to a feed and permeate flowrate of 0.18 m^3/h. Combining this feed flowrate

with a circulation flowrate of 0.91 m^3/h created an inlet crossflow velocity of 0.21 m/s, an outlet crossflow velocity of 0.17 m/s, and a mean crossflow velocity of 0.19 m/s . Increasing the circulation flowrate at this flux to 1.09 m^3/h created an inlet crossflow velocity of 0.24 m/s, an outlet crossflow velocity of 0.21 m/2, and a mean crossflow velocity of 0.22 m/s. This represented an increase in mean crossflow velocity of 18 percent. A permeate flux of 22 Lmh was equivalent to a feed and permeate flowrate of 0.11 m^3/h. At this flux, a circulation flowrate of 0.57 m^3/h created an inlet crossflow velocity of 0.13 m/s, an outlet crossflow velocity of 0.11 m/s and a mean crossflow velocity of 0.12 m/s. Increasing the circulation flowrate to 0.68 m^3/h raised the inlet crossflow velocity to 0.15 m/s and the outlet crossflow velocity of 0.13 m/s. The mean crossflow velocity at this flux was 0.14 m/s, representing an increase in mean crossflow velocity of 18 percent. Conductivity data presented in Figure 4.26 indicated that increases in crossflow velocity of this magnitude did not significantly reduce permeate conductivity or improve permeate quality in terms of TDS concentration for test conditions. A permeate flux of 26 Lmh corresponded to a feed and permeate flowrate of 0.14 m^3/h. A circulation flowrate of 0.68 m^3/h at this flux created an inlet crossflow velocity of 0.16 m/s, an outlet crossflow velocity of 0.13 m/s and a mean crossflow velocity of 0.14 m/s. Raising the circulation flowrate to 0.91 m^3/h increased the inlet crossflow velocity to 0.20 m/s, the outlet crossflow velocity to 0.17 m/s and the mean crossflow velocity to 0.19 m/s. The corresponding increase in mean crossflow velocity represented an increase of 30 percent. Data presented in Figure 4.27 indicated that an increase in mean crossflow velocity of this magnitude resulted in a slight reduction in permeate conductivity and a small improvement in permeate quality in terms of TDS concentration.

Based upon the role of antiscalants in the brackish RO process, it was expected that the addition of antiscalant or an increase in antiscalant concentration had the potential to improve permeate quality. In order to demonstrate the effect of antiscalant, permeate conductivities are presented in Table 4.8 for desalination of Well 1 and Well 2 groundwater at recoveries of approximately 50 percent and 80 percent for a target permeate flux of 35 Lmh.

Table 4.8 Permeate conductivities at select recoveries for desalination of Well 1 and Well 2 groundwater. Effect of antiscalant.

Source	Permeate Flux (Lmh)	Circulation Flowrate (m^3/h	Mean Crossflow Velocity (m/s	Recovery (%)	Antiscalant Concentration (mg/L)	Permeate Conductivity (μS/cm)
Well 1	35	1.09	0.23	53.3	10.0	7.3
Well 1	35	1.09	0.23	79.7	10.0	22.0
Well 1	35	1.09	0.23	52.0	5.4	8.1
Well 1	35	1.09	0.23	79.8	5.4	14.7
Well 1	35	0.91	0.19	49.6	10.0	7.3
Well 1	35	0.91	0.19	79.9	10.0	22.0
Well 1	35	0.91	0.19	49.8	5.4	8.5
Well 1	35	0.91	0.19	79.8	5.4	14.7
Well 2	35	1.09	0.23	54.3	30.6	76.5
Well 2	35	1.09	0.23	79.9	30.6	197.0
Well 2	35	1.09	0.23	53.8	0.0	65.9
Well 2	35	1.09	0.23	79.6	0.0	150.0
Well 2	35	0.91	0.19	52.6	30.6	81.4
Well 2	35	0.91	0.19	79.8	30.6	198.6
Well 2	35	0.91	0.19	52.3	0.0	56.2
Well 2	35	0.91	0.19	79.8	0.0	156.3

[1]Reported conductivity values are three-minute averages.

For desalination of Well 2 groundwater at a target flux of 35 Lmh and recoveries of approximately 80 and 50 percent, adding antiscalant had the opposite effect to what was expected, based on the role of antiscalants in the RO process. Rather than reducing permeate conductivity and improving permeate quality, the addition of antiscalant at a concentration of 30.0 mg/L actually increased permeate conductivity. Similar behavior was observed for desalination of Well 1 groundwater for the same flow conditions and recovery of approximately 80 percent, when the antiscalant concentration was increased from 5.4 to 10.0 mg/L. For desalination of Well 1 groundwater at approximately 50 percent, the permeate conductivity was actually higher at the lower antiscalant concentration. This can be partially explained on the basis of relative fluctuations at very low conductivity readings. Because Well 1 groundwater had a much lower TDS level than Well 2 groundwater, the permeate had a much lower conductivity, assuming a similar salt rejection. Conductivity readings for desalination of Well 1 groundwater had a much smaller signal to noise ratio and greater potential relative error than conductivity measurements for desalination of Well 2 groundwater. The higher conductivity readings for desalination of Well 2 groundwater at increased antiscalant doses, however, may be indicative of undesirable side effects of antiscalants when these chemicals are used at very high concentrations. Side effects listed by other researchers include biofouling (Vrouwenvelder and others, 2000) and enhanced scaling (Maeleb and Ayoub, 2011). Biofouling is not a likely cause due to the short timeframes involved in the desalination tests described here. A more plausible explanation may be due to behavior described by Amiri and Samei (2007), who observed improved permeate quality and salt rejection, accompanied by flux decline. They attributed this to inorganic fouling, i.e., scaling. It is possible that what was observed during the present study was an example of increased salt rejection accompanying membrane scaling by sparingly soluble salts. When antiscalant concentration was increased, scaling was reduced, also resulting in a reduction in salt rejection. It is possible that the scaling layer, while providing resistance to water flux, provided even greater resistance to salt flux, leading to an actual net improvement in permeate quality. Another possible explanation for this behavior would be a higher

concentration of free ions, for example, sulfate, at the membrane surface resulting from the binding of potential attachment sites on the scaling layer by antiscalants. More of these ions would be free to pass through membranes at higher antiscalant concentrations. It is also possible that negatively charged antiscalant species passed through the membrane at higher antiscalant concentrations. Regardless of the precise mechanism responsible for increasing permeate conductivity, these results indicated that antiscalant concentrations may need to be more tightly controlled to optimize permeate quality, permeate flux, and energy consumption.

Conclusions

A small-scale RO system employing closed concentrate circulation (VCCC) and single parallel membrane elements was used to desalinate brackish groundwater from three wells at the BGNDRF facility in Alamogordo, New Mexico. The small-scale system incorporated features used in a similar process (CCD), patented by Efraty (2009, 2010, and 2011). The three groundwater sources provided a wide range of TDS levels and potentials for inorganic fouling. Antiscalant was added to all three groundwaters in concentrations based upon assessed scaling potential of combined feed and circulating concentrate at target recoveries. The small-scale system was operated at recoveries up to approximately 90 percent. Specific energy was determined for permeate production at target permeate fluxes ranging from 22 Lmh to 44 Lmh. Manufacturer permeate flux recommendations for desalination of feed water of similar quality range from 14 to 18 gfd (24 to 31 Lmh).

The feed pump component of the specific energy was below 1.0 kWh/m^3 at maximum first cycle recovery for desalination of all groundwaters tested for all feed and circulation flowrates and antiscalant concentrations. This includes desalination of Well 2 groundwater containing no added antiscalant. Total specific energy did not exceed 1.0 kWh/m^3 at 90 percent first cycle recovery for desalination of groundwater from Well 1 at a target permeate flux up to 26 Lmh for all circulation flowrates and antiscalant concentrations. In addition, total specific energy for desalination of Well 1 groundwater did not exceed 1.0 kWh/m^3 for a flux of 35 Lmh at circulation flowrates up to 1.0 m^3/h. Total specific energy for desalination of Well 2 and Well 3

groundwater did not exceed 1.0 kWh/m^3 at a target permeate flux of 26 Lmh for all circulation flowrates, with the exception of 0.91 m^3/h. These results were achieved at recoveries approaching 90 percent.

Experimental results demonstrated that an RO system using VCCC and a parallel configuration of single membrane elements can achieve recovery and energy efficiency comparable to or superior to those of conventional RO systems with large numbers of membrane elements arranged in multiple stages of long pressure vessels, if operated at permeate fluxes appropriate to the water being treated. The small-scale RO system described here demonstrated that it could achieve these results in the treatment of brackish groundwaters of variable scaling potential, using antiscalant in concentrations ranging from approximately 5 mg/L to 30 mg/L, depending upon the assessed scaling potential.

Tests indicated that addition of antiscalant reduced energy consumption in desalination of groundwater with potential for inorganic fouling, and that increases in antiscalant concentration up to an "optimal" concentration can result in further reductions in specific energy. For one groundwater source tested, increasing the antiscalant concentration reduced energy consumption by several percent. Results of these tests also indicated that the use of circulation flowrate as a means to increase crossflow velocity and shear has the potential to reduce energy consumption in desalination of brackish groundwater with potential for inorganic fouling, with or without added antiscalant. It is noteworthy that the beneficial effects of antiscalant were observed in relatively short-term tests of one- to two-hour duration. The energy-saving benefits of increased crossflow velocity are potentially due to reduced CP at the higher circulation flowrates in desalination of high TDS groundwater.

BIBLIOGRAPHY

Amiri, M. C. & Samiei, M. (2007). Enhancing permeate flux in a RO plant by controlling membrane fouling. *Desalination, 207,* 361-369.

Austin, A. E., Miller, J. F., Vaughan, D. A. & Kircher, J. F. (1975). Chemical additives for calcium sulfate scale control. *Desalination, 16,* 345-357.

Bartman, A. R., Lyster, E., Rallo, R., Christofides, P. D. & Cohen, Y. (2011). Mineral scale monitoring for reverse osmosis desalination via real-time membrane surface image analysis. *Desalination, 273,* 64-71.

Borden, J., Gilron, J. & Hasson, D. (1987) Analysis of RO flux decline due to membrane surface blockage. *Desalination, 66,* 257-269.

Bratt, R. I. (1989). *U.S. Patent No. 4,814,086*. Washington D.C. U.S. Patent and Trademark Office.

Desaulniers, J. W. (1997). *U.S. Patent No. 5,647,973*. Washington D.C. U.S. Patent and Trademark Office.

Dow Chemical Company. (2011) Technical manual excerpt: Filmtec membranes. System design: membrane system design guidelines. Retrieved in 2011 from company website: http://dowwaterandprocess.com/resources/en.

Dow Chemical Company, (Filmtec® Membrane) Answer Center. (2013). Information obtained through email correspondence with Filmtec® membrane technical assistance personnel on December 16, 2013.

Efraty, A. (2009). *U.S. Patent No. 7,628,921*. Washington, DC: U.S. Patent and Trademark Office.

Efraty, A. (2010). *U.S. Patent No. 7,695,614*. Washington, DC: U.S. Patent and Trademark Office.

Efraty, A. (2011). *U.S. Patent No. 8,025,804*. Washington, DC: U.S. Patent and Trademark Office.

Efraty, A. (2012). Closed circuit desalination series no.-4: high recovery low energy desalination of brackish water by a new single stage method without any loss of brine energy. *Desalination and Water Treatment, 42,* 262-268.

Efraty, A., Barak, R. N. & Gal, Z. (2011). Closed circuit desalination—A new low energy high recovery technology without energy recovery. Desalination and Water Treatment, 31, 95-101.

Elimelech, M., Zhu, X., Childress, A. E. & Hong, S. (1997). Role of membrane surface morphology in colloidal fouling of cellulose acetate and composite aromatic polyamide reverse osmosis membranes. *Journal of Membrane Science, 127*, 101-109.

Ghermandi, A. & Messalem, R. (2009). Solar-driven desalination with reverse osmosis: the state of the art. *Desalination & Water Treatment, 7*, 285-296.

Gleick, P. H. (2006). *The world's water 2006-2007, the biennial report on freshwater resources*. Washington, DC: Island Press/Center for Resource Economics.

Greenlee, L.F., Lawler, D. F., Freeman, B. D., Marrot, B. & Moulin, P. (2009). Reverse osmosis desalination: water sources, technology, and today's challenges. *Water Research, 43*, 2317-2348.

Greenlee, L.F., Testa, F., Lawler, D. F., Freeman, B. D.& Moulin, P. (2010). The effect of antiscalant addition on calcium carbonate precipitation for a simplified synthetic brackish water reverse osmosis concentrate. *Water Research, 44*, 2957-2969.

Gross, M. C. (1974). *U.S. Patent No. 3,836,457*. Washington D.C.: U.S. Patent and Trademark Office.

Gude, V. G. (2011). Energy consumption and recovery in reverse osmosis. *Desalination and Water Treatment, 36*, 239-260.

Herzberg, M., Kang, S. & Elimilech, M. (2009). Role of extracellular polymeric substances (EPS) in biofouling of reverse osmosis membranes. *Environmental Science & Technology, 43*, 4393-4398.

Hoek, E. M. , Kim, A. S. & Elimilech, M. (2002). Influence of crossflow membrane filter geometry and shear rate on colloidal fouling in reverse osmosis and nanofiltration separations. *Environmental Engineering Science, 19*, 357-372.

Hoek, E. M. & Elimilech, M. (2003) Cake-enhanced concentration polarization: a new fouling mechanism for salt-rejecting membranes. *Environmental Science & Technology, 37*, 5581-5588.

Kang, N. W., Lee, S., Kim, D., Hong, S. & Kweon, J. H. (2011). Analyses of calcium carbonate scale deposition on four RO membranes under a seawater desalination condition. *Water Science and Technology, 64*, 1573-1580.

Karagiannis, I. C. & Soldatos, P. G. (2008). Water desalination cost literature: review and assessment. *Desalination, 223*, 448-456.

Kim, S. & Hoek, E. M.. (2007). Interactions controlling biopolymer fouling of reverse osmosis membranes. *Desalination, 202*, 333-342.

Lee, S., Lee, E., Elimelech, M. & Hong, S. (2011). Membrane characterization by dynamic hysteresis: Measurements, mechanisms, and implications for membrane fouling. *Journal of Membrane Science, 366*, 17-24.

.

Lenntech Corporation (2011). Reverse osmosis plants. Retrieved in 2011 from website, http://www.lenntech.com/systems/reverse-osmosis/ro/rosmosis.htm.

Maeleb, L. & Ayoub, G. M. (2011). Reverse osmosis technology for water treatment: State of the art review. *Desalination 267*, 1-8.

McCool, B. C., Rahardianto, A., Faria, J., Kovac, K., Lara, D. & Cohen, Y. (2010). Feasibility of reverse osmosis desalination of brackish agricultural drainage water in the San Joaquin Valley. *Desalination, 261*, 240-250.

McHarg, J. (2010). What are efficient methods to reduce the energy requirements of brackish groundwater desalination. Presentation to the Texas Water Conference, 2010.

McHarg, J. (September 2011). *Energy optimization of brackish groundwater reverse osmosis desalination*. Final report for Contract No. 0804830845, Texas Water Development Board, Austin, TX. Retrieved in 2011 from web address http://www.twdb.state.tx.us/innovativewater/desal/projects/adc/doc/2011_09_adc_final_rpt.pdf

Qiu, T. & Davies, P. A. (2012). Comparison of configurations for high recovery inland desalination systems. *Water, 4*, 690-706.

Rahardianto, A., Shih, W. Y., Lee, R. W. & Cohen, Y. (2006). Diagnostic characterization of gypsum scale formation and control in RO membrane desalination of brackish water. *Journal of Membrane Science, 279*, 655-668.

Ramon, G. Z. & Hoek, E. M. (2012). On the enhanced drag force induced by permeation through a filtration membrane. *Journal of Membrane Science., 392-393*, 1-8.

Robbins, A. (2001). *U.S. Patent No. 6,190,558*. Washington DC: U.S. Patent and Trademark Office.

Shih, W. Y., Rahardianto, A., Lee, R. W. & Cohen, Y. (2005). Morphometric characterization of calcium sulfate dihydrate (gypsum) scale on reverse osmosis membranes. *Journal of Membrane Science, 252*, 253-263.

Shirazi, S., Lin, C. J. & Chen, D. (2010). Inorganic fouling of pressure-driven membrane processes--a critical revew. *Desalination, 250*, 236-248.

Song, L., Schuetze, B. D., Rainwater, K. (December 2012). *Demonstration of a high recovery and energy-efficient RO system for small-scale brackish desalination*. Final report. for Contract No. 1004831107, Texas Water Development Board, Austin, TX. Document found at web address http://www.twdb.state.tx.us/innovativewater/desal/projects/texastech/doc/texas_tech_final_rpt.pdf

Song, L., Hong, S., Hu, J. Y., Ong, S. L. & Eng, W. J. (2002). Simulations of full-scale reverse osmosis process. *Journal of Environmental Engineering, 128*, 960-966.

Spectrawatermakers (2009). *Pearson high-pressure pump application guide*. Accessed in September 2013 from website www.spectrawatermakers.com.

Stover, R. L., (2009). *Energy recovery devices in desalination applications.* Manuscript prepared for presentation at the 2009 IWA Membrane Research Conference.

Stover, R. L. (2011). CCD starts a new generation for RO. *Desalination November-December*, (6), 34-35.

Stover, R. L. & Efraty, N. (2012). Low-energy consumption with closed-circuit desalination. *IDA Journal of Desalination and Water Reuse, 4*(3), 12-19.

Stover, R. L. (2013). Industrial and brackish water treatment with closed circuit reverse osmosis. *Desalination and Water Treatment, 51*, 1124-1130.

Szucz, L. (1991). *U.S. Patent No. 4,983,301*. Washington DC: U.S. Patent and Trademark Office.

Tran, T., Bolto, B., Gray, S., Hoang, M. & Ostarcevic, E. (2007), An autopsy study of a fouled reverse osmosis membrane element used in a brackish water treatment plant. *Water Research, 41*, 3915-3923.

Tetra Tech (October 2011). *Analysis of Water from Four Wells at the Brackish Groundwater National Desalination Research Facility.* Report for Contract No. R10PC40009, prepared for the U.S. Bureau of Reclamation, Alamogordo, NM.

Vince, F.,Maréchal, F..,Bréant, P., Aoustin, E. (August, 27, 2007). *Process optimization on economic and environmental objectives*. Presentation by Veolia at the 3rd Conference on Lifecycle Management.

Vrijenhoek, E. M., Hong, S. & Elimelech, M. (2001). Infuence of membrane surface properties on initial rate of colloidal fouling of reverse osmosis and nanofiltration membranes. *Journal of Membrane Science, 188,* 115-128.

Vrouwenvelder, J. S., Manolarakis, S. A., Veenendaal, H. R. & Van der Kooij, D. (2000). Biofouling potential of chemicals used for scale control in RO and NF membranes. *Desalination 132,* 1-10.

Wood, R. (2007). Sun- and wind-powered solar cube is a self-contained water purification system. *Journal of American Water Works Association, 99*(7), 38-40.

Yiantsios, S. G., Sioutopoulos, D. & Karabelas, A. J. (2005). Colloidal fouling of RO membranes: an overview of key issues and efforts to develop improved prediction techniques. *Desalination 183,* 257-272.

Yu, Y., Lee, S. & Hong, S. (2010). Effect of solution chemistry on organic fouling of reverse osmosis membranes in seawater desalination. *Journal of Membrane Science, 351,* 205-213.

Zhu, A., Christofides, P. D. & Cohen, Y. (2009). Effect of thermodynamic restriction on energy cost optimization of RO membrane water desalination. *Industrial & Engineering Chemistry Research, 48,* 6010-6021.

Zhu, A., Christofides, P. D. & Cohen, Y. (2009). Energy consumption optimization of reverse osmosis membrane water desalination subject to feed salinity fluctuation. *Industrial & Engineering Chemistry Research, 48,* 9581-9589.

Zhu, X.& Elimelech, M. (1995). Fouling of reverse osmosis membranes by aluminum oxide colloids. *Journal of Environmental Engineering, 121,* 884-892.

Zhu, X.& Elimelech, M. (1997). Colloidal fouling of reverse osmosis membranes: measurements and fouling mechanisms. *Environmental Science & Technology, 31,* 3654-3662.

APPENDIX A: TEMPERATURE CORRECTION FACTORS FOR SELECTED TESTS

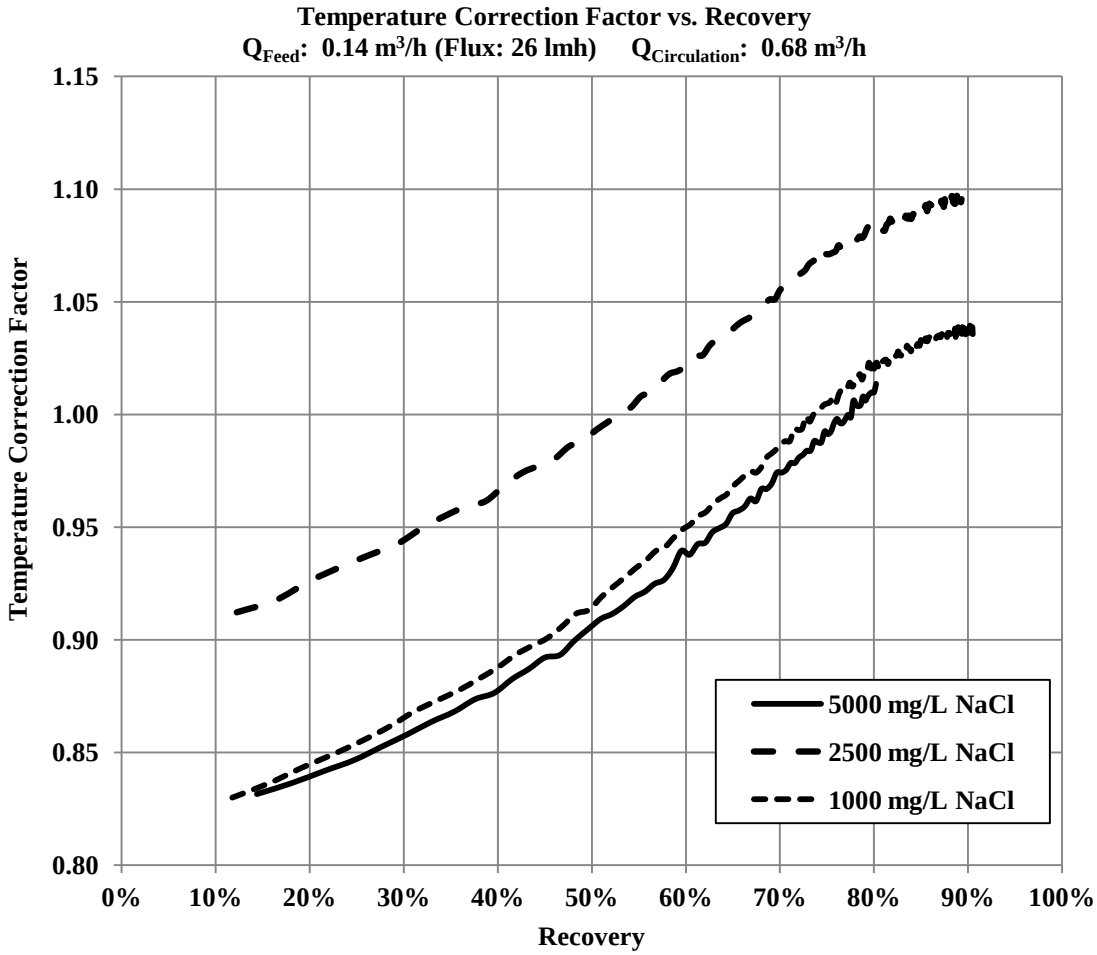

Figure A.1 Temperature correction factor vs. recovery. Feed NaCl (water softener salt) concentrations: 1,000, 2,500, and 5,000 mg/L. Permeate flux: 26 Lmh. Circulation flowrate: 0.68 m^3/h.

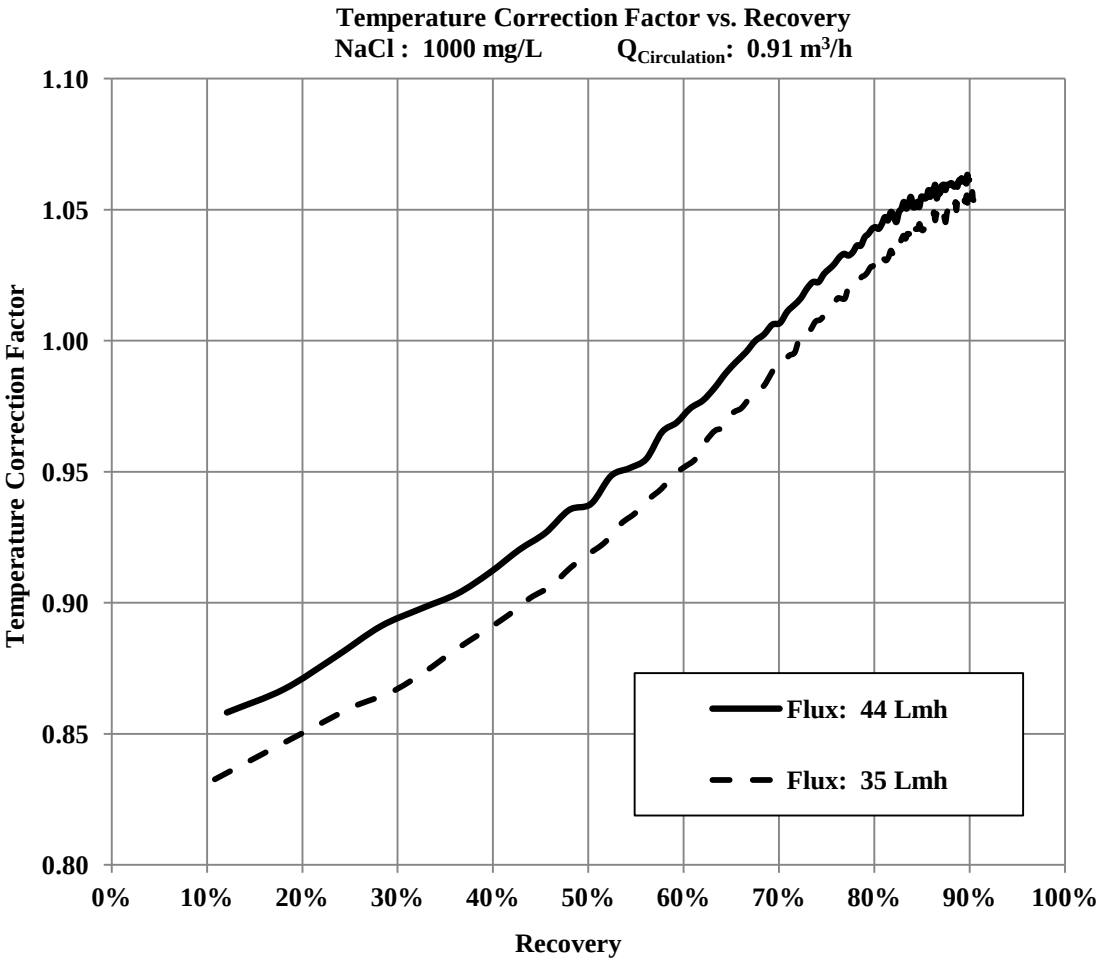

Figure A.2 Temperature correction factor vs. recovery. Feed NaCl (water softener salt) concentration: 1,000 mg/L. Permeate fluxes: 35 Lmh and 44 Lmh. Circulation flowrate: 0.91 m^3/h.

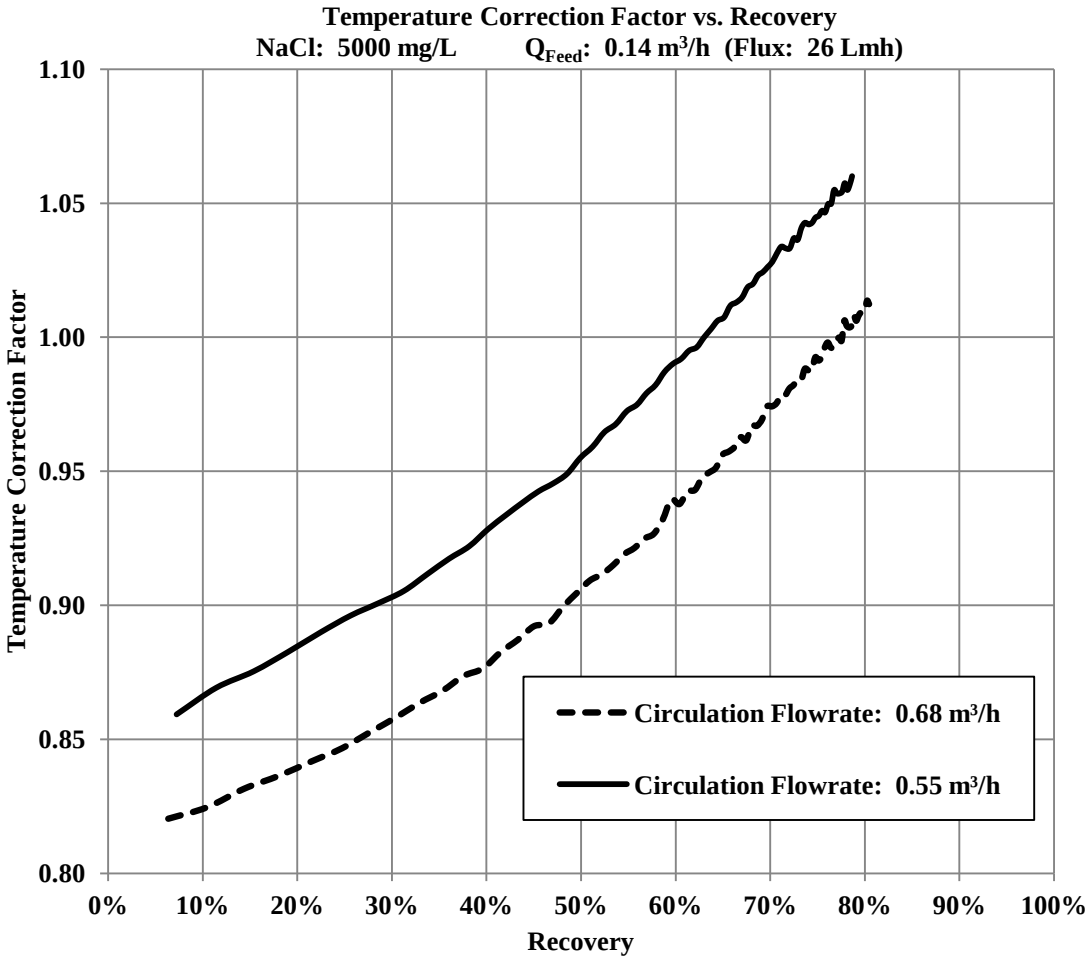

Figure A.3 Temperature correction factor vs. recovery. Feed NaCl (water softener salt) concentration: 5,000 mg/L. Permeate flux: 26 Lmh. Circulation flowrates: 0.55 m^3/h and 0.68 m^3/h.

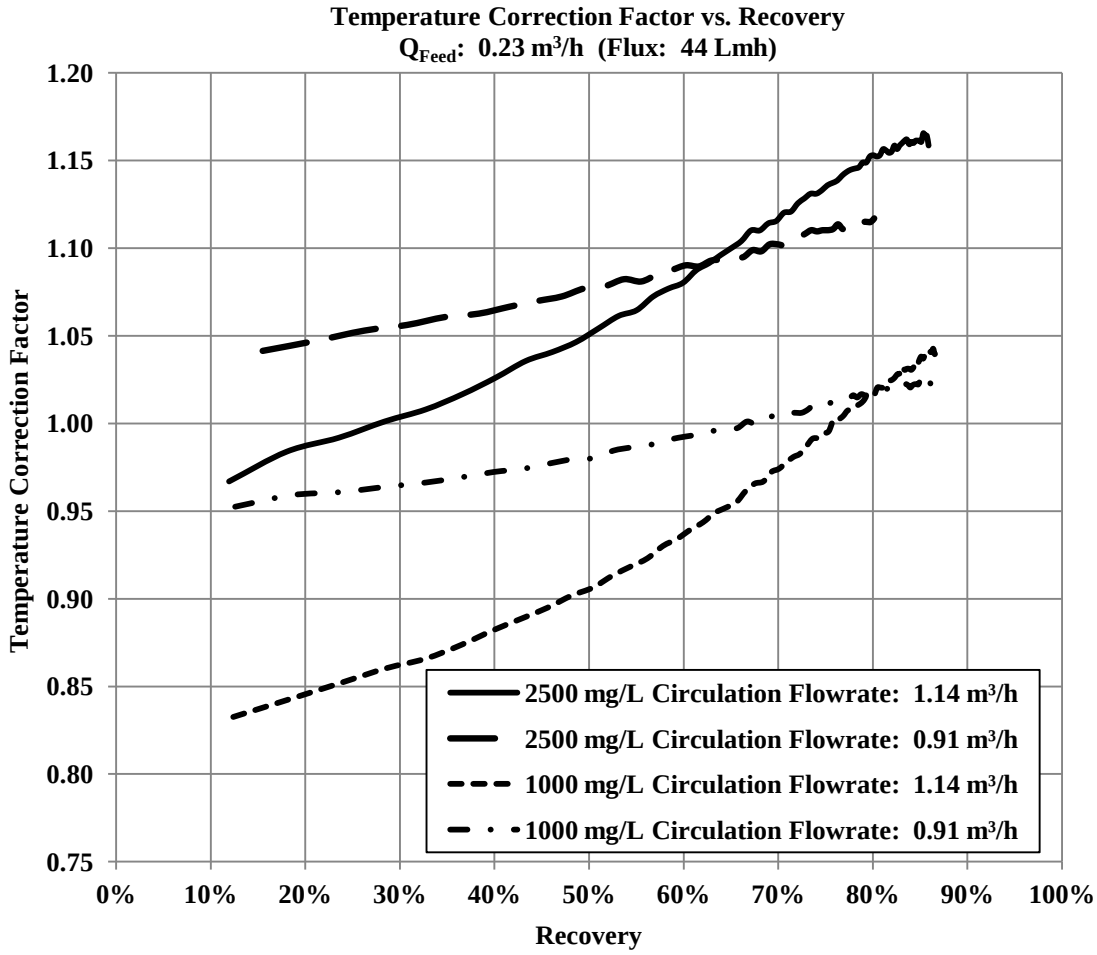

Figure A.4 Temperature correction factor vs. recovery. Feed NaCl (water softener salt) concentrations: 1,000 and 2,500 mg/L. Permeate flux: 44 Lmh. Circulation flowrates: 0.91 m^3/h and 1.14 m^3/h.

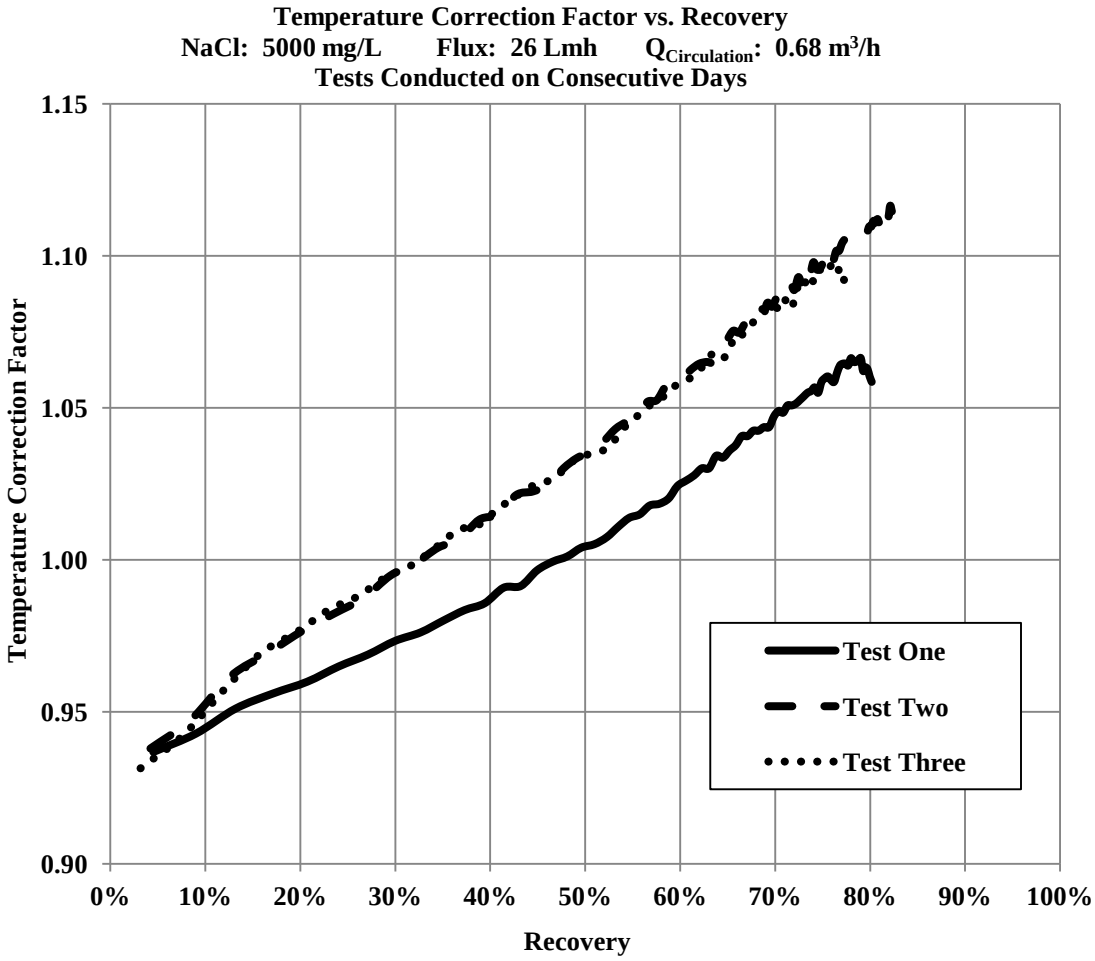

Figure A.5 Temperature correction factor vs. recovery. Feed NaCl (reagent) concentration: 5,000 mg/L. Permeate flux: 26 Lmh. Circulation flowrate: 0.68 m^3/h.

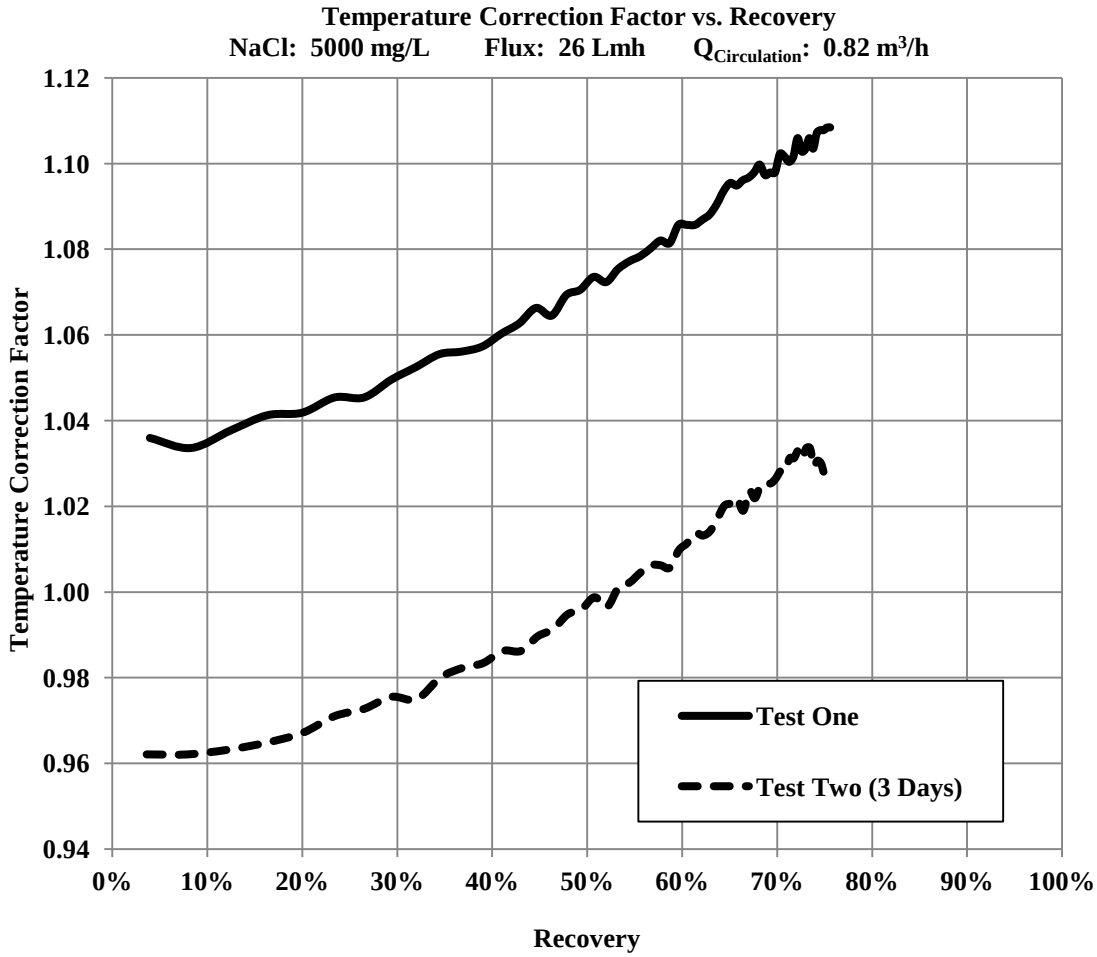

Figure A.6 Temperature correction factor vs. recovery. Feed NaCl (reagent) concentration: 5,000 mg/L. Permeate flux: 26 Lmh. $Q_{Circulation}$: 0.82 m^3/h.

As stated in Chapter I, timespans between duplicate tests are provided on the legend in parentheses.

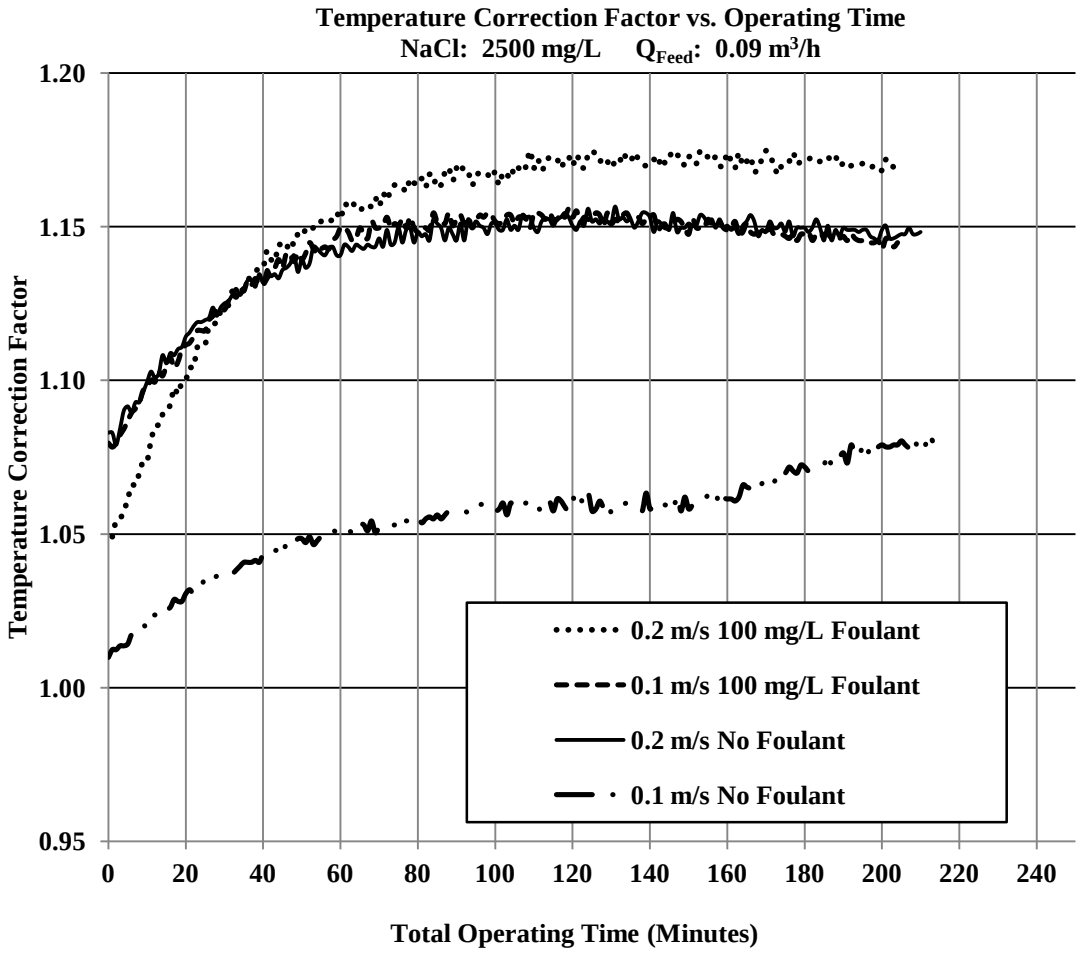

Figure A.7 Temperature correction factor vs. operating time. Feed foulant concentrations: 100 mg/L and baseline (no foulant). Fleed flowrate:: 0.09 m^3/h. Permeate flux: 17 Lmh. Inlet crossflow velocities: 0.1 m/s and 0.2 m/s.

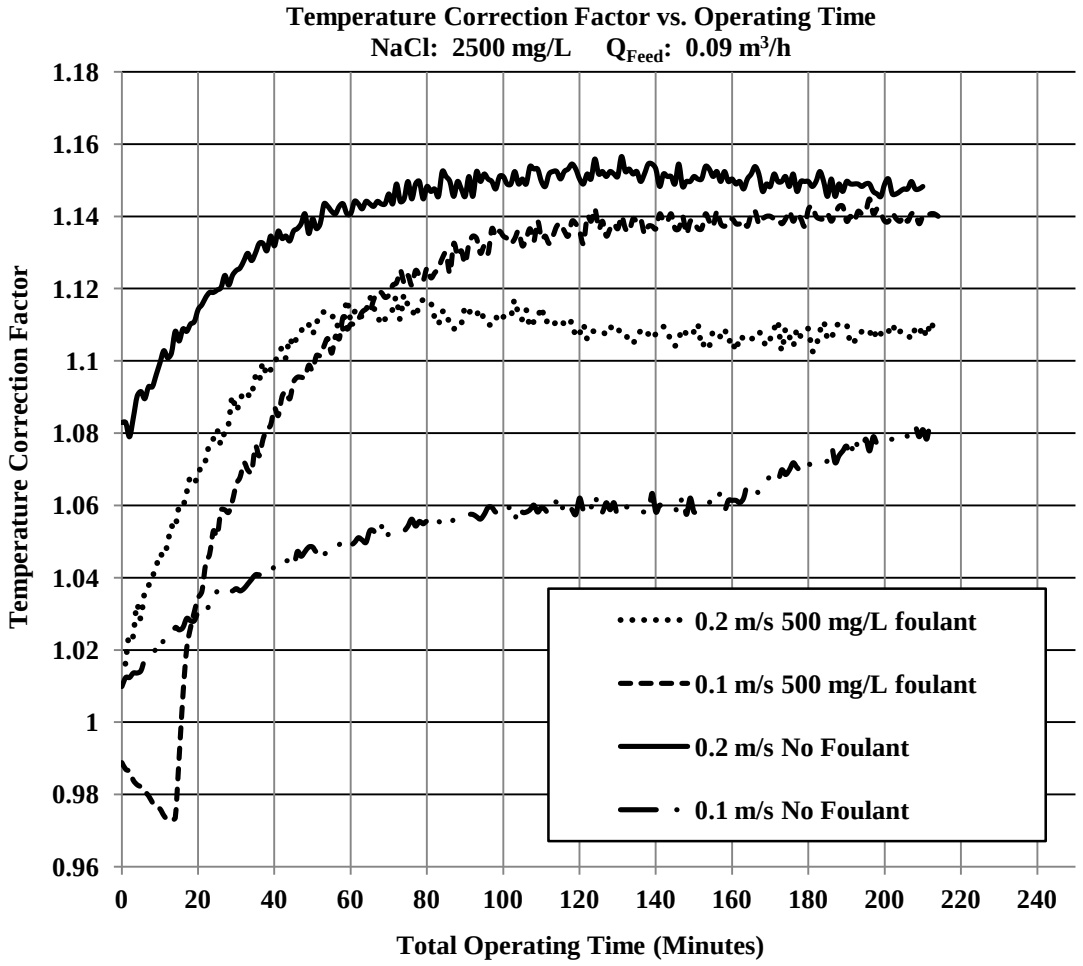

Figure A.8 Temperature correction factor vs. operating time. Feed foulant concentrations: 500 mg/L and baseline (no foulant). Feed flowrate: 0.09 m^3/h. Permeate flux: 17 Lmh. Inlet crossflow velocities: 0.1 m/s and 0.2 m/s.

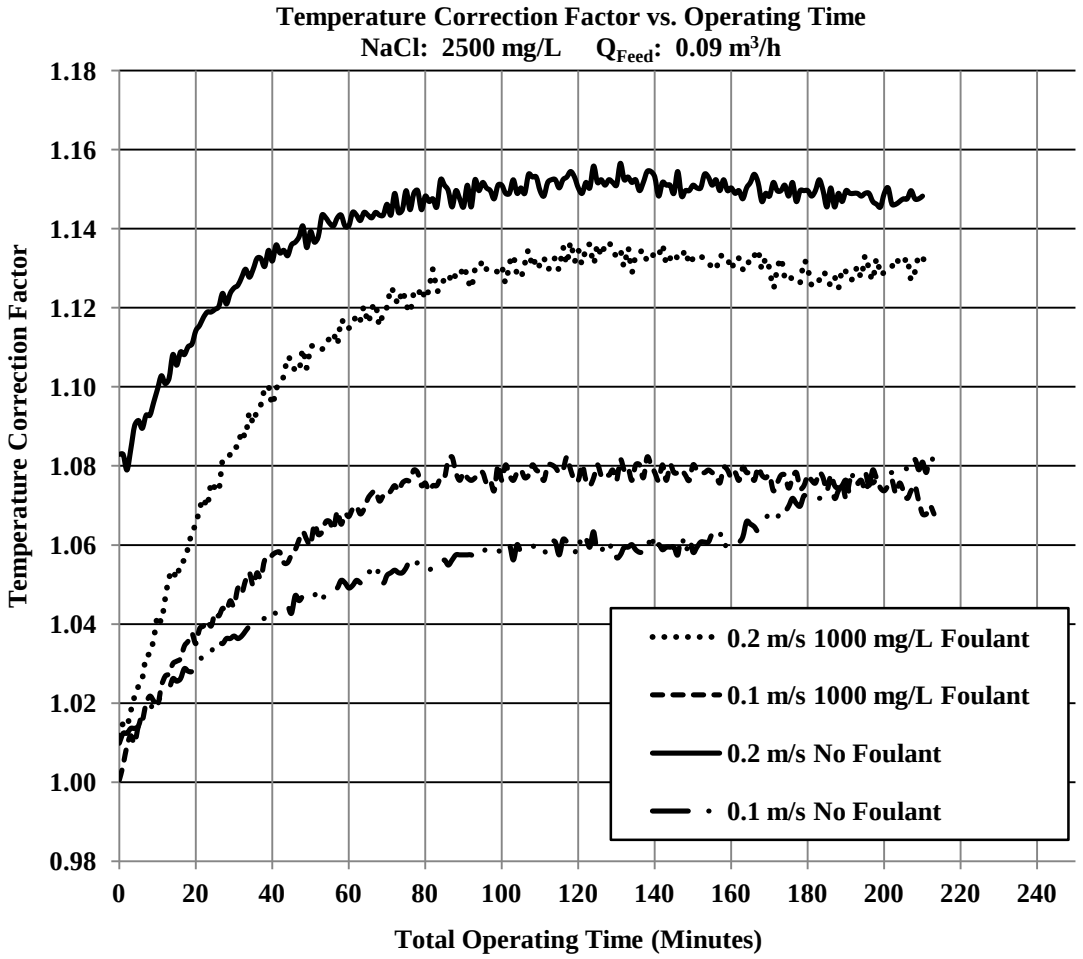

Figure A.9 Temperature correction factor vs. operating time. Feed foulant concentrations: 1,000 mg/L and baseline (no foulant). Feed flowrate: 0.09 m^3/h. Permeate flux: 17 Lmh. Inlet crossflow velocities: 0.1 m/s and 0.2 m/s.

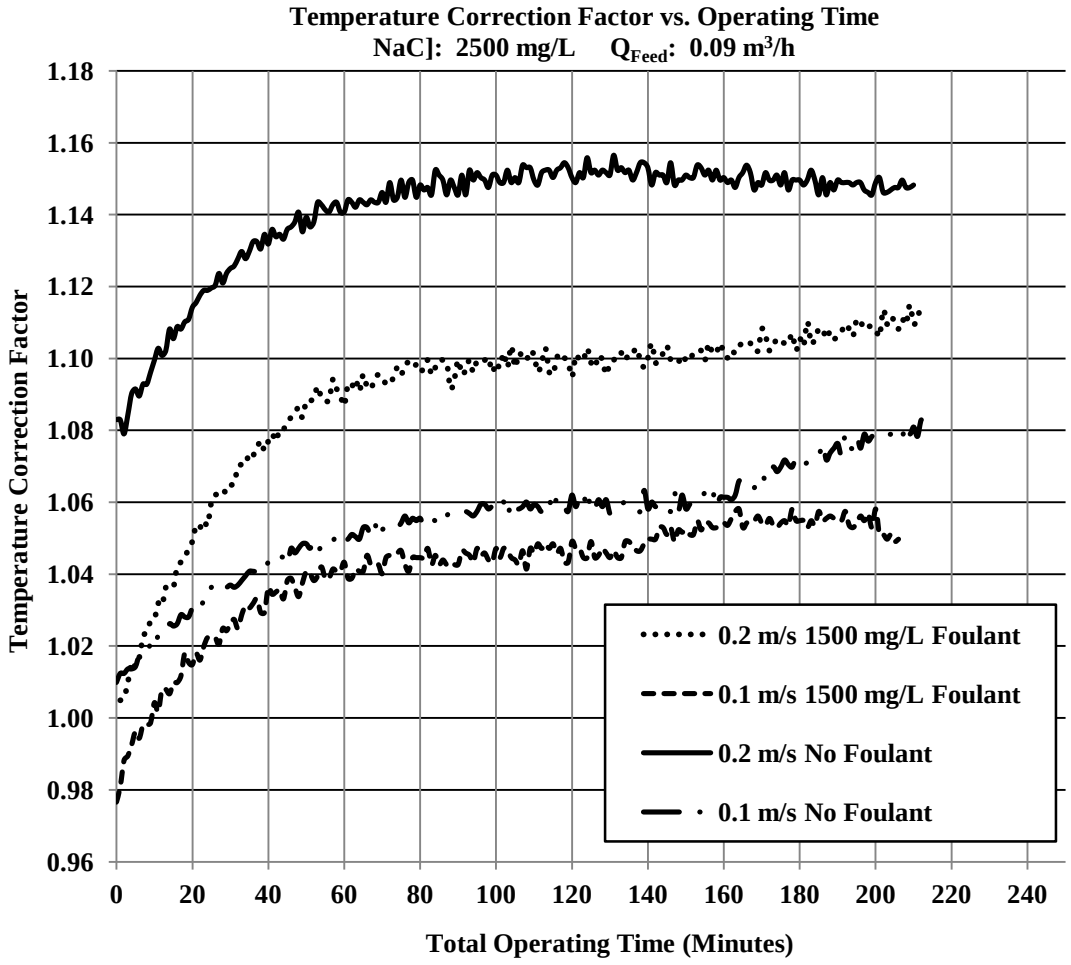

Figure A.10 Temperature correction factor vs. operating time. Foulant concentrations: 1,500 mg/L and baseline (no foulant). Feed flowrate: 0.09 m^3/h. Permeate flux: 17 Lmh. Inlet crossflow velocities: 0.1 m/s and 0.2 m/s.

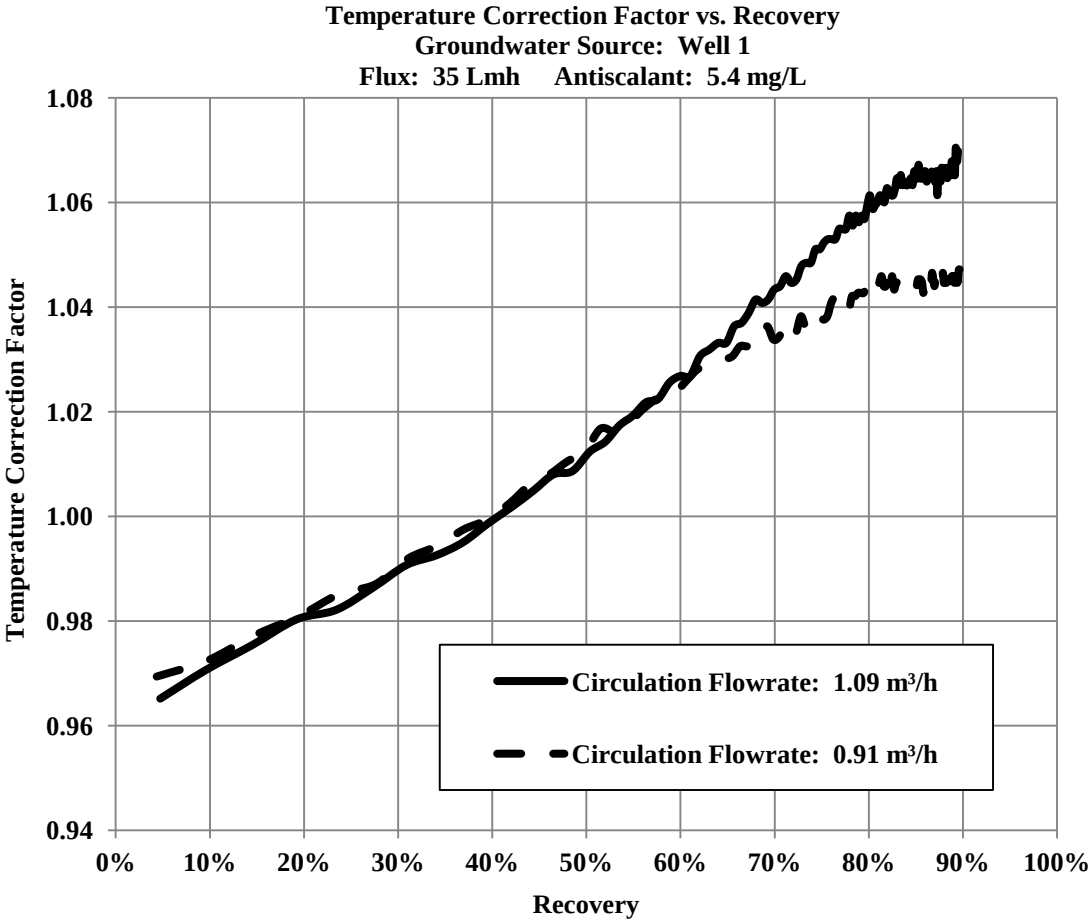

Figure A.11 Temperature correction factor vs. recovery. Reference temperature: 25 C. Groundwater source: Well 1. Permeate flux: 35 Lmh. Circulation flowrates: 0.91 m^3/h and 1.09 m^3/h. Antiscalant: 5.4 mg/L

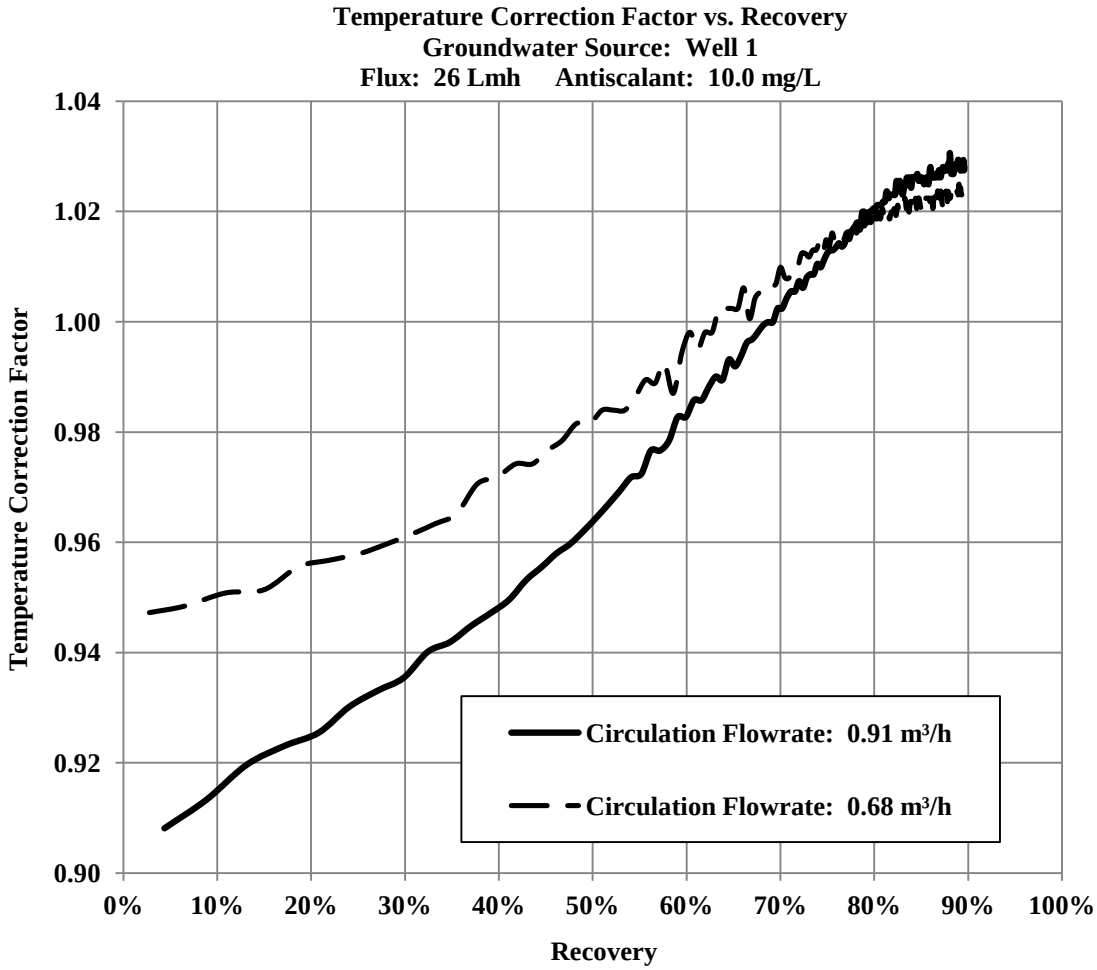

Figure A.12 Temperature correction factor vs. recovery. Reference temperature: 25 C. Groundwater source: Well 1. Permeate flux: 26 Lmh. Circulation flowrates: 0.68 m^3/h and 0.91 m^3/h. Antiscalant: 10.0 mg/L.

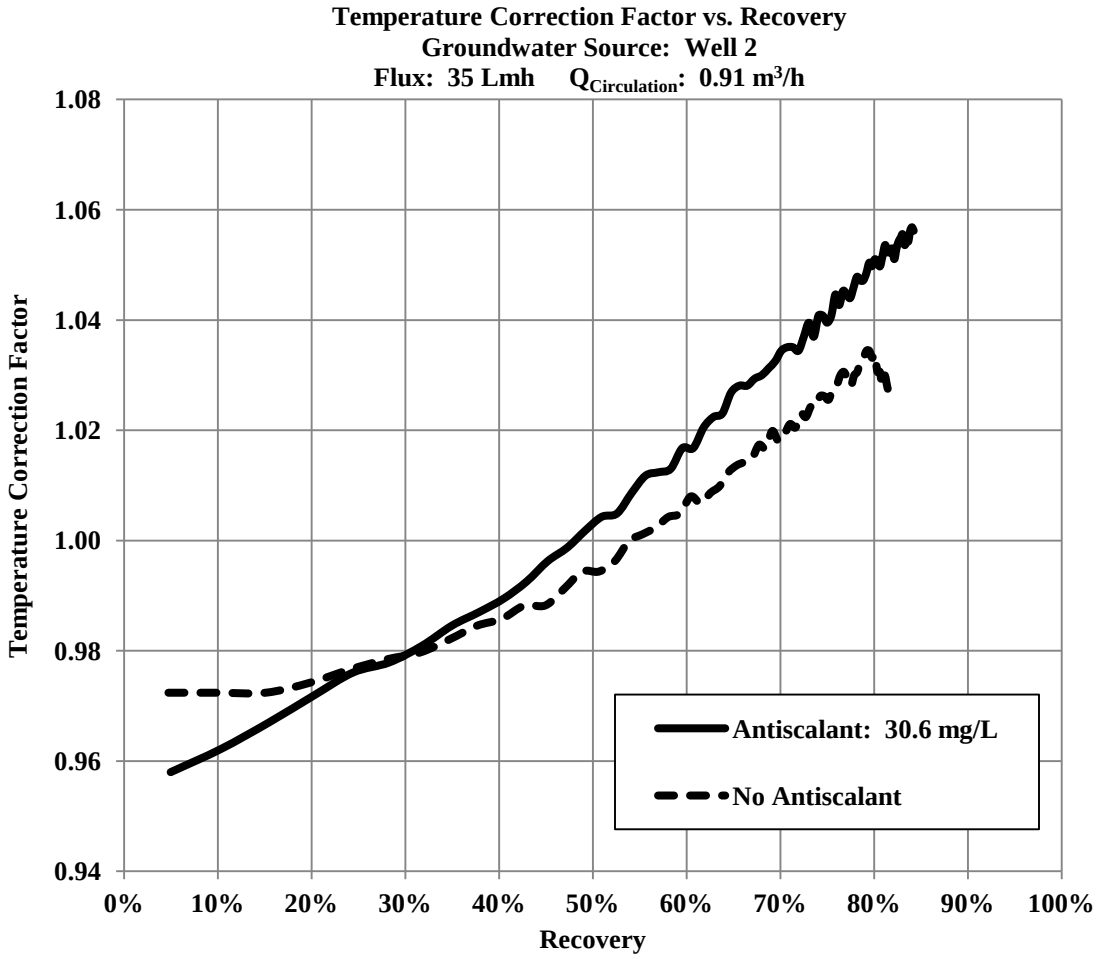

Figure A.13 Temperature correction factor vs. recovery. Reference temperature: 25 C. Groundwater source: Well 2. Permeate flux: 35 Lmh. Circulation flowrate: 0.91 m^3/h. Antiscalant: 30.6 mg/L and 0.0 mg/L.

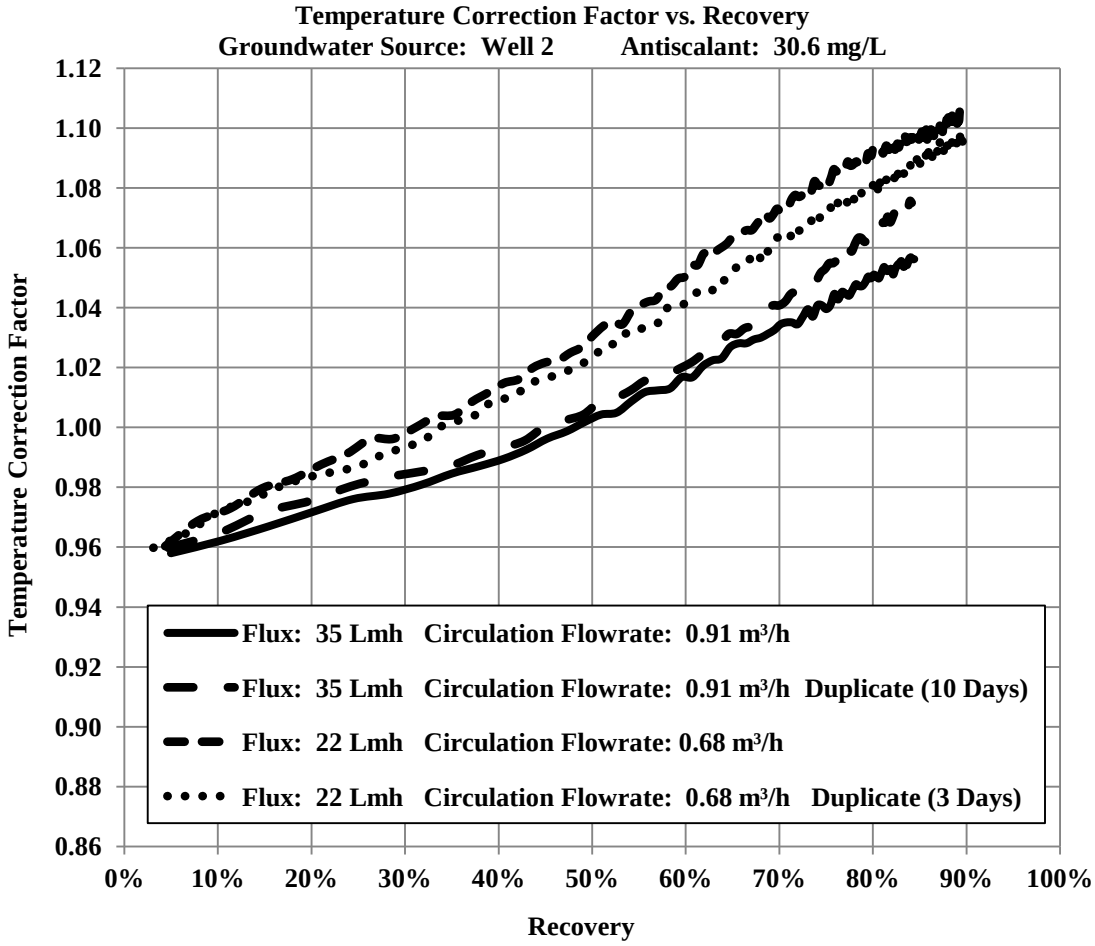

Figure A.14 Temperature correction factor vs. recovery. Reference temperature: 25 C. Groundwater source: Well 2. Permeate fluxes: 22 Lmh and 35 Lmh. Circulation flowrates: 0.68 m^3/h and 0.91 m^3/h. Antiscalant: 30.6 mg/L.

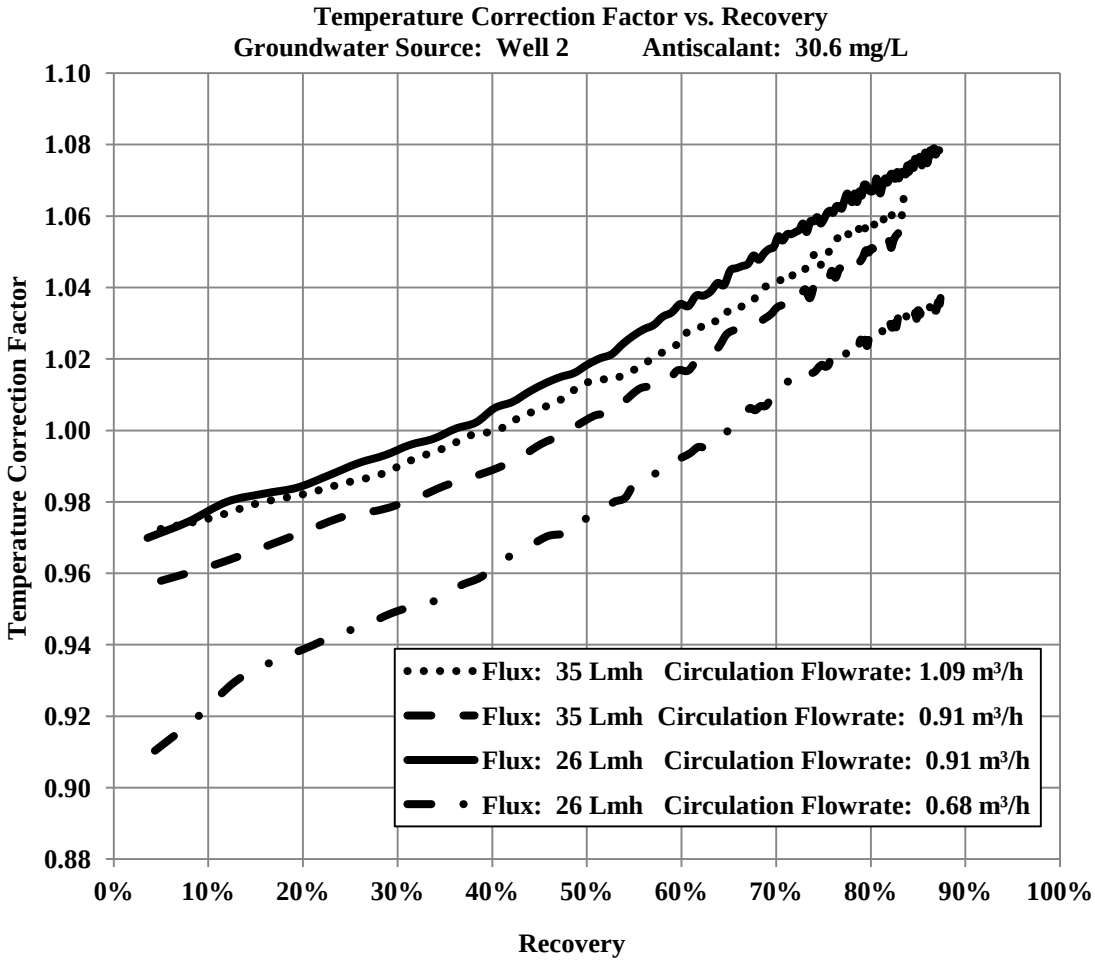

Figure A.15 Temperature correction factor vs. recovery. Reference temperature: 25 C. Groundwater source: Well 2. Permeate fluxes: 26 Lmh and 35 Lmh. Circulation flowrates: 0.68 m^3/h, 0.91 m^3/h, and 1.09 m^3/h. Antiscalant: 30.6 mg/L.

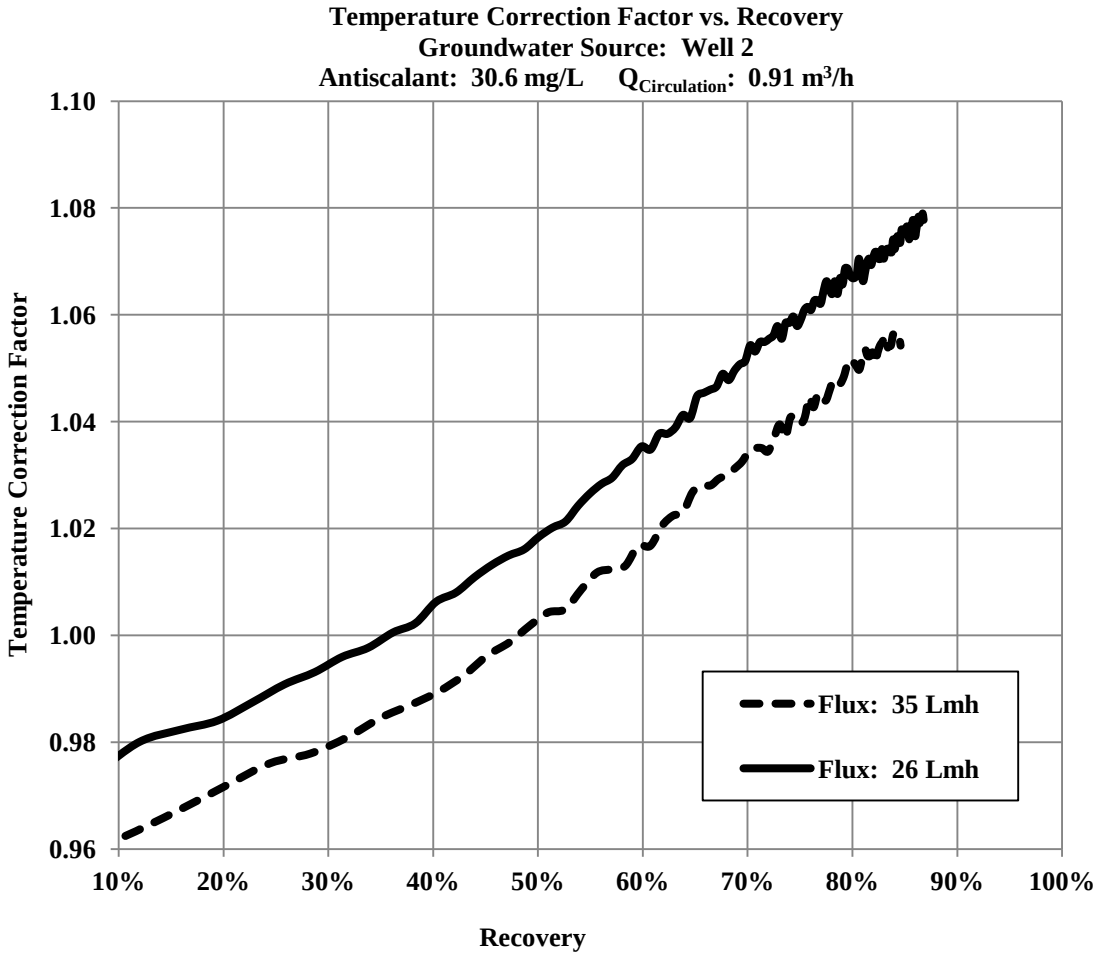

Figure A.16 Temperature correction factor vs. recovery. Reference temperature: 25 C. Groundwater Source: Well 2. Permeate fluxes: 26 Lmh and 35 Lmh. Circulation flowrate: 0.91 m^3/h. Antiscalant: 30.6 mg/L.

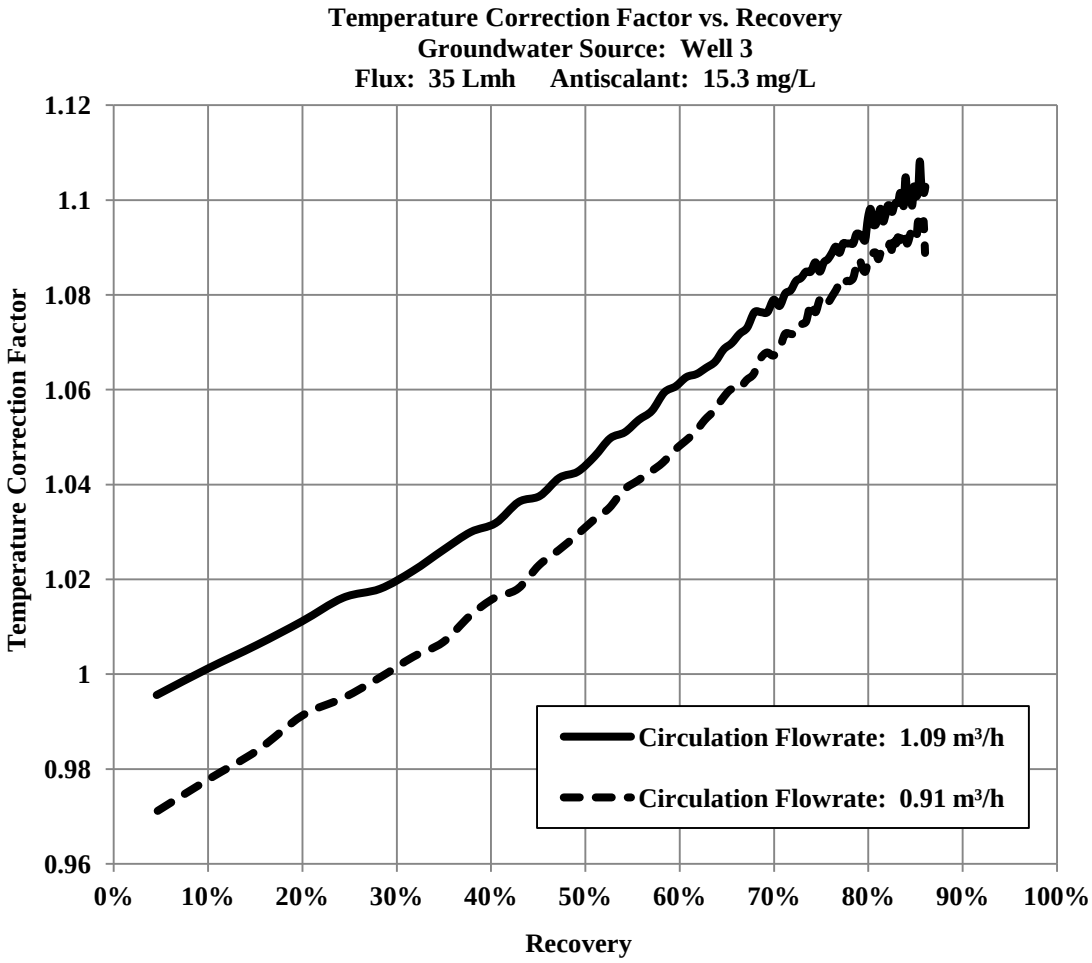

Figure A.17 Temperature correction factor vs. recovery. Reference temperature: 25 C. Groundwater source: Well 3. Permeate flux: 35 Lmh. Circulation flowrates: 0.91 m^3/h and 1.09 m^3/h. Antiscalant: 15.3 mg/L.

APPENDIX B: RESULTS OF DUPLICATE TESTS

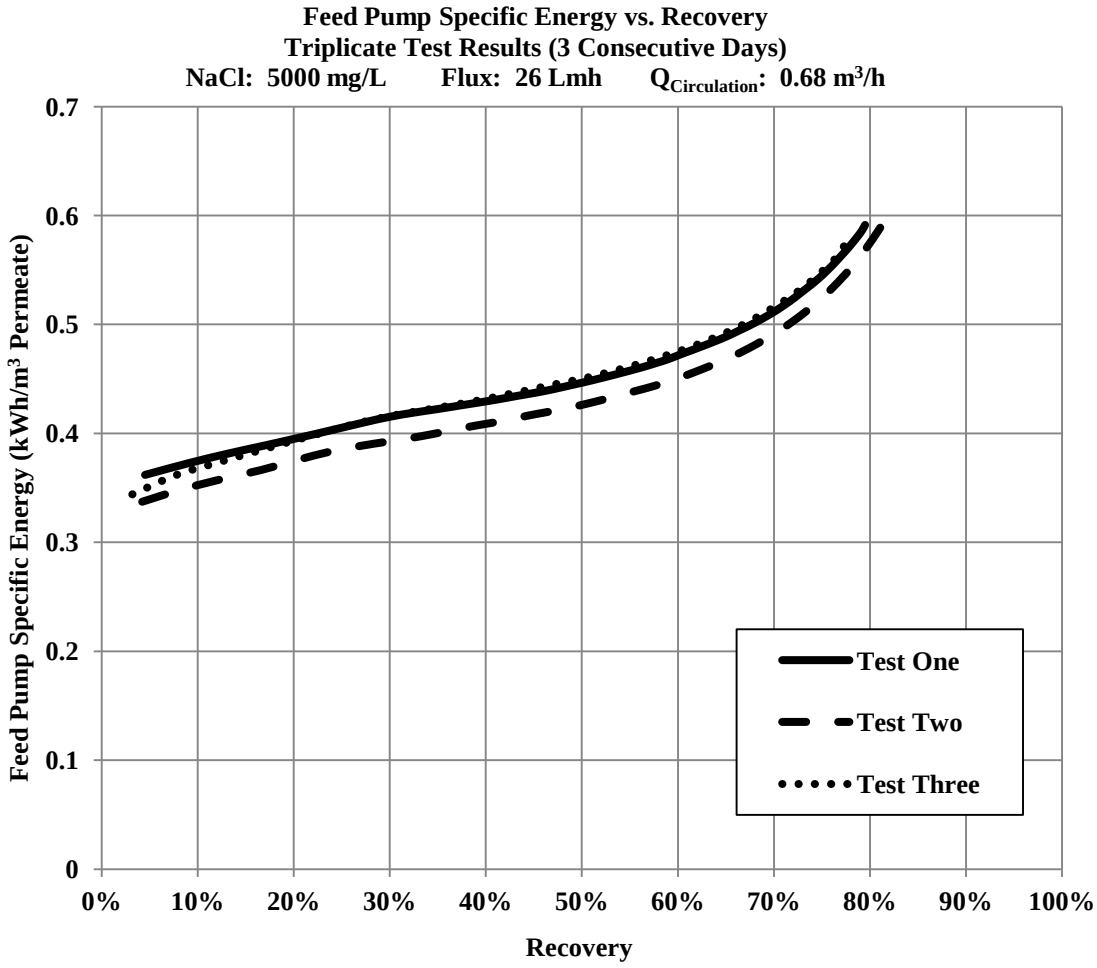

Figure B.1 Feed pump specific energy vs. recovery. Results of triplicate tests. Feed NaCl (reagent) concentration: 5,000 mg/L. Permeate flux: 26 Lmh. Circulation flowrate: 0.68 m^3/h.

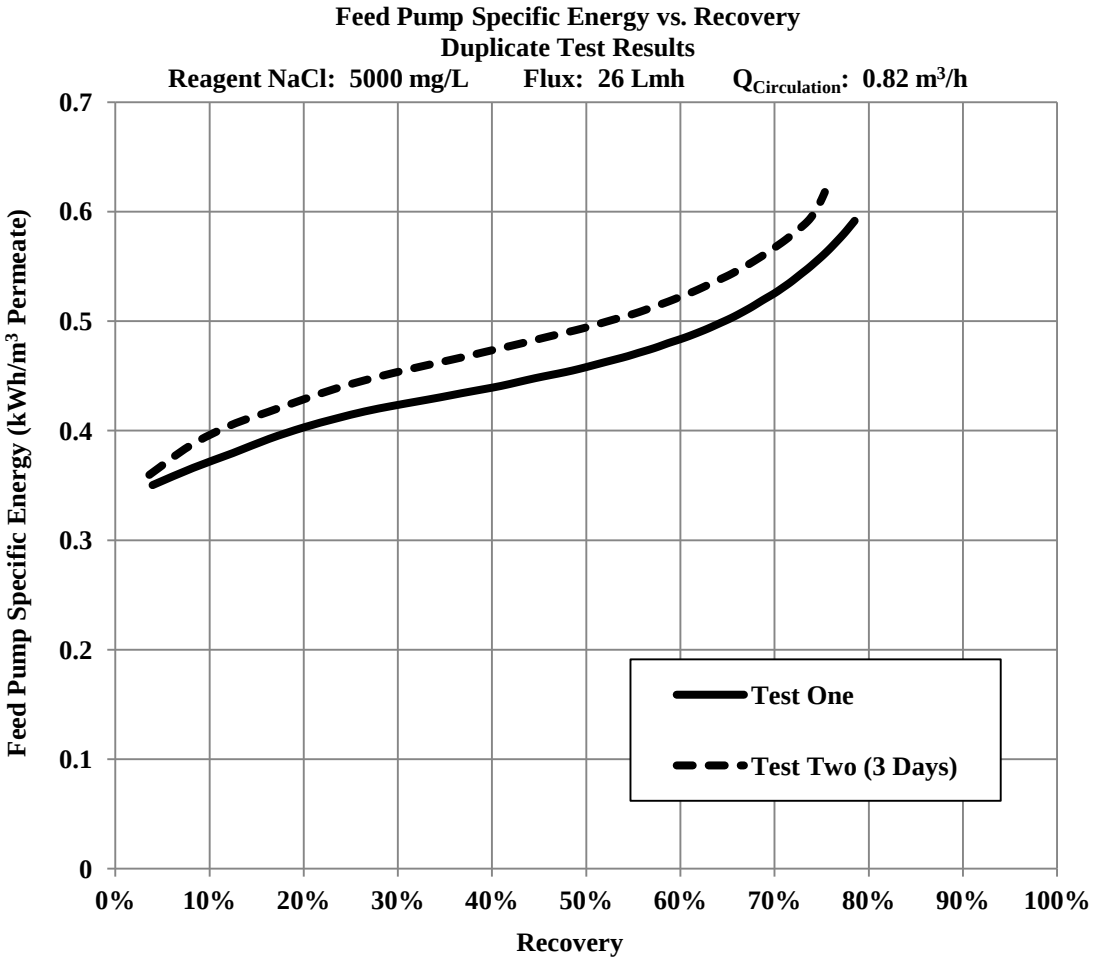

Figure B.2 Feed pump specific energy vs. recovery. Results of duplicate tests. Feed NaCl (reagent) concentration: 5,000 mg/L. Permeate flux: 26 Lmh. . Circulation flowrate: 0.82 m^3/h.

Please note that timespans between duplicate tests are provided on the legend in parentheses.

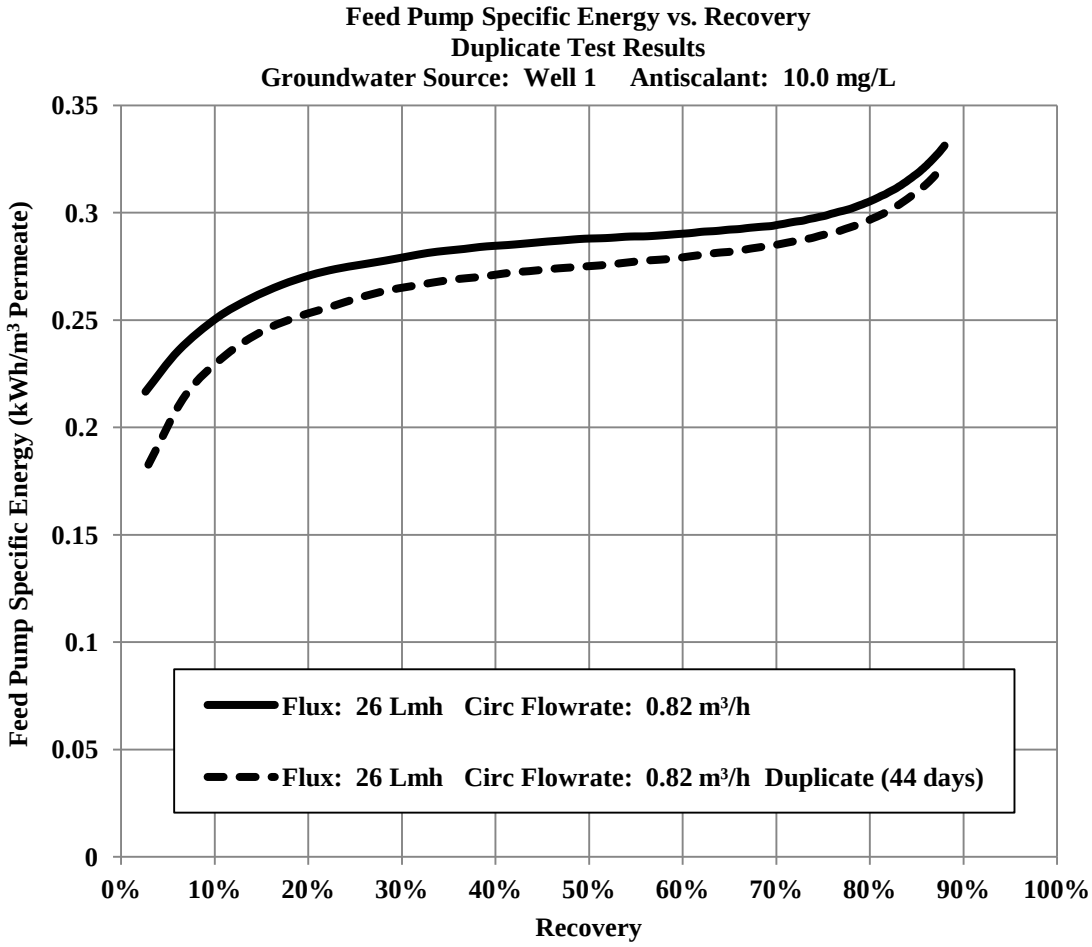

Figure B.3 Feed pump specific energy vs. recovery. Results of duplicate tests. Groundwater source: Well 1. Permeate flux: 26 Lmh. Circulation flowrate: 0.82 m^3/h. Antiscalant: 10.0 mg/L.

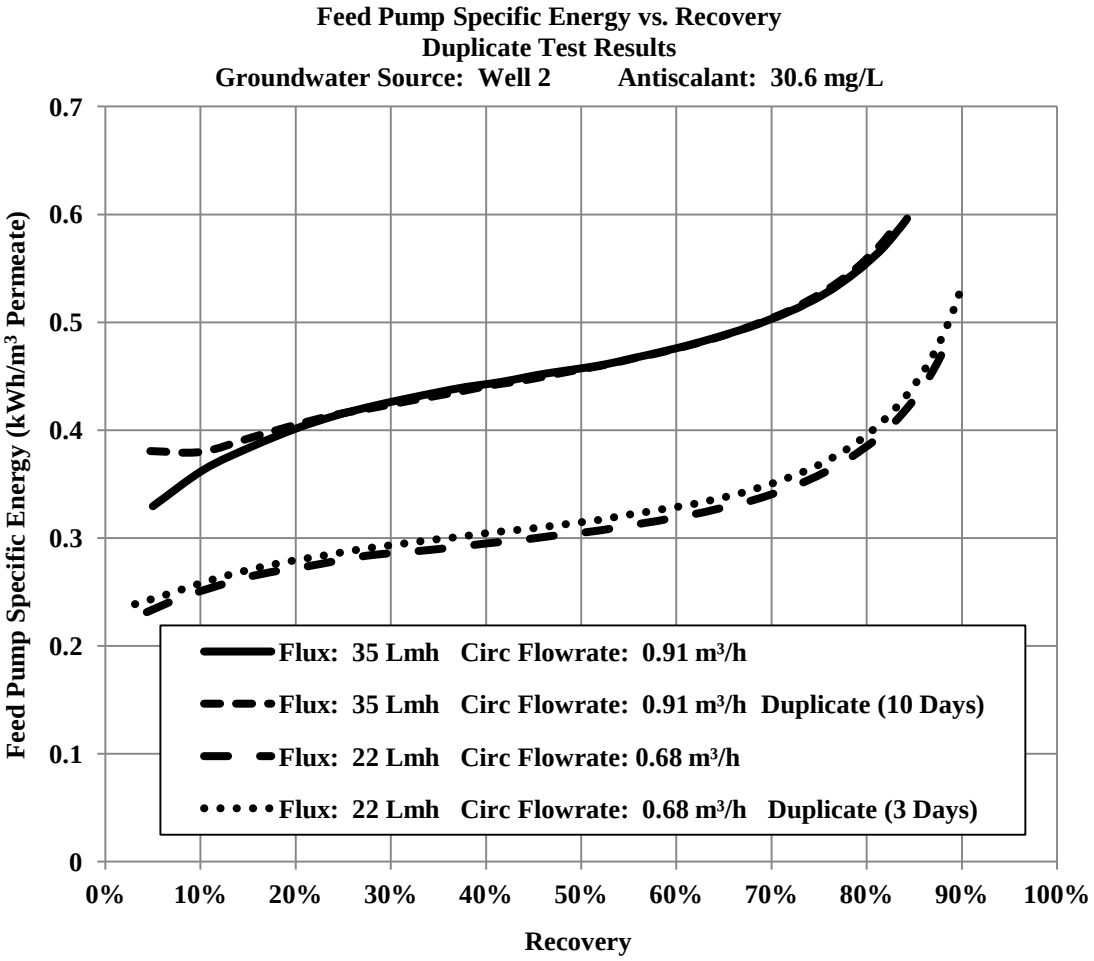

Figure B. 4 Feed pump specific energy vs. recovery. Results of duplicate tests. Groundwater source: Well 2. Permeate fluxes: 22 Lmh and 35 Lmh. Circulation flowrates: 0.68 m^3/h and 0.91 m^3/h. Antiscalant: 30.6 mg/L.

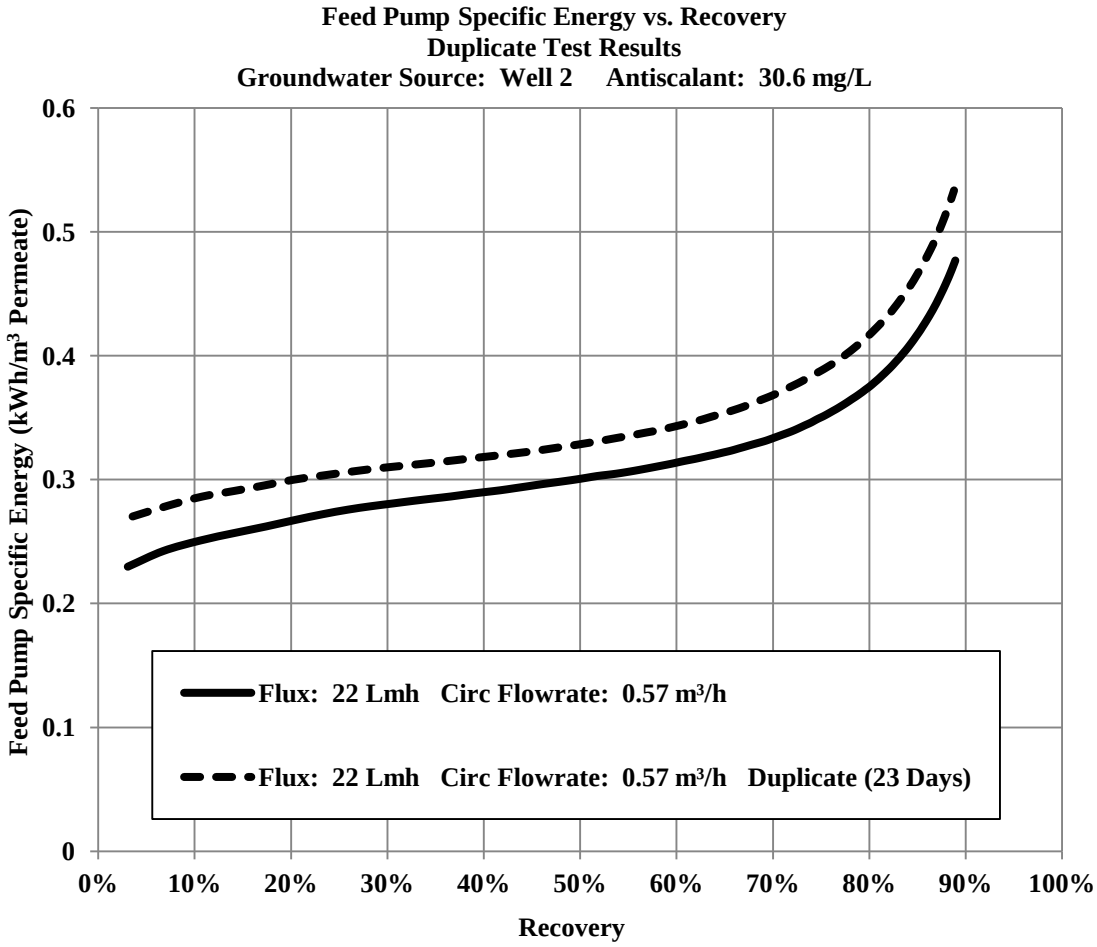

Figure B.5 Feed pump specific energy vs. recovery. Results of duplicate tests. Groundwater source: Well 2. Permeate flux: 22 Lmh. Circulation flowrate: 0.57 m^3/h. Antiscalant: 30.6 mg/L.

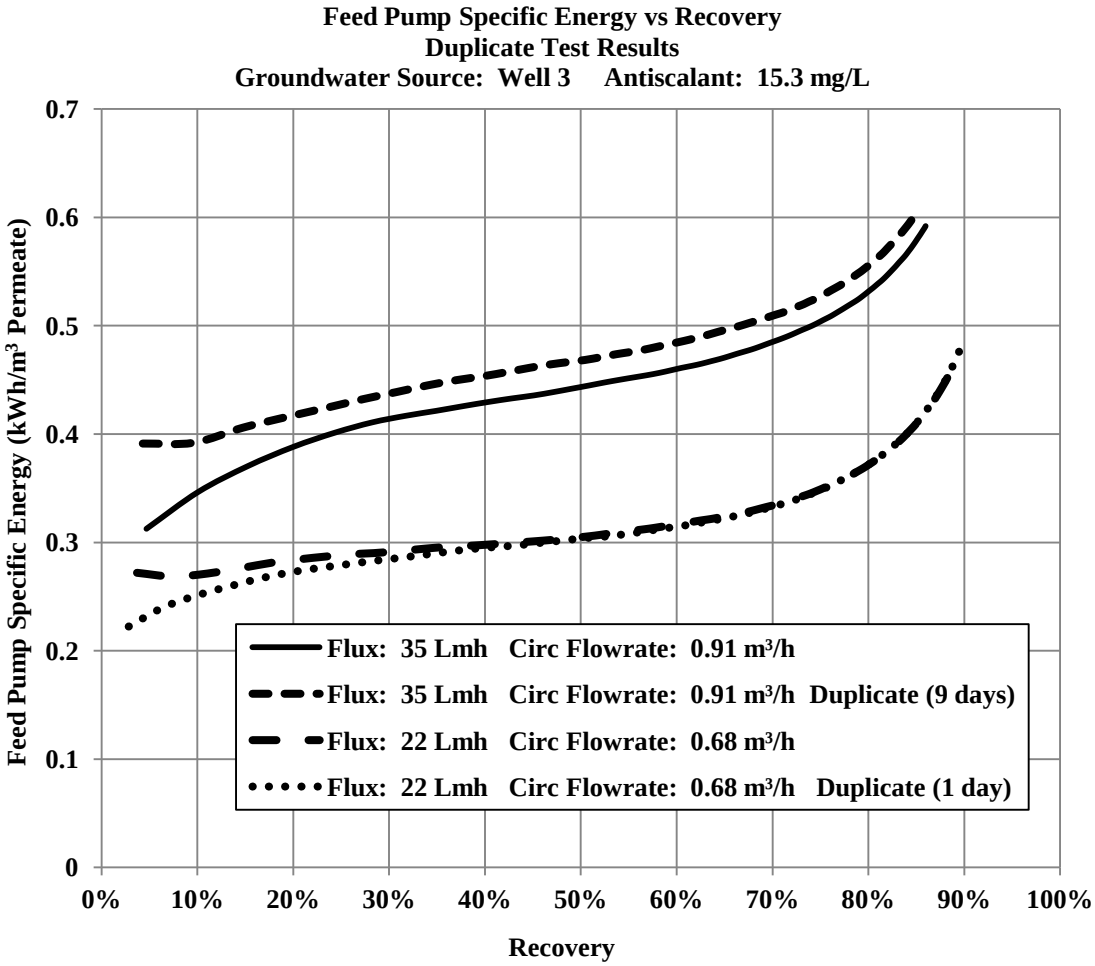

Figure B.6 Feed pump specific energy vs. recovery. Results of duplicate tests. Groundwater source: Well 3. Permeate fluxes: 22 Lmh and 35 Lmh. Circulation flowrates: 0.68 m^3/h and 0.91 m^3/h. Antiscalant: 15.3 mg/L.